/CDF/PHYS/BOTTOM/CDFR/6285
Version 1.1
August 29, 2003

Measurement of the b-Hadron Inclusive Cross-section in CDF Run II using $H_b \to J/\psi X$

Mary Bishai[1], Jonathan Lewis[1], Thomas J. LeCompte[2], Pat Lukens[1], Ting Miao[1], Rick Tesarek[1], Richard St. Denis[3], Slawomir Tkaczyk[1], Simon Waschke[3]

[1] *Fermi National Accelerator Laboratory*
[2] *Argonne National Laboratory*
[3] *Glasgow University*

Abstract

Using 37 pb^{-1} of the Run-II J/ψ data sample collected from February to September 2002, a measurement of the inclusive b-hadron production cross-section in the decay channel $H_b \to J/\psi X$ is performed, where H_b denotes all b-hadrons that decay to J/ψ. The b-fraction is extracted using an unbinned likelihood fit to the proper decay length of the J/ψ in bins of $p_T(J/\psi)$ for $p_T(J/\psi) > 1.25$ GeV/c. The b-fractions obtained are applied to the measurement of the inclusive J/ψ cross-section to obtain a measurement of the differential $H_b \to J/\psi X$ production cross-section as a function of $p_T(J/\psi)$. The first measurement of the total b-hadron cross-section at a hadronic machine has been extracted from the measurement of the cross-section with J/ψ transverse momenta > 1.25 GeV/c and < 17.0 GeV/c using a Monte Carlo modeling of the decay kinematics of b hadrons to charmonium. We find $\sigma(p\bar{p} \to H_b X, |y| < 0.6).Br(H_b \to J/\psi X).Br(J/\psi \to \mu\mu) = 24.5 \pm 0.5(stat)^{+4.7}_{-3.9}(syst)$ nb, where H_b denotes both hadron and anti-hadron states. The total single b-quark cross-section integrated over one unit of rapidity is $\sigma(p\bar{p} \to \bar{b}X, |y| < 1.0) = 29.4 \pm 0.6(stat)^{+6.2}_{-5.4}(syst)\mu$b.

Contents

1 Introduction

The Run I central b production cross-section results, which included only b hadrons with $p_T > 5$ GeV, were more than a factor of two greater than NLO QCD predictions [1]. Dozens of theoretical explanations were offered: NNLO corrections were large, intrinsic k_T effects are large, extreme value of the renormalization scales are required, new methods of resummation and fragmentation were required [2] [3] [4] [5], and even theories of new and exotic sources of b hadrons were proposed [6]. Results from CDF Run I and various theoretical predictions from NLO QCD calculations are summarized in Figures 1 2 3.

These theories can broadly be categorized as "size" theories and "shape" theories. Because CDF measured only about 10% of the spectrum (the typical fraction above the p_T threshold), it's not evident from the data whether the excess is due to an overall increase in the $b\bar{b}$ production rate or instead a shift in the spectrum towards higher p_T.

An inclusive measurement of bottom quark production over all transverse momenta can help resolve this ambiguity. Because of the copious production of J/ψ

mesons from bottom hadrons, H_b, decays at the Tevatron, we have a sample of tens of thousands of $H_b \to J/\psi X$ decays from which we can extract this cross-section.

This is done by taking the previously measured total J/ψ cross-section [7], and determining the fraction of these particles that are bottom hadron decay products by measuring the position of the J/ψ vertex relative to the H_b's. The long-lived H_b daughters have J/ψ daughters hundreds or thousands of microns from the primary vertex, unlike directly produced charmonium which has the J/ψ vertex at the proton-antiproton interaction point. We use an unbinned maximum liklihood fit to statistically separate the two components. The combination of the inclusive J/ψ cross-section and the fraction of those J/ψ's that are H_b daughters (along with the appropriate branching fractions) is then used to extract the b-hadron inclusive cross-section.

The lower in $p_T(J/\psi)$ we can probe, the more of the $H_b \to J/\psi X$ cross-section we observe, and the more accurate our measurement will be. However, because the bottom decay imparts up to about 1.7 GeV/c of momentum to the J/ψ, once we can probe $p_T(J/\psi)$ below this value, we gain some sensitivity to b's near $p_T = 0$. The key to the inclusive b measurement using J/ψ decays is to push the J/ψ p_T threshold as low as possible, but it is not necessary to push it all the way to zero.

2 Event Selection

The data sample used in this study are J/ψ events from the dimuon trigger paths in runs 138425 to 152625. This corresponds to the 2-miss operation mode of the level 1 XFT track trigger. The data was processed with version 4.8.4a of the CDF production software and analyzed using version 4.9.1.

2.1 COT and CMU selection criteria

The following selection criteria were applied to the COT and CMU μ track parameters [7]:

L3 selection criteria:

- CMU muons
- $p_T(\mu)_{COT} > 1.5$ GeV/c
- Opposite sign muons
- $|z_0(\mu_1) - z_0(\mu_2)| < 5$ cm
- $2.7 < M(\mu\mu) < 4.0$ GeV/c^2
- $\Delta\phi(\mu\mu) < 130^0$ when $p_T(J/[y]) > 2.0$ GeV/c

- stub-track match: $\Delta(r\phi)_{CMU} < 30cm$

Additional COT/CMU offline selection:

- Explicitly require CMU-only or CMUP muons
- $\chi^2(\Delta r\phi)_{CMU} < 9$
- $\mid y(J/\psi) \mid < 0.6$
- COT hits: axial≥ 20, stereo≥ 16.
- Both muon stubs are required to be seperated by $\Delta\phi = 5^0$

2.2 Silicon track selection

Both μ tracks are required to be COT-SVXII tracks. Additional silicon track selections were made to assure a good lifetime measurement as outlined in [15]; both CMU muon tracks were required to have a hit in the innermost layer of the SVXII and a hit in the next layer out if it was functioning; the total number of hits expected in SVXII alone was computed using the SiExpected module v4.9.1. Tracks with greater than 1 missing hit in the SVXII were rejected. Tracks crossing SVXII mechanical barrel boundries are also rejected.

The COT-SVXII muon tracks were refit using v4.9.1 of the SiTrackFitter module with alignment table 100030 1 GOOD. All 3-D hits found in SVXII during pattern recognition are used. L00 and ISL hits are dropped during the track refit. Energy loss corrections using a μ particle hypothesis were applied to the candidate tracks during track refit using the GEANT material integrator, G3X. A 3-D constrained vertex fit (CTVMFT) is applied to the two muon tracks to reconstruct the J/ψ decay vertex position. The probability of χ^2 of the 3-D vertex fit to the $\mu\mu$ vertex is required to be > 0.001. The events were also required to have the run-averaged beam line position calculated from silicon tracks in inclusive jet data with history code 19.

The J/ψ mass distribution of accepted events in the run range 138425-152625 is shown in Figure 4. We find $139,200 \pm 500$ events.

3 Monte Carlo Simulation

To extract the fraction of inclusive J/ψ events from the decays of b-hadrons and thus measure the b-hadron inclusive cross-section, the number of J/ψ events with long lived displaced vertices needs to be counted. A MC simulation is needed to model the kinematic distributions of J/ψs from b-hadron decays. Kinematic distributions of the momentum spectrum of J/ψ from b-hadrons and the long-lived flight distances can then be used to distinguish prompt J/ψ events from $H_b \rightarrow J/\psi$ events.

We use a parameteric simulation of the COT smearing, energy loss in SVXII material, CMU fiducial volume, calorimeter range-out and kinematic acceptance as described in [7]. The measured L1 muon trigger efficiency curve as a function of the μ transverse momentum is used to simulate the acceptance of the L1 trigger [9] [1]. The rapidity of the J/ψ is required to be $|y(J/\psi)| < 0.6$ to be compatible with the inclusive cross-section measurement.

3.1 Choosing an initial b-hadron production spectrum

The Bgenerator package [10] (version 4.9.1) is used to generate b hadrons using an input b quark $d\sigma/dp_T dy$ spectrum. The input spectrum to Bgenerator from Equation is produced using the HVQ package (version 4.9.1) such that:

- The parton distribution functions used the MRST 2000 proton structure functions.
- The default normalization scale used is $\mu = \mu_0$ where $\mu_0 = \sqrt{m_b^2 + p_T^2}$
- The mass of the b quark is $m_b = 4.75$ GeV/c.

The spectra from HVQ are histograms with 200 MeV/c granularity in $p_T(b)$. A mix of b hadron states is produced in the following ratios: $B_d : B_u : B_s : \Lambda_b = 0.389 : 0.389 : 0.106 : 0.116$ [11]. The b hadrons are decayed using the QQ package to final states containing $J/\psi \to \mu\mu$. The input masses and lifetime of the b-hadrons used are listed in Table 1.

In Figure 5, the 2-D p_T, y distribution of the input b-quark and output b-hadron spectra when fragmentation is turned on in Bgenerator [2] reveals a large excess of very low momenta b-hadrons is produced. The source of the excess is not well understood at the moment. To properly model the shape of the low momentum b-hadron spectrum used for the MC in this analysis, the fragmentation option in Bgenerator is switched off and the b-hadron spectrum used is as shown in Figure 6.

3.2 Modeling the $H_b \to J/\psi X$ decay spectra

The inclusive decay spectra of charmonium from B meson decays produced at the $\Upsilon(4S)$ have been recently remeasured using larger data samples at CLEO [12] and BaBar [13]. We find that the QQ decay table used in this analysis (version 20010328) to simulate $B^{\pm,0} \to J/\psi X$ agrees well with the measured spectrum of $B^{\pm,0} \to J/\psi(direct)X$ decays from CLEO 2001 data as shown in Figure 7. From

[1] The simulation also includes the effect of the trigger inefficiency near the center of the COT wire planes.

[2] A Peterson fragmentation function is used to form the final b-hadronic states in Bgenerator.

the CLEO analysis details [14], it was pointed out that the spectra of $\psi(2s)$ and χ_{c1} from the default QQ decay tables is harder than the measured spectra in data. Therefore, the branching fractions of unknown modes in the inclusive $B \rightarrow \psi(2s)X$ decays was changed until good agreement was obtained between the inclusive J/ψ spectrum in the CLEO data and CDF generator level MC in the $\Upsilon(4S)$ rest frame. We find that including a branching fraction of $B \rightarrow \psi(2S)K^*(892)\pi\pi$ of 44% of the total $B \rightarrow \psi(2s)X$ produces an inclusive J/ψ spectrum in good agreement with the CLEO data as illustrated in the bottom plot of Figure 7. We use a mixture of $B \rightarrow J/\psi(direct)X$ and $B \rightarrow \psi(2S)(direct)X, \psi(2S) \rightarrow J/\psi X$ in the ratio 1:0.295 respectively. A χ^2 test of the MC distribtuion fit to CLEO data has a confidence level of 31.4%. The decay of the inclusive $B_s \rightarrow J/\psi X$ in the tuned decay table is chosen to exactly mirror the $B^{\pm,0}$. The decay dynamics of the baryons are still not well measured so only the two body decay of the $\Lambda_b \rightarrow J/\psi\Lambda$ is currently included in the MC model. Since the baryon contribution to inclusive J/ψ at CDF is small, we treat it as a systematic uncertainty on the MC modeling by measuring the effect of varying the fraction of the baryon contribution and the lifetime.

3.3 Transverse momentum reach of b-hadrons decaying to J/ψ

To assess whether our tuned production and decay MC models are a reasonable starting point for our studies, we compared the J/ψ transverse momentum distribution from the current analysis of the $b \rightarrow J/\psi X$ cross-section to the MC predictions using the hard $B \rightarrow J/\psi(direct)X$ and the much softer $B \rightarrow \psi(2s)X, \psi(2S) \rightarrow J/\psi X$ decay spectra is shown in Figure 8. We find that the MC spectrum is harder than the data distribution but is still consistent within statistical and systematic uncertainties with the initial measurement.

The transverse momenta of the parent b-hadron, vis-a-vis the transverse momentum of the reconstructed J/ψ is shown in Figure 9. At $p_T(J/\psi)$ between 2.00 and 2.25 GeV/c, b-hadrons down to p_T of 500 MeV/c are probed. This corresponds to $\gamma\beta c\tau \approx 45\mu$m which is similar to the 50μm measured resolution of the flight distance of J/ψ events [15]. Since the cross-section falls rapidly near $p_T(H_b) = 0$ GeV/c, the number of J/ψ from bs with $p_T < 500 MeV/c$ is only 4% at $p_T(J/\psi) = 1.0$ GeV/c. Table 2 summarizes the fraction of b-hadrons probed (shown in Figure 9) with transverse momenta below 500 MeV/c for $0 < p_T(J/\psi) < 2.0$ GeV/c. We find that there is a linear correlation between the average J/ψ transverse momentum and the average b-hadron transverse momentum for all J/ψ momenta above 1.0 GeV/c. A straight line fit to the mean of the b-hadron transverse momentum distribution in each 250

MeV/c $p_T(J/\psi)$ bin from 1- 17 GeV/c is shown in Figure 9. We find

$$< p_T(b-hadron) >= 1.36 < p_T(J/\psi) > +0.42 \text{ GeV/c}, \quad p_T(J/\psi) > 1.0 \text{ GeV/c} \quad (1)$$

Below $p_T(J/\psi) \sim 1.0$ GeV/c there is no strong correlation between the transverse momenta of the b-hadron and the daughter J/ψ; the H_b momentum spectrum is approximately constant. Therefore, information about the shape of the b-hadron cross-section cannot be extracted from the $b \to J/\psi X$ events with $J/\psi < 1.0$ GeV/c.

4 b-Fraction Fitting Method

The transverse flight distance of the long lived b-hadrons in the transverse plane R_{xy} is the basic starting quantity used to separate the long lived b J/ψ events from prompts. The signed projection on the flight distance of the reconstructed J/ψ momentum, L_{xy} as illustrated in Figure 10, can also be used to separate prompt J/ψ from long-lived $b \to J/\psi X$ events:

$$L_{xy}(J/\psi) = \vec{L}.\vec{p_T}(J/\psi)/|p_T(J/\psi)| \quad (2)$$

Studies with simple MC reveal that L_{xy} and R_{xy} have similar separation power for J/ψ with momenta > 1 GeV/c but at lower momenta R_{xy} shows better separation power. Details can be found in Appendix F. The L_{xy} distribution is a signed quantity and for the prompt J/ψ signal, which dominates the inclusive J/ψ events, it is symmetrically distributed around $L_{xy} = 0$ and can be used to extract the shape of the resolution function simultaneously from the fit to the same data. Ultimately the choice of which flight distance variable to use is a question of statistical power versus systematic control. Since we extract the b-fractions from J/ψ with momenta > 1 GeV/c - which is sufficient to probe 0 momentum b-hadrons - the signed projection, L_{xy}, is used to extract the b-hadron fraction.

The J/ψ pseudo-lifetime is defined as

$$x = L_{xy}(J/\psi)/p_T(J/\psi) \cdot M(J/\psi). \quad (3)$$

Using the quantity $L_{xy}(J/\psi)/p_T(J/\psi)$ in bins of p_T versus using L_{xy} alone reduces our dependence on the J/ψ transverse momentum bin size and placement.

4.1 Extracting the b-hadron fraction in inclusive J/ψ data

At high transverse momenta, $p_T(J/\psi) > 5.0$ GeV/c, range (Figure 11) the pseudo-lifetime of J/ψ events from b decays is a pure exponential distribution with an invariant slope of 378μm. The J/ψ pseudo-lifetime is chosen as the kinematic variable used for all $p_T(J/\psi)$ ranges to minimize variations in the signal shape between the different bins and reduce the dependency on the MC simulation of the production b-hadron spectrum. A MC simulation is needed to model the distribution of $x(J/\psi)$ from b signal events and can be done in two ways:

1. The distribution of MC generated x values of accepted events as a function of J/ψ momentum, $\mathcal{X}_{mc}(x, p_T^{J/\psi})$, is shown in Figure 11. The $\mathcal{X}_{mc}(x, p_T^{J/\psi})$ MC distributions are generated for all J/ψ transverse momentum ranges and are directly convoluted with the value of the x resolution function measured in the data without allowing any of the parameters governing the shape of the MC distributions to vary. The MC shapes are used to separate the $H_b \to J/\psi X$ events from the prompt J/ψ x distributions in the signal region.

2. The Lorentz-invariant proper decay length of the b hadron parent of the J/ψ is given by

$$c\tau_b = \frac{L}{\beta\gamma} = L_{xy}(B) \cdot \frac{M(B)}{p_T(B)} = \frac{x}{F} \tag{4}$$

   The scale factor F is defined as

$$F \equiv \frac{p_T(B) \cdot M(J/\psi) \cdot cos\Theta}{p_T(J/\psi) \cdot M(B)} \tag{5}$$

   where Θ is the angle between the B and J/ψ momentum. The F distribution is calculated using the $H_b \to J/\psi X$ Monte Carlo simulation (see Appendix D for distributions). The value of the b-hadron proper decay length obtained by correcting x measured in data by the F-factors from MC is convoluted with the x resolution function measured in the data and an exponential function to extract the b-hadron inclusive lifetime (slope of the exponential) simultaneously from the same fit as the b-fraction. This method only works in J/ψ transverse momentum ranges where there are no parent b-hadrons produced at rest and where the J/ψ and H_b flight directions are strongly correlated. Below J/ψ momenta of 2 GeV/c, b-hadrons produced at rest are probed (see Table 2).

The b-fractions are extracted using method 1) for the central value for all J/ψ transverse momentum ranges.

For J/ψ momenta > 2 GeV/c where $p_T(H_b) > 500$ MeV/c, we use method 2) to extract an average b-hadron lifetime as well as a b-fraction as a cross-check. Since, *a priori*, both the mix of b-hadrons in the data and the b-hadron spectrum is not known, allowing the lifetime to vary in the fit is equivalent to a) changing the lifetime mix in the MC and/or b) changing the mean of the $p_T(b - hadron)$ distribution used in the MC model.

4.2 Unbinned Maximum Likelihood Fit

An unbinned maximum likelihood fit is used to extract the b fraction, f_B, from the data. The J/ψ pseudo-lifetime, x, its error, σ, and the invariant mass of the di-muon pair, $m_{\mu\mu}$, are the input variables. A simultaneous mass and lifetime fit is performed using a log-likelihood function:

$$\ln \mathcal{L} = \sum_{i=1}^{N} ln\mathcal{F}(x, m_{\mu\mu}) \tag{6}$$

where N is the total number of events between $m_{\mu\mu}^{min} = 2.85$ GeV/c^2 and $m_{\mu\mu}^{max} = 3.35$ GeV/c^2.

The invariant mass and pseudo-lifetime distribution is described by the following function,

$$\mathcal{F}(x, m_{\mu\mu}) = f_{Sig} \cdot \mathcal{F}_{Sig}(x) \times \mathcal{M}_{Sig}(m_{\mu\mu}) + (1 - f_{Sig}) \cdot \mathcal{F}_{Bkg}(x) \times \mathcal{M}_{Bkg}(m_{\mu\mu})$$

where the fraction of signal $J/\psi \to \mu\mu$ in the invariant mass signal region, f_{Sig}, is a fit parameter. $\mathcal{F}_{Sig,Bkg}(x)$ is the functional form describing the J/ψ pseudo-$c\tau$ distribution in the signal and background regions respectively. $\mathcal{M}_{Sig,Bkg}$ is the functional form describing the invariant mass distribution in the signal and background regions respectively.

4.2.1 Modeling the J/ψ signal pseudo-$c\tau$ distribution

The function for modeling the J/ψ pseudo-$c\tau$ signal distribution consists of two parts, the $H_b \to J/\psi X$ decay and prompt decay functions labeled $\mathcal{F}_B(x)$ and $\mathcal{F}_P(x)$ respectively:

$$\mathcal{F}_{Sig}(x) = [f_B \cdot \mathcal{F}_B(x) + (1 - f_B) \cdot \mathcal{F}_P(x)] \tag{7}$$

where f_B is the b fraction.

The shape of the $H_b \to J/\psi X$ inclusive signal is modeled using the generated x distributions of accepted events from MC, $\mathcal{X}_{mc}$, as templates for the x distribution of b-hadron events in data. The distributions used are as shown in Figure 11. The generated distributions are convoluted with a resolution function, $R(x' - x, s\sigma)$ such that the $H_b \to J/\psi X$ signal shape is given by

$$\mathcal{F}_B(x) = R(x' - x, s\sigma) \otimes \mathcal{X}_{mc}(x') \tag{8}$$

where s is an overall error scale factor which represents the possible amount we underestimate or overestimate the uncertainty on x in the data The function for prompt J/ψ, $\mathcal{F}_P = R(x, s\sigma)$, is assumed to have zero lifetime and is, therefore, the resolution function.

In order to extract the b-hadron average lifetime to use as a cross-check, the fit is also performed by modeling the shape of the the b-hadron lifetime distribution using the J/ψ pseudo-$c\tau$ measured in the data. The distribution of the F-factor in each momentum bin, $\mathcal{H}(F, p_T(J/\psi))$, shown in the histograms in Appendix D, are convoluted with the resolution function and the b-lifetime exponential such that

$$\mathcal{F}'_B(x) = R(x' - x, s\sigma) \otimes \frac{1}{F.c\tau_b} \exp(-\frac{x}{F.c\tau_b}) \otimes \mathcal{H}(F, p_T(J/\psi)) \tag{9}$$

where $c\tau_B$ is the average inclusive b hadron lifetime extracted from the fit.

The shape of the resolution function $R(x' - x, s\sigma)$ and the motivation for the choice is discussed in section 5.2. We find that $R(x' - x, s\sigma)$ is best described by a double Gaussian distribution centered at $x = 0$.

4.2.2 Modeling the J/ψ background pseudo-$c\tau$ distribution

The pseudo-lifetime background function is composed of four parts, the zero lifetime component, a positive slope exponential function, a negative slope exponential function, and a symmetric exponential function with both positive and negative slopes. The positive slope exponential function is chosen to model the background which may be from other long lived b events that produce opposite sign muons, such as $b \to c\mu^-\nu X, c \to \mu^+\nu X$. The zero lifetime component is chosen to be the same shape as the resolution function and the prompt signal component. The extra exponentials are added to parameterize the remaining components of the background pseudo-$c\tau$ distributions which are from unknown sources. The background exponential tails are also convoluted with the resolution function.

The background functional form is parameterized as follows:

$$\begin{aligned}\mathcal{F}_{Bkg}(x) = \; & (1 - f_+ - f_- - f_{sym}) R(x, s\sigma) \\ & + \frac{f_+}{\lambda_+} \exp(-\frac{x'}{\lambda_+}) \otimes R(x' - x, s\sigma) + \frac{f_-}{\lambda_-} \exp(\frac{x'}{\lambda_-}) \otimes R(x' - x, s\sigma) \\ & + \frac{f_{sym}}{2\lambda_{sym}} \exp(-\frac{x'}{\lambda_{sym}}) \otimes R(x' - x, s\sigma) + \frac{f_{sym}}{2\lambda_{sym}} \exp(\frac{x'}{\lambda_{sym}}) \otimes R(x' - x, s\sigma).\end{aligned}$$

where $f_{-,+,sym}$ is the fraction of the background distribution in the negative, positive and symmetric exponential tails respectively, and $\lambda_{-,+,sym}$ are the corresponding exponential slopes.

4.2.3 The invariant mass line shape

The dimuon invariant mass shape, $\mathcal{M}_{Sig}$ is chosen to be a double Gaussian to correctly parameterize the $m_{\mu\mu}$ distribution at low invariant mass due to radiative decays of $J/\psi \to \mu\mu\gamma$. The mean of both Gaussians are allowed to float independantly:

$$\mathcal{M}_{Sig}(m_{\mu\mu}) = G_1(m_{\mu\mu} - M, \sigma_M) + f_2 \cdot G_2(m_{\mu\mu} - (M + D), r_2\sigma_M) \qquad (10)$$

The invariant mass fit parameters are M, the mean of the mass distribution, σ_M, the width of the first Gaussian, f_2, the fraction of the second Gaussian, D, the shift in the mean of the second Gaussian, and r_2, the ratio of the widths of the two Gaussians. The invariant mass background is modeled using a 1^{st} order polynomial as such:

$$\mathcal{M}_{Bkg}(m_{\mu\mu}) = \frac{1}{m_{\mu\mu}^{max} - m_{\mu\mu}^{min}} + M_{slope}(m_{\mu\mu} - \frac{m_{\mu\mu}^{max} + m_{\mu\mu}^{min}}{2}), \qquad (11)$$

where $m_{\mu\mu}^{min}$ to $m_{\mu\mu}^{max}$ is the di-muon invariant mass range over which the fit is performed and M_{slope} is the slope of the linear mass background distribution.

The 19 fit parameters used are summarized in Table 3.

5 Modeling the resolution function shape

The most important element of extracting the b fraction from inclusive J/ψ events is understanding and modeling the resolution function shape. The measurement of the b-fraction is strongly dependent on how well we can model and constrain the shape of the prompt J/ψ distribution, which is also used to extract the resolution function from the data.

5.1 Measurement of the decay length resolutions in data

The measured L_{xy} resolution from a single Gaussian fit to the core of the inclusive J/ψ lifetime distribution, after all silicon quality cuts are applied, is shown in Figure 12 and the results are summarized in Table 4. The raw L_{xy} resolution varies from 50 to 90 μm in the range $2 - 14$ GeV/c. The pseudo-lifetime resolution used in the fit, defined as $\sigma(x, p_T(J/\psi)) = \sigma(L_{xy}, p_T(J/\psi)) * M(J/\psi)/p_T(J/\psi)$, is shown in Figure 12. The distribution fits well to a parameteric function such that

$$\sigma(x, p_T(J/\psi)) = (25 \pm 4) \times \left(1 + \exp\left[-\frac{p_T - (3.4 \pm 0.7)}{(2.1 \pm 0.7)}\right]\right). \qquad (12)$$

The L_{xy} resolution is determined both by mutliple scattering in the SVXII, which degrades the position resolution of low momentum tracks, and the opening angle between the two muons in the $r - \phi$ plane. In Figure 13 the width of the core of the L_{xy} distribution from a fit to a single Gaussian is plotted as a function of the opening angle in the $r - \phi$ plane using both a hard $p_T(\mu) > 3.0$ GeV/c cut to minimize multiple scattering and the default $p_T(\mu) > 1.5$ GeV/c requirement. We find the variation in the L_{xy} distribution as a function of the opening angle is $\sigma(L_{xy}) \sim 90\mu m$ for $\Delta\phi < 10^0$ and $\sigma(L_{xy}) \sim 50\mu m$ for $\Delta\phi \sim 130^0$.

5.2 Determining the functional form of the resolution function

The distribution of $L_{xy}/\sigma(L_{xy})$ for J/ψ data events with $L_{xy} < 150\mu$m is shown in Figure 14. Events with $L_{xy}/\sigma(L_{xy}) < 3$ are fit to both a single Gaussian and double Gaussian. The double Gaussian fit has a better $\chi^2/D.O.F$ but does not fully describe the resolution component which is a non-Gaussian tail. The amount of non-Gaussian tails is at the sub-percent level and varies with the momentum of the muon tracks.

Several exponential distributions are used to model non-Gaussian tails in the J/ψ background region. To determine whether these distributions are part of the resolution function, the distribution of J/ψ pseudo-lifetime in the mass sideband and sideband subtracted mass signal region are examined in Figure 15. The two distributions are normalized to the number of events in the 0th bin. A fit using a double Gaussian resolution function is overlaid. The non-Gaussian tails in the sideband fit in the low momentum bins is dominated by the symmetric exponential component which represents about $7-8\%$ of the total background shape. From Figure 15, it is clear that the non-Gaussian tails in the background are much larger than in the the negative tails of the sideband subtracted signal region. Therefore, the exponential tails in the J/ψ mass background are treated separately in the fit and are not included in the resolution function fit parameters.

A scale factor is used to correct for inaccuracies in the $\sigma(L_{xy})$ value returned from CTVMFT. The scale factor determines the width of the zero lifetime distributions and the resolution function used in both the background and signal regions. Preliminary fits to the x distributions using the same scale factor for signal and background shapes indicate that the zero lifetime component in the signal region is poorly described, as shown in Figure 16. A series of toy MC studies was conducted using the fit shapes extracted in the $2.0-2.25$ GeV/c bin using the same and different scale factors for signal and background. We find that there is a $+1.0\sigma$ bias in the pull of the scale factor used to describe the width of the prompt J/ψ lifetime Gaussian component when the same scale factor is used to fit the zero lifetime component in signal and background. This bias in the scale factor describing the prompt signal shape is reduced if different scale factors are used for signal and background. The effect is illustrated by the pull distribution from 100 toy MC experiments shown in Figure 17. Therefore, for the final fit model, the signal and background zero lifetime shapes are decoupled in the fit and a different scale factor is used for signal, s_{sig}, and background, s_{bkg}.

The final resolution functional shape used for the central fit result is a double Gaussian. Studies of tracking parameters and their pulls in an independent data sample [19] indicate that the the track parameter resolutions are worse for tracks passing through the hybrid/bulkhead region, and the pulls vary by up to 37% in different regions of the SVXII. The double Gaussian form is chosen as an approximate parameterization of these effects. Given the large number of bins, the statistics in each bin and the contributions/correlations from other fit parameters make it difficult to reliably determine all the double Gaussian parameters in the unbinned likelihood fit in each momentum bin. The wider Gaussian relative area, f_t, and relative width, μ, are fixed to the values obtained from the fit to the sideband subtracted binned $L_{xy}/\sigma(L_{xy})$ distribution shown in Figure 14. The fit is performed in the range (-6,3) and is the average value for all $p_T(J/\psi)$. With the means fixed at 0, we find the double Gaussian area $= 11 \pm 1\%$ of the total and the relative width $= 1.9 \pm 0.05$. The width of the narrow dominant Gaussian is allowed to float in the fit and is set by σx measured in the data multiplied by the scale factors s_{sig} and s_{bkg} for signal and background respectively. The relative width and area of the wider Gaussian is fixed to the values obtained above. From Figure 14 we can see that there are residual non-Gaussian tails in the pull distribution from unknown effects. With our choice of the double Gaussian resolution function parameters, the fraction of events in these tails are small and is of order 0.1% of the resolution function shape. The excess of events in the tails not modeled by the resolution function shape is used to assign a systematic uncertainty.

6 b-fraction Measurement

We use the simultaneous fit to the invariant mass and pseudo-lifetime with MC templates (method 1) described in Section 4.1 to extract the b-fraction in different J/ψ transverse momentum ranges. The fits in the range $1.25 - 17.0$ GeV/c converged properly and were stable with changes made to estimate systematic uncertainties. A fit using the x distributions from MC was attempted in the range $1.0 - 1.25$ GeV/c with all the resolution function parameters fixed to the values obtained from the fit in the range $1.25 - 1.5$ GeV/c. The fit failed to converge. The b-fraction results are thus quoted for all measurements above $p_T(J/\psi) > 1.25$ GeV/c.

The value of all fit parameters are listed in tables 23, 24 and 25 in Appendix A. The J/ψ pseudo-lifetime distributions in the data, with the projection of the fitted functional forms overlaid, are shown in Figures 56 to 81 in Appendix B. The distributions of the b-fractions obtained in the range 1.25-2 GeV/c with statistical errors only are shown in Figure 18. From 2.5-20 GeV/c, the b-fractions increase linearly as a function of $p_T(J/\psi)$ varying from $\sim 10\%$ to $\sim 50\%$. At low transverse momenta the fraction is constant and is $9 - 10\%$ in the range 1.25-2.5 GeV/c.

The error scale factors measured in the signal and background region extracted from the fit differ by $\sim 15\%$ up to $p_T(J/\psi) \sim 10$ GeV/c. The scale factor extracted from the background region is the larger of the two. In the four transverse momentum bins with $p_T(J/\psi) > 10$ GeV/c, both scale factors are the same within statistical uncertainties. The scale factors increase as a function of $p_T(J/\psi)$ in the lower transverse momentum bins as shown in Figure 18.

The background and mass fit results in the various p_t bins are shown in Figures 19 and 20. We find the fraction of the symmetric exponential in the background is approximately constant in all momentum bins and is $\sim 7\%$ of the background. The slope of the symmetric exponential decreases with transverse momentum; the largest slope being 800μm in the bin 1.25 -1.5 GeV/c. The fraction of background events in the positive exponential tail increases with transverse momentum, varying from 4 - 25 % in the range 4 - 20 GeV/c and is approximately constant at $2-3\%$ from 1.75 - 4 GeV/c, indicating the presence of a long lived physics signal in the background.

6.1 Correlations between fit parameters

The correlation matrix parameters of the b-fraction with the other fit parameters in the different transverse momentum bins is shown in Figures 21 and Figures 22. The largest correlation is with the average b-lifetime value, $cor(f_b, c\tau_b) = -0.18$ to -0.56 which is extracted from the F-factor fit. The correlation decreases as the transverse momenta of the J/ψ increases and the kinematic separation between prompt and non-prompt J/ψ improves. The standard method used to extract the b-fractions uses MC x templates where the lifetime is determined and fixed by the MC. The average b-hadron lifetime, measured in the CDF Run II data, is 456μm which is shorter than the average lifetime of 475μm used to generate the MC x templates. Therefore, we find that the b-fractions extracted from the F-factor method are higher than the direct fit to MC x templates and that the difference is larger in the lower momentum bins where the correlation with the lifetime is larger. A systematic uncertainty is assigned as discussed in Section 7.7.

In addition to the correlation between the average b-hadron lifetime used to model x and the value of the b-fraction extracted, there are small but significant correlations between the b-fraction and the scale factor, $cor(f_b, s_{sig}) = -0.14$ to -0.26 and the positive exponential tail in the background, $cor(f_b, f+) = -0.08$ to -0.21. The background parameters are extracted from a fit to the sideband data distributions only, where the sidebands are chosen such that no significant contribution is expected from the radiative J/ψ tail. The fit is repeated in each bin with the values of the background parameters fixed to the values obtained from the sideband fit. The difference is taken as a systematic uncertainty.

Despite the existance of long-lived symmetric background tails in the lower momentum bins, we find that the correlation between the symmetric background and the b-fraction is small, the largest being $cor(f_b, f_{sym}) = -0.129$ in the 1.25-1.5 GeV/c bin. Therefore, no systematic bias is expected. The correlation coefficients returned from MINUIT for the fit in the lowest momentum bin are show in Table 5.

7 Systematic uncertainties on the b-fraction measurement

7.1 Goodness-of-Fit

The fit shapes for signal and background are histogramed into bins and compared to the data distributions. A Kolmogorov-Smirnov test [16] is used to compare the fit and data distribtions to estimate the goodness-of-fit. The HDIFF function from the HBOOK libraries is used. The bin size chosen is 5 μm for the x distributions. Four comparisons are considered:

1. Comparison between the total pseudo-lifetime distribution and the data.
2. The pseudo-lifetime distribution from the mass sideband subtracted region is compared to the J/ψ prompt signal and $b \to J/\psi X$ fit distributions. The signal region is taken to be 3σ around the mean mass, where the mean mass and the width are the weighted averages of the 2 Gaussians used in the invariant mass fits. The sidebands are shown as shaded regions on the mass fits in Figures 58 to 81.
3. The sideband regions from 2). are compared to the background fit histogram.
4. The comparison between the invariant mass distribution for signal and background events is considered.

The distribution of K-S probability values for each distribution listed above in the different transverse momentum bins is shown in Figure 23 and listed in Table 6.

To determine how well these values represent the quality of the fits, the distribution of K-S probabilities from $\sim$ 80 statistically independent toy MC samples is shown in Figure 24 . Each MC sample was generated to match the data x, $\sigma(x)$ and $M(\mu\mu)$ distributions in the bin $2.0 - 2.25$ GeV/c and fit in the same manner as the data. Table 7 summarizes the mean of the K-S probability value in the 13 bins from 1.75 - 5.0 GeV/c and the mean value of the toy MC K-S probability distribution. The means are in reasonable agreement (difference is less than 0.1) for the sideband subtracted signal and sideband distribtion.

In addition to the K-S tests, the difference between the data and fit projections, $pull_{fit} = (Data - fit)/\sigma(stat)$, is compared in every transverse momentum bin. Firstly, the data and fit projections are histogrammed using unequal bin sizes such that the number of data events in each bin > 20 events thus ensuring Gaussian statistical errors (Figure 25). Secondly, the $pull_{fit}$ distributions are examined in each bin, as shown in 4 representative bins in Figure 26. The mean and width distributions from a single Gaussian fit to the $pull_{fit}$ distributions in all 26 transverse momentum bins is shown in Figure 27. We find no obvious discrepencies between the fit projection and data distributions. The projections of data and fit in uneven bin sizes is used to calculate the χ^2 per degree-of-freedom of the fit to the J/ψ proper decay length. The χ^2, number of degrees of freedom and the probability of χ^2 are listed in Table 8.

7.2 Toy MC Studies

In the previous section a toy MC was used to determine the quality of the fits, in addition, a toy Monte Carlo is also used to determine the reliability of the b fraction value extracted from the fit. The MC distribution, $\mathcal{X}_{mc}(x)$, in the 1.25 -1.5 GeV/c bin is used to generate 500 statistically independent MC samples with an identical distribution as data. Five different values of the b-fraction - $5\%, 7\%, 9\%, 11\%$, and 13% - are generated. The average reconstructed values of the b-fractions from each set of 100 tests are compared to the generated value in Table 9 and are found to be in good agreement. The mean of the $\frac{Value_{fit}-Value_{generated}}{\sigma_{fit}}$ from all 500 tests is found to be 0.10 ± 0.04 and the width is 0.97 ± 0.03 (Figure 30). The bias is not statistically significant and no systematic uncertainty is applied to the 3 lowest momentum bins. The distribution of the minimum likelihood values obtained from the toy MC tests is shown in Figure 31 with the value obtained from the fit to the data in the first bin overlaid. We find good agreement with the expected value of the minimum Likelihood between data and the toy MC tests.

The fit parameters in 3 other representative transverse momentum ranges of $2.0-2.25, 5-5.5, 10-12$ GeV/c are used to generate MC events with the same invariant mass and pseudo-lifetime distributions as the data. The number of events generated is chosen to match the data with the same signal fraction f_{sig}. The b lifetime generated is smeared by the F-factor distribution for each bin to simulate the pseudo-lifetime distribution in the data. The uncertainty on the x measurement in the toy MC events is taken from the data distributions of $\sigma(x)$. In each test bin, 500 statistically independent MC samples are generated. The distribution of $\frac{Value_{fit}-Value_{generated}}{\sigma_{fit}}$ for the b-lifetime and b-fraction is shown in Figure 28. A small but significant bias in the b-fractions extracted is evident at low momentum. The bias is $0.3\sigma \sim 0.3 \cdot 0.006 = 0.002$. The bias is included as a systematic uncertainty on the b-fraction measurement in these and neighbouring bins.

Using the signal and background fit shape parameters extracted from the fit to the data in the $2.0 - 2.25$ GeV/c bin, the b-fraction is varied and the fit performed. Figure 29 shows the generated versus reconstructed values of the b fractions. The reconstructed values are consistent with the generated values within statistical errors. A straight line fit to the reconstructed versus generated values is found to have a slope of 1.060 ± 0.045 and a $\chi^2/D.O.F = 0.7$.

Table 14 summarizes the value of the systematic uncertainties assigned to the b-fraction measurement in each transverse momentum bin due to the biases observed in the toy MC studies.

7.3 Fitting model

The resolution function is modeled by a double Gaussian where the dominant Gaussian width (scale factor) is allowed to float and is determined by the fit. The double Gaussian parameters are fixed using the values obtained from a binned fit to $L_{xy}/\sigma(L_{xy})$ averaged over all $p_T(J/\psi)$. The double Gaussian resolution function is not an exact description of the resolution function shape but only an approximate paramterization of many different resolution effects. Therefore, to estimate the systematic uncertainty on the shape of the double Gaussian model in each transverse momentum bin, the maximum range of values for the relative area and width supported by the data needs to be estimated. We i) redo the $L_{xy}/\sigma(L_{xy})$ fit in the range (-4,3), ii) allow the means to float and, iii) redo the fit in 4 different J/ψ momentum ranges (1-3,3-6,6-9,9-20) (Table 10). We find that the relative width in the signal region varies in the range $1.5-2.5$ and relative area varies in the range $5-15\%$ and we use that range of variations to estimate the systematic uncertainty on the resolution function model as shown in Table 11.

The systematic uncertainty is largest in the lowest momentum bin where the maximum positive variation is +8% and the largest -ve deviation is -6% and decreases with increasing $p_T(J/\psi)$.

To estimate the systematic uncertainty on the long lived tails not modeled by the prompt signal double Gaussian a box fit is added to the J/ψ x signal distribution in the range (-2500,2500) μm. The height of the box is fixed in the fit using the following method:

1. The number of events in the sideband subtracted binned distribution of the J/ψ proper decay length in the range (-2500, -150) μ m is counted.

2. The number of events in the J/ψ signal fit projection in the same range is also counted.

3. The difference between the number of events in the data and fit projection is the excess that is not modeled by the resolution function shape.

4. The size of the box is determined by the excess calculated in 3) as shown in Figure 32.

5. To reduce the statistical uncertainty on the box size from counting small number of events, the total excess in the tails in the range 1.25-4.0 GeV/c and 4.0-12GeV/c is used to set the box size in those ranges respectively. The fractional box sizes are 0.0070 ± 0.0004 and 0.0041 ± 0.0004.

The b-fraction values returned from the fit with the box function are used to estimate the systematic uncertainty from the tails that are not modeled properly. We find the b-fraction values decrease by about 5% in the lowest momentum bins when the box shape is added to the prompt J/ψ distribution. The excess modeled by the box can also be assigned to the b signal which causes a systematic increase. Figure 33 displays the projection from the box fit in the J/ψ signal region. The change in the b-fraction decreases in the higher transverse momentum bins.

Since there are correlations between the systematic uncertainties from the shape of the resolution function and the negative tails, the maximum positive and negative deviation from the central value of the b-fraction in the 4 columns in Table 11, is used the systematic uncertainty on the resolution function parameterization. This method is a conservative estimate of the uncertainty on the resolution function shape.

7.4 Modeling the background shape

The fit was repeated with the background shape changed such that only a positive and negative exponential is used with no symmetric exponential. The differences in the b-fractions observed are negligible.

The background parameters are extracted from a fit to the sideband data distributions only, where the sidebands are chosen such that no significant contribution is expected from the radiative J/ψ tail. The fit is repeated in each bin with the values of the background parameters fixed to the values obtained from the sideband fit. The background parameters extracted from the fit to the whole mass range and the fit to the sideband mass region only are overlaid in Figure 34. No significant difference between the value of the parameters extracted is observed. The difference in the b-fraction extracted using the parameters obtained from the sideband fit is taken as a systematic uncertainty. In the lowest and highest momentum bin the difference is $2-3\%$ and is less than 1% in all other bins.

These systematic uncertainties are listed in Table 12 and plotted in Figure 35.

7.5 MC modeling of b-hadron production and decay spectra

To study the dependency of the b fractions extracted on the modeling of the b-hadron spectrum used in the MC, a flat distribution in p_T and y of the b production spectrum is used to regenerate both the x and F-factor distributions and the fits repeated. The differences in the value of the b-fractions extracted from the direct fit to MC templates of x produced from a flat $p_T(b), y(b)$ input spectrum are examined. The variation in the b-fractions extracted in the range $1.25-2.0$ GeV/c are the largest, the maximum variation being an increase of 18% in the bin $1.5-1.75$ GeV/c. The study is repeated using the F-factor method with the b-lifetime parameter allowed to float, a significantly smaller dependency on the input production spectrum shape from MC is found for all bins $> 2.5 GeV/c$. The results are summarized in Table 13. The flat $p_T(b), y(b)$ input spectrum is unrealistic, therefore the systematic uncertainty is taken as 1/2 of the size of the variation observed in the b-fraction when the flat model is used. Using 1/2 of the values in column 1 of Table 13 as a guideline, we assign systematic uncertainties of $\pm 7\%, 3\%$, and 2% for measurements in the transverse momentum ranges of $1-3$, $3-8$ and $8-20$ GeV/c respectively. To check that the systematic uncertainty due to the MC production spectrum modeling assigned using the flat spectrum is sufficient, the shape of the b-hadron production spectrum is extracted from the initial measurement of the cross-section as a function of $p_T(J/\psi)$, as detailed in section 8.3. We find that the default MC spectrum is still consistent with the data but is harder than the measured b-hadron spectrum (see Figure 52). The spectrum measured in the data is used to reweight the generated $H_b \to J/\psi$ MC events. The analysis is repeated using the new b-hadron spectrum and the difference between the b-fractions extracted is listed in Table 13 under the column headed b spectrum 3. We find that the b-fraction extracted in the lower momentum bins decreases when the spectrum used is harder and the decrease is between 1-3% in the range $1.25 < p_T(J/\psi) < 2.0$ GeV/c and is less than 1% for all momenta > 2.0 GeV/c. These variations are smaller than the systematic uncertainty assigned using the flat spectrum. There are many variations of the production spectrum that are possible that would be consistent with the measurement of the b-hadron spectrum in the data: softer spectra, harder, narrower, wider ...etc. Not all possible variations on the measured spectra have been studied at this time that can be used to extract a more accurate systematic uncertainty.

In addition, we examine the change in the b-fraction extracted when varying the $H_b \to J/\psi X$ decay spectrum while keeping the H_b production spectrum fixed as listed in the last column of Table 13. The decay spectra of $H_b \to J/\psi(direct)X$ and $H_b \to J/\psi(inclusive)X$ are used. The difference is found to be 2-4% in the lowest momentum bins and $< 1\%$ for $p_T(J/\psi) > 2.5$ GeV/c

The variations in the b-fraction observed for the systematic studies discussed in this section are plotted in Figure 36.

7.6 MC modeling of the b-hadron average lifetime

The mix of hadrons and their respective lifetimes is a contributing factor to the shape of the J/ψ pseudo-$c\tau$ distributions. To assess the systematic uncertainty due to the uncertainty on the b-hadron average lifetime we vary the average lifetime in the MC by 11μm, which is the size of the systematic uncertainty on the average b-hadron lifetime measured at CDF run II [20]. Figure 36 shows the fractional difference in the b-fractions extracted when the average b-hadron lifetime is changed. We find that the measured b-fraction decreases in all transverse momentum bins when the lifetime is increased. The fractional decrease is -4% in the lowest momentum bin and less than 1% for bins with $p_T(J/\psi) > 12$ GeV/c (Table 15. The variation in the b-fraction observed when the average b-hadron lifetime is varied by $\pm 11\mu$m is taken as a systematic uncertainty on the b-fraction measurement.

7.7 Cross-check with F-factor method

In the transverse momentum range of $p_T > 2.0$ GeV/c, where both the F-factor method with the lifetime allowed to float and the direct fit to $\mathcal{X}_{mc}$ templates can be used, the difference in the extracted b-fractions is taken as a systematic uncertainty on the fitting technique. The values of the parameters from the fits in different J/ψ p_T bins, obtained using F-factors to extract the b-lifetime and fraction simultaneosly, are shown in Tables 26, 27 and 28 of Appendix A. The value of the b-lifetime extracted from the F-factor fit used as a cross-check is shown in Figure 37. From a fit to a straight line in the transverse momentum range $>$ 2 GeV/c, we find $< c\tau_b >= 455 \pm 5(stat)\mu$m. If we exclude the lower momentum bins and fit only the range $p_T(J/\psi) > 5$ GeV/c, we find $< c\tau_b >= 456 \pm 6(stat)\mu$m. This value is in good agreement with previous measurements of $< c\tau_b >$ in the same data sample. The average b-lifetime is fixed to $< c\tau_b >= 456\mu$ m and the F-factor fits redone. The difference in the b-fractions extracted with the F-factor method from our standard method is shown in the first column of Table 12 and plotted in Figure 38. We find that the b-fraction extracted using the F-factor method with the lifetime fixed to 456 μ m is larger than that extracted using our standard method and the largest difference is +3%. The difference between the b-fraction extracted using both methods is much smaller when the average b-hadron lifetime value is fixed to the nominal value in the MC of 475μm as shown in Figure 38. No significant variation is therefore observed when the two different fit methods are used to extract the b-fraction, provided the same value of the average b-hadron lifetime is used.

7.8 Using 3-D versus 2-D SVXII hit information

To crosscheck if there is any bias introduced by using the 3-D silicon hits, the mean and RMS of the difference in the L_{xy} measured using 3-D and 2-D hits is shown in Figure 39. No significant deviation in the mean of the distribution away from zero is observed. The value of the b-hadron lifetime is expected to be sensitive to biases in SVXII, therefore, the b-lifetime extracted using 3-D and 2-D hit information (more data events are accepted when 2-D hit information only is used with worse S:B) as a function of $p_T(J/\psi)$ is also shown in Figure 39. The variation in the b-fraction when 3-D hit and 3-D vertex quality cuts versus 2-D hit and vertex quality cuts are used is listed in Table 12. No significant bias in the lifetime or b-fraction is observed and the changes are consistent within statistical uncertainties.

7.9 Invariant mass line shapes

MC mass line shapes from a realistic SVXII MC simulation of J/ψ events are generated and used to fit the invariant mass distribution in the simultaneous mass and lifetime fit instead of a double Gaussian parameterization. The data and MC mass templates are shown in Figure 40. The realistic MC reproduces the data invariant mass distributions well in the lower momentum bins, but underestimates the resolution in the higher momentum bins. Therefore, an extra Gaussian smearing parameter is added to the realistic MC mass templates used in the fit. The value of the width is allowed to float and is determined by data. A smearing of 3 MeV/c^2 in the lowest momentum bin and 13 MeV/c^2 in the highest momentum bin is sufficient to improve the agreement between the realistic MC simulation and data as shown in Figure 41. Since the MC models the contribution of the long J/ψ radiative tail at small invariant masses based on a physics calculation, this comparison is used as a cross-check that no significant bias in the signal fraction has been introduced due to the double Gaussian parameterization. The difference in the b-fraction extracted using the double Gaussian line shape and the smeared SVXII MC line shape is listed in Table 12. We find no discrepancies larger than 1.7% which is much smaller than the statistical uncertainties on the b-fraction, therefore no systematic uncertainties are assigned to the modeling of the mass shape.

7.10 Detector and selection criteria bias

Since the momentum spectrum of prompt J/ψ is softer than $H_b \rightarrow J/\psi X$, a bias in acceptance as a function of opening angle and/or momentum could introduce a systematic bias in the fraction of H_bs counted in that bin. The relative SVXII/COT acceptance in each transverse momentum bin is listed in Table 17. We find a $\pm 4-5\%$ variation in the SVXII acceptance compared to COT over the entire J/ψ transverse momentum range of 19 GeV/c. At higher momentum the SVXII acceptance is expected to increase due to the smaller opening angle between the two muons. When the angle between the two muons is smaller than the 30^0 angular acceptance of a single SVXII wedge, the SVXII track reconstruction efficiency for both tracks is the same as for a single track. The analysis is performed in bins of $\Delta(p_T(J/\psi)) << 19 GeV/c$ where the largest bin size is 3.0 GeV/c. We therefore conclude that since the systematic bias on the momentum spectrum within a bin is $< 1\%$ and has a negligible effect on the b-fraction.

8 Measurement of the Inclusive $H_b \rightarrow J/\psi X$ cross-section

The value of the b-fraction from the final fit models with statistical and systematic uncertainties is listed in Table 16 and the distribution is shown in Figure 42. The Run I results are also listed. Both Run II and Run I measurements of the b-fractions are in good agreement for $p_T > 5$ GeV/c. The statistical accuracy of the Run II measurements in the high transverse momentum bins is similar to Run I. The Run II measurement has been extended down to J/ψ transverse momenta of 1.25 GeV/c. This measurement of the b-fraction is in conjunction with the measurement of the absolute inclusive J/ψ cross-section to calculate the inclusive b-hadron cross-section.

8.1 Polarization of J/ψ from b-hadron decays

The CDF detector kinematic acceptance of $J/\psi \rightarrow \mu\mu$ events depends on the J/ψ polarization. The polarization for prompt J/ψ compared to J/ψ from b-hadrons could be different and therefore the acceptance values have to be correctly treated for the different J/ψ sources. We use the same J/ψ polarization parameter for prompt and b J/ψ in the measurement of the inclusive cross-section. The value used is an average of the CDF Run I measurement for both prompt J/ψ and J/ψ from H_b with $p_T > 4.0$ GeV/c: $\alpha = 0.15 \pm 0.3$. A larger uncertainty is used to account for the extrapolation to $p_T = 0.0$ [7] [21]. The CDF run I measurement of the polarization of J/ψ from b-hadrons as a function of $p_T(J/\psi)$ for $p_T > 4.0$ GeV/c is consistent with zero where $< \alpha(B) > (p_T(J/\psi) > 4.0GeV/c) = -0.090 \pm 0.095$ (Run I). BaBar (and CLEO) measure $\alpha(B) = -0.46 \pm 0.06$ where the helicity angle of the J/ψ is measured in the $\Upsilon(4S)$ rest frame [13]. Since both the Babar and CDF data are measured in very different rest frames it is not obvious whether the results are consistent or not. Earlier studies indicate that the boost of H_b in the CDF lab frame smears out the helicity distribution and could possibly reduce the observed decay asymmetry [22]. In addition, different J/ψ momentum ranges probe different portions of 2-body (maximum polarization) and multibody $H_b \to J/\psi X$ decays (smaller polarization). It is difficult to use the Babar number to predict what the observed polarization is for $1.0 < p_T(J/\psi) < 4.0$ GeV/c as measured in the CDF lab frame, therefore for $H_b \to J/\psi X$ acceptance we use $\alpha(B) = 0.0 \pm 0.5$ instead of $\alpha = 0.15 \pm 0.3$ used previously for the inclusive cross-section measurement. This combines the central value measured in CDF with the largest possible deviation from zero based on the Babar measurement. The acceptance increases by $3-6\%$ compared to the acceptance reported for $\alpha = 0.15$ in [7]. The acceptance values for $\alpha = 0.15$ and $\alpha = 0.0$ are listed in Table 18. The systematic uncertainty on the acceptance due to the polarization of the J/ψ is listed in Table 19. The uncertainty varies from $8 - 19\%$ and is smallest in the high momentum range.

8.2 Measurement of $d\sigma/dp_T(J/\psi).Br(H_b \to J/\psi X).Br(J/\psi \to \mu\mu)$

The b fractions thus obtained are multiplied with the measurements of the inclusive J/ψ cross-section listed in Table 21 [7]. The central value is corrected for the different J/ψ acceptance due to polarization (Table 18) to obtain the differential b hadron inclusive cross-section: $\sigma(p\bar{p} \to bX) \cdot Br(H_b \to J/\psi X)$ such that:

$$\frac{d\sigma(H_b \to J/\psi)}{dp_T(J/\psi)} = f_B \times \frac{d\sigma(J/\psi^{inclusive})}{dp_T(J/\psi)} \times \frac{\mathcal{A}(\alpha = 0.15)}{\mathcal{A}(\alpha = 0.0)} \tag{13}$$

Table 20 summarizes the systematic uncertainties on the b-hadron inclusive cross-section considered so far. The p_T dependent systematic uncertainties on $\frac{d\sigma(H_b \to J/\psi)}{dp_T(J/\psi)}$ are obtained by adding in quadrature the non-polarization systematic uncertainties on the inclusive measurement, the polarization systematic uncertainties in Table 19, and the b-fraction systematic uncertainties summarized in the first section of Table 20.

The J/ψ and b-hadron inclusive cross-section results with statistical and p_T dependent systematic uncertainties are shown in Table 21. The differential cross-section with all statistical and systematic errors added is plotted in Figure 43. A comparison with theory [4] and the Run I results are shown in Figure 44.

The integrated b-hadron cross-section is the integral of the differential cross-section results in Table 21 and is measured to be $\sigma(p\bar{p} \to bX, p_T(J/\psi) > 1.25$ GeV/c, $|y(J/\psi)| < 0.6|) \cdot Br(H_b \to J/\psi X) \cdot Br(J/\psi \to \mu\mu) = 19.9 \pm 0.3(stat)^{+3.8}_{-3.2}(syst)$ nb. The systematic uncertainty quoted includes the fully correlated uncertainty of 6.7% obtained from the inclusive J/ψ cross-section measurement. For comparison with Run I we find:

$$\sigma(H_b \to J/\psi, p_T(J/\psi) > 5.0\ GeV/c, |y| < 0.6)^{RunII} = 3.30 \pm 0.05(stat)^{+0.47}_{-0.41} \text{ nb}$$
$$\sigma(H_b \to J/\psi, p_T(J/\psi) > 5.0\ GeV/c, |\eta| < 0.6)^{RunI} = 3.23 \pm 0.05(stat)^{+0.28}_{-0.30} \text{ nb}$$

8.3 Measurement of the total b-hadron cross-section

Since J/ψ with transverse momenta < 2.0 GeV/c probe b-hadrons with transverse momenta down to 0 GeV/c and J/ψ with transverse momenta ≈ 17 GeV/c probe b-hadrons up to 40 GeV/c, the measurement of the differential cross-section using $1.25 < p_T(J/[y]) < 17.0$ GeV/c can be used to extract the total b-hadron cross-section as well as measure the shape of the differential cross-section as a function of $p_T(b - hadron)$. The fraction of the total b-hadron cross-section probed by a given range of J/ψ momenta is largely dependent on the decay kinematics of b-hadrons to charmonium and not the production mechanisms. In Figure 45, the fraction of the b-hadron cross-section, f_σ, probed by J/ψ with $1.25 < p_T(J/\psi) < 17.0$ GeV/c from generator level MC studies is shown using a realistic and flat input spectrum. We find that before acceptance is taken into account, we probe $> 25\%$ of the b-hadron spectrum from $0 - 2.0$ GeV/c and 10% at 40 GeV/c with no dependence on the input spectrum. The acceptance extracted from the MC can be used to correct the cross-section measured using a limited J/ψ transverse momentum range and extract the total cross-section. The uncertainty on the total cross-section thus extracted will depend on the measured uncertainties in $d\sigma/dp_T(J/\psi)$ and the uncertainty from the MC modeling of the $H_b \to J/\psi X$ decay dynamics.

To extract the differential b-hadron spectrum from $d\sigma/dp_T(J/\psi)$, a convolution is performed with the transverse momentum distribution of b-hadrons as a function of $p_T(J/\psi)$ obtained from MC:

$$\frac{d\sigma}{dp_T(H_b)} = \frac{1}{f_\sigma(p_T(H_b))}\frac{d\sigma}{dp_T(J/\psi)} \otimes H(p_T(J/\psi), p_T(H_b)) \tag{14}$$

where $H(p_T(J/\psi), p_T(H_b))$ is the MC distribution of b-hadron transverse momenta in each J/ψ transverse momentum bin as shown in Figure 46 and $f_\sigma(p_T(H_b))$ is the efficiency with which the cross-section measured with $1.25 < p_T(J/\psi) < 17.0$ GeV/c and $|y|(J/\psi) < 0.6$ probes the total cross-section (Figure 45). From MC, we find that

$$N^{H_b}_{generated}(|y(J/\psi)| < 0.6) = 0.999 N^{H_b}_{generated}(|y(H_b)| < 0.6). \quad (15)$$

The MC distribution of $y(b - quark) = y(H_b)$ is shown in Figure 54. A numerical convolution is performed as follows:

$$N^b_i = \sum_{j=1}^{N} w_{ij} N^{J/\psi}_j, \quad (16)$$

where N^b_i is the number of b-hadrons in the i^{th} $p_T(H_b)$ bin, $N^{J/\psi}_j$ is the number of J/ψs from H_b in the j^{th} $p_T(J/\psi)$ bin and w_{ij} is the fraction of H_b events in the i^{th} $p_T(H_b)$ bin relative to the total in the j^{th} $p_T(J/\psi)$ bin obtained from MC. The sum of the weights w_{ij} in each $p_T(J/\psi)$ bin is normalized to 1.0. The statistical error in each $p_T(H_b)$ bin is given by:

$$\delta_{stat}(N^b_i) = \sqrt{\sum_{j=1}^{N} w_{ij} \delta^2_{stat}(N^{J/\psi}_j)} \quad (17)$$

The systematic uncertainties on $N^{J/\psi}$ as a function of $p_T(J/\psi)$ are correlated, therefore, we add the uncertainties to obtain the total systematic uncertainty on the b-hadron cross-section:

$$\delta_{syst}(N^b_i) = \sum_{j=1}^{N} w_{ij} \delta_{syst}(N^{J/\psi}_j) \quad (18)$$

We use 200 MeV/c momentum bins $p_T(H_b)$ bins.

Several iterations of the procedure are repeated where each time the input production spectrum used in the MC is the spectrum measured in the previous iteration. A χ^2 comparison between the input and output spectra is performed after each iteration until the value is stable as shown in Figure 47. The procedure is also applied to the J/ψ spectrum obtained from the same MC sample used in the fit and the results shown in Figure 47. We find the MC converges after a single iteration as expected and the data after 8-9 iterations. The resulting data distribution is shown in Figure 49. We repeated the analysis using 1 GeV/c $p_T(H_b)$ bins for the unfolding and found no difference in the integrated or differential cross-section shape as shown in Figure 50.

The differential cross-section as a function of $p^2_T(H_b)$ is also extracted and plotted in Figure 51. The ratio of the measured cross-section and the generated cross-section used in this analysis is shown in Figure 48. The measured cross-section is softer than the generated spectrum in the mid momentum range.

The generated b-hadron spectrum is reweighted to match the data measurement and the resultant MC J/ψ spectrum is compared to the J/ψ spectrum in data. We find that the agreement between the MC J/ψ spectrum produced using the above procedure and the data is good as shown in Figure 52. The b-fractions are remeasured using MC distributions generated from the reweighted b-hadron spectrum. The change in the b fraction is taken as the systematic uncertainty from the MC modeling of the shape of the b-hadron momentum spectrum and is included in the uncertainty on the b-fraction measurement.

The total value of the Run II inclusive b-hadron cross-section is the integral of the differential cross-section extracted above and is found to be:

$$\sigma(p\bar{p} \to bX, |y| < 0.6).Br(H_b \to J/\psi X).Br(J/\psi \to \mu\mu) = 24.5 \pm 0.5(stat)^{+4.7}_{-3.9}(syst) \text{ nb}, \tag{19}$$

were H_b denotes both hadron and anti-hadron states.

8.4 Measuring the B^+ cross-section

As a cross-check we extract the B^+ cross-section from the inclusive b-hadron cross-section:

$$\sigma(p\bar{p} \to B^+X, |y| < 1.0)^{Run\ II} = \frac{This\ measurement/2.f_u}{Br(b \to J/\psi X).Br(J/\psi \to \mu\mu).(|y| < 0.6)/(|y| < 1.0)} \tag{20}$$

where the values of the branching fractions and the fragmentation fraction f_u are given as follows:

$$Br(H_b \to J/\psi(anything)X) = 1.16 \pm 0.10\% \text{ (PDG 2003)} \tag{21}$$

$$Br(J/\psi \to \mu\mu) = 5.88 \pm 0.10\% \text{ (PDG 2003)} \tag{22}$$

$$f_{u,d} = 0.401 \pm 0.010 \text{ (LEP 2003)} \tag{23}$$

$$(|y| < 0.6)/(|y| < 1.0) = 0.61\ (MC) \tag{24}$$

The Run II results compared to the Run I cross-sections are listed in Table 22 and plotted in Figure 53. To the fully correlated uncertainty on the b-hadron inclusive cross-section of $\pm 6.7\%$, we add the uncertainties on the correction factors used to estimate the B^+ cross-section ($\pm 6\%$). The Run II cross-sections are expected to be $\sim 10\%$ higher than the Run I measurements due to higher center-of-mass energy. We find the measurements are consistent within fully correlated errors. The integrated cross-section for B^+ above 6 GeV/c from Run I and II are :

$$\sigma(p\bar{p} \to B^+X, p_T > 6.0\ GeV/c, |y| < 1.0)^{RunII} = 2.8 \pm 0.4(stat \oplus syst)\mu b$$
$$\sigma(p\bar{p} \to B^+X, p_T > 6.0\ GeV/c, |y| < 1.0)^{RunIb} = 3.6 \pm 0.6(stat \oplus syst)\mu b$$
$$\sigma(p\bar{p} \to B^+X, p_T > 6.0\ GeV/c, |y| < 1.0)^{RunIa} = 2.7 \pm 0.6(stat \oplus syst)\mu b$$

8.5 Checking for model dependence

To check for model dependence of the measured $p_T(H_b)$ spectrum on the input MC production spectrum, we generated 2 independent MC samples: sample A with a realistic $p_T(H_b), y(H_b)$ spectrum and sample B with a flat $p_T(H_b), y(H_b)$ spectrum. The b-hadrons in both samples were decayed using the same QQ decay tables. Starting from the J/ψ transverse momentum of sample A in the range 1.25 - 17 GeV/c divided into the same $p_T(J/\psi)$ bin sizes as our data, we repeat the procedure to extract $d\sigma/p_T(H_b)$ from $d\sigma/p_T(J/\psi)$ using sample B as the initial start point. We find that it requires at least 20 iterations for the spectrum to converge. The measured and expected $d\sigma/p_T(H_b)$ distributions are compared in Figure 55. We find a small dependence on the input spectrum below 2 GeV/c where the input flat spectrum used for the unfolding is unphysical and does not decrease with decreasing momentum.

9 Conclusion

A preliminary measurement of the b-hadron inclusive cross-section in CDF Run II has been conducted using inclusive J/ψ decays. The differential cross-section is measured for J/ψ transverse momenta > 1.25 GeV/c which probes b-hadron transverse momenta down to zero. The integrated cross-section measured is $\sigma(p\bar{p} \to bX, p_T(J/\psi) > 1.25 \text{ GeV/c}, |y(J/\psi)| < 0.6|) \cdot Br(H_b \to J/\psi X) \cdot Br(J/\psi \to \mu\mu) = 19.9 \pm 0.3(stat)^{+3.8}_{-3.2}(syst)$ nb. The first measurement of the total b-hadron cross-section at a hadronic machine has been extracted from the measurement of the cross-section with J/ψ transverse momenta > 1.25 GeV/c and < 17.0 GeV/c using a MC modeling of the decay kinematics of b hadrons to charmonium. We find

$$\begin{aligned}\sigma(p\bar{p} \to H_b X, |y| < 0.6).Br(H_b \to J/\psi X).Br(J/\psi \to \mu\mu) &= \\ 24.5 \pm 0.5(stat)^{+4.7}_{-3.9}(syst) \text{ nb} &,\end{aligned}$$

were H_b denotes both hadron and anti-hadron states. This measurement divided by two, the branching fractions, and rapidity correction factors in Equations 21, 22 and 24 is the total single b-quark cross-section in one unit of rapidity. We find:

$\sigma(p\bar{p} \to bX, |y| < 1.0) = 29.4 \pm 0.6(stat)^{+6.2}_{-5.4}(syst)\mu$b

where a 9% systematic uncertainty from the branching fraction measurements has been added.

10 Acknowledgements

We would like to thank the proponents of the Run I measurement for developing many of the methods used in this analysis. Thanks to Stan Thompson from Glasgow for running many of the toy MC studies. Special mention for Saverio D'Auria and the SVXII MC developers who were instrumental in producing the realistic SVXII MC used in some of our studies.

b-hadron	QQ mass (GeV/c^2)	QQ lifetime (μm)	Fragmentation Fraction
$B^{\pm}$	5.28	493	0.389
B^0	5.28	486	0.389
B_s	5.38	465	0.106
Λ_b	5.641	387	0.116

Table 1: b-hadron properties used in the MC simulation.

$p_T(J/\psi)$ GeV/c	Fraction of b events with $p_T(b - hadron) < 500 MeV/c$
$0.00 - 0.25$	0.06
$0.25 - 0.5$	0.06
$0.5 - 0.75$	0.06
$0.75 - 1.0$	0.06
$1.0 - 1.25$	0.04
$1.25 - 1.5$	0.04
$1.5 - 1.75$	0.03
$1.75 - 2.0$	0.01
$2.0 - 2.25$	0.002

Table 2: Fraction of $b \to J/\psi X$ decays with $p_T(b - hadron) < 500 MeV/c$ as a function of J/ψ transverse momenta.

Parameter	Description
	b signal lifetime fit parameters
$c\tau_b$	inclusive b hadron lifetime
f_B	$b \to J/\psi X$ fraction
s_{sig}	Scale factor on X measurement uncertainty for signal events
f_{sig}	fraction of J/ψ signal events in $\mu^+\mu^-$ combinations
f_t	fraction of the resolution function in the wider Gaussian
μ	Relative width of the 2^{nd} Gaussian in the resolution function
	$M(\mu\mu)$ invariant mass fit paramaters
M	mean of the J/ψ signal mass distribution
σ_M	the width of the first Gaussian
f_2	the fraction of the second Gaussian
D	the shift in the mean of the second Gaussian
r_2	the ratio of the widths of the two Gaussians
M_{slope}	slope of the linear mass background
	J/ψ pseudo-lifetime background fit parameters
f_-	fraction of the background distribution in the negative exponential tails
λ_-	the slope of the negative exponential background
f_+	fraction of the background distribution in the positive exponential tails
λ_+	the slope of the positive exponential background
f_{sym}	fraction of the background distribution in the symmetric exponential tails
λ_{sym}	the slope of the symmetric exponential background
s_{bg}	Scale factor on X measurement uncertainty for background events

Table 3: Fit parameters used in the simulateneous mass and pseudo-lifetime fit used to extract the fraction of $b \to J/\psi X$ events from the inclusive J/ψ data.

$p_T(J/\psi)$ GeV/c	L_{xy} resolution (μm)
$1.75 - 2.0$	48.90 ± 0.66
$2.0 - 2.25$	50.14 ± 0.67
$2.25 - 2.5$	50.70 ± 0.62
$2.5 - 2.75$	49.61 ± 0.65
$2.75 - 3.0$	50.54 ± 0.65
$3.0 - 3.25$	52.13 ± 0.68
$3.25 - 3.5$	51.17 ± 0.67
$3.5 - 3.75$	52.40 ± 0.68
$3.75 - 4.0$	53.05 ± 0.82
$4.0 - 4.25$	56.48 ± 0.87
$4.25 - 4.5$	55.71 ± 0.91
$4.5 - 4.75$	57.56 ± 0.97
$4.75 - 5.0$	57.88 ± 1.1
$5.0 - 5.5$	60.41 ± 0.85
$5.5 - 6.0$	60.15 ± 0.96
$6.0 - 6.5$	63.1 ± 1.1
$6.5 - 7.0$	67.8 ± 1.4
$7.0 - 8.0$	67.7 ± 1.2
$8.0 - 9.0$	74.4 ± 1.9
$9.0 - 10.0$	75.9 ± 2.5
$10.0 - 12.0$	78.5 ± 2.6
$12.0 - 14.0$	91.0 ± 6.9

Table 4: Width of the prompt core of the J/ψ L_{xy} distributions from a fit to a single Gaussian.

PARAMETER CORRELATION COEFFICIENTS

NO.	GLOBAL	2	3	10	11	12	13	14	15	16	17	18	19
2	0.28872	1.000	-0.246	-0.129	0.029	0.016	0.004	0.000	-0.002	0.018	-0.007	-0.014	0.011
3	0.34771	-0.246	1.000	0.066	-0.025	-0.061	-0.003	0.035	0.012	-0.032	0.018	0.033	-0.222
10	0.55776	-0.129	0.066	1.000	-0.467	-0.036	-0.006	0.006	0.019	-0.014	0.023	0.022	-0.387
11	0.48524	0.029	-0.025	-0.467	1.000	-0.045	-0.003	-0.009	0.046	0.015	0.046	0.018	0.288
12	0.76390	0.016	-0.061	-0.036	-0.045	1.000	0.068	-0.011	-0.609	-0.040	-0.601	-0.347	-0.115
13	0.26543	0.004	-0.003	-0.006	-0.003	0.068	1.000	-0.051	-0.024	-0.114	-0.183	-0.028	-0.012
14	0.55945	0.000	0.035	0.006	-0.009	-0.011	-0.051	1.000	-0.418	-0.397	-0.074	0.114	-0.030
15	0.80489	-0.002	0.012	0.019	0.046	-0.609	-0.024	-0.418	1.000	0.442	0.459	0.170	0.127
16	0.66844	0.018	-0.032	-0.014	0.015	-0.040	-0.114	-0.397	0.442	1.000	0.046	-0.365	0.032
17	0.64762	-0.007	0.018	0.023	0.046	-0.601	-0.183	-0.074	0.459	0.046	1.000	0.333	0.120
18	0.56275	-0.014	0.033	0.022	0.018	-0.347	-0.028	0.114	0.170	-0.365	0.333	1.000	0.052
19	0.48465	0.011	-0.222	-0.387	0.288	-0.115	-0.012	-0.030	0.127	0.032	0.120	0.052	1.000

Table 5: Table of the correlation co-efficients returned from MINUIT for the fit in the lowest momentum bin. The parameter definitions are as follows: 2=b-fraction, 3=signal scale factor, 10=fraction of background in symmetric exponential, 11=slope of symmetric exponential,12=Background fraction, 13=Mass mean, 14=Mass width (narrow), 15=Relative area of second Gaussian, 16=Mass shift of 2nd Gaussian, 17=Relative width of second Gaussian, 18=Slope of mass background, 19=background scale factor.

$p_T(J/\psi)$ GeV/c GeV/c	K-S probability (all x)	K-S Prob (signal x)	K-S prob. (bkgd x)	K-S prob. (mass)
$1.25 - 1.5$	0.76	0.94	0.93	0.95
$1.5 - 1.75$	0.48	0.93	0.11	0.000169
$1.75 - 2.0$	0.66	0.99	0.58	0.81
$2.0 - 2.25$	0.84	0.81	0.57	0.00
$2.25 - 2.5$	0.66	0.71	0.36	0.24
$2.5 - 2.75$	0.77	0.47	0.60	0.22
$2.75 - 3.0$	0.46	0.99	0.07	0.45
$3.0 - 3.25$	0.18	0.98	0.11	0.76
$3.25 - 3.5$	0.87	0.99	0.70	0.05
$3.5 - 3.75$	0.88	0.46	0.04	0.07
$3.75 - 4.0$	0.94	0.77	0.52	0.41
$4.0 - 4.25$	0.29	0.82	0.50	0.21
$4.25 - 4.5$	0.67	0.93	0.88	0.48
$4.5 - 4.75$	0.68	0.69	0.91	0.69
$4.75 - 5.0$	0.60	0.95	0.35	0.27
$5.0 - 5.5$	0.76	0.55	0.53	0.34
$5.5 - 6.0$	0.95	0.94	0.39	0.43
$6.0 - 6.5$	0.94	0.99	0.31	0.59
$6.5 - 7.0$	0.46	0.99	0.37	0.86
$7.0 - 8.0$	0.68	0.77	0.34	0.15
$8.0 - 9.0$	0.98	0.99	0.88	0.65
$9.0 - 10.0$	0.49	0.52	0.81	0.89
$10.0 - 12.0$	0.98	0.99	0.71	0.71
$12.0 - 14.0$	0.97	0.99	0.82	0.70
$14.0 - 17.0$	0.99	0.85	0.29	0.23
$17.0 - 20.0$	0.94	0.81	0.70	0.71

Table 6: K-S probability values of the data distributions compared to the fit distributions returned by HDIFF.

Distributions compared	K-S probability mean Lowest 13 bins in data	K-S probability mean Toy MC
x distribution of all events in fit	0.59	0.71
x distribution in signal region	0.69	0.74
x distribution in sideband region	0.49	0.42
Invariant mass distribution	0.36	0.49

Table 7: Average K-S probability values returned from the comparison between data and fit in the bins from 1.75 - 5.0 GeV/c compared to the expected mean obtained from toy MC studies.

$p_T(J/\psi)$ GeV/c	χ^2/D.O.F	Prob(χ^2)
$1.25 - 1.5$	115/106	0.25
$1.5 - 1.75$	168/129	0.01
$1.75 - 2.0$	131/126	0.36
$2.0 - 2.25$	133/130	0.40
$2.25 - 2.5$	171/128	0.006
$2.5 - 2.75$	174/119	0.0007
$2.75 - 3.0$	149/114	0.01
$3.0 - 3.25$	129/111	0.11
$3.25 - 3.5$	125/106	0.10
$3.5 - 3.75$	129/97	0.01
$3.75 - 4.0$	82/91	0.72
$4.0 - 4.25$	95/86	0.22
$4.25 - 4.5$	92/80	0.17
$4.5 - 4.75$	76/77	0.48
$4.75 - 5.0$	99/74	0.03
$5.0 - 5.5$	137/101	0.009
$5.5 - 6.0$	129/91	0.006
$6.0 - 6.5$	106/79	0.02
$6.5 - 7.0$	68/70	0.52
$7.0 - 8.0$	120/93	0.03
$8.0 - 9.0$	72/69	0.37
$9.0 - 10.0$	72/52	0.03
$10.0 - 12.0$	62/55	0.22
$12.0 - 14.0$	30/30	0.44
$14.0 - 17.0$	24/24	0.44
$17.0 - 20.0$	12/8	0.13

Table 8: χ^2 goodness-of-fit comparison using the data and fit projections in different width bins.

b-fraction generated	b-fraction reconstructed	width of the pull
0.05	0.051 ± 0.0008	0.93 ± 0.08
0.07	0.072 ± 0.001	1.08 ± 0.12
0.09*(data value)	0.091 ± 0.001	1.00 ± 0.10
0.11	0.111 ± 0.001	0.88 ± 0.08
0.13	0.129 ± 0.001	0.99 ± 0.10

Table 9: Results from Toy MC studies with generated distributions chosen to match the data distributions in bin $1.25 - 1.5$ GeV/c. The reconstructed values are the mean of the Gaussian distribution of the results from a 100 trials. The average pull, $(generated - reco)/error$, of all 500 trials combined was 0.10 ± 0.04 and the width of the pull distribution was 0.97 ± 0.03

p_T bin	Mean Gaussian 2	Relative width (W2/W1)	Fractional area (A2/Total)
$1- > 3$	0.8 ± 0.4 (fixed to 0)	$2.3 \pm 0.3(1.8 \pm 0.1)$	$7 \pm 2(12 \pm 4)\%$
$3- > 6$	0.5 ± 0.2 (fixed to 0)	$2.0 \pm 0.2(1.8 \pm 0.1)$	$10 \pm 3(14 \pm 3)\%$
$6- > 9$	0.3 ± 0.2 (fixed to 0)	$2.5 \pm 0.3(2.2 \pm 0.2)$	$5 \pm 2(5 \pm 1)\%$
$9- > 20$	-3.7 ± 1.4 (fixed to 0)	$1.1 \pm 0.6(2.9 \pm 0.9)$	$1.0 \pm 0.4(2 \pm 1)\%$

Table 10: Fit parameters of the second broader Gaussian in a binned double Gaussian fit to the sideband subtracted $L_{xy}/\sigma(L_{xy})$. The fit is performed in the region (-6,3). The fit results with the means allowed to float is shown. The fit result with the means are fixed to 0.0 are shown in between brackets. Weighted average for the first three bins: $W2/W1 = 2.2 \pm 0.2$, $A2/Total = 10.0 \pm 2\%$

$p_T(J/\psi)$ GeV/c	Double Gauss $\mu = 2.5$	Double Gauss $\mu = 1.5$	Double Gauss $f_t = 15\%$,	Double Gauss $f_t = 5\%$	Box function
$1.25 - 1.5$	-6.1%	$+8.2\%$	-3.1%	$+4.7\%$	$\pm 5.5\%$
$1.5 - 1.75$	-5.1%	$+7.1\%$	-2.9%	$+4.2\%$	$\pm 5.6\%$
$1.75 - 2.0$	-5.4%	$+7.0\%$	-2.5%	$+4.0\%$	$\pm 5.8\%$
$2.0 - 2.25$	-4.3%	$+7.0\%$	-2.2%	$+3.3\%$	$\pm 4.9\%$
$2.25 - 2.5$	-4.6%	$+6.5\%$	-2.5%	$+3.7\%$	$\pm 5.7\%$
$2.5 - 2.75$	-3.9%	$+5.7\%$	-2.3%	$+3.3\%$	$\pm 4.4\%$
$2.75 - 3.0$	-3.0%	$+5.3\%$	-2.0%	$+3.0\%$	$\pm 4.3\%$
$3.0 - 3.25$	-2.9%	$+4.3\%$	-1.7%	$+2.5\%$	$\pm 4.2\%$
$3.25 - 3.5$	-3.0%	$+4.7\%$	-1.7%	$+2.6\%$	$\pm 3.5\%$
$3.5 - 3.75$	-3.3%	$+5.2\%$	-2.0%	$+3.0\%$	$\pm 3.0\%$
$3.75 - 4.0$	-2.2%	$+3.0\%$	-1.2%	$+1.8\%$	$\pm 2.1\%$
$4.0 - 4.25$	-2.9%	$+4.6\%$	-1.8%	$+2.7\%$	$\pm 2.1\%$
$4.25 - 4.5$	-2.6%	$+3.5\%$	-1.4%	$+2.0\%$	$\pm 2.1\%$
$4.5 - 4.75$	-2.2%	$+3.5\%$	-1.3%	$+1.9\%$	$\pm 2.2\%$
$4.75 - 5.0$	-2.0%	$+3.6\%$	-1.3%	$+2.0\%$	$\pm 1.7\%$
$5.0 - 5.5$	-2.0%	$+2.6\%$	-1.0%	$+1.5\%$	$\pm 1.6\%$
$5.5 - 6.0$	-3.1%	$+2.9\%$	-1.1%	$+1.6\%$	$\pm 1.4\%$
$6.0 - 6.5$	-1.5%	$+2.7\%$	-1.0%	$+1.5\%$	$\pm 1.6\%$
$6.5 - 7.0$	-1.4%	$+1.9\%$	-0.70%	$+1.1\%$	$\pm 1.4\%$
$7.0 - 8.0$	-1.3%	$+2.1\%$	-0.86%	$+1.2\%$	$\pm 1.1\%$
$8.0 - 9.0$	-1.1%	$+1.6\%$	-0.74%	$+1.0\%$	$\pm 1.2\%$
$9.0 - 10.0$	-0.91%	$+1.4\%$	-0.6%	$+0.8\%$	$\pm 1.0\%$
$10.0 - 12.0$	-0.85%	$+1.0\%$	-0.50%	$+0.8\%$	$\pm 0.91\%$
$12.0 - 14.0$	-0.54%	$+0.92\%$	-0.4%	$+0.6\%$	0.0%
$14.0 - 17.0$	-0.23%	$+0.36\%$	-0.25%	$+0.3\%$	0.0%
$17.0 - 20.0$	-0.46%	$+0.62\%$	-0.27%	$+0.4\%$	0.0%

Table 11: The p_T dependent J/ψ inclusive lifetime fit systematic uncertainties related to the modeling of the resolution function. The values in the first 4 columns are the changes in the b-fractions obtained when the relative area f_t and relative width μ are fixed to the indicated amounts. When the area is changed the width remains fixed and vice versa. The maximum positive and negative deviation of the results in this table is taken as the systematic uncertainty.

$p_T(J/\psi)$ GeV/c	Fix background using sideband	No symmetric exponential	Use F-factor method*	MC mass templates*	Drop r-z hits*
$1.25 - 1.5$	$+1.9\%$	-0.7%	N/A	-0.2%	$\%$
$1.5 - 1.75$	-0.6%	$+0.3\%$	N/A	$+0.6\%$	$\%$
$1.75 - 2.0$	-0.2%	-0.4%	N/A	-0.2%	$\%$
$2.0 - 2.25$	-0.2%	-0.1%	$+1.7\%$	$+1.3\%$	$+2.2\%$
$2.25 - 2.5$	$+0.3\%$	$+0.0\%$	$+1.8\%$	$+0.8\%$	$+6.6\%$
$2.5 - 2.75$	-0.2%	$+0.0\%$	$+2.1\%$	$+0.3\%$	$+1.7\%$
$2.75 - 3.0$	-0.3%	0.0%	$+1.8\%$	$+1.3\%$	$+2.7\%$
$3.0 - 3.25$	-0.3%	-0.2%	$+1.8\%$	$+1.0\%$	$+4.3\%$
$3.25 - 3.5$	-0.3%	-0.0%	$+1.9\%$	$+1.0\%$	$+2.8\%$
$3.5 - 3.75$	$+1.3\%$	0.0%	$+1.6\%$	$+1.7$	$+0.6\%$
$3.75 - 4.0$	-0.3%	$+0.1\%$	$+1.1\%$	$+0.1\%$	$+6.8\%$
$4.0 - 4.25$	-1.0%	$+0.1\%$	$+1.4\%$	$+0.5\%$	$+0.02\%$
$4.25 - 4.5$	$+0.2\%$	$+0.2\%$	$+1.7\%$	$+0.5\%$	$+2.0\%$
$4.5 - 4.75$	$+0.8\%$	-0.1%	$+1.2\%$	$+0.3\%$	$+2.5\%$
$4.75 - 5.0$	-0.3%	$+0.1\%$	$+1.3\%$	$+0.6\%$	$+1.0\%$
$5.0 - 5.5$	-0.3%	-0.1%	$+1.1\%$	$+0.6\%$	$+2.1\%$
$5.5 - 6.0$	$+0.2\%$	0.0%	$+0.7\%$	$+0.4\%$	-0.08%
$6.0 - 6.5$	$+0.3\%$	0.0%	$+0.8\%$	$+0.5\%$	$+2.2\%$
$6.5 - 7.0$	-0.6%	0.0%	$+1.0\%$	$+0.8\%$	$+3.7\%$
$7.0 - 8.0$	-0.5%	0.0%	$+0.4\%$	$+0.5\%$	$+0.7\%$
$8.0 - 9.0$	-0.9%	0.0%	$+0.9\%$	$+0.7\%$	$+0.2\%$
$9.0 - 10.0$	$+0.0\%$	0.0%	$+1.0\%$	$+0.0\%$	$+3.4\%$
$10.0 - 12.0$	-0.3%	0.0%	$+0.3\%$	$+0.4\%$	$+0.7\%$
$12.0 - 14.0$	$+0.4\%$	0.0%	$+0.4\%$	$+0.7\%$	$+6.1\%$
$14.0 - 17.0$	-0.7%	$+0.1\%$	$+0.2\%$	-0.1%	$+3.1\%$
$17.0 - 20.0$	$+3.0\%$	0.0%	$+1.3\%$	$+0.7\%$	$\%$

Table 12: The p_T dependent J/ψ inclusive lifetime fit systematic uncertainties related to the modeling of the signal and background lifetime shapes and invariant mass shape. * These results are for cross-checks only.

$p_T(J/\psi)$	b Spectrum 1		b Spectrum 3		J/ψ decay spectrum	
(GeV/c)	Method 2	1	2	1	2	1
$1.25-1.5$	N/A	$+12\%$	N/A	-2.6%	N/A	$\pm3.3\%$
$1.5-1.75$	N/A	$+18\%$	N/A	-2.1%	N/A	$\pm3.4\%$
$1.75-2.0$	N/A	$+0.5\%$	N/A	-1.4%	N/A	$\pm2.9\%$
$2.0-2.25$	$+3.3$	-1.5%	$+0.33$	-0.85%	2.3	$\pm2.2\%$
$2.25-2.5$	$+2.5$	-1.8%	$+0.15$	-0.67%	0.6	$\pm1.5\%$
$2.5-2.75$	$+1.4$	-7.0%	< 0.1	-0.47%	1.0	$\pm1.0\%$
$2.75-3.0$	$+0.68$	-4.8%	$''$	-0.36%	0.8	$\pm1.0\%$
$3.0-3.25$	$+0.69$	-4.7%	$''$	-0.27%	1.5	$\pm1.1\%$
$3.25-3.5$	$+0.62$	-4.6%	$''$	-0.26%	1.7	$\pm1.0\%$
$3.5-3.75$	$+0.64$	-5.0%	$''$	-0.77%	0.5	$\pm1.0\%$
$3.75-4.0$	$+0.56$	-6.0%		-1.0%	0.0	$\pm0.8\%$
$4.0-4.25$	$+0.62$	-6.0%		$< -1.0\%$	0.5	$\pm0.7\%$
$4.25-4.5$	$+0.52$	-6.1%		$< -1.0\%$	0.5	$\pm0.4\%$
$4.5-4.75$	$+0.52$	-5.2%		$< -1.0\%$	0.4	$\pm1.1\%$
$4.75-5.0$	$+0.58$	-6.4%		$< -1.0\%$	0.0	$\pm0.4\%$
$5.0-5.5$	$+0.53$	-6.2%		$< -1.0\%$	0.6	$\pm0.4\%$
$5.5-6.0$	$+0.51$	-5.8%		$< -1.0\%$	< 1	$\pm0.5\%$
$6.0-6.5$	$+0.48$	-5.9%		$< -1.0\%$	$''$	$\pm0.6\%$
$6.5-7.0$	$+0.48$	-4.8%		$< -1.0\%$	$''$	$\pm0.6\%$
$7.0-8.0$	$+0.42$	-5.1%		$< -1.0\%$	$''$	$\pm0.9\%$
$8.0-9.0$	$+0.38$	-4.6%		$< -1.0\%$	$''$	$\pm0.5\%$
$9.0-10.0$	$+0.35$	-4.5%		$< -1.0\%$	$''$	$\pm1.0\%$
$10.0-12.0$	$+0.23$	-4.5%		$< -1.0\%$	$''$	$\pm1.0\%$
$12.0-14.0$	$+0.05$	-4.5%		$< -1.0\%$	$''$	$\pm1.2\%$
$14.0-17.0$	$+0.05$	-4.5%		$< -1.0\%$	$+1.3$	$\pm0.8\%$
$17.0-20.0$	$+0.06$	-4.5%	-0.15	$< -1.0\%$	$+2.6$	$\pm1.0\%$

Table 13: The p_T dependant J/ψ inclusive lifetime fit systematic uncertainties related to the modeling of the input b hadron production and decay spectra. The effect on the b-fractions extracted using both the direct fit to L_{xy}/p_T (1) and the F-factor fit (2) is shown. Spectrum 1 is the difference in b-fractions obtained when a flat $(p_T(b-hadron), y(b-hadron)$ distribution is used. Spectrum 3 is the effect when a harder b-hadron spectrum still consistent with the data is used. The systematic uncertainty is taken as 1/2 of the size of the variation observed in the b-fraction when the flat model is used. The J/ψ decay spectrum is the uncertainty in b-fraction obtained when the decay model used is varied.

$p_T(J/\psi)$ (Gev/c)	Syst. bias
$1.25 - 1.5$	$+0\%$
$1.5 - 1.75$	$\sim 0\%$
$1.75 - 2.0$	$\sim 0\%$
$2.0 - 2.25$	$+2\%$
$2.25 - 2.5$	$\sim 2\%$
$2.5 - 2.75$	$\sim 2\%$
$2.75 - 3.0$	$\sim 2\%$
$3.0 - 3.25$	$\sim 2\%$
$3.25 - 3.5$	$\sim 2\%$
$3.5 - 3.75$	$\sim 2\%$
$3.75 - 4.0$	$\sim 2\%$
$4.0 - 4.25$	$\sim 2\%$
$4.25 - 4.5$	$\sim 2\%$
$4.5 - 4.75$	$\sim 2\%$
$4.75 - 5.0$	$\sim 2\%$
$5.0 - 5.5$	$+1\%$
$5.5 - 6.0$	$\sim 1\%$
$6.0 - 6.5$	$\sim 1\%$
$6.5 - 7.0$	$\sim 1\%$
$7.0 - 8.0$	$\sim 1\%$
$8.0 - 9.0$	$\sim 1\%$
$9.0 - 10.0$	$\sim 1\%$
$10.0 - 12.0$	$\sim 1\%$
$12.0 - 14.0$	$+0\%$
$14.0 - 17.0$	$+0\%$

Table 14: The p_T dependent J/ψ inclusive lifetime fit systematic bias from toyMC studies.

$p_T(J/\psi)$ (Gev/c)	Syst. bias
$1.25 - 1.5$	$\pm 3.7\%$
$1.5 - 1.75$	$\pm 3.2\%$
$1.75 - 2.0$	$\pm 3.4\%$
$2.0 - 2.25$	$\pm 3.3\%$
$2.25 - 2.5$	$\pm 2.9\%$
$2.5 - 2.75$	$\pm 2.5\%$
$2.75 - 3.0$	$\pm 2.4\%$
$3.0 - 3.25$	$\pm 2.2\%$
$3.25 - 3.5$	$\pm 2.0\%$
$3.5 - 3.75$	$\pm 1.9\%$
$3.75 - 4.0$	$\pm 1.6\%$
$4.0 - 4.25$	$\pm 1.8\%$
$4.25 - 4.5$	$\pm 1.6\%$
$4.5 - 4.75$	$\pm 1.7\%$
$4.75 - 5.0$	$\pm 1.5\%$
$5.0 - 5.5$	$\pm 1.6\%$
$5.5 - 6.0$	$\pm 1.3\%$
$6.0 - 6.5$	$\pm 1.7\%$
$6.5 - 7.0$	$\pm 1.3\%$
$7.0 - 8.0$	$\pm 1.0\%$
$8.0 - 9.0$	$\pm 1.0\%$
$9.0 - 10.0$	$\pm 1.0\%$
$10.0 - 12.0$	$\pm 0.7\%$
$12.0 - 14.0$	$\pm 0.7\%$
$14.0 - 17.0$	$\pm 0.5\%$

Table 15: The change in the b-fraction measured when the average b-hadron lifetime is changed by 11 μm.

$p_T(J/\psi)$ GeV/c	Run II b-Fraction	Run I b-Fraction
$1.25 - 1.5$	$0.097 \pm 0.010(stat)^{0.012}_{-0.010}(syst)$	
$1.5 - 1.75$	$0.094 \pm 0.006^{+0.010}_{-0.009}$	
$1.75 - 2.0$	$0.087 \pm 0.006^{+0.009}_{-0.009}$	
$2.0 - 2.25$	$0.100 \pm 0.005^{+0.011}_{-0.009}$	
$2.25 - 2.5$	$0.092 \pm 0.005^{+0.009}_{-0.008}$	
$2.5 - 2.75$	$0.102 \pm 0.005^{+0.010}_{-0.009}$	
$2.75 - 3.0$	$0.099 \pm 0.005^{+0.009}_{-0.008}$	
$3.0 - 3.25$	$0.108 \pm 0.005^{+0.007}_{-0.005}$	
$3.25 - 3.5$	$0.112 \pm 0.005^{+0.007}_{-0.006}$	
$3.5 - 3.75$	$0.113 \pm 0.005^{+0.008}_{-0.006}$	
$3.75 - 4.0$	$0.133 \pm 0.005^{+0.007}_{-0.006}$	
$4.0 - 4.25$	$0.115 \pm 0.005^{+0.007}_{-0.005}$	
$4.25 - 4.5$	$0.126 \pm 0.006^{+0.007}_{-0.006}$	
$4.5 - 4.75$	$0.133 \pm 0.006^{+0.007}_{-0.005}$	
$4.75 - 5.0$	$0.144 \pm 0.007^{+0.008}_{-0.006}$	
$5.0 - 5.5$	$0.143 \pm 0.005^{+0.006}_{-0.006}$	$0.148 \pm 0.005(stat)$
$5.5 - 6.0$	$0.157 \pm 0.006^{+0.007}_{-0.007}$	$0.165 \pm 0.005(stat)$
$6.0 - 6.5$	$0.170 \pm 0.007^{+0.007}_{-0.006}$	$0.178 \pm 0.006(stat)$
$6.5 - 7.0$	$0.184 \pm 0.007^{+0.008}_{-0.007}$	$0.191 \pm 0.006(stat)$
$7.0 - 8.0$	$0.209 \pm 0.006^{+0.009}_{-0.008}$	$0.207 \pm 0.005(stat)$
$8.0 - 9.0$	$0.229 \pm 0.009^{+0.007}_{-0.006}$	$0.232 \pm 0.007(stat)$
$9.0 - 10.0$	$0.250 \pm 0.011^{+0.008}_{-0.007}$	$0.236 \pm 0.010(stat)$
$10.0 - 12.0$	$0.279 \pm 0.012^{+0.008}_{-0.007}$	$0.300 \pm 0.010(stat)$
$12.0 - 14.0$	$0.336 \pm 0.019^{+0.009}_{-0.008}$	$0.317 \pm 0.017(stat)$
$14.0 - 17.0$	$0.396 \pm 0.025^{+0.009}_{-0.009}$	$0.387 \pm 0.024(stat)$
$17.0 - 20.0$	$0.470 \pm 0.045^{+0.017}_{-0.011}$	$0.379 \pm 0.046(stat)$

Table 16: Fraction of inclusive J/ψ from b-hadron decays.

5all bins to account for the variation in L_{xy} asymmetry as a

$p_{\mathrm{T}}(\mathrm{J}/\psi)$	SVXII/COT Acceptance
1.75 - 2.0	0.3618 ± 0.0034
2.0 - 2.25	0.3605 ± 0.0025
2.25 - 2.5	0.3592 ± 0.0017
2.5 - 2.75	0.3580 ± 0.0009
2.75 - 3.0	0.3568 ± 0.0002
3.0 - 3.25	0.3557 ± 0.0004
3.25 - 3.5	0.3547 ± 0.0010
3.5 - 3.75	0.3537 ± 0.0015
3.75 - 4.0	0.3528 ± 0.0020
4.0 - 4.25	0.3519 ± 0.0024
4.25 - 4.5	0.3511 ± 0.0027
4.5 - 4.75	0.3504 ± 0.0030
4.75 - 5.0	0.3497 ± 0.0032
5.0 - 5.5	0.3488 ± 0.0035
5.5 - 6.0	0.3478 ± 0.0035
6.0 - 6.5	0.3470 ± 0.0034
6.5 - 7.0	0.3465 ± 0.0030
7.0 - 8.0	0.3461 ± 0.0020
8.0 - 9.0	0.3465 ± 0.0002
9.0 - 10.0	0.3478 ± 0.0034
10.0 - 12.0	0.3515 ± 0.0099
12.0 - 14.0	0.3598 ± 0.0218
14.0 - 17.0	0.3755 ± 0.0422

Table 17: The relative J/ψ acceptance in the SVXII measured with respect to COT.

$p_T(J/\psi)$ GeV/c	Acceptance $J/\psi^{inclusive}$ $\mathcal{A}(\alpha=+0.15)$	Acceptance J/ψ^{H_b} $\mathcal{A}(\alpha=0.0)$
$1.25-1.5$	0.01636 ± 0.00039	0.01714 ± 0.00041
$1.5-1.75$	0.01992 ± 0.00045	0.02086 ± 0.00047
$1.75-2.0$	0.02413 ± 0.00051	0.02523 ± 0.00054
$2.0-2.25$	0.02749 ± 0.00024	0.02885 ± 0.00028
$2.25-2.5$	0.03328 ± 0.00028	0.03469 ± 0.00033
$2.5-2.75$	0.03699 ± 0.00032	0.03845 ± 0.00038
$2.75-3.0$	0.04199 ± 0.00037	0.04368 ± 0.00043
$3.0-3.25$	0.04792 ± 0.00042	0.04975 ± 0.00050
$3.25-3.5$	0.05367 ± 0.00048	0.05528 ± 0.00056
$3.5-3.75$	0.05914 ± 0.00054	0.06179 ± 0.00064
$3.75-4.0$	0.06339 ± 0.00060	0.06600 ± 0.00071
$4.0-4.25$	0.06909 ± 0.00067	0.07236 ± 0.00080
$4.25-4.5$	0.07689 ± 0.00076	0.07903 ± 0.00090
$4.5-4.75$	0.08252 ± 0.00084	0.0850 ± 0.0010
$4.75-5.0$	0.09114 ± 0.00095	0.0940 ± 0.0011
$5.0-5.5$	0.10029 ± 0.00078	0.10337 ± 0.00092
$5.5-6.0$	0.11378 ± 0.00096	0.11773 ± 0.0011
$6.0-6.5$	0.1251 ± 0.0012	0.1295 ± 0.0014
$6.5-7.0$	0.1344 ± 0.0014	0.1388 ± 0.0016
$7.0-8.0$	0.1498 ± 0.0013	0.1536 ± 0.0015
$8.0-9.0$	0.1609 ± 0.0018	0.1642 ± 0.0020
$9.0-10.0$	0.1643 ± 0.0024	0.1710 ± 0.0028
$10.0-12.0$	0.1692 ± 0.0025	0.1723 ± 0.0030
$12.0-14.0$	0.1555 ± 0.0041	0.1613 ± 0.0049
$14.0-17.0$	0.1219 ± 0.0052	0.1300 ± 0.0062

Table 18: The p_T dependent J/ψ acceptance. The values for $\alpha = +0.15$ used for the inclusive measurement and the value for $\alpha = 0.0$ to be used for the $H_b \rightarrow J/\psi X$ measurement. The uncertainty on the $H_b \rightarrow J/\psi X$ acceptance from the J/ψ polarization is $\alpha = 0.0 \pm 0.5$.

$p_T(J/\psi)$ GeV/c	syst. uncert(%) $\Delta(\alpha) = \pm 0.5$
$1.25 - 1.5$	$+16 - 13\%$
$1.5 - 1.75$	$+16 - 13\%$
$1.75 - 2.0$	$+15 - 12\%$
$2.0 - 2.25$	$+15 - 12\%$
$2.25 - 2.5$	$+15 - 12\%$
$2.5 - 2.75$	$+13 - 11\%$
$2.75 - 3.0$	$+13 - 11\%$
$3.0 - 3.25$	$+13 - 11\%$
$3.25 - 3.5$	$+12 - 9.8\%$
$3.5 - 3.75$	$+13 - 11\%$
$3.75 - 4.0$	$+12 - 10\%$
$4.0 - 4.25$	$+13 - 11\%$
$4.25 - 4.5$	$+11 - 9.0\%$
$4.5 - 4.75$	$+11 - 9.2\%$
$4.75 - 5.0$	$+11 - 9.0\%$
$5.0 - 5.5$	$+11 - 8.7\%$
$5.5 - 6.0$	$+11 - 8.8\%$
$6.0 - 6.5$	$+11 - 8.7\%$
$6.5 - 7.0$	$+10 - 8.2\%$
$7.0 - 8.0$	$+8.8 - 7.3\%$
$8.0 - 9.0$	$+7.6 - 6.3\%$
$9.0 - 10.0$	$+9.6 - 8.0\%$
$10.0 - 12.0$	$+6.8 - 5.7\%$
$12.0 - 14.0$	$+9.2 - 7.6\%$
$14.0 - 17.0$	$+10 - 8.5\%$

Table 19: The uncertainty on the $H_b \rightarrow J/\psi X$ acceptance from the J/ψ polarization for $\mathcal{A}(\alpha = 0.0 \pm 0.5)$.

Source of uncertainty	Value
Resolution function shape (including tails)	1-8% (p_T dependent)
MC production spectrum	$2 - 7\%$ (p_T dependent)
MC decay spectrum	$0.5 - 4\%$ (p_T dependent)
MC b-hadron lifetime	$1 - 4\%$ (p_T dependent)
Background fit model	$< 3\%$ (p_T dependent)
Acceptance	$9 - 16\%$ (p_T dependent)
Inclusive J/ψ cross-section	$6 - 15\%$ (p_T dependent)
Fully correlated (from inclusive)	$\pm 6.7\%$

Table 20: Summary of systmatic uncertainties

$p_T(J/\psi)$	$< p_T(J/\psi) >$	$\frac{d\sigma}{dp_T} \cdot \mathcal{B}$ (nb/GeV/c)	$\frac{d\sigma}{dp_T} \cdot \mathcal{B}$ (nb/GeV/c)
(GeV/c)	(GeV/c)	J/ψ inclusive	J/ψ from b
$1.25 - 1.5$	1.38	$70.9 \pm 1.7^{+10.6}_{-7.8}$	$6.57 \pm 0.72(stat)^{+1.50}_{-1.19}(syst_{p_T})$
$1.5 - 1.75$	1.63	$74.1 \pm 1.6^{+10.9}_{-7.5}$	$6.65 \pm 0.46^{+1.49}_{-1.16}$
$1.75 - 2.0$	1.87	$71.5 \pm 1.4^{+9.4}_{-7.0}$	$5.95 \pm 0.39^{+1.22}_{-0.99}$
$2.0 - 2.25$	2.13	$69.4 \pm 0.8^{+8.6}_{-6.8}$	$6.65 \pm 0.36^{+1.35}_{-1.09}$
$2.25 - 2.5$	2.38	$66.0 \pm 1.0^{+7.8}_{-5.9}$	$5.81 \pm 0.31^{+1.14}_{-0.91}$
$2.5 - 2.75$	2.62	$57.2 \pm 0.9^{+6.4}_{-4.9}$	$5.62 \pm 0.27^{+0.98}_{-0.82}$
$2.75 - 3.0$	2.87	$51.9 \pm 0.8^{+5.5}_{-4.3}$	$4.93 \pm 0.24^{+0.84}_{-0.70}$
$3.0 - 3.25$	3.12	$43.3 \pm 0.7^{+4.4}_{-3.4}$	$4.52 \pm 0.21^{+0.69}_{-0.56}$
$3.25 - 3.5$	3.38	$37.5 \pm 0.8^{+3.7}_{-2.9}$	$4.06 \pm 0.18^{+0.59}_{-0.47}$
$3.5 - 3.75$	3.62	$30.8 \pm 0.5^{+2.9}_{-2.3}$	$3.33 \pm 0.15^{+0.51}_{-0.41}$
$3.75 - 4.0$	3.87	$26.5 \pm 0.4^{+2.4}_{-1.9}$	$3.39 \pm 0.15^{+0.47}_{-0.38}$
$4.0 - 4.25$	4.12	$22.9 \pm 0.4^{+2.1}_{-1.7}$	$2.52 \pm 0.12^{+0.38}_{-0.31}$
$4.25 - 4.5$	4.38	$18.5 \pm 0.3^{+1.7}_{-1.4}$	$2.27 \pm 0.11^{+0.30}_{-0.24}$
$4.5 - 4.75$	4.62	$16.8 \pm 0.3^{+1.5}_{-1.2}$	$2.16 \pm 0.10^{+0.28}_{-0.23}$
$4.75 - 5.0$	4.88	$13.3 \pm 0.3^{+1.1}_{-0.9}$	$1.87 \pm 0.089^{+0.24}_{-0.20}$
$5.0 - 5.5$	5.24	$10.4 \pm 0.15^{+0.9}_{-0.71}$	$1.44 \pm 0.051^{+0.18}_{-0.15}$
$5.5 - 6.0$	5.74	$7.32 \pm 0.12^{+0.58}_{-0.48}$	$1.11 \pm 0.041^{+0.14}_{-0.12}$
$6.0 - 6.5$	6.24	$5.21 \pm 0.09^{+0.39}_{-0.33}$	$0.857 \pm 0.034^{+0.11}_{-0.09}$
$6.5 - 7.0$	6.74	$3.62 \pm 0.07^{+0.26}_{-0.22}$	$0.644 \pm 0.027^{+0.074}_{-0.062}$
$7.0 - 8.0$	7.45	$2.36 \pm 0.04^{+0.16}_{-0.14}$	$0.481 \pm 0.015^{+0.050}_{-0.042}$
$8.0 - 9.0$	8.46	$1.24 \pm 0.03^{+0.08}_{-0.07}$	$0.279 \pm 0.011^{+0.025}_{-0.021}$
$9.0 - 10.0$	9.46	$0.672 \pm 0.018^{+0.077}_{-0.074}$	$0.162 \pm 0.0075^{+0.023}_{-0.021}$
$10.0 - 12.0$	10.8	$0.320 \pm 0.009^{+0.051}_{-0.050}$	$0.0875 \pm 0.0037^{+0.015}_{-0.014}$
$12.0 - 14.0$	12.8	$0.146 \pm 0.006^{+0.023}_{-0.023}$	$0.0474 \pm 0.0028^{+0.0085}_{-0.0081}$
$14.0 - 17.0$	15.4	$0.072 \pm 0.004^{+0.014}_{-0.011}$	$0.0266 \pm 0.0018^{+0.0057}_{-0.0046}$

Table 21: Run II inclusive b-Hadron differential cross-section with statistical and p_T dependent systematic uncertainties. The fully correlated systematic uncertainty, $syst_{fc} = 6.7\%$, from the measurement of the inclusive J/ψ cross-section is not included.

$< p_T(B^+) >$ GeV/c	$\sigma(B^+)(\lvert y\rvert < 1.0) nb/(GeV/c)$ Run I	$\sigma(B^+)(\lvert y\rvert < 1.0) nb/(GeV/c)$ Run II (from inclusive)
7.34	$815 \pm 117(stat) \pm 31(syst_{p_T}) \pm 104(syst_{f_c})$	$604 \pm 12(stat) \pm 79(syst_{p_T}) \pm 72(syst_{f_c})$
10.35	$222 \pm 33(stat) \pm 8(syst_{p_T}) \pm 28(syst_{f_c})$	$204 \pm 5(stat) \pm 23(syst_{p_T}) \pm 24(syst_{f_c})$
13.36	$77.5 \pm 16.2(stat) \pm 2.4(syst_{p_T}) \pm 9.9(syst_{f_c})$	$71.3 \pm 2.4(stat) \pm 8.6(syst_{p_T}) \pm 8.6(syst_{f_c})$
18.87	$18.7 \pm 2.6(stat) \pm 0.6(syst_{p_T}) \pm 2.4(syst_{f_c})$	$16.5 \pm 0.6(stat) \pm 2.6(syst_{p_T}) \pm 2.0(syst_{f_c})$

Table 22: Run II B^+ cross-section values extrapolated from the inclusive b-hadron cross-section compared with Run I values. The integrated cross-section for $p_T(B) > 6.0$ GeV/c is 2.8 ± 0.4.

THEORY FIGURES

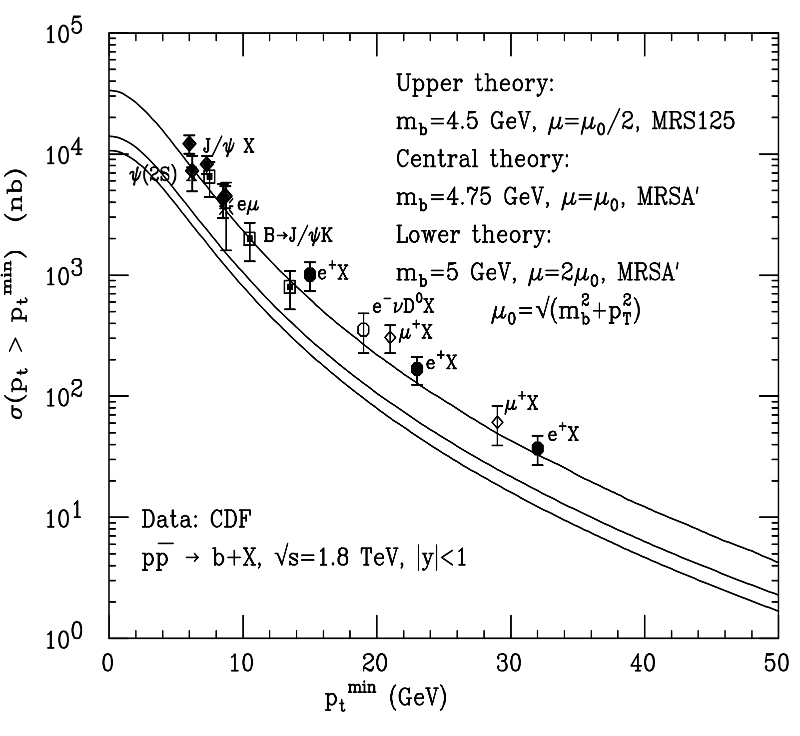

Figure 1: CDF Run I inclusive b cross-sections with theoretical predictions from [1].

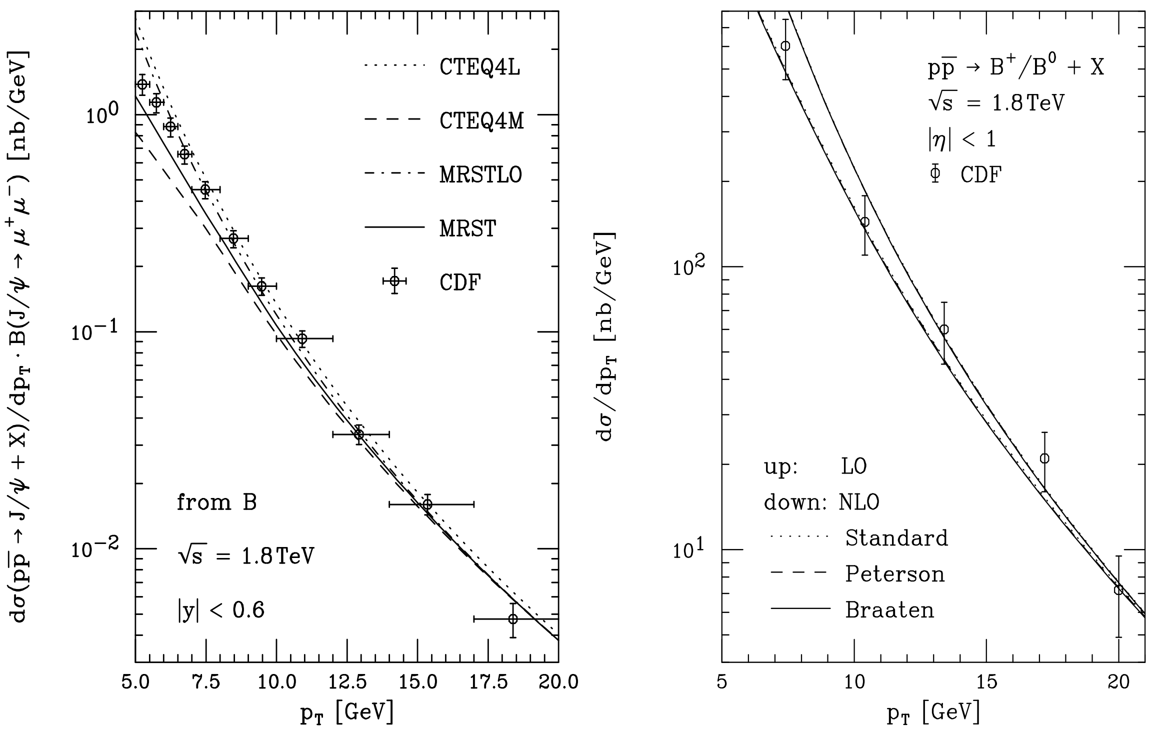

Figure 2: CDF Run I inclusive $b \to J/\psi X$ and B meson cross-sections with theoretical predictions from [2] [4] .

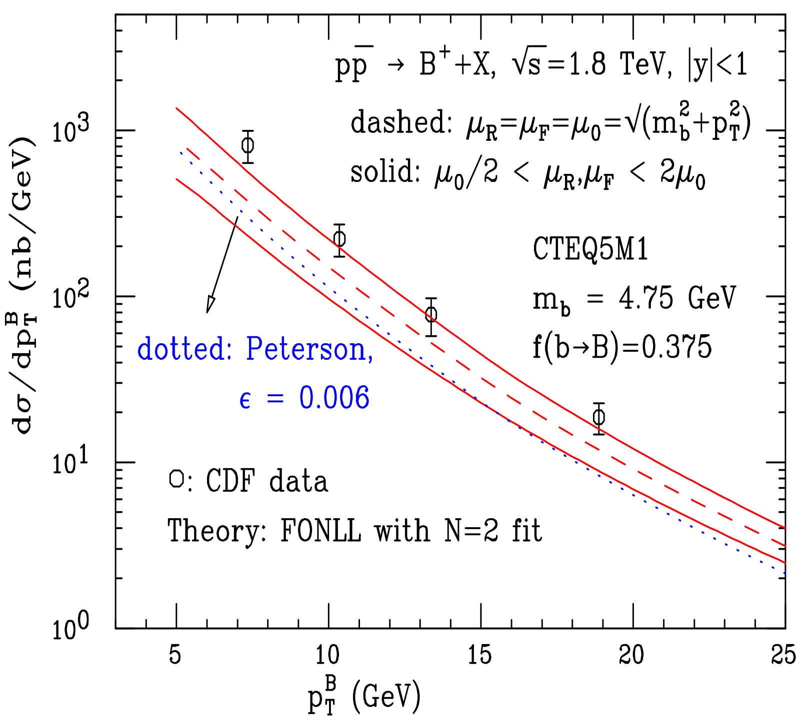

Figure 3: CDF Run I B meson cross-sections with theoretical predictions from [3].

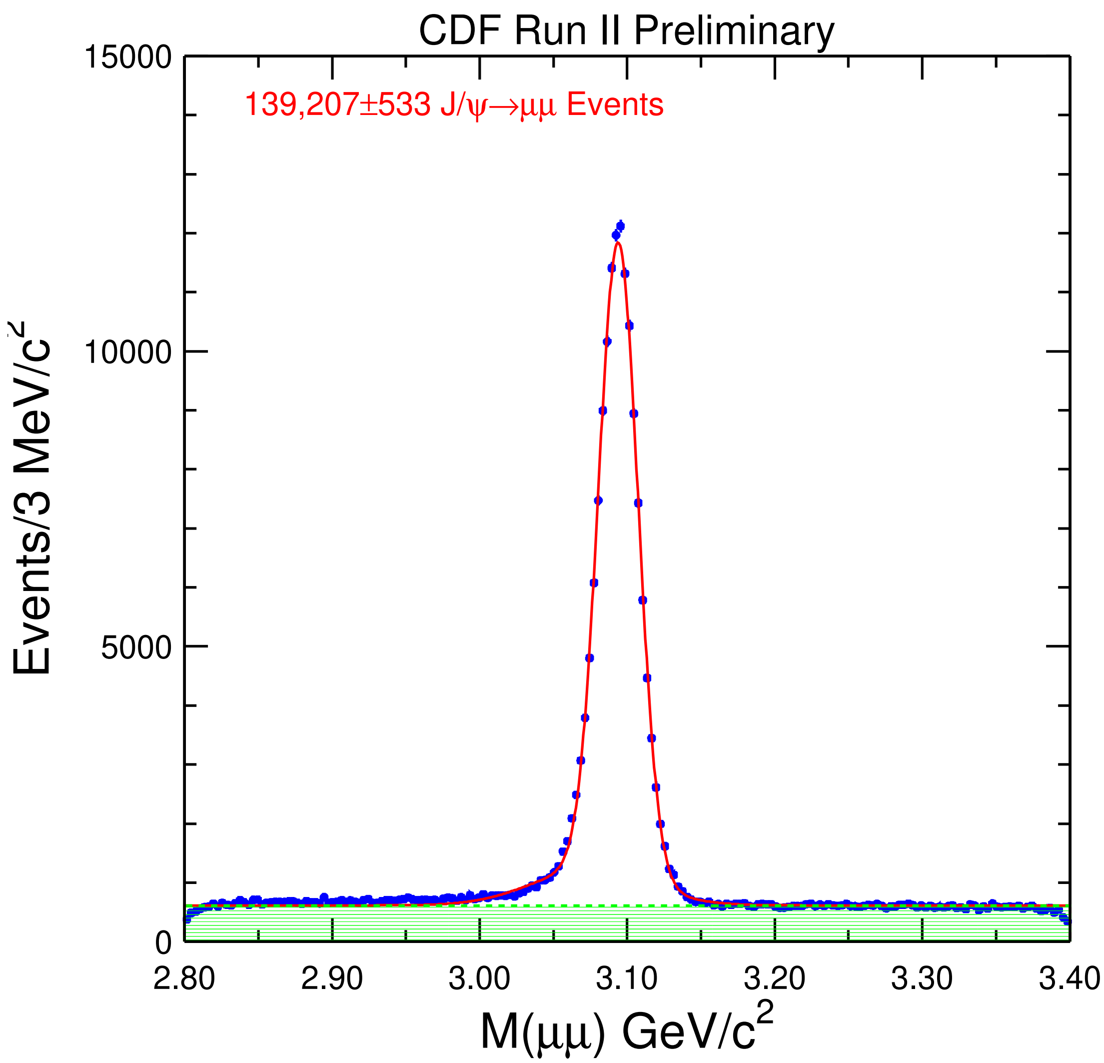

Figure 4: The dimuon invariant mass for J/ψ with $p_T \geq 1.25$ GeV/c

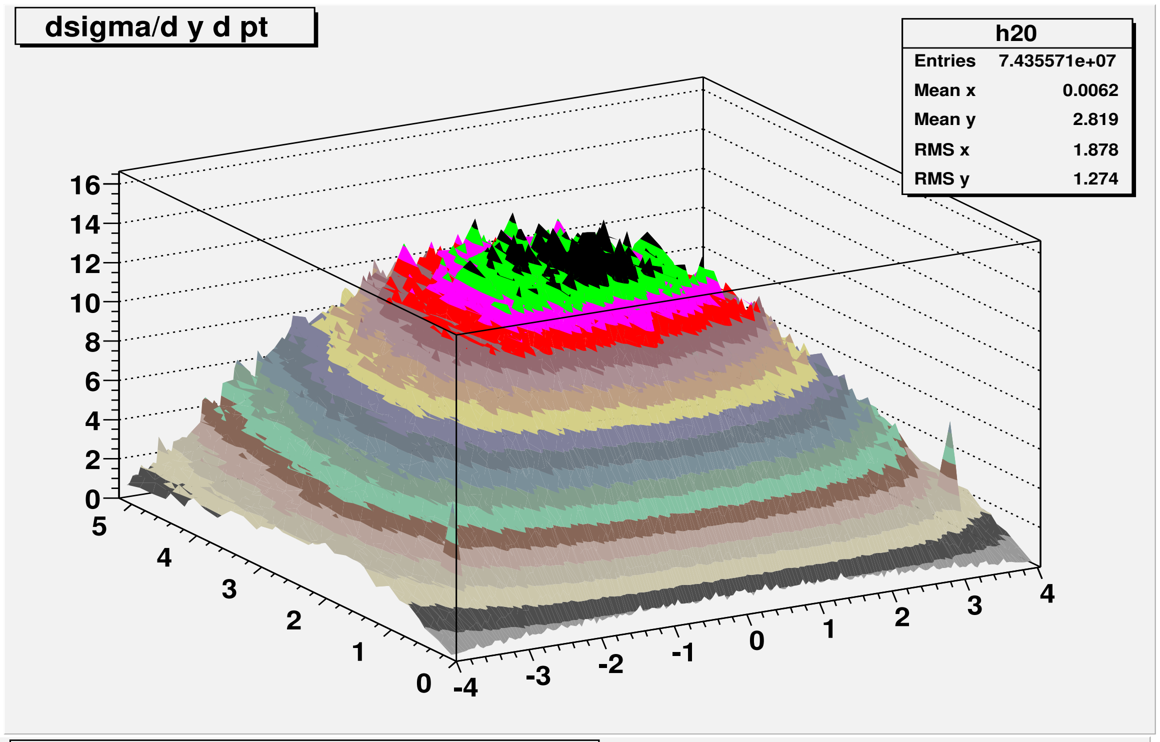

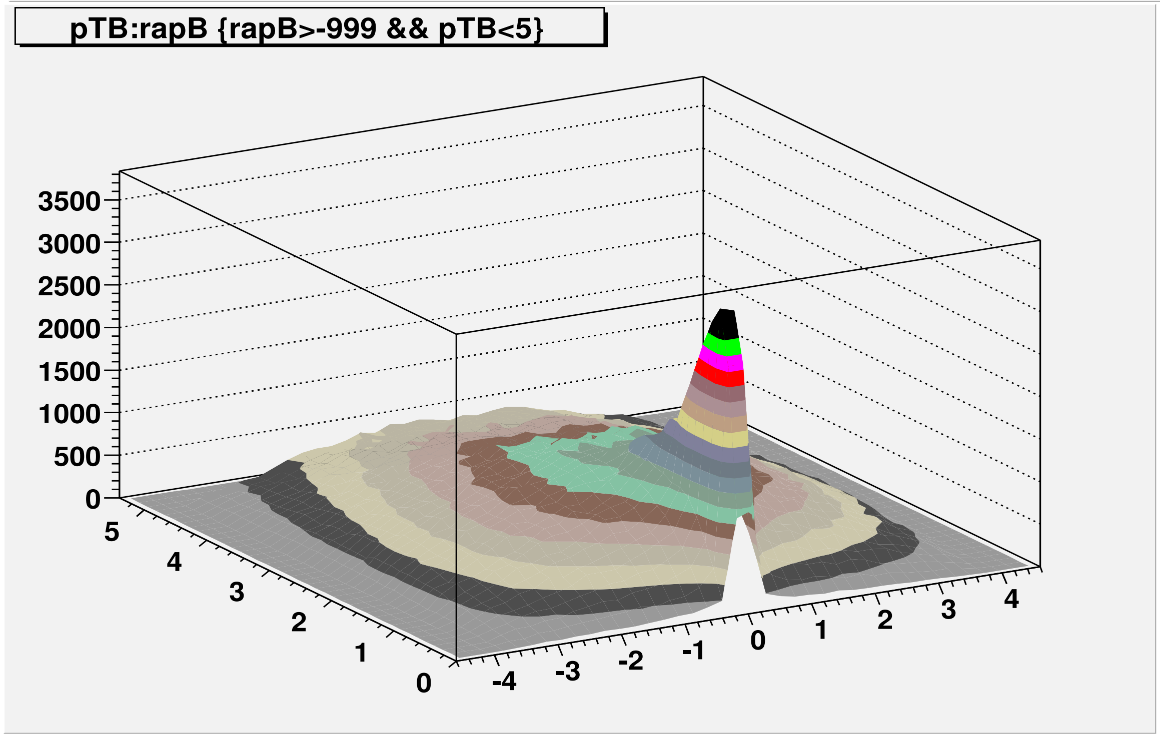

Figure 5: The b-quark $d\sigma/dp_T dy$ spectrum input to Bgenerator(above) and the resultant b-hadron spectrum (below) after fragmentation using a Peterson function with $\epsilon_q = 0.006$

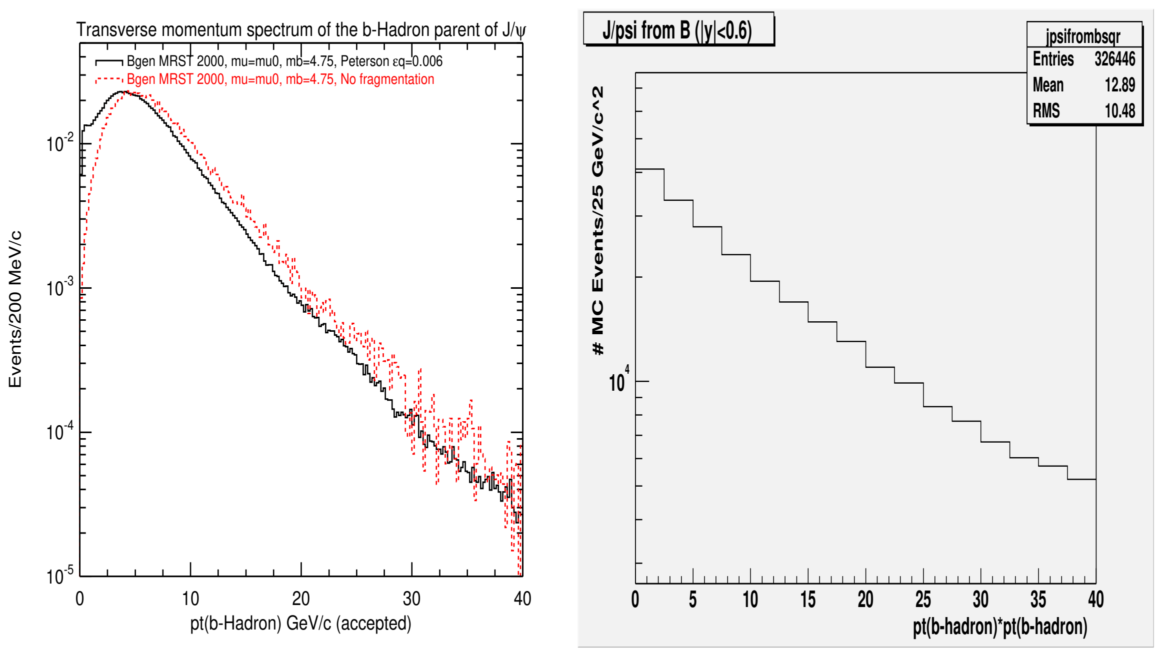

Figure 6: b-hadron transverse momentum spectra from Bgenerator when fragmentation is switched off. On the left plot the solid line is the spectrum of b-hadron parents with the fragmentation turned on and the dashed line is the spectrum with the fragmentation turned off. The dashed spectrum is the default spectrum used in the following analysis. The right plot is the distribtution of MC events as a function of the invariant quantity $p_T^2(b - hadron)$ in the lowest transverse momentum range with fragmentation switched off.

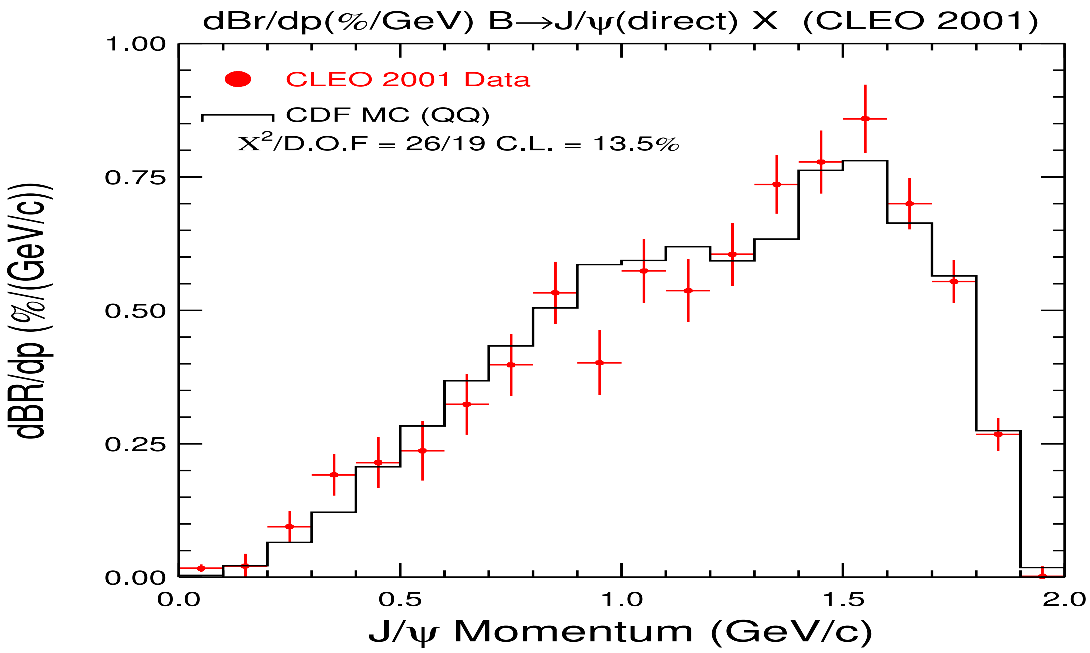

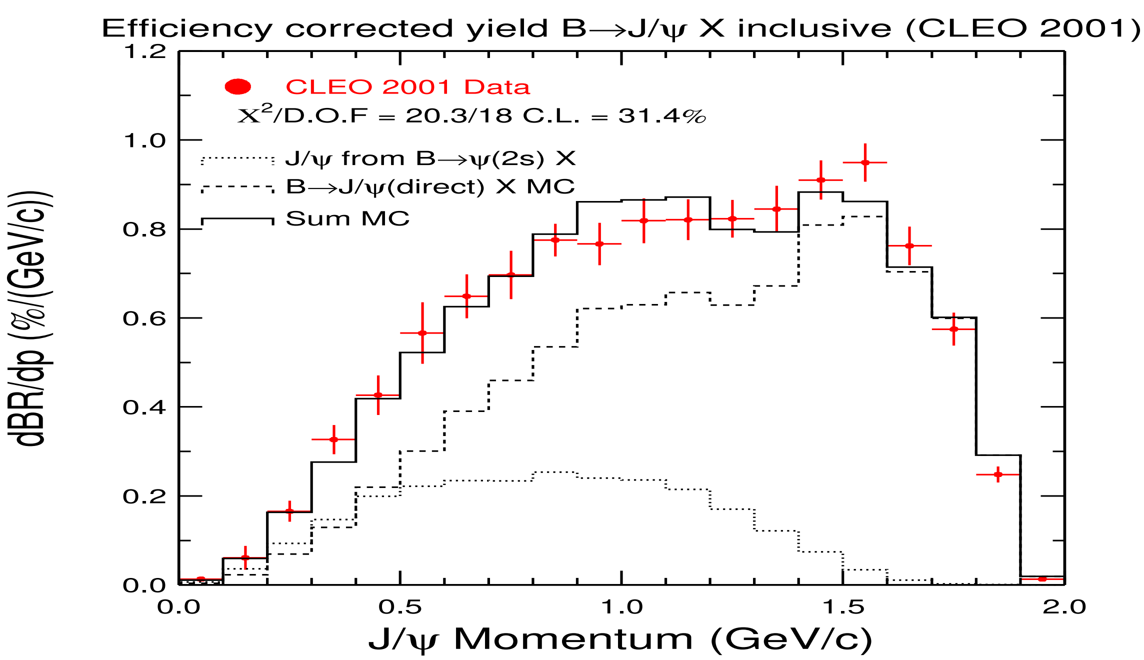

Figure 7: Left: $B \to J/\psi(1S)(direct)X$ decay spectrum. The points are published CLEO 2001 data and the histogram is from CDF Bgenerator+QQ generator level MC. Right:The points with error bars are the $B \to J/\psi(inclusive)X$ CLEO data extrapolated from published results. The solid histogram is the sum of the contribution from $B \to J/\psi(1S)(direct)X$ (dashed line) and a tuned $B \to \psi(2S)X$ contribution (dotted line) which includes a large $B \to \psi(2S)K^*(892)\pi\pi$ br. fraction

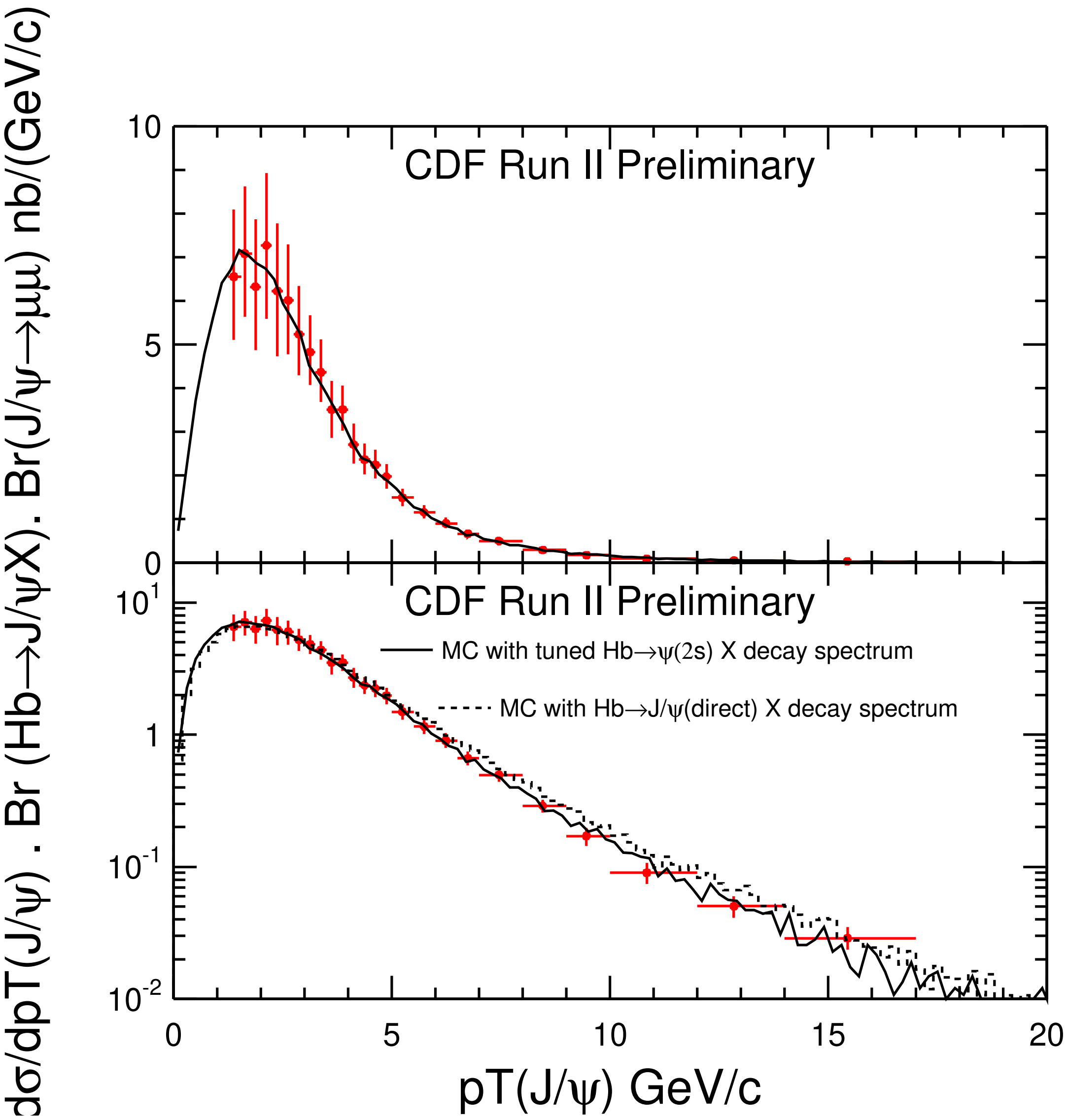

Figure 8: A comparison between the current measurement of the $b \to J/\psi$ transverse momentum spectrum measured in data and the input spectrum used for the MC modeling using the tuned and untuned decay spectrum. The $\chi^2/D.O.F$ of the MC spectrum compared to the data is 10.5/25 with a C.L. of 99.2%.

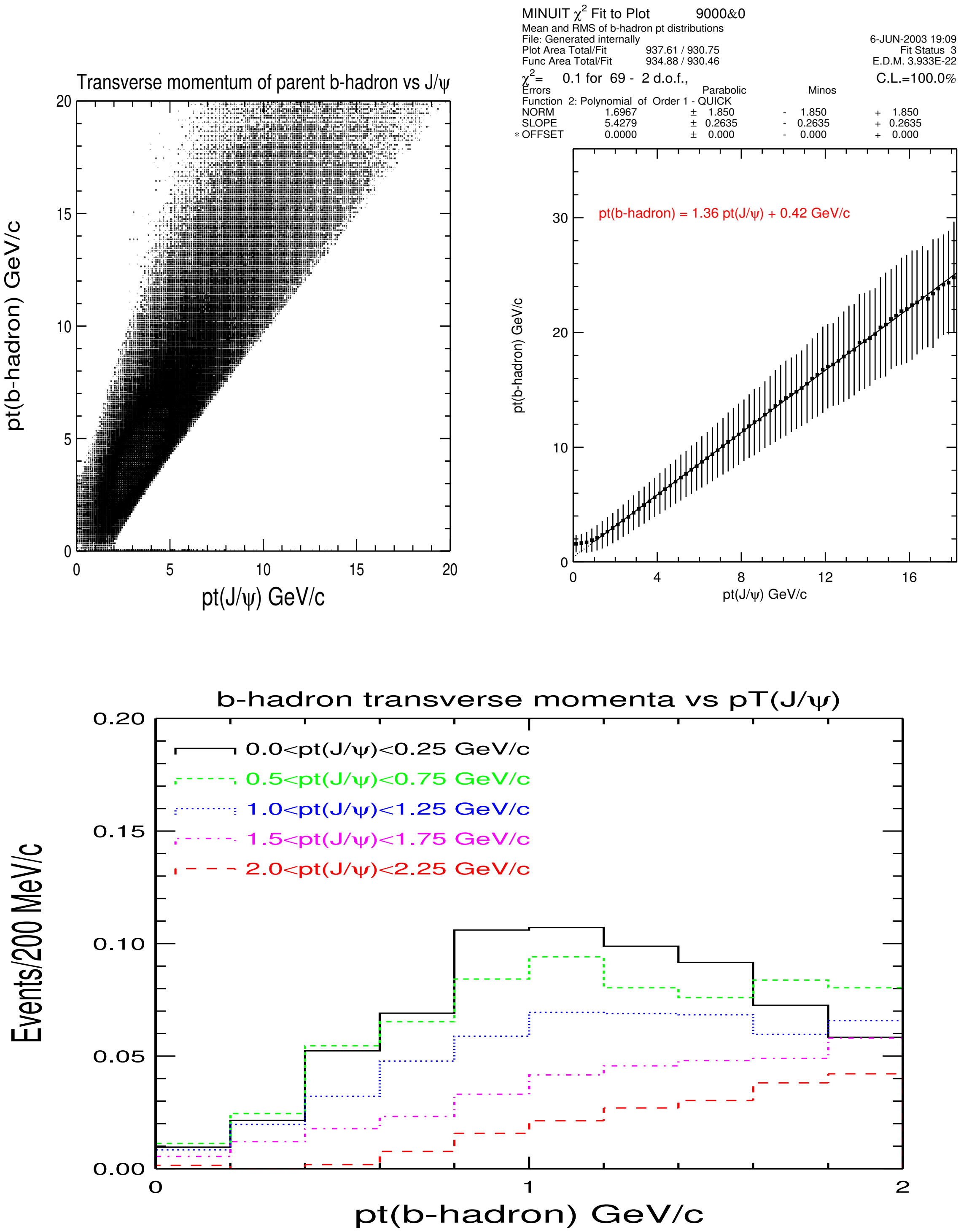

Figure 9: Transverse momentum of the input b-hadron versus the J/ψ from Bgenerator with no fragmentation. Top left plot is the scatter plot of the distribution of b-hadron versus J/ψ momenta. Top right plot, the points are the mean of the b-hadron momentum distribution in each 250 MeV/c J/ψ bin and the error bars are the rms of the distribution. Bottom plot is the transverse momentum distribution of b-hadrons in several J/ψ momentum bins.

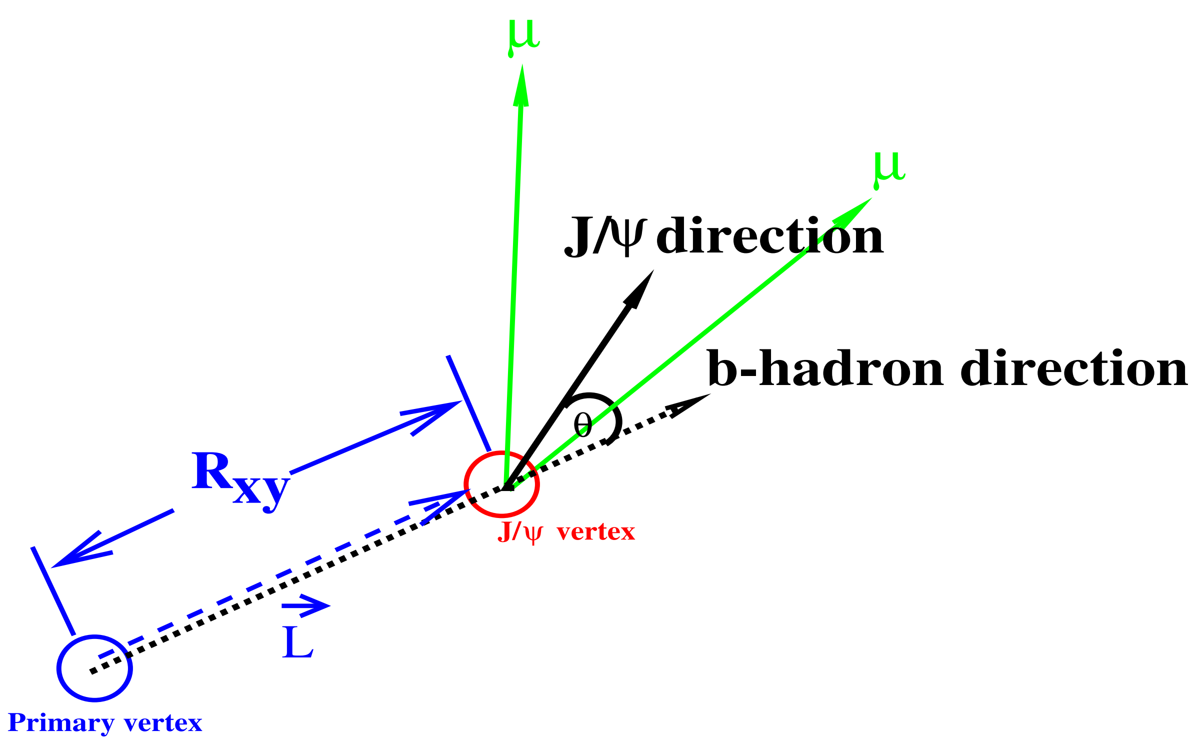

Figure 10: Variables used to define L_{xy} shown in the $r-\phi$ plane. $L_{xy} = \vec{L}.\vec{p_T}^{\psi}/|p_T^{\psi}| = R_{xy}\cos\theta$.

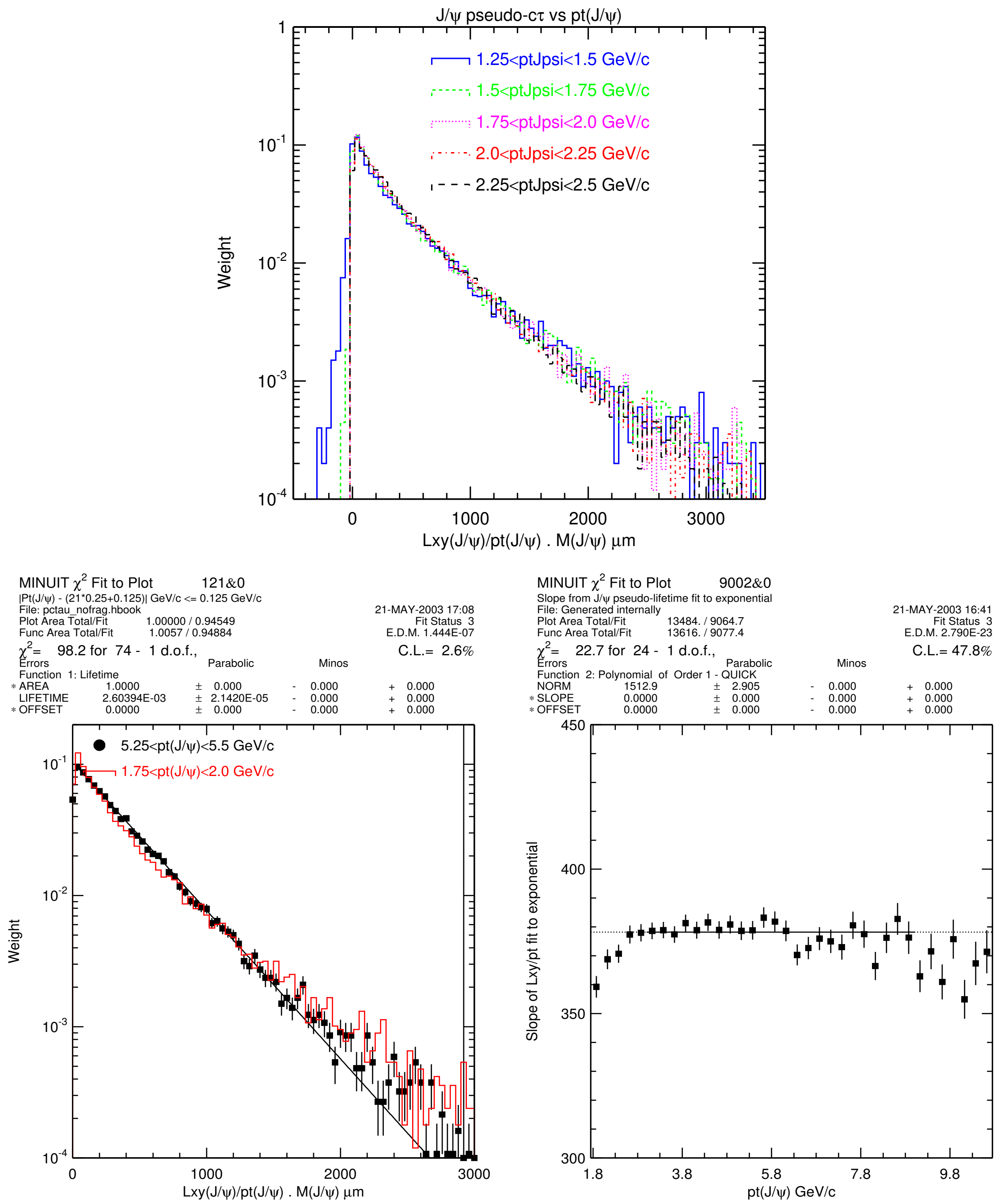

Figure 11: J/ψ pseudo-lifetime distributions from generator level MC in the lower transverse momentum bins (top). For $p_T(J/\psi) > 5.0$ GeV/c the pseudo-$c\tau$ distribution is well described by a single exponential with a characteristic slope of 378μm (bottom left). The value of the slope from a fit to a pure exponential function for various J/ψ transverse momentum bins (bottom right).

LIFETIME RESOLUTIONS

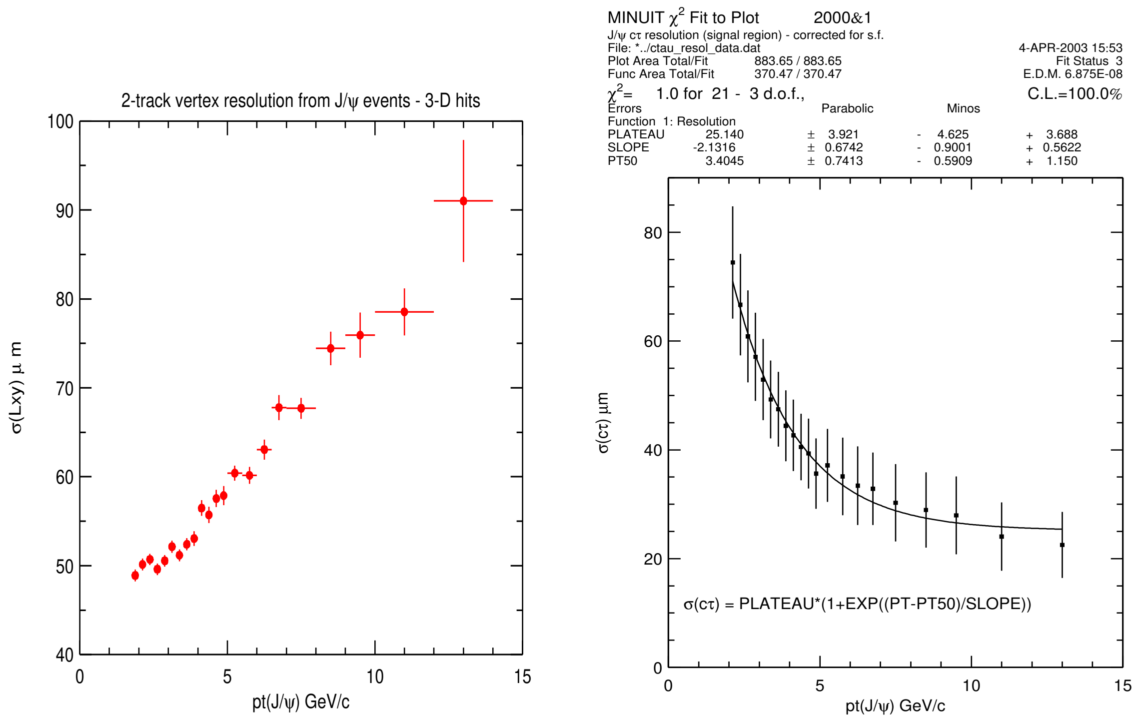

Figure 12: J/ψ L_{xy} and pseudo-$c\tau$ resolutions as a function of transverse momentum. The plot on the left is the resolution of L_{xy}

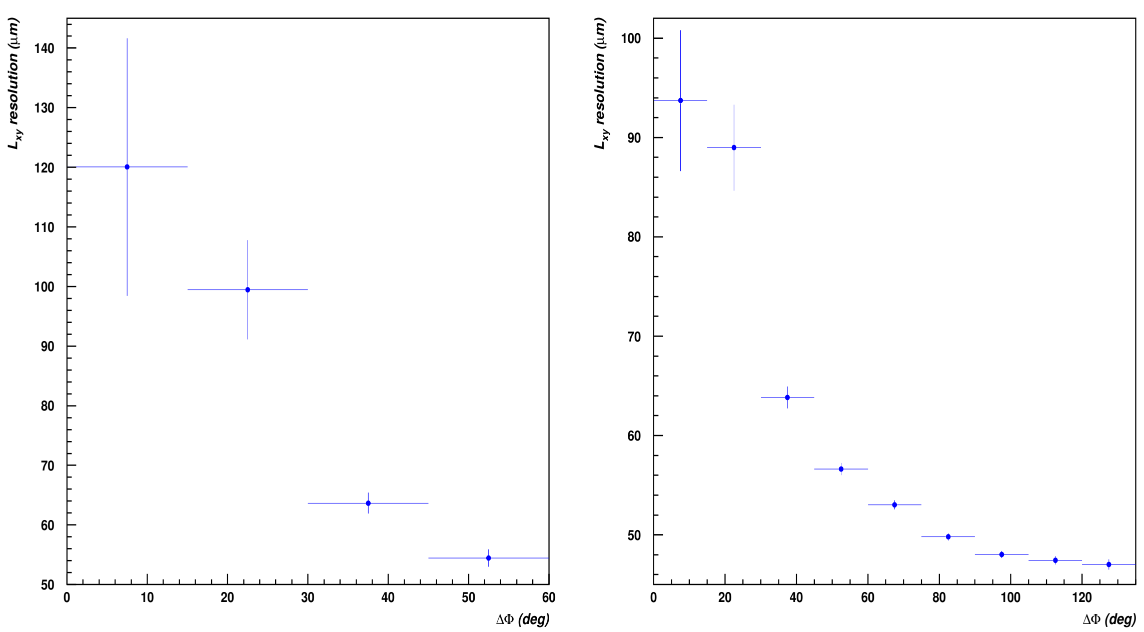

Figure 13: J/ψ L_{xy} resolutions as a function of opening angle in the $r - phi$. The plot on the left is the resolution of L_{xy} using a cut on the muon $p_T(\mu) > 3.0$ GeV/c to minimize multiple scatter and on the right is all J/ψ with $p_T(\mu) > 1.5$ GeV/c.

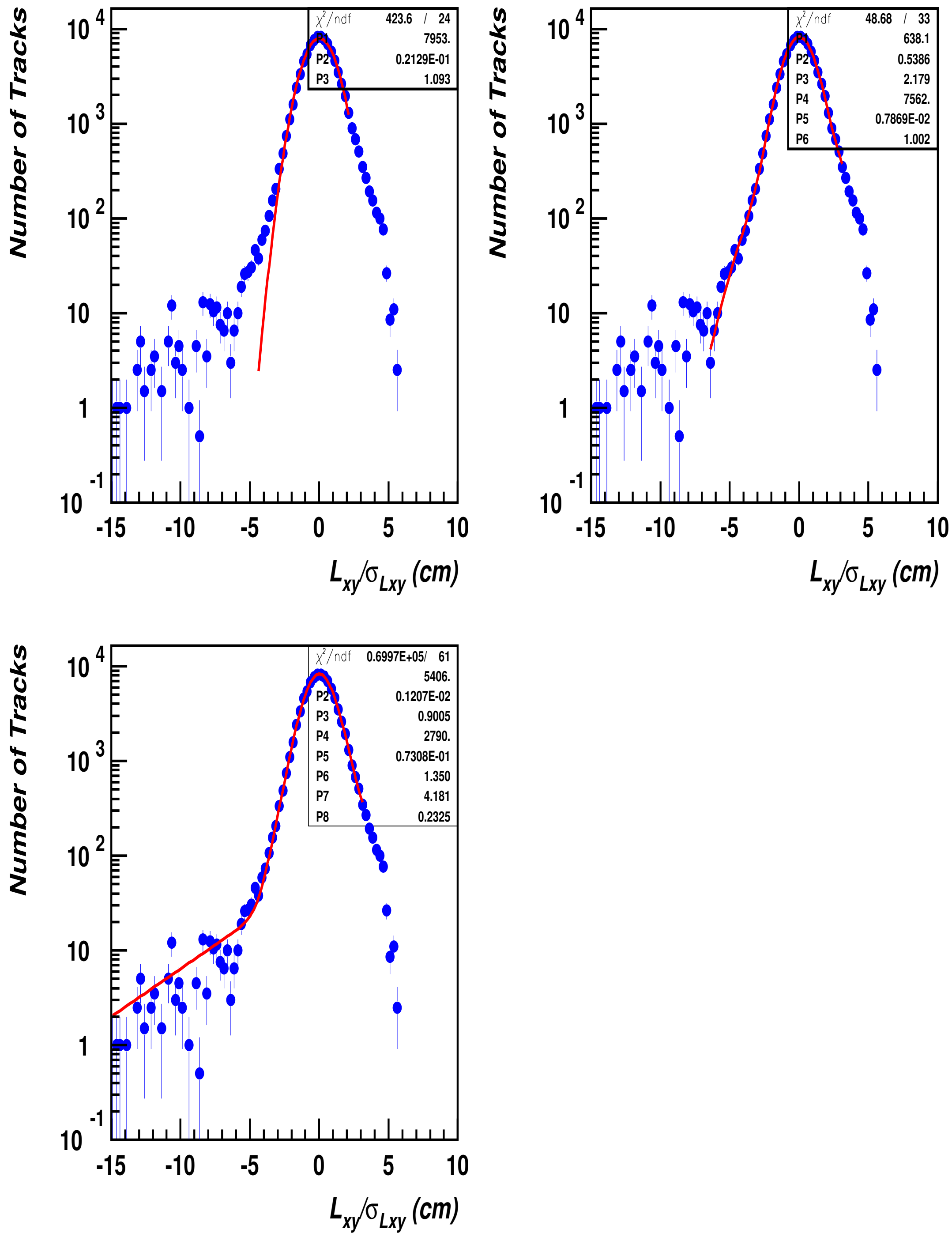

Figure 14: $L_{xy}/\sigma(L_{xy})$ pull in data - all momenta. Top left is the fit in the range (-6,3) to a single Gaussian, top right is the fit to a double Gaussian, bottom is the fit to a double Gaussian and an exponential -ve tail.

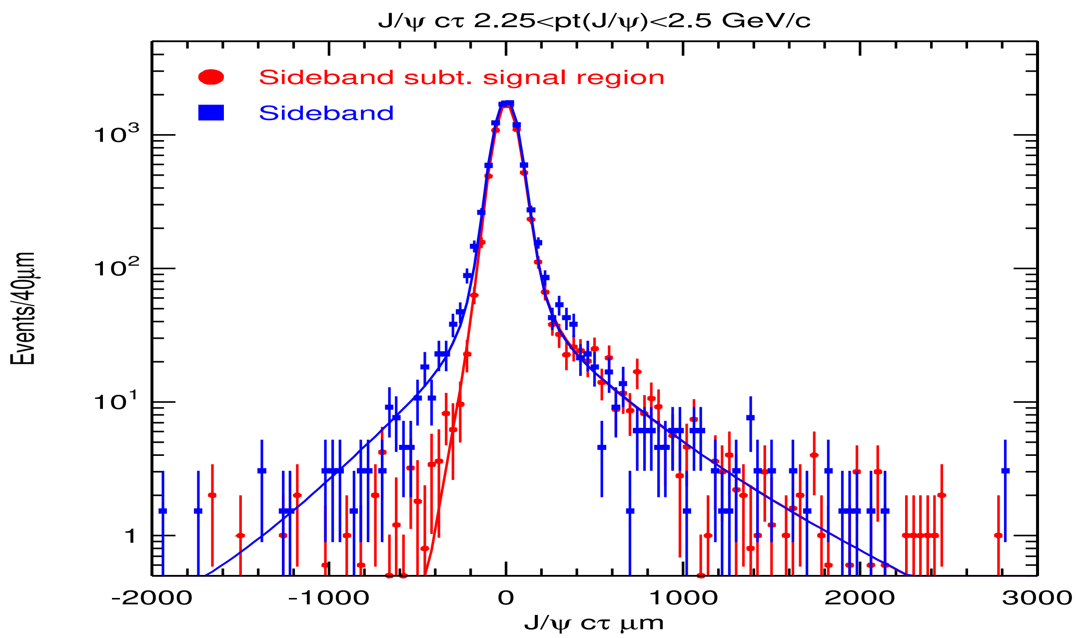

Figure 15: Background shape overlaid with the sideband subtracted signal shape and a preliminary fit. Symmetric tails in the background from fake J/ψ are not evident in the sideband subtracted mass signal region.

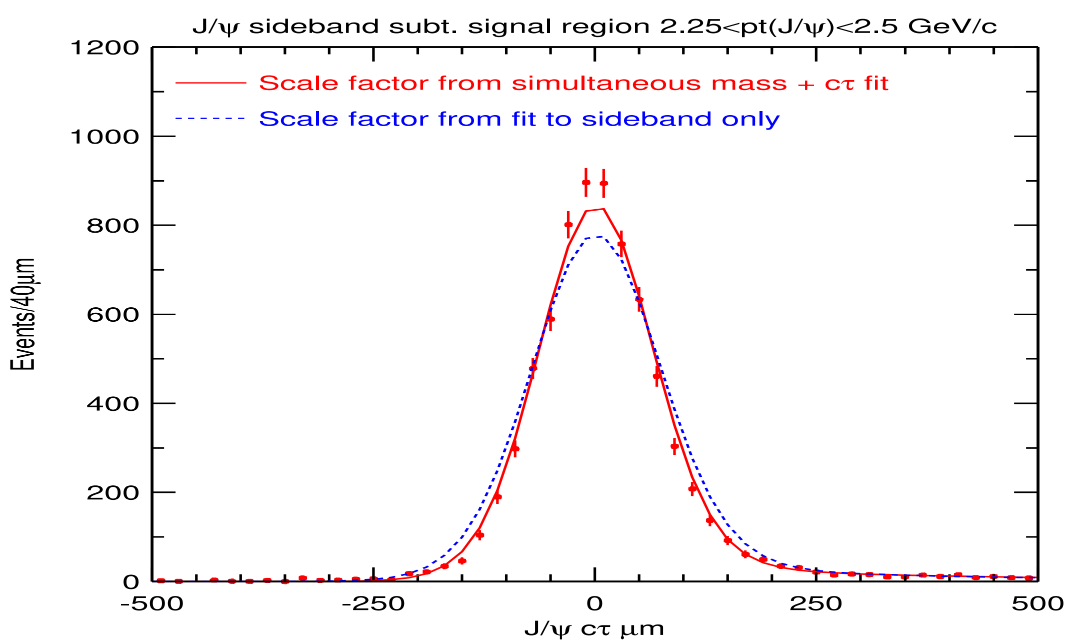

Figure 16: Fit using the same pseudo-$c\tau$ scale factor to fit 0 lifetime component in signal and background and using different scale factors.

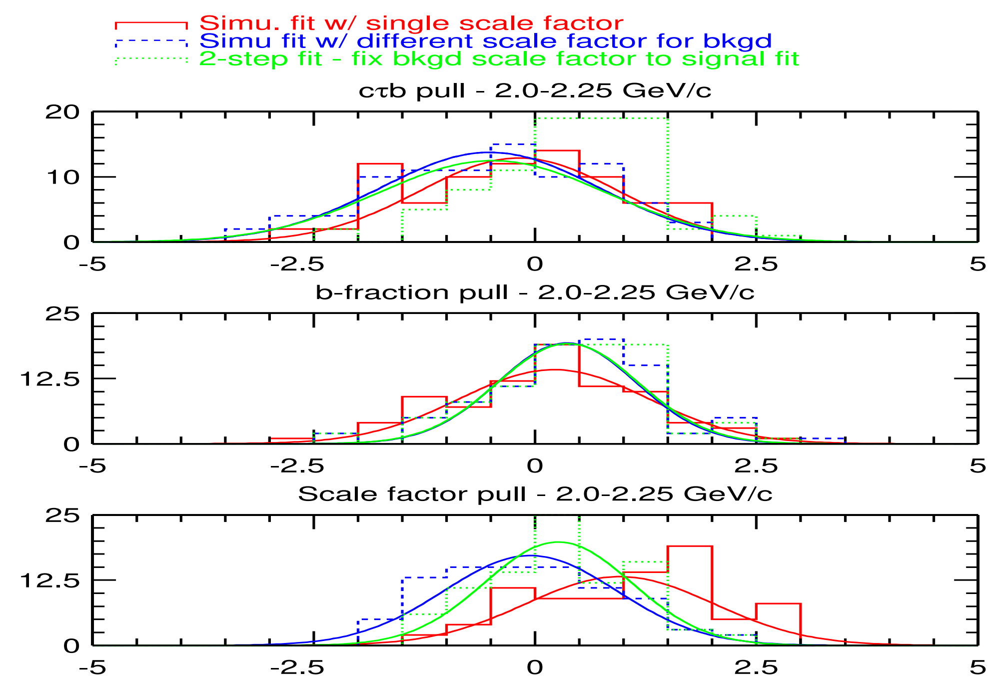

Figure 17: Pull distributions for the prompt signal scale factor, b-fraction and b-lifetime using different fit models for the scale factor. These are the results from 100 toy MC experiments.

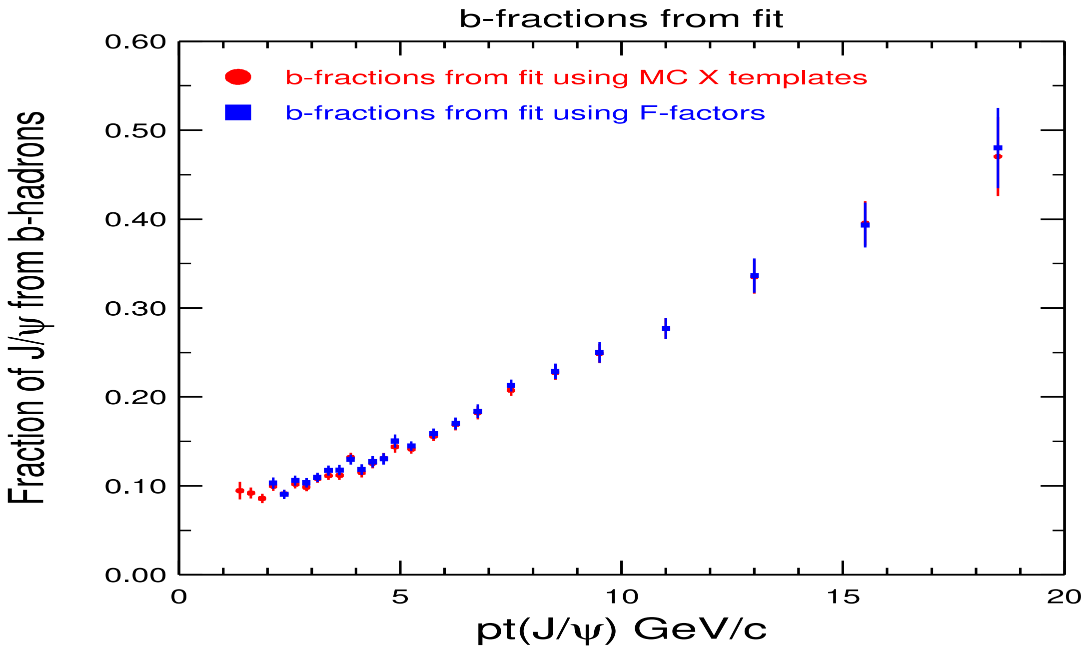

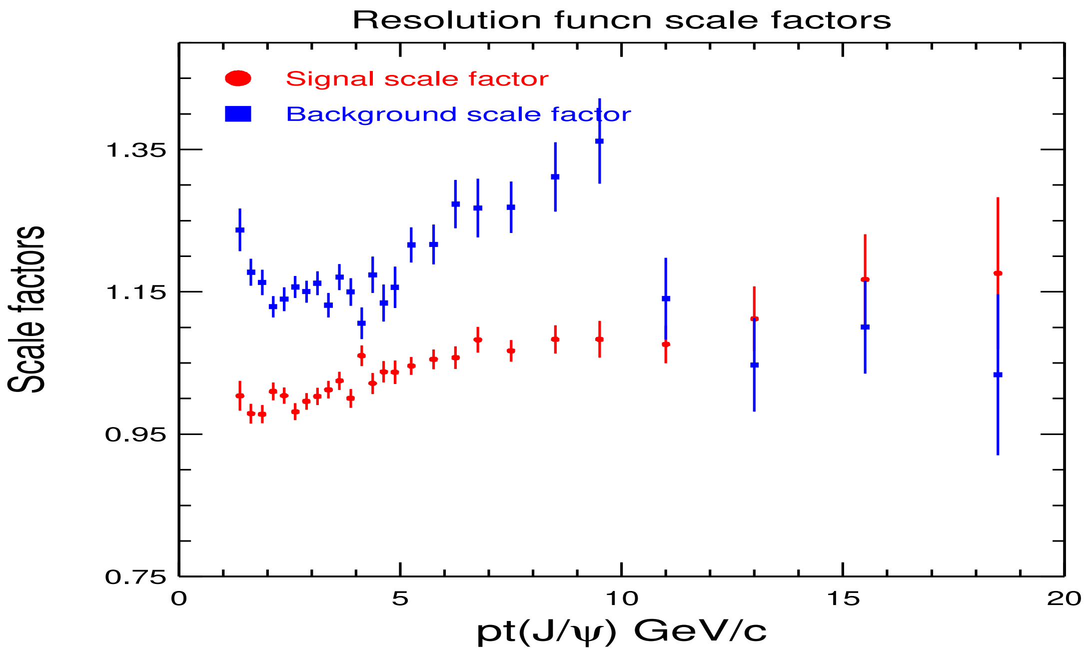

Figure 18: b-fraction as a function of J/ψ p_T bins (left). Lifetime uncertainty scale factors as a function of J/ψ p_T (right).

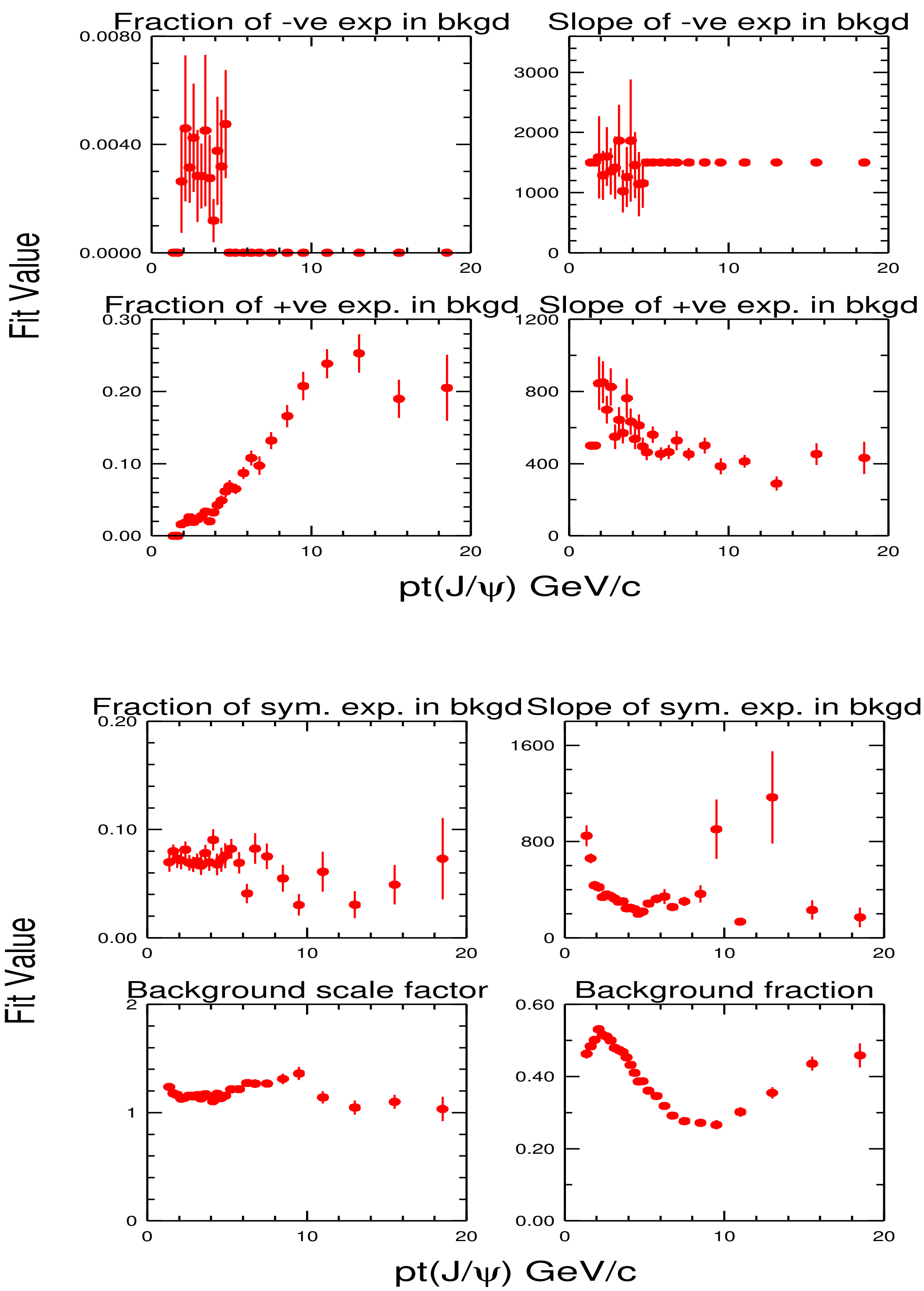

Figure 19: Lifetime background fit parameters as a function of J/ψ p_T returned from the simultaneous J/ψ mass and b-fraction fit.

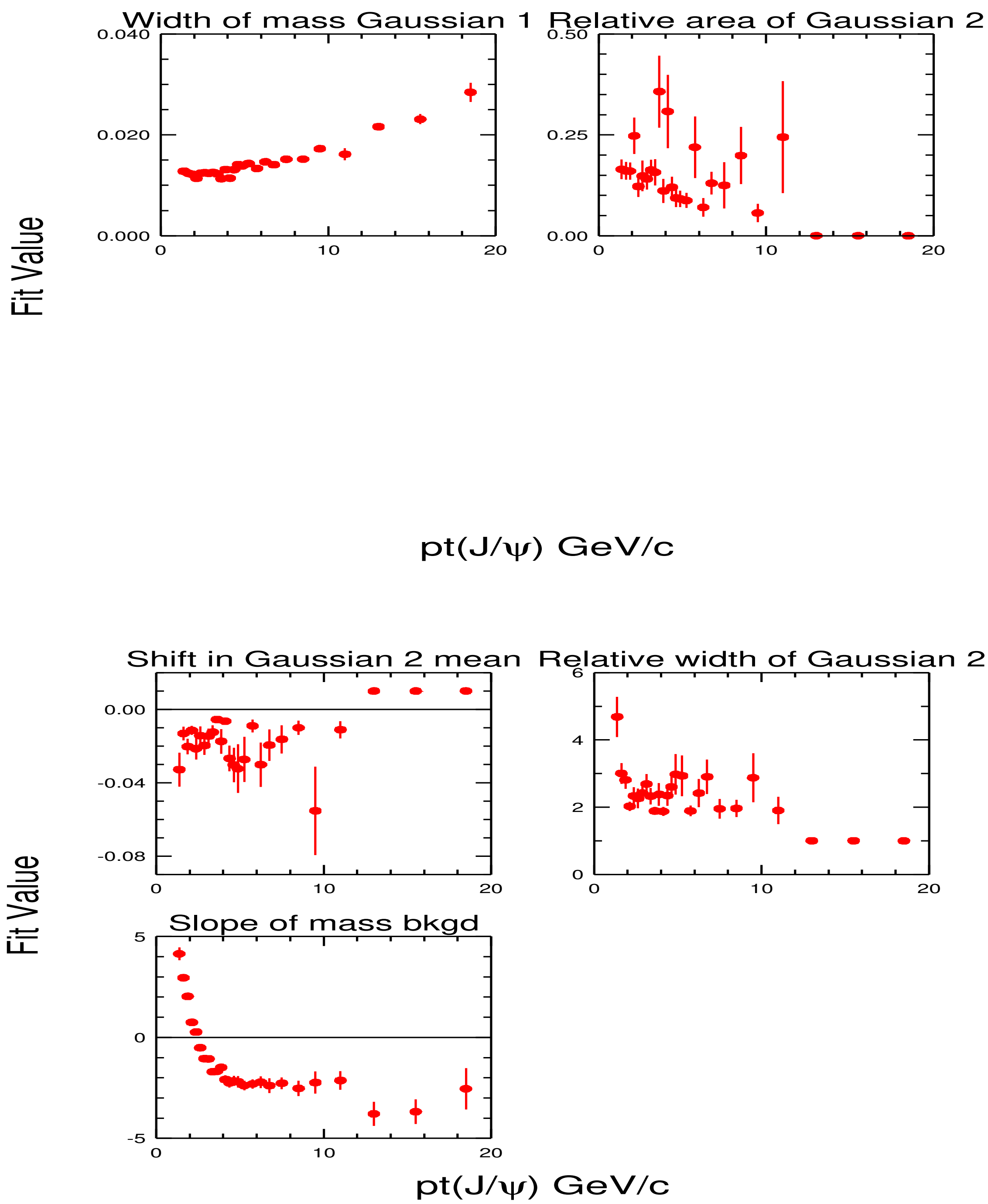

Figure 20: Invariant mass fit parameters as a function of J/ψ p_T returned from the simultaneous J/ψ mass and b-fraction fit.

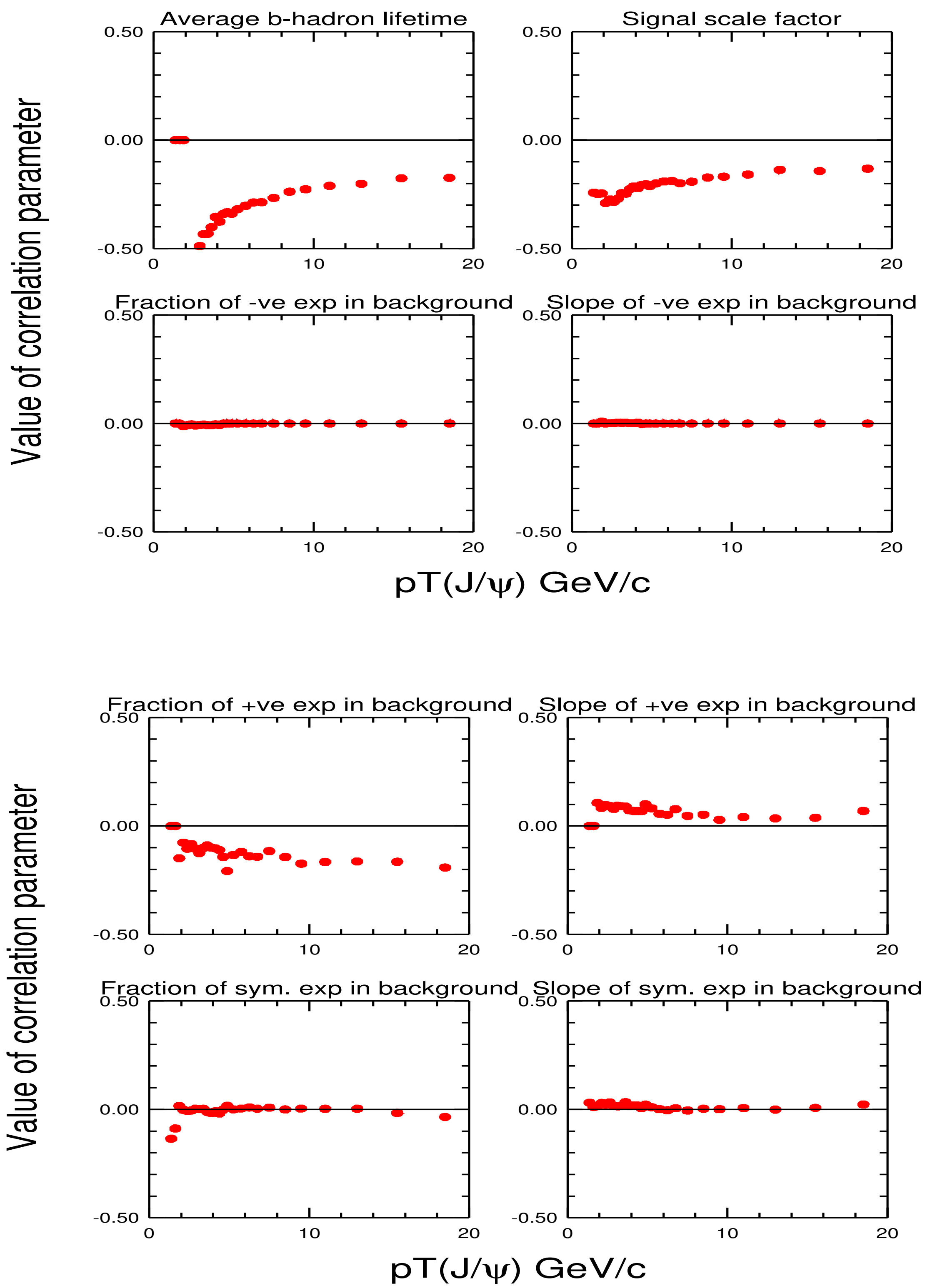

Figure 21: Value of the correlation matrix elements of the b fraction paramater versus other fit parameters

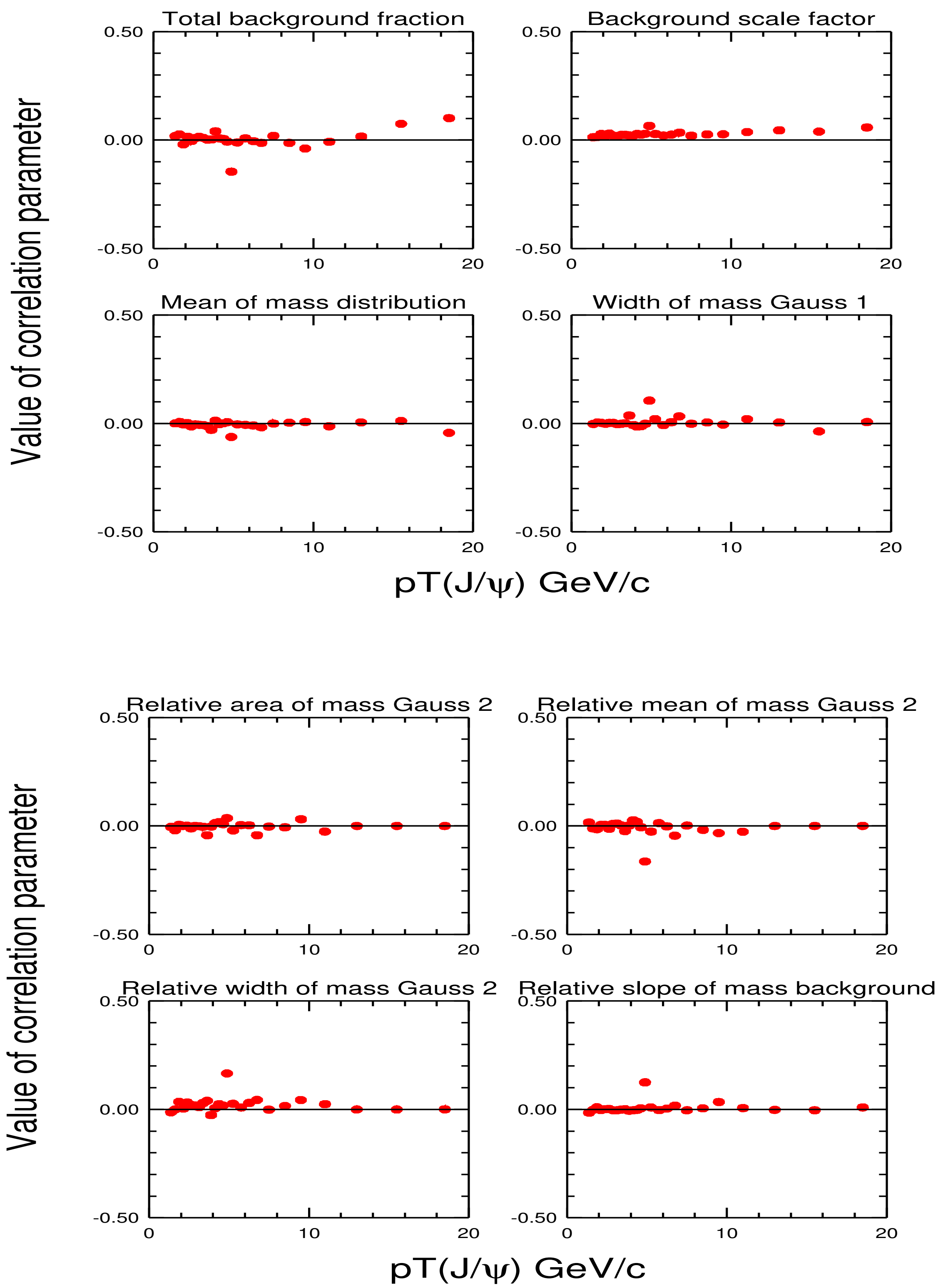

Figure 22: Value of the correlation matrix elements of the b fraction paramater versus other fit parameters

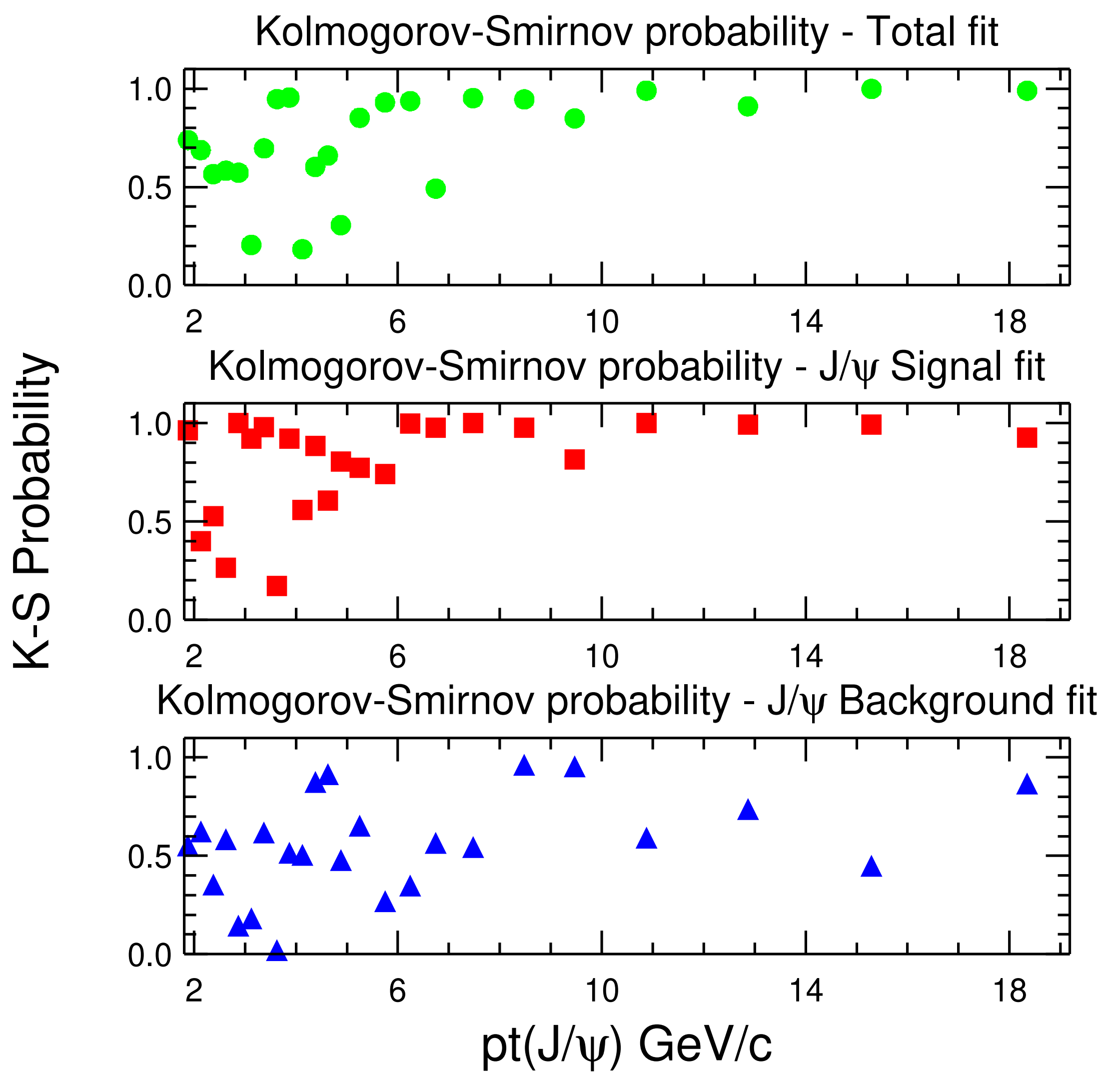

Figure 23: Probability values returned from a Kolmogorov-Smirnov comparison between the data distributions and the final fit distributions.

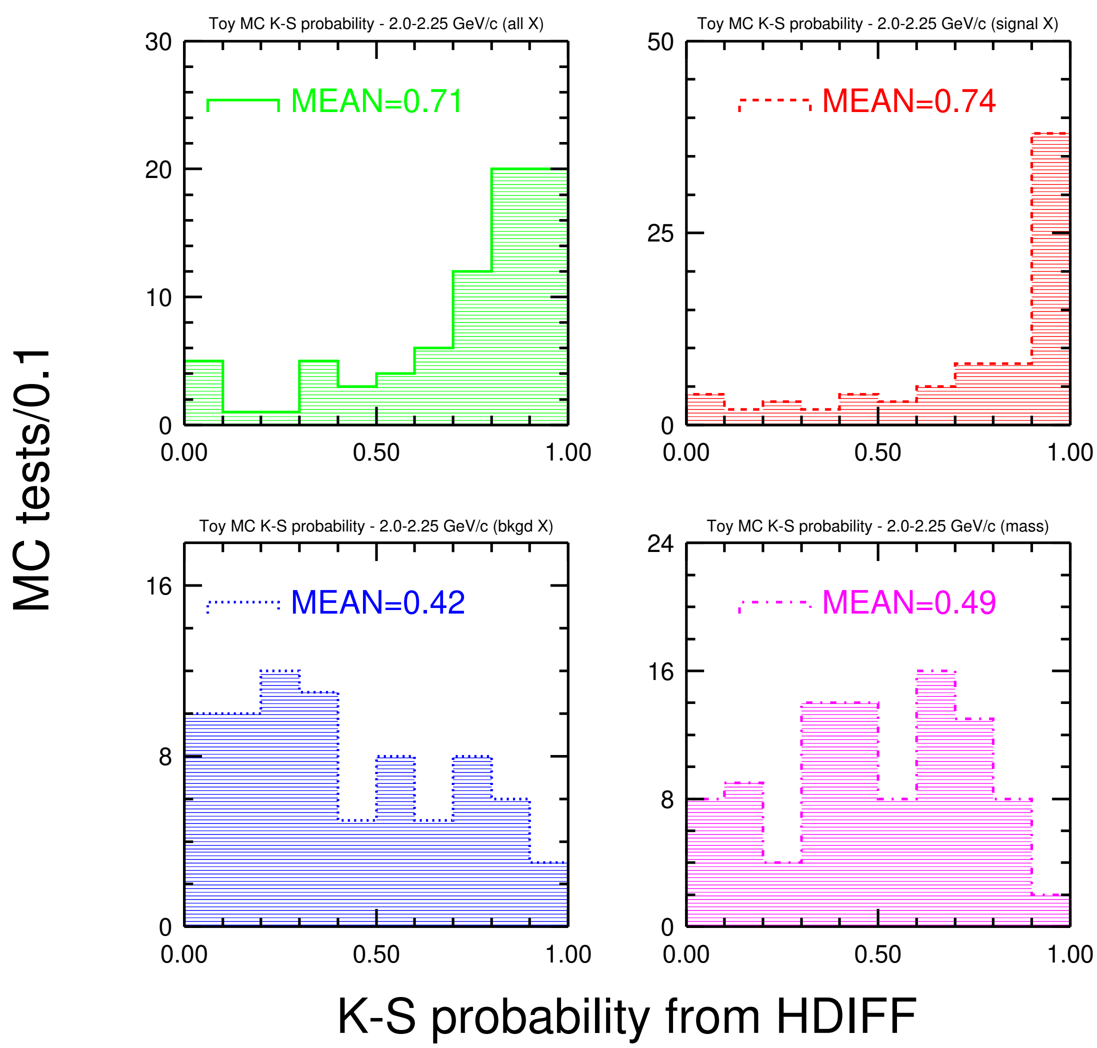

Figure 24: Distribution of probability values returned from a Kolmogorov-Smirnov comparison between toy MC distributions and the corresponding fit distributions. About 80 statistically independent MC samples generated to match the data distributions of X and $M(\mu\mu)$ in the bin 2.0-2.25 GeV/c are used.

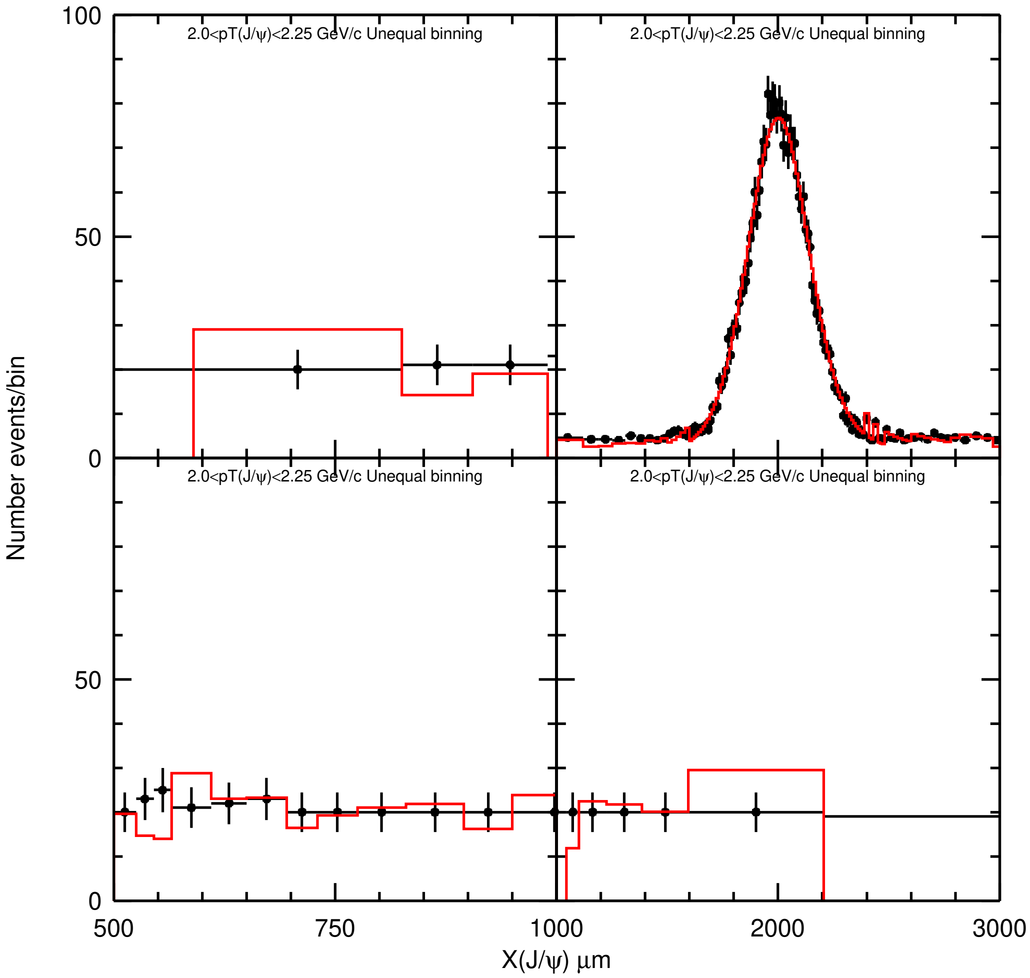

Figure 25: Distribution of the J/ψ pseudo-lifetime and the total fit overlaid using unequal bin sizes in the range 2.0-2.25 GeV/c.

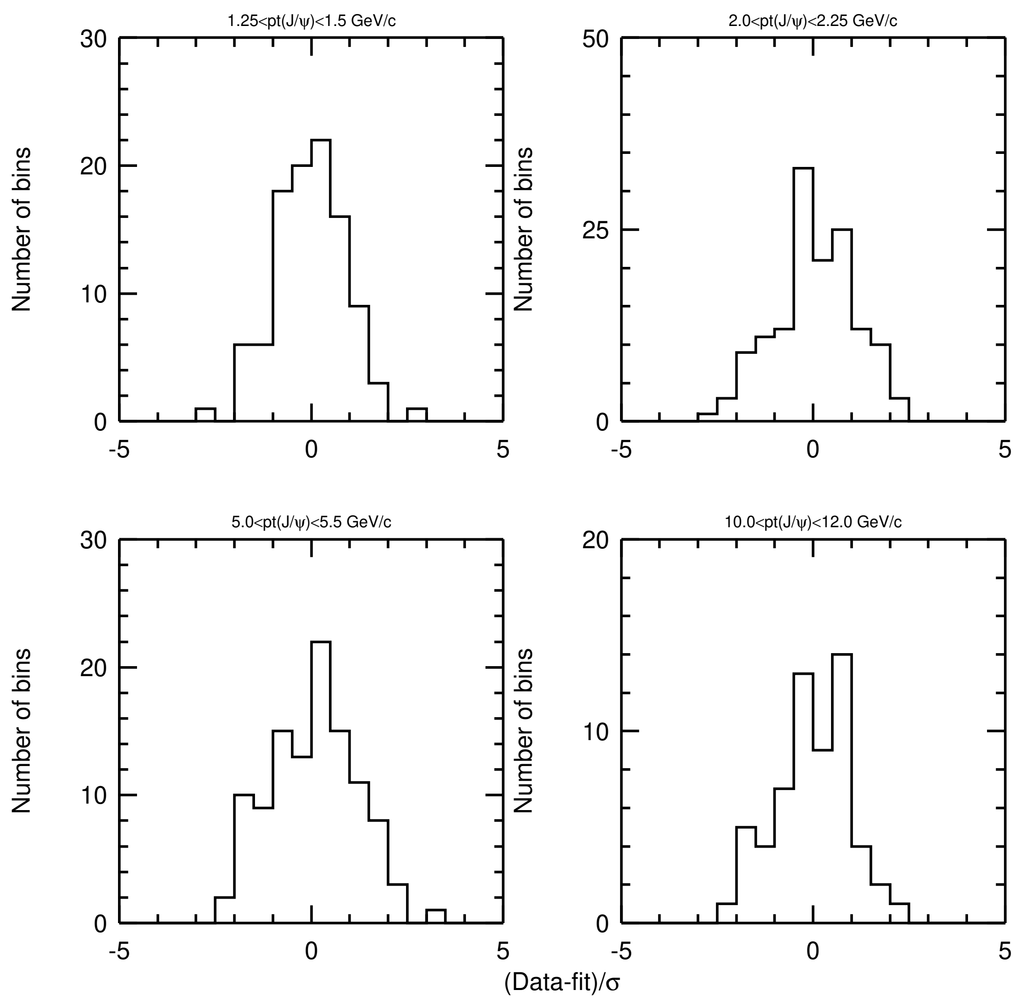

Figure 26: The distribution of the (data-fit)/statistical error using unequal bin sizes so that the statistical errors are Gaussian in 4 represenative transverse momentum bins

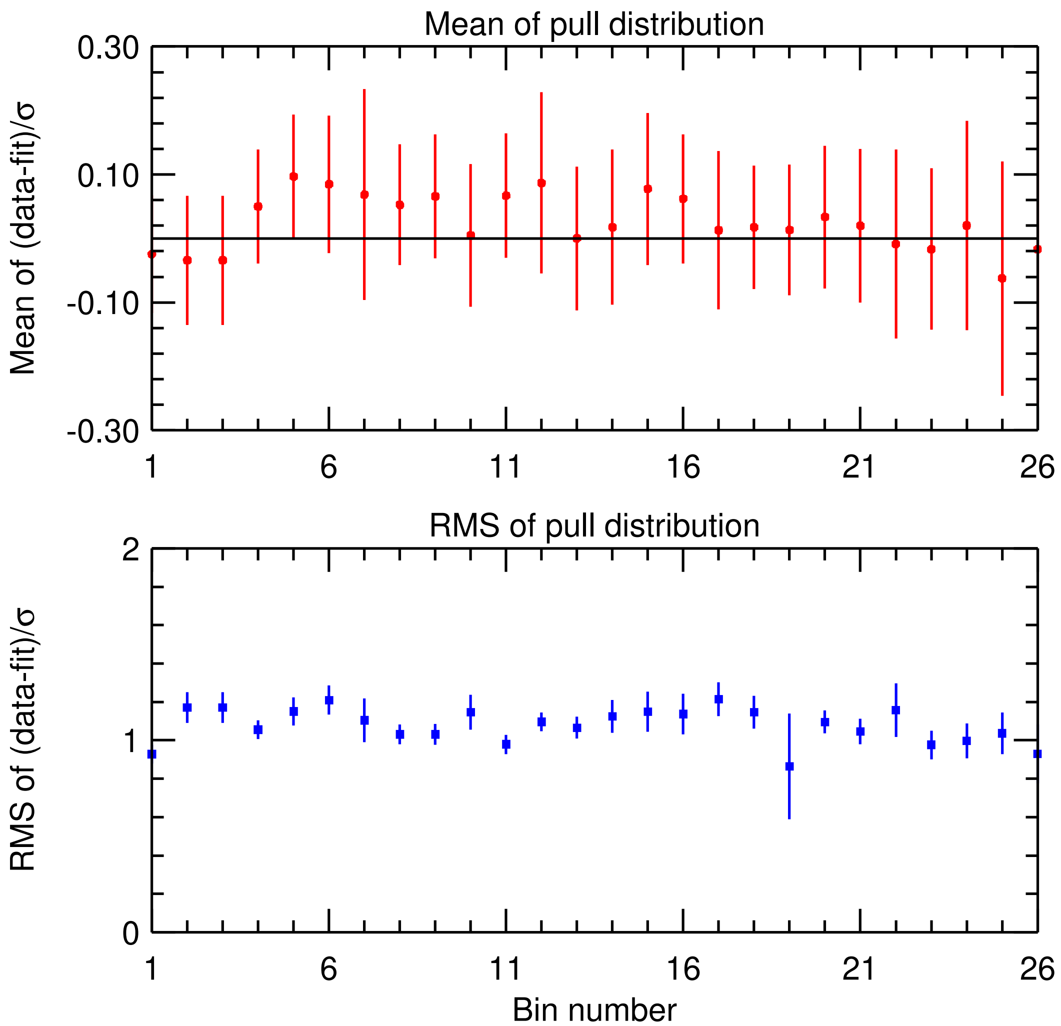

Figure 27: The mean and RMS of the (data-fit)/error distributions in all 26 transverse momentum bins.

2.0 - 2.25 GeV/c   5-5.5 GeV/c   10 - 12 GeV/c

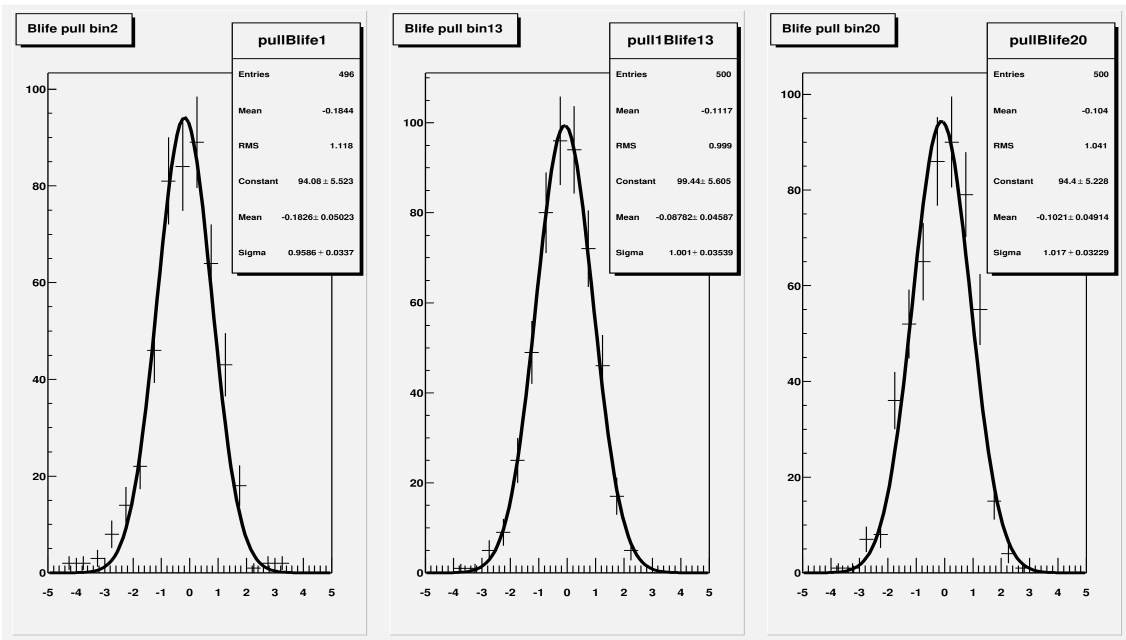

$MEAN = 0.18 \pm 0.05$ $\sigma = 0.96 \pm 0.03$

$MEAN = -0.09 \pm 0.05$ $\sigma = 1.00 \pm 0.04$

$MEAN = -0.10 \pm 0.05$ $\sigma = 1.02 \pm 0.03$

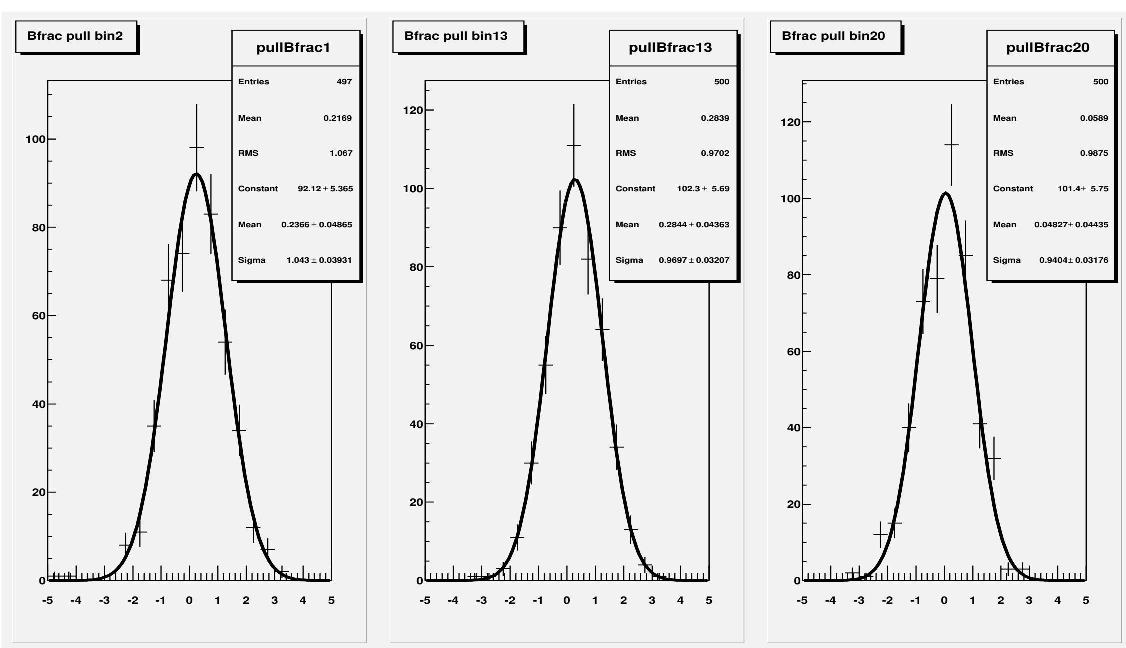

$MEAN = 0.24 \pm 0.05$ $\sigma = 1.04 \pm 0.04$

$MEAN = 0.28 \pm 0.04$ $\sigma = 0.97 \pm 0.04$

$MEAN = 0.05 \pm 0.05$ $\sigma = 0.94 \pm 0.03$

Figure 28: Reconstructed versus generated b fractions and b lifetimes in a Toy MC sample generated to match the data distributions in 3 transverse momentum bins. The top plots are for the b hadron inclusive lifetime and the bottom plots are the pull distributions for the b-fractions.

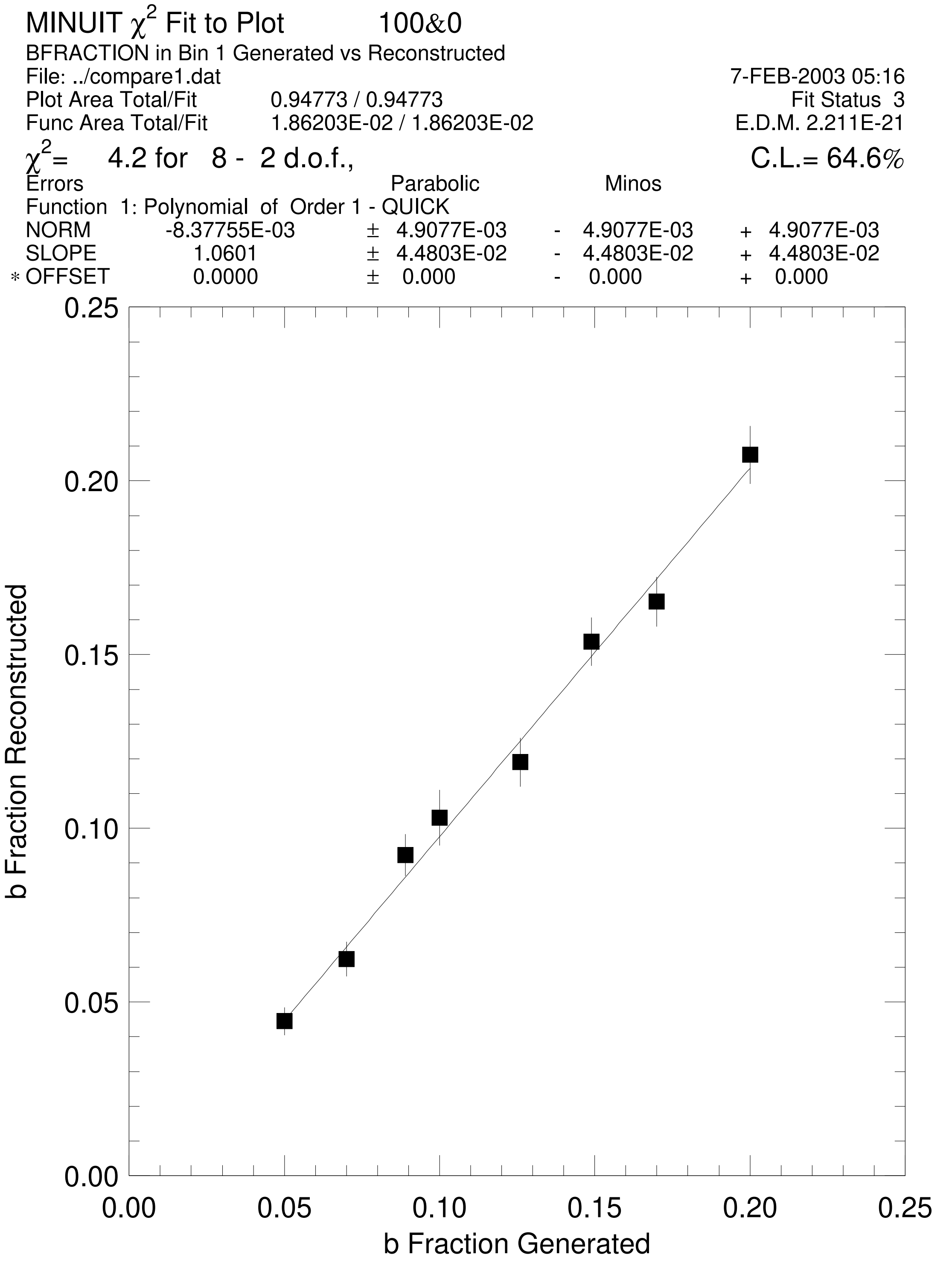

Figure 29: Reconstructed versus generated b fractions in a Toy MC sample generated to match the data distributions in bin $2 - 2.25$ GeV/c.

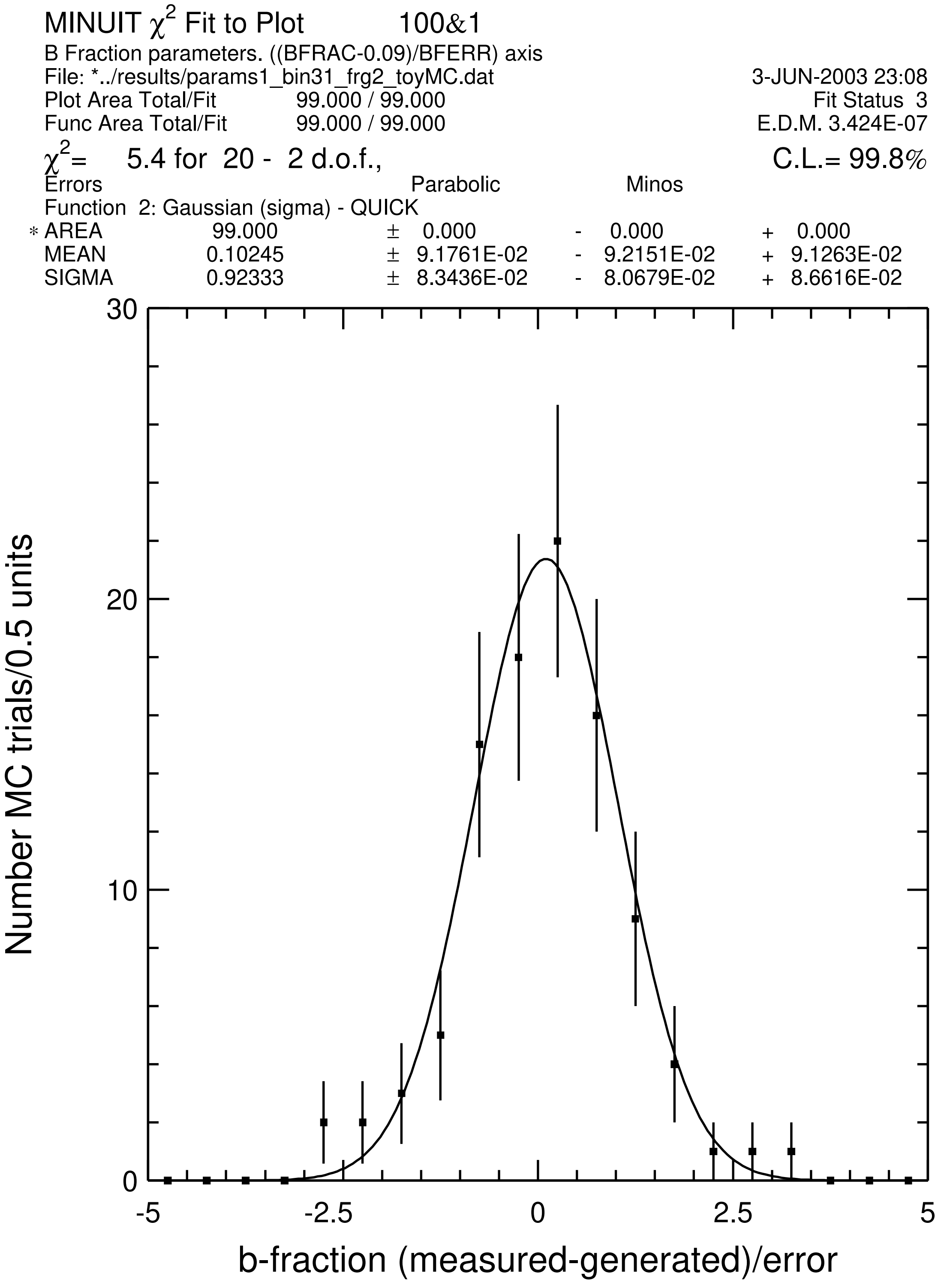

Figure 30: Reconstructed versus generated b fractions in a toy MC sample generated to match the data distributions in the 1.25 - 1.5 GeV/c momentum bin.

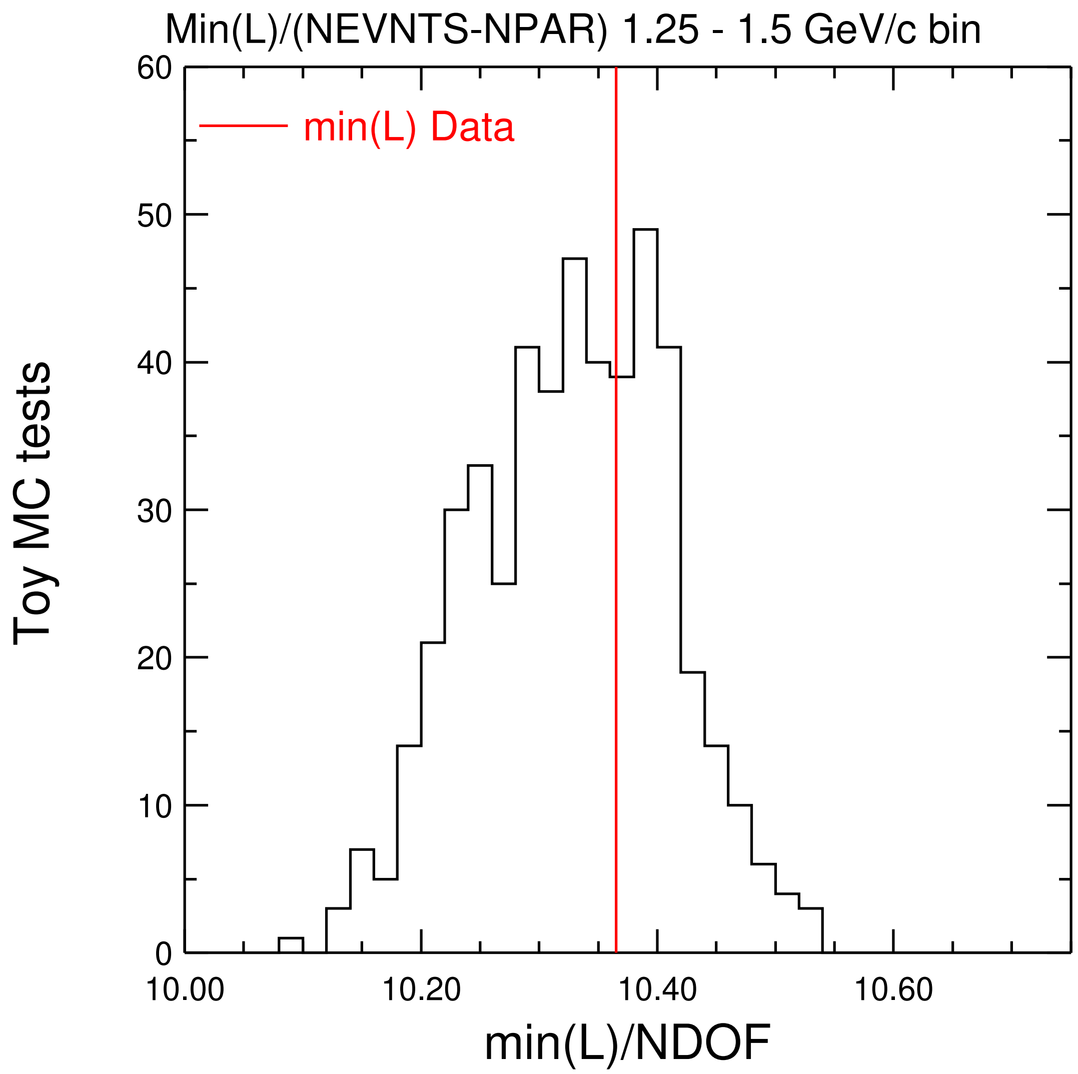

Figure 31: The distribution of the minimum Likelihood value in toy MC samples generated to match the data distributions in the 1.25 - 1.5 GeV/c momentum bin. The straight line is the value obtained from the data.

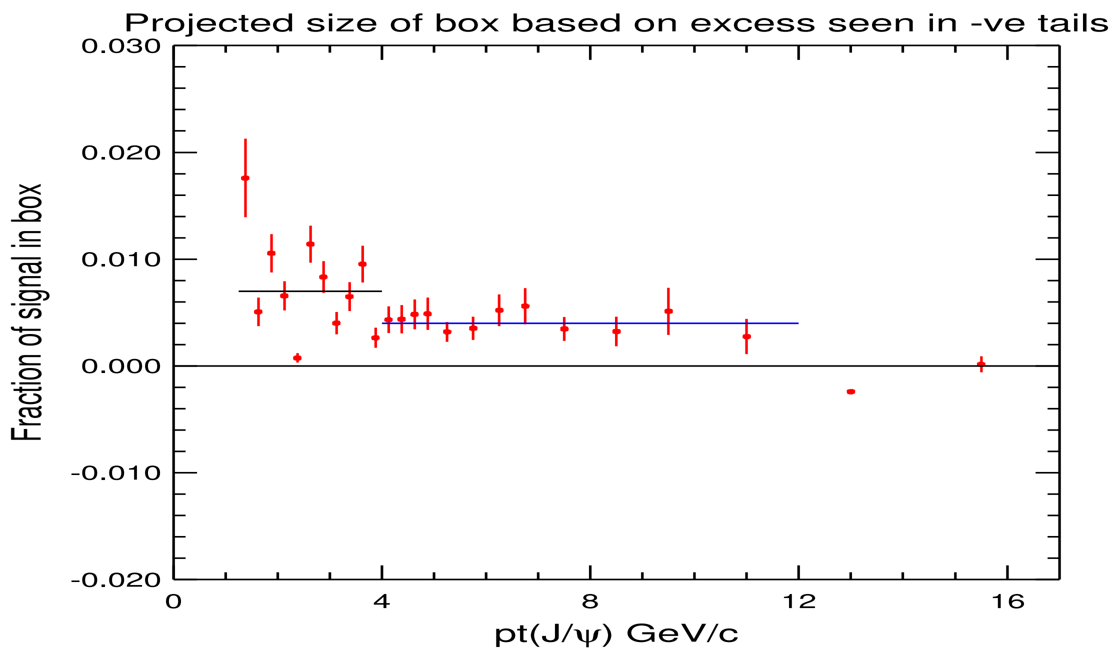

Figure 32: Size of the box used in the loglikelihood fit estimated from the excess of data events compared with the fit in the -ve x region.

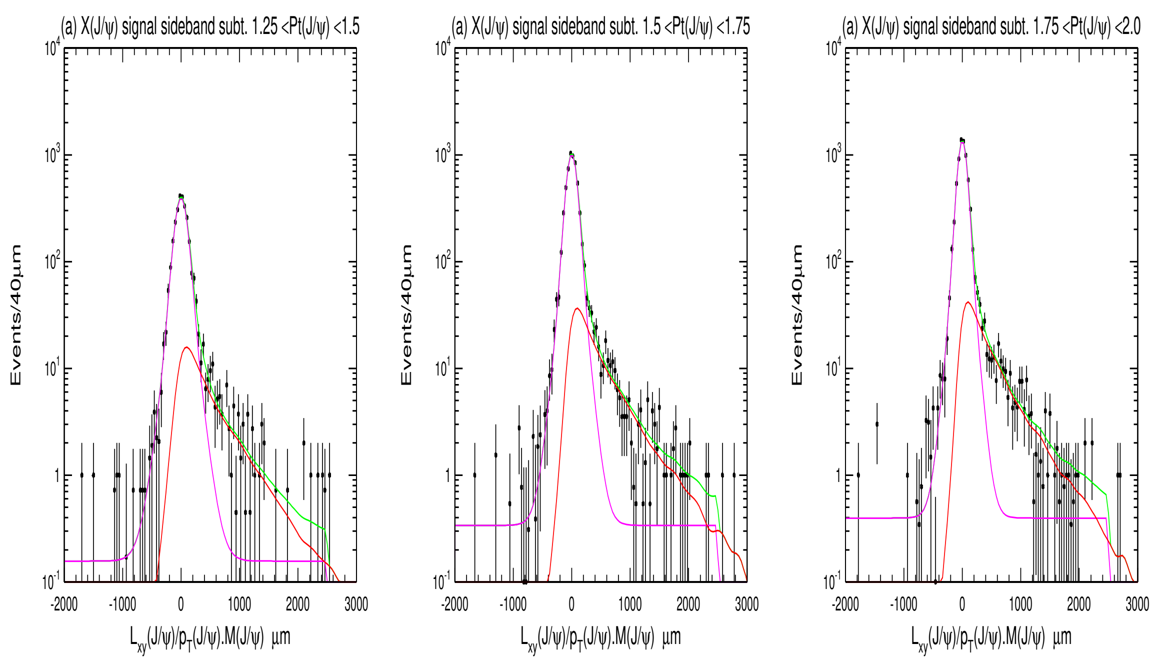

Figure 33: Projection of the box fit in the x signal region in the lowest transverse momentum bins.

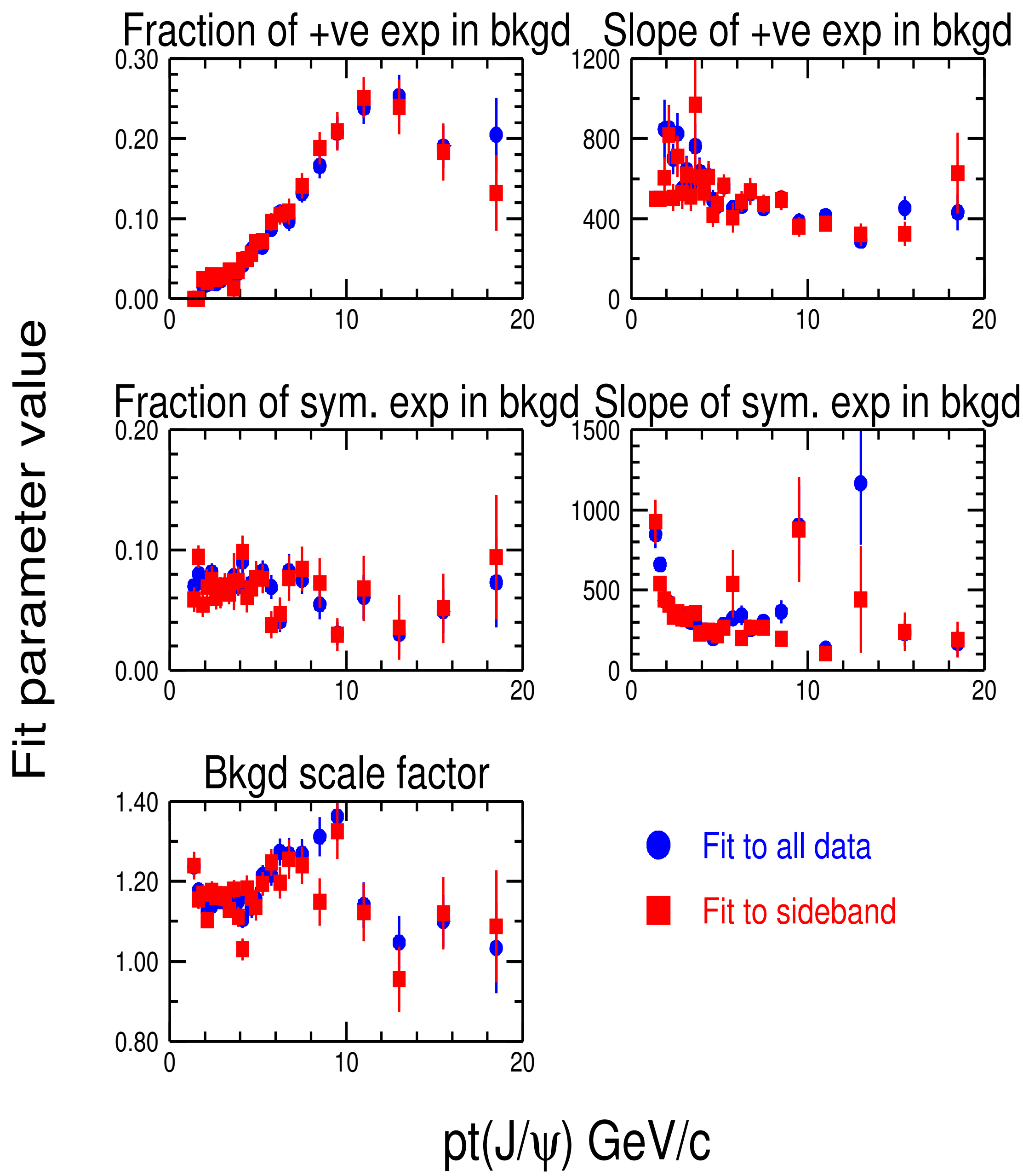

Figure 34: The background parameters extracted from the fit to the whole mass range and the fit to the sideband mass region only are overlaid

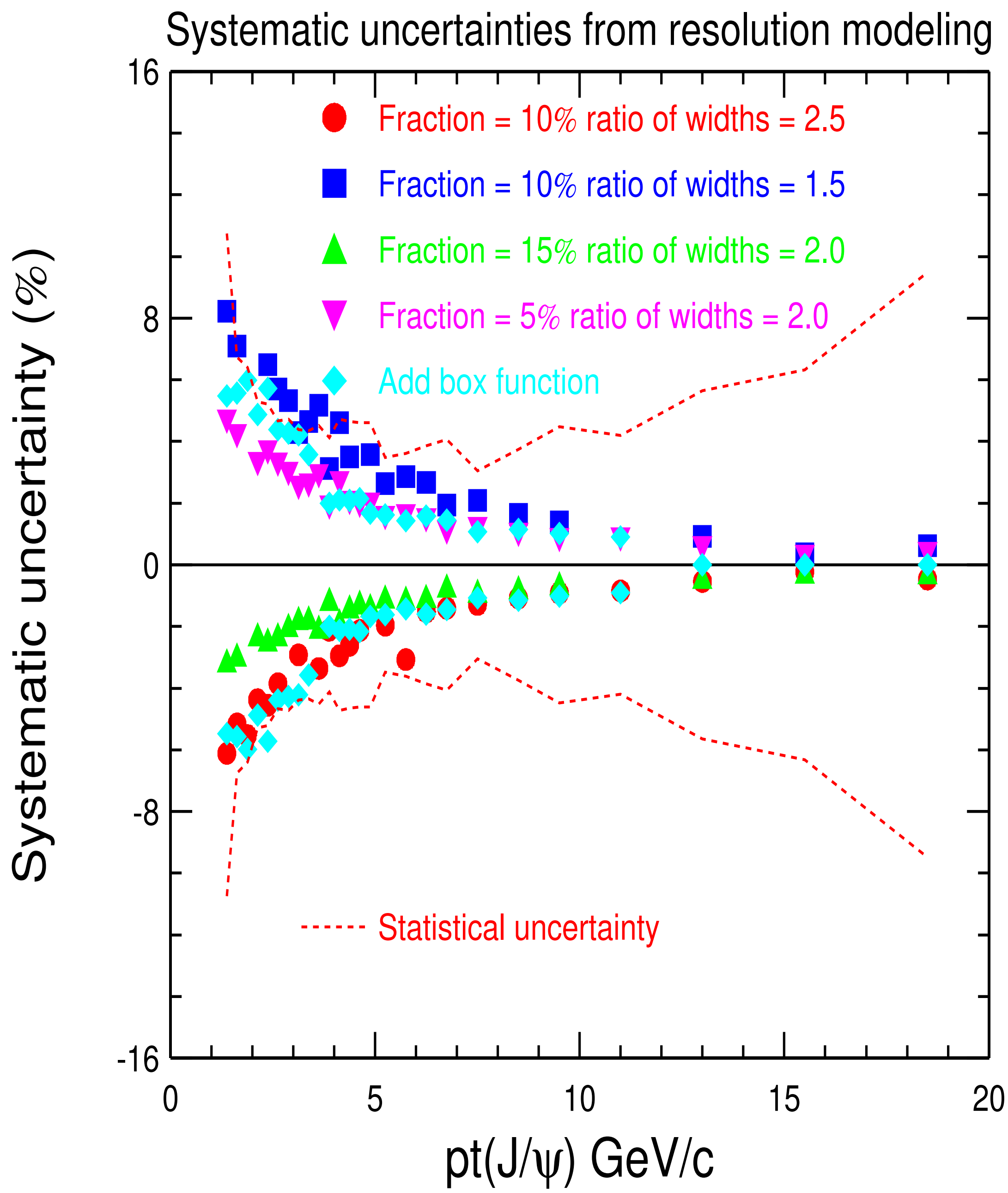

Figure 35: Plot of the systematic uncertainties listed in Table 11

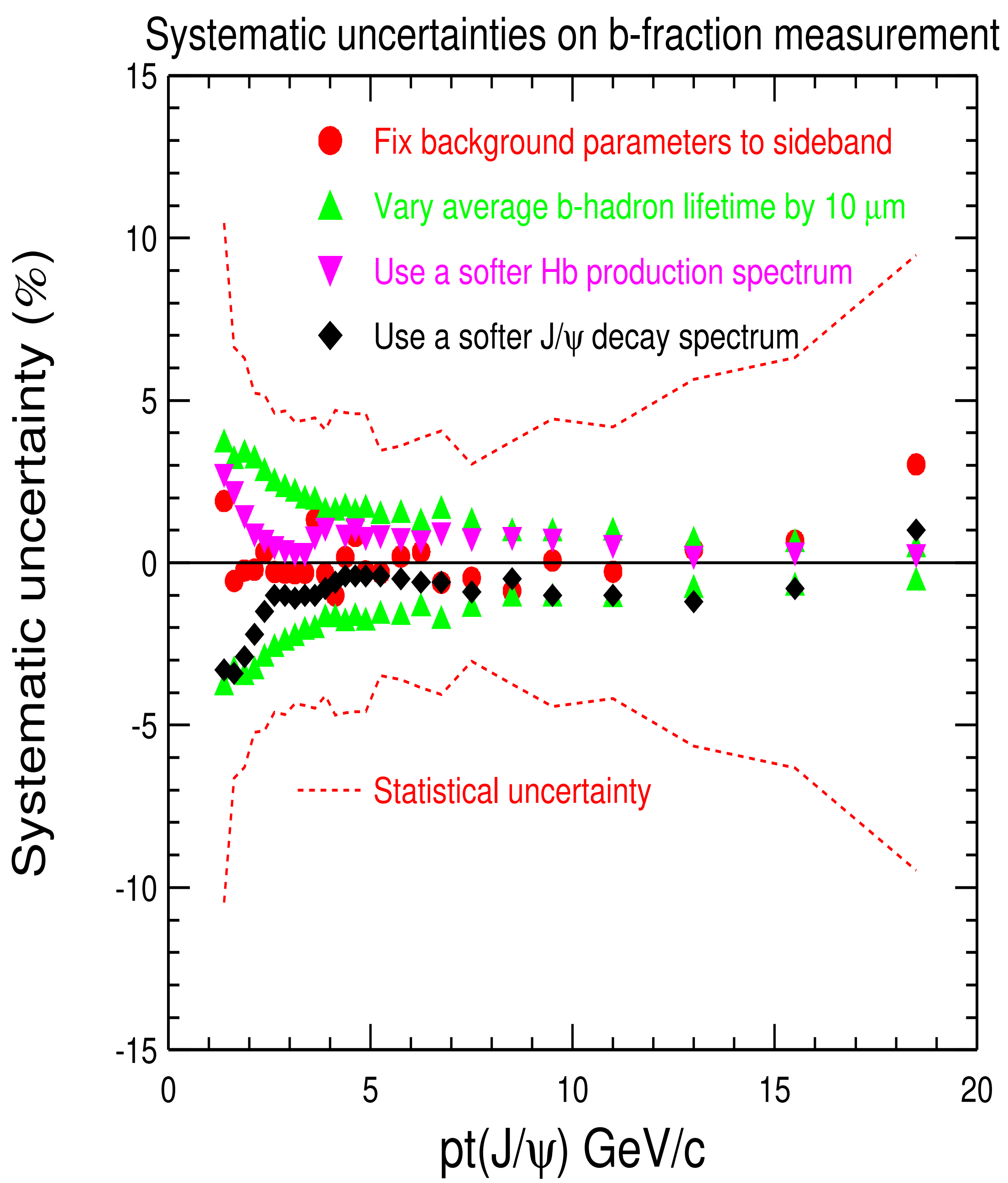

Figure 36: Plot of the systematic uncertainties listed in Table 12

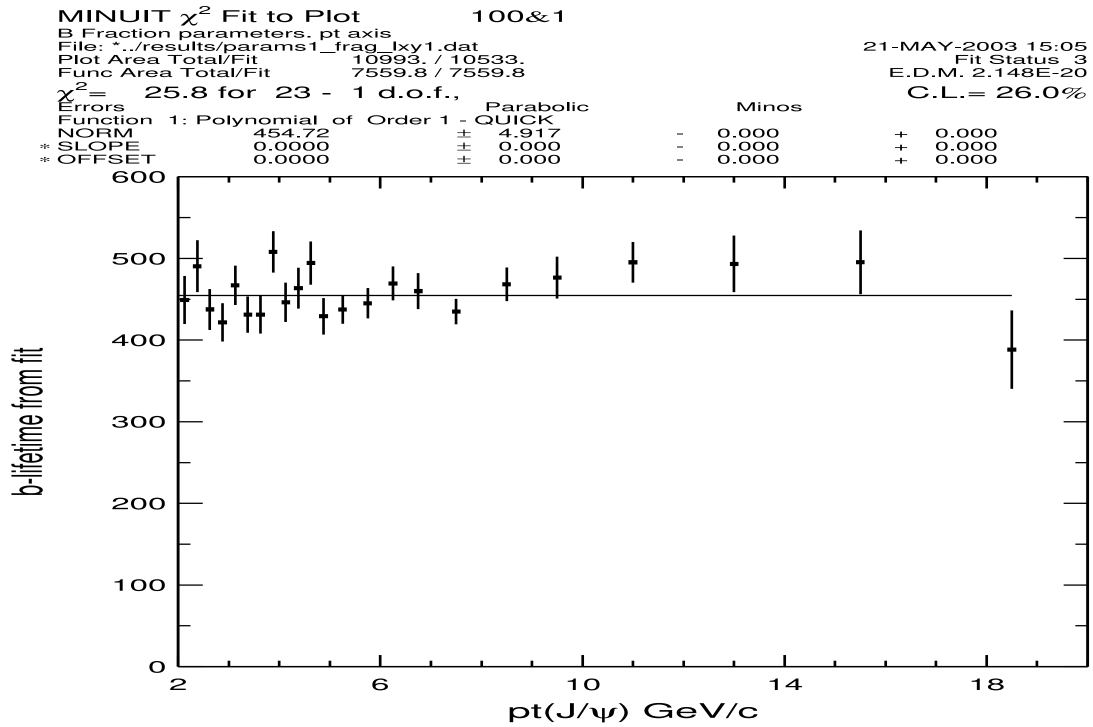

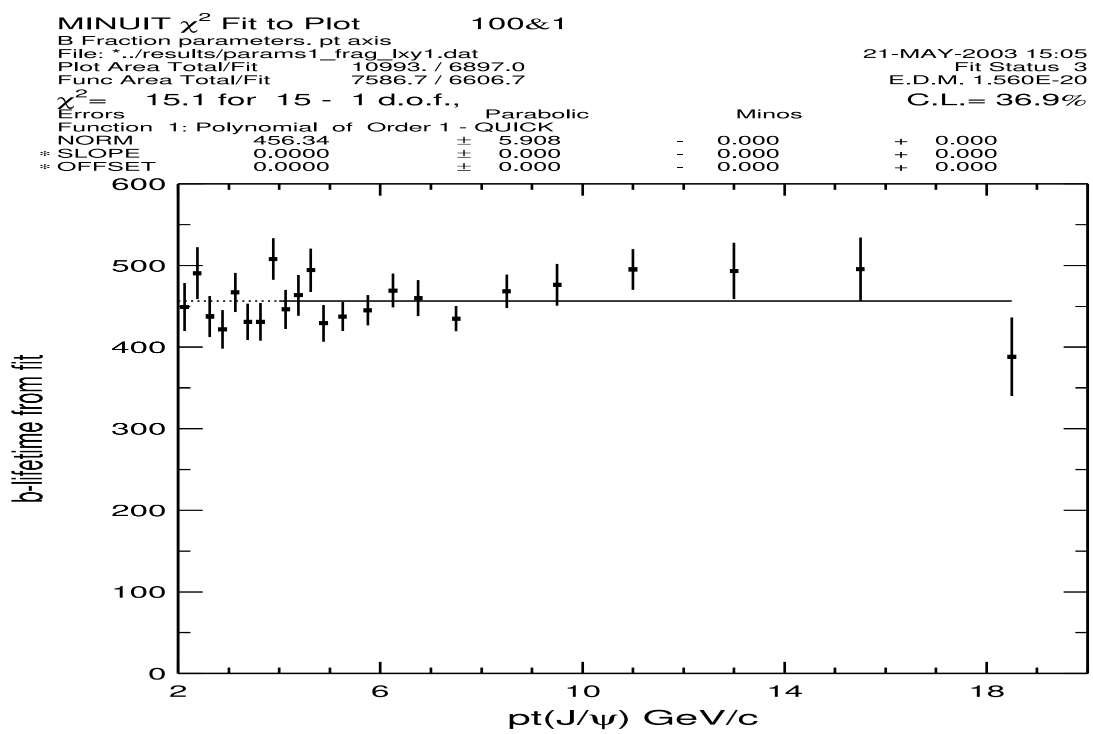

Figure 37: B lifetime as a function of J/ψ p_T bins using F-factor convolutions in the fitting procedure. On the left is a straight line fit to the transverse momentum range > 2 GeV/c, $< c\tau_b >= 455 \pm 5\mu$m and to the right is the fit to the range > 5 GeV/c, $< c\tau_b >= 456 \pm 6\mu$m

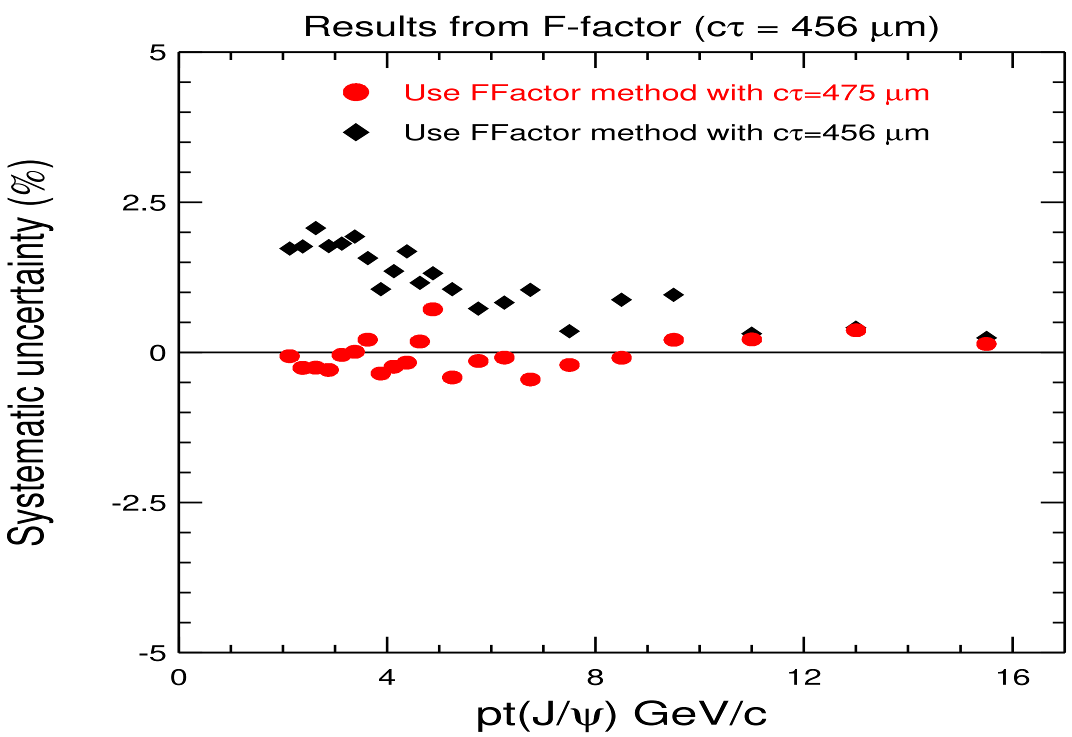

Figure 38: Difference in the b-fraction extracted using the F-factor method with lifetime fixed and the method using MC templates of X as a function of $p_T(J/\psi)$ and the value of the lifetime.

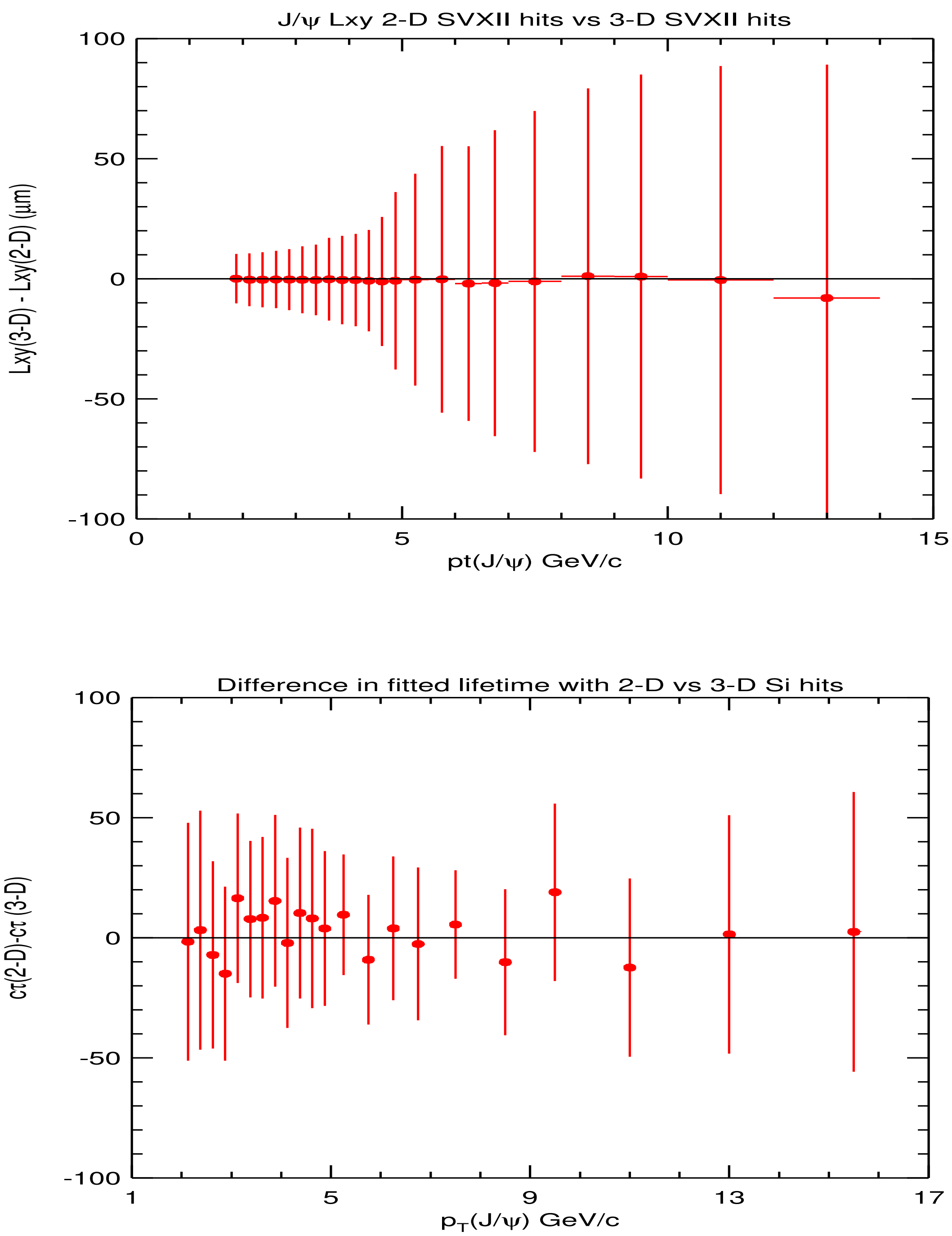

Figure 39: Difference in L_{xy} using 2-D and 3-D Si hits (top). b inclusive lifetime values calculated from fits to data using 3-D and 2-D Si hit information only. Note that there are larger backgrounds present when only 2-D hits are used.

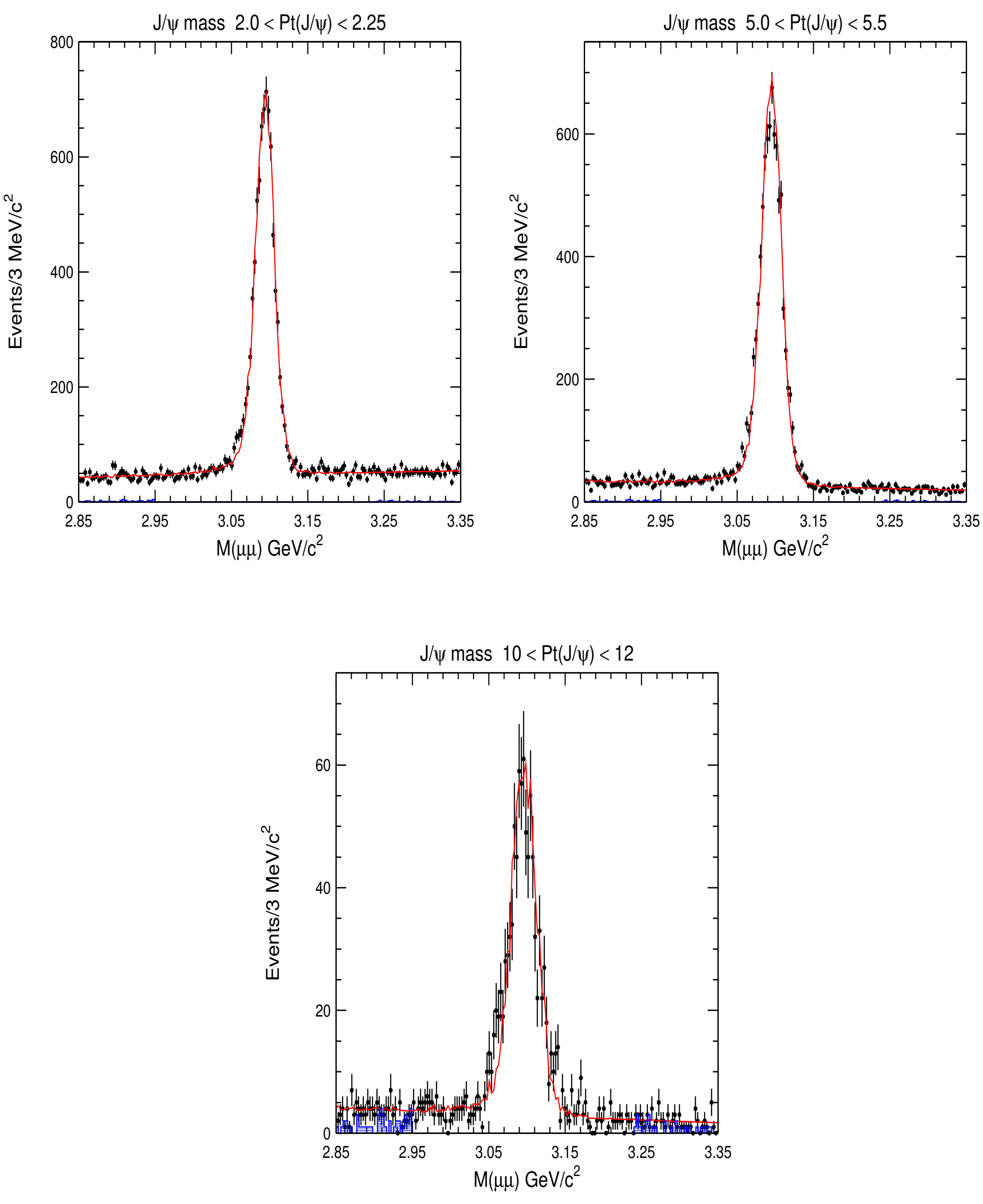

Figure 40: The histograms are MC realistic $\mu\mu$ invariant mass distributions obtained from the default SVXII simulation and the points with error bars are the data.

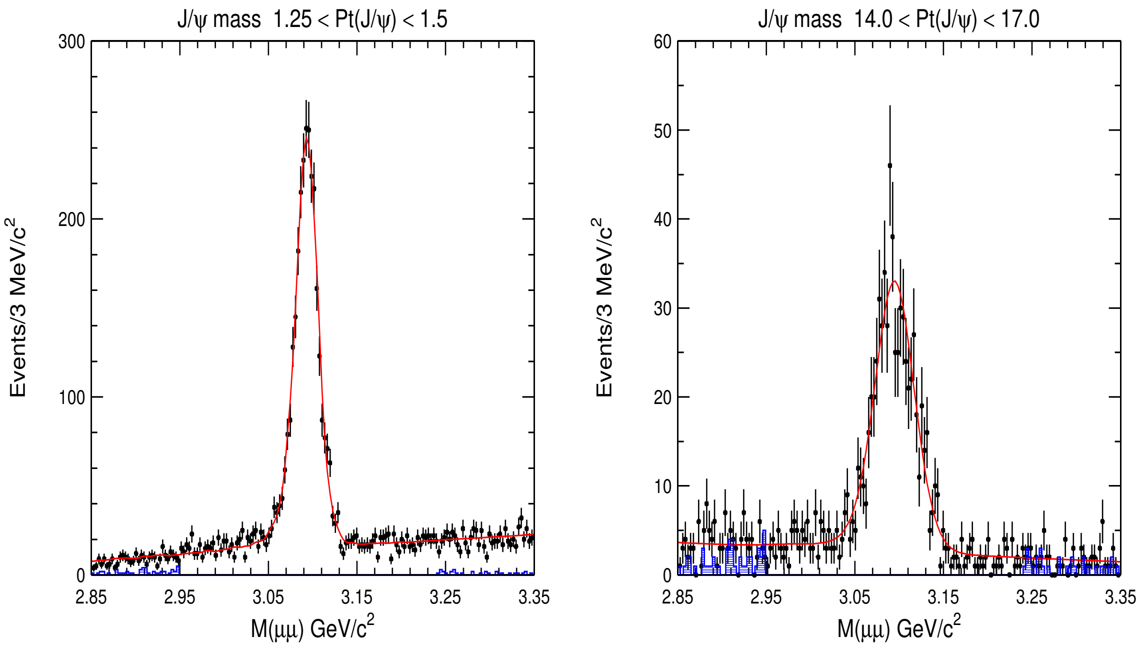

Figure 41: MC binned $\mu\mu$ invariant mass templates obtained from default 4.9.1 realistic SVXII simulation after an extra Gaussian smearing is applied to improve agreement with data.

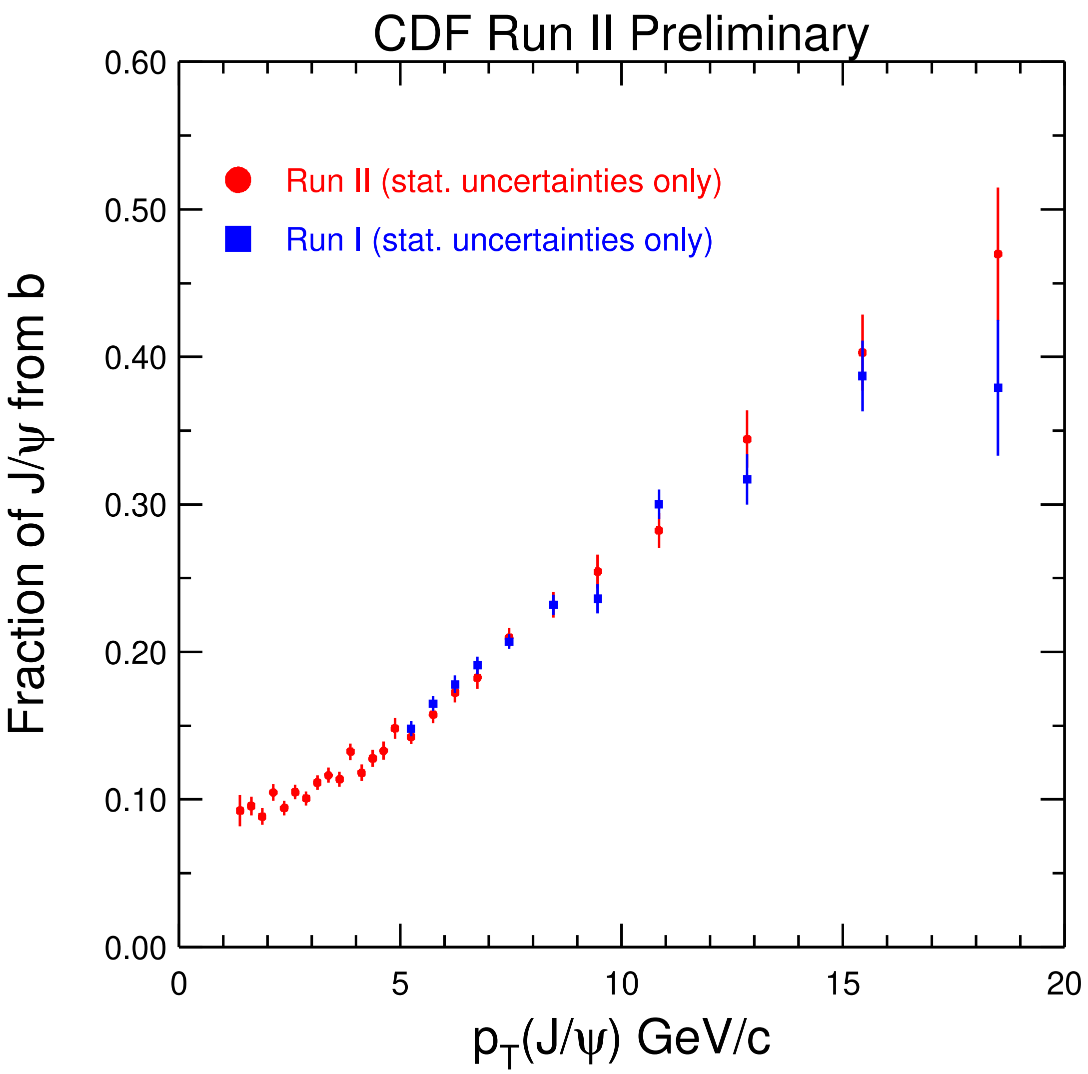

Figure 42: Fraction of J/ψ events from b.

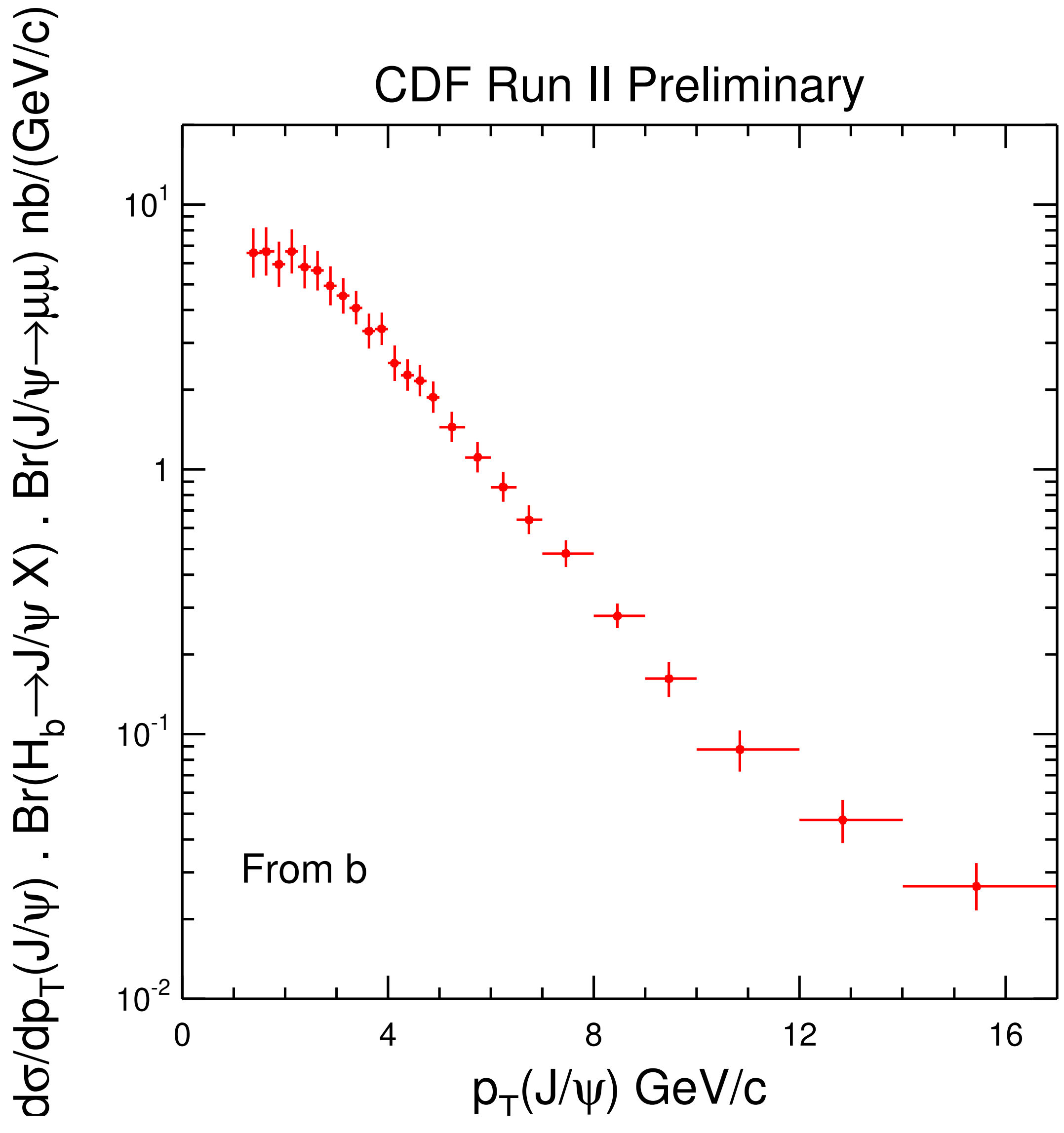

Figure 43: Differential cross-section for $b \to J/\psi X$ as a function of $J/\psi\ p_T$.

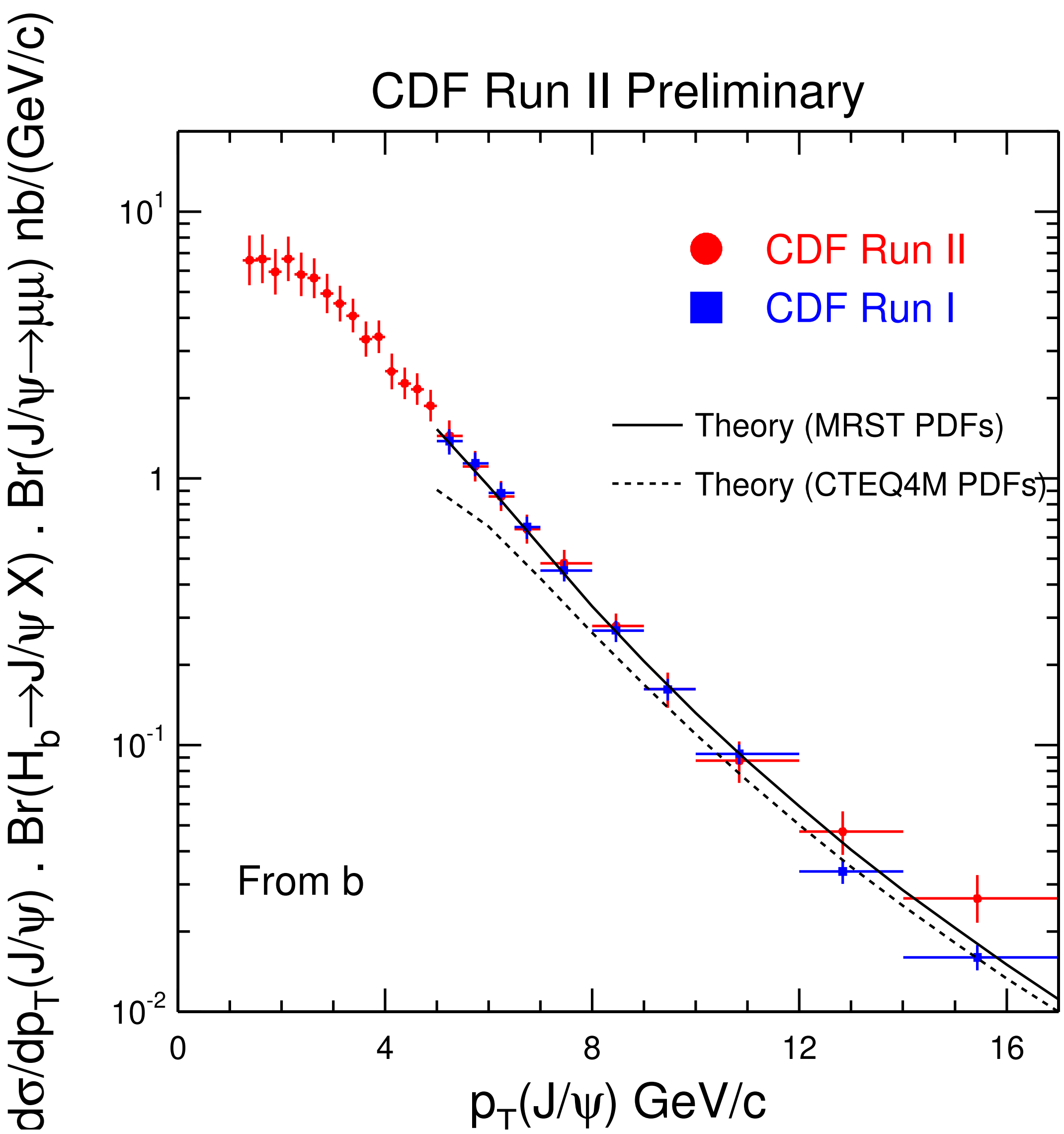

Figure 44: Cross-section for $b \to J/\psi X$ as a function of J/ψ p_T. Comparison with Run I and theory predictions

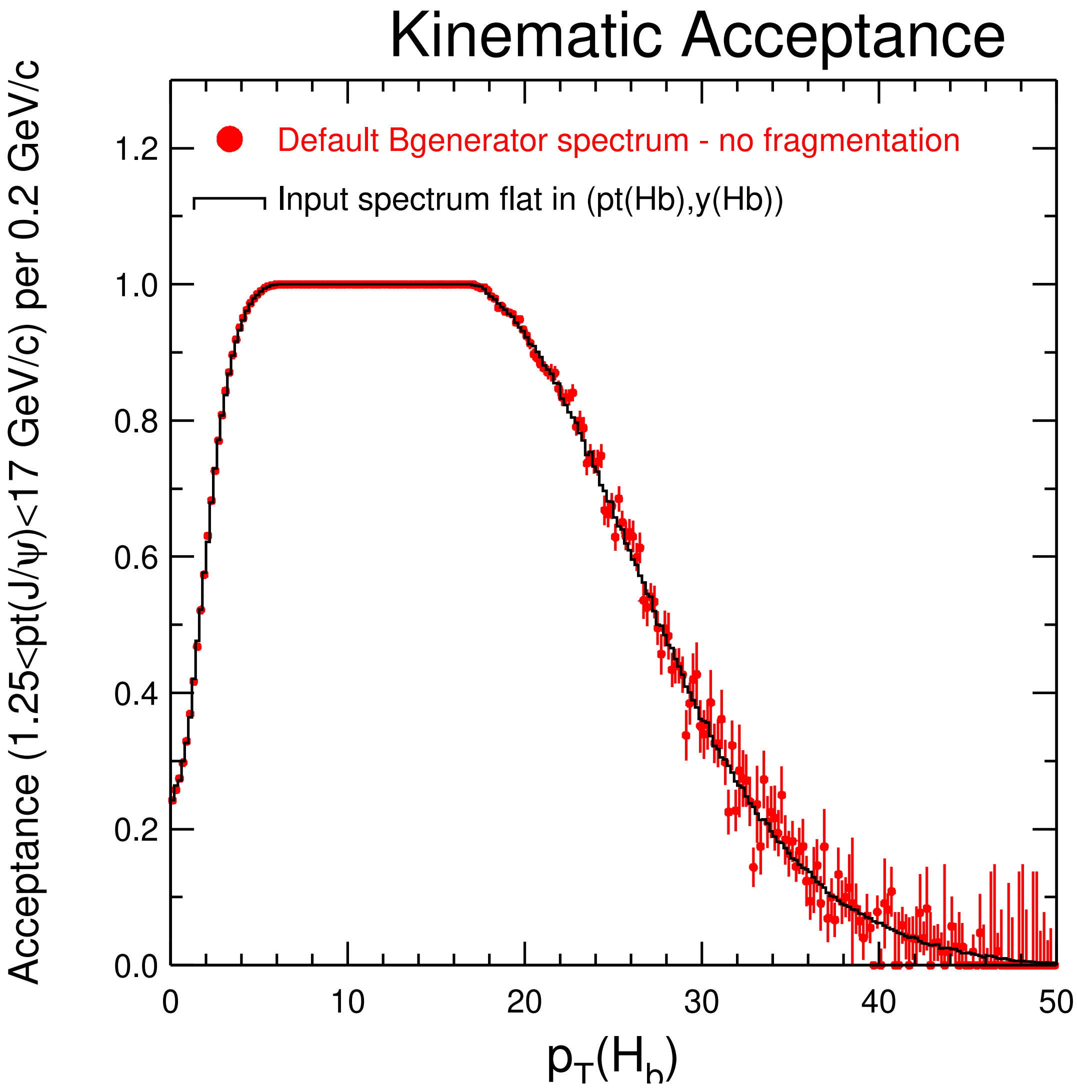

Figure 45: Ratio of the differential cross-section for $b \to J/\psi X$ as a function of $p_T(b - hadron)$ for $1.25 < p_T(J/\psi) < 17.0$/Total.

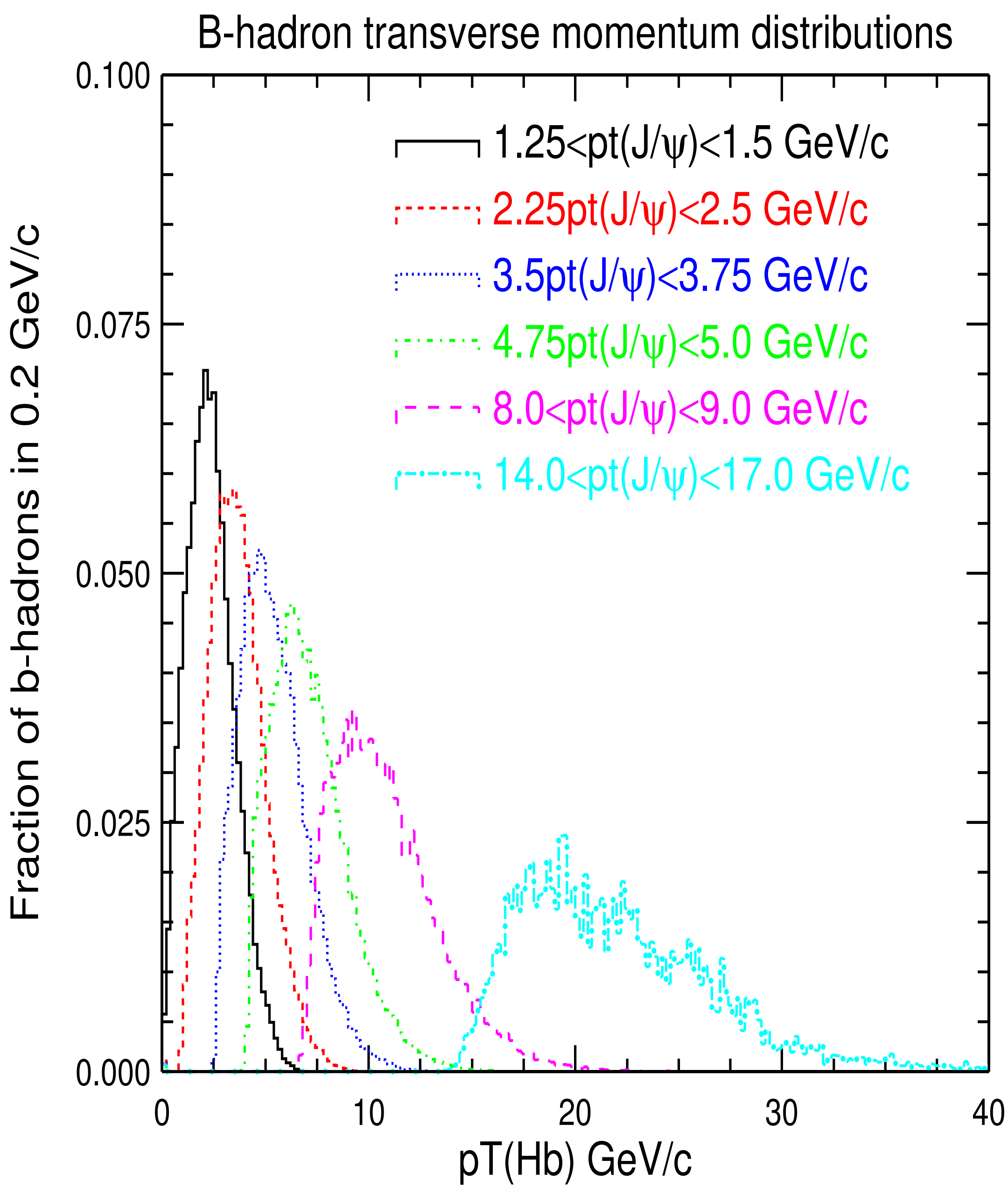

Figure 46: Transverse momentum of the input b-hadron versus the J/ψ from Bgenerator with no fragmentation.

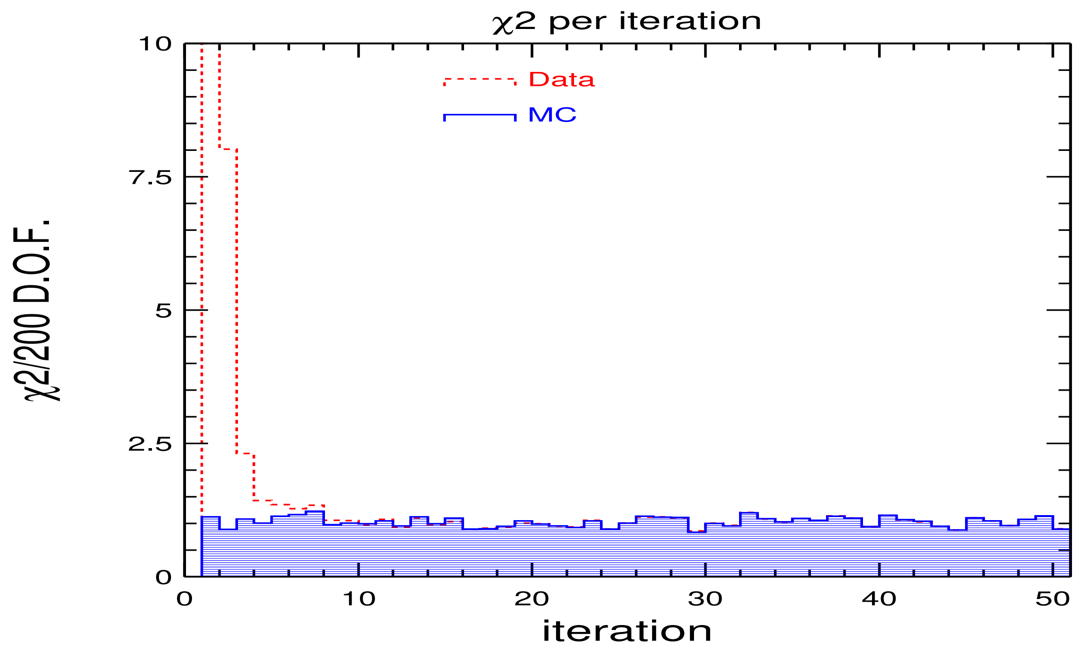

Figure 47: χ^2 comparison of input and output b-hadron spectrum extracted as a function of iteration. The red dashed line is the distribution using the J/ψ spectrum obtained from data and the solid histogram is the distribution when starting from the J/ψ spectrum obtained from the same MC sample used in the fit.

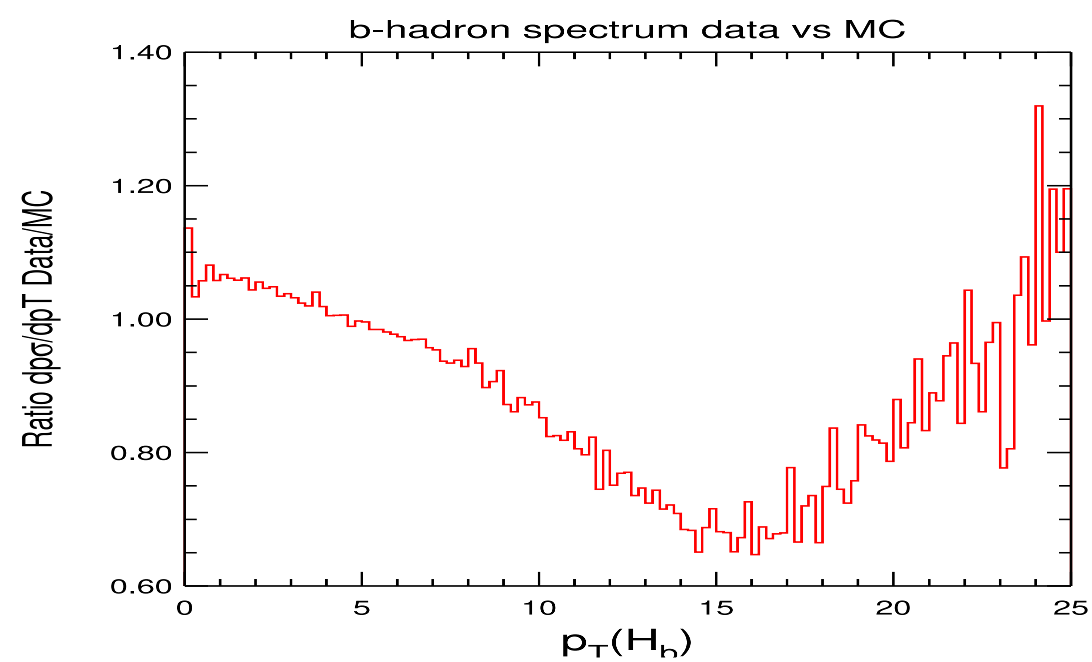

Figure 48: Difference between the measured b-hadron spectrum in data and the initial MC production spectrum with no fragmentation.

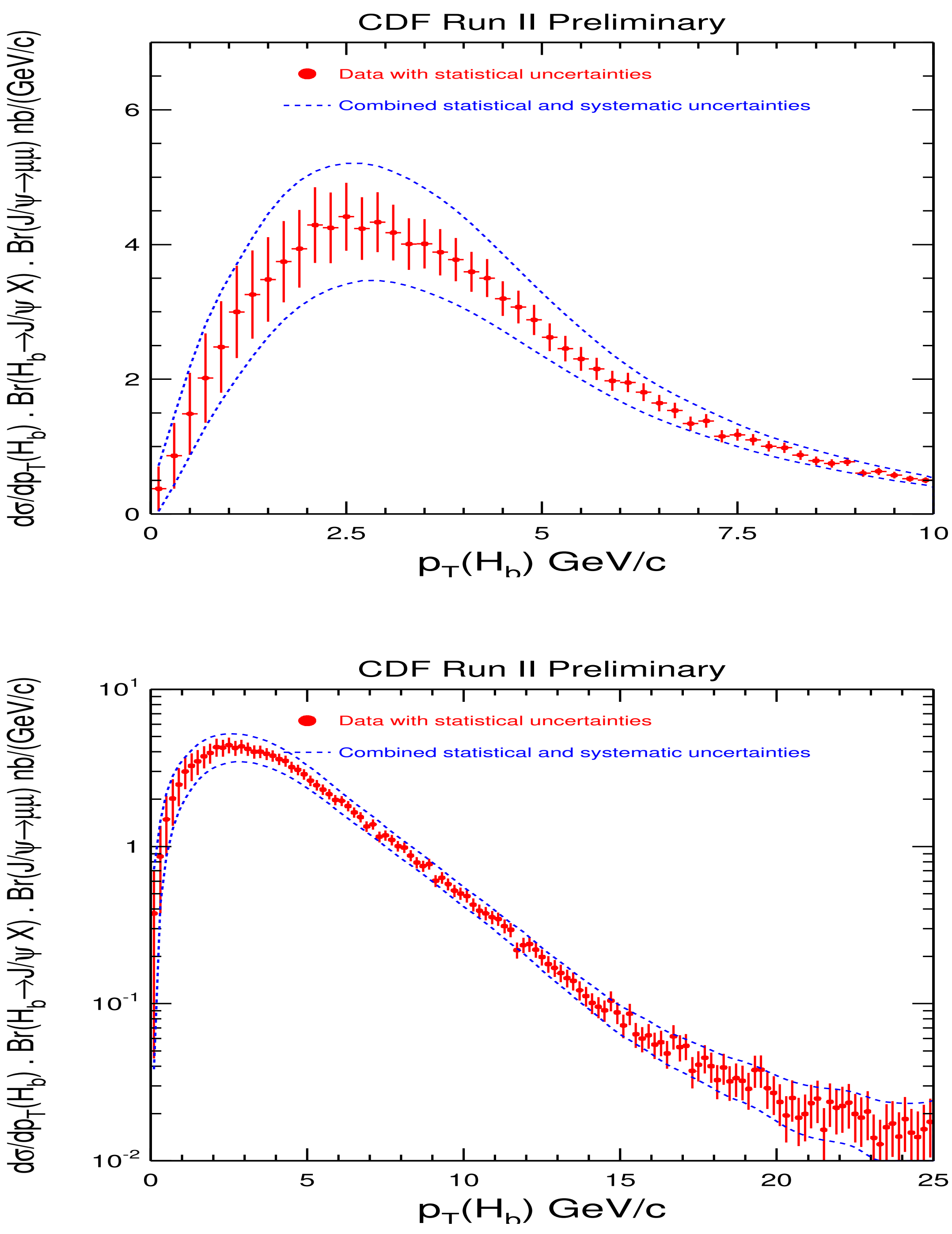

Figure 49: Differential cross-section for $b \to J/\psi X$ as a function of b-hadron p_T.

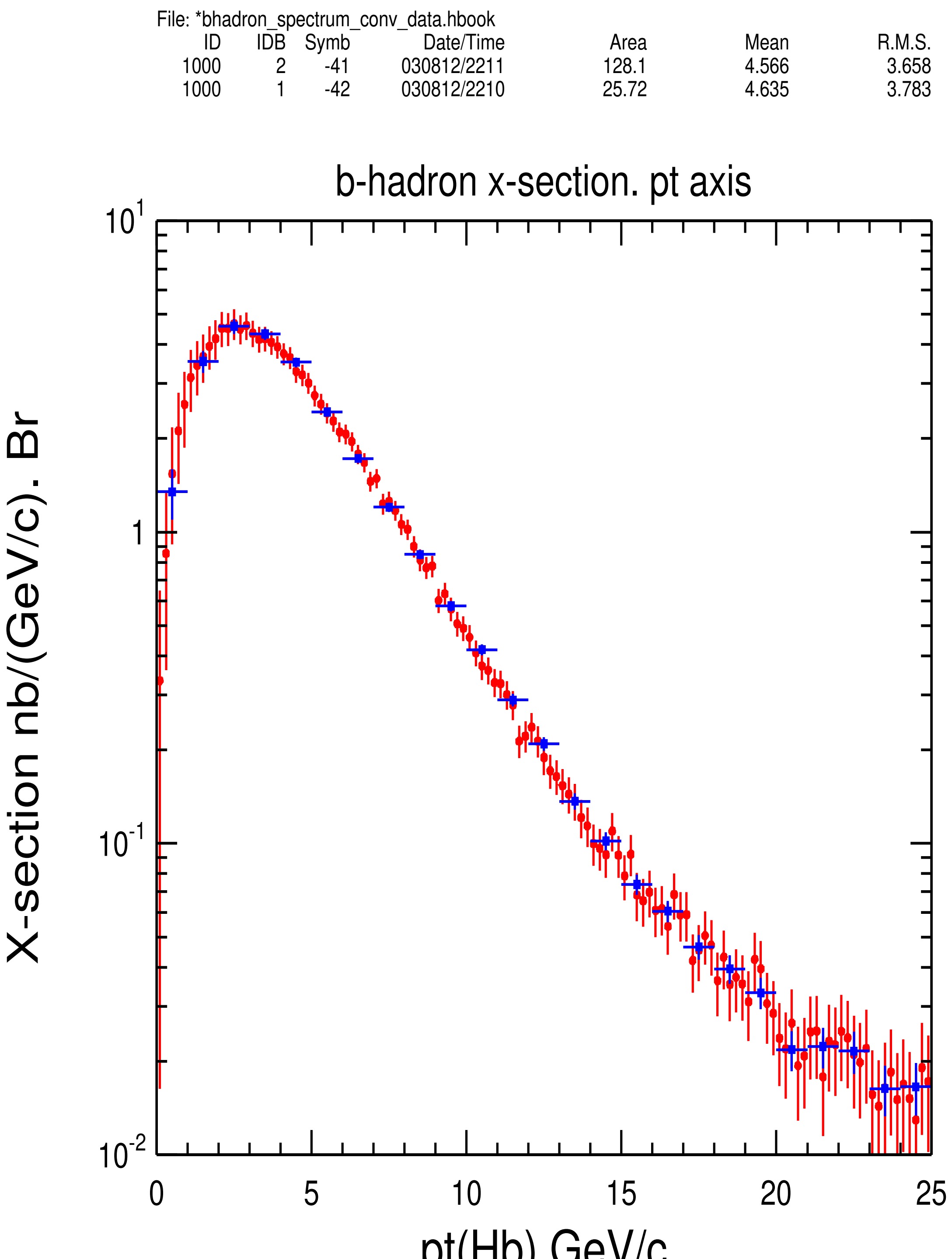

Figure 50: Differential cross-section for $b \rightarrow J/\psi X$ as a function of b-hadron p_T when using 200 MeV/c and 1 GeV/c bins in the unfolding.

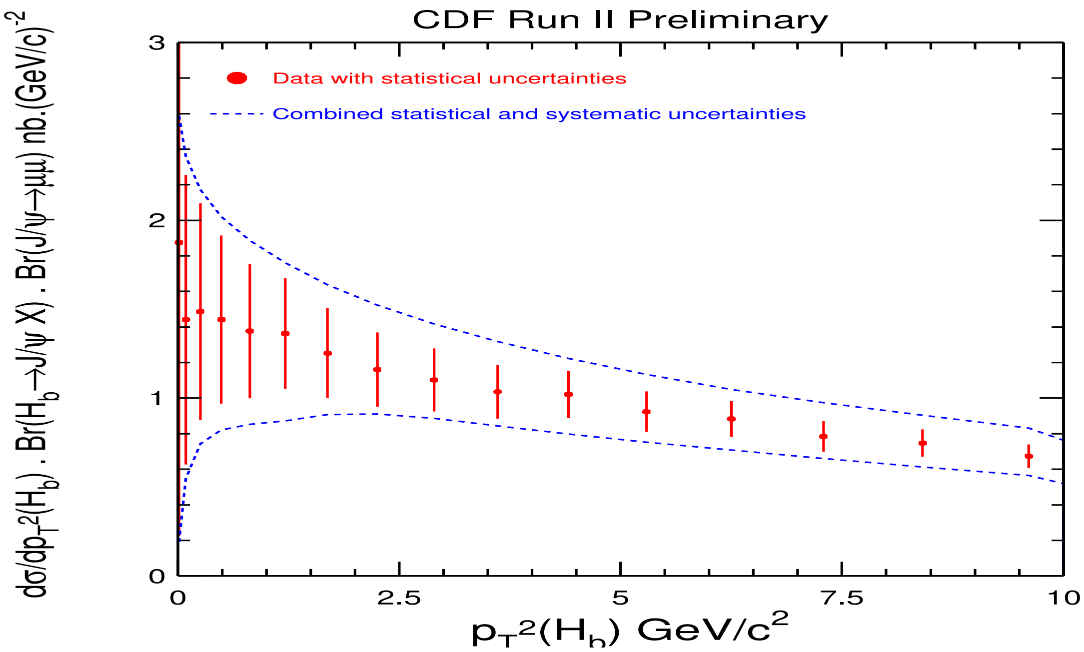

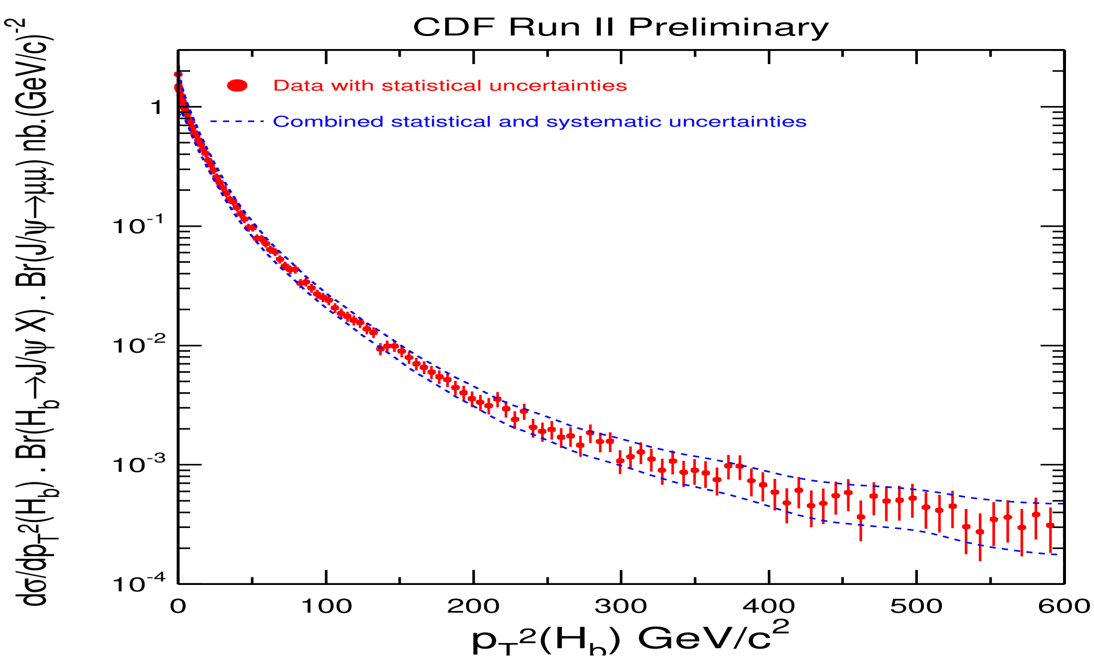

Figure 51: Differential cross-section for $b \to J/\psi X$ as a function of b-hadron p_T^2.

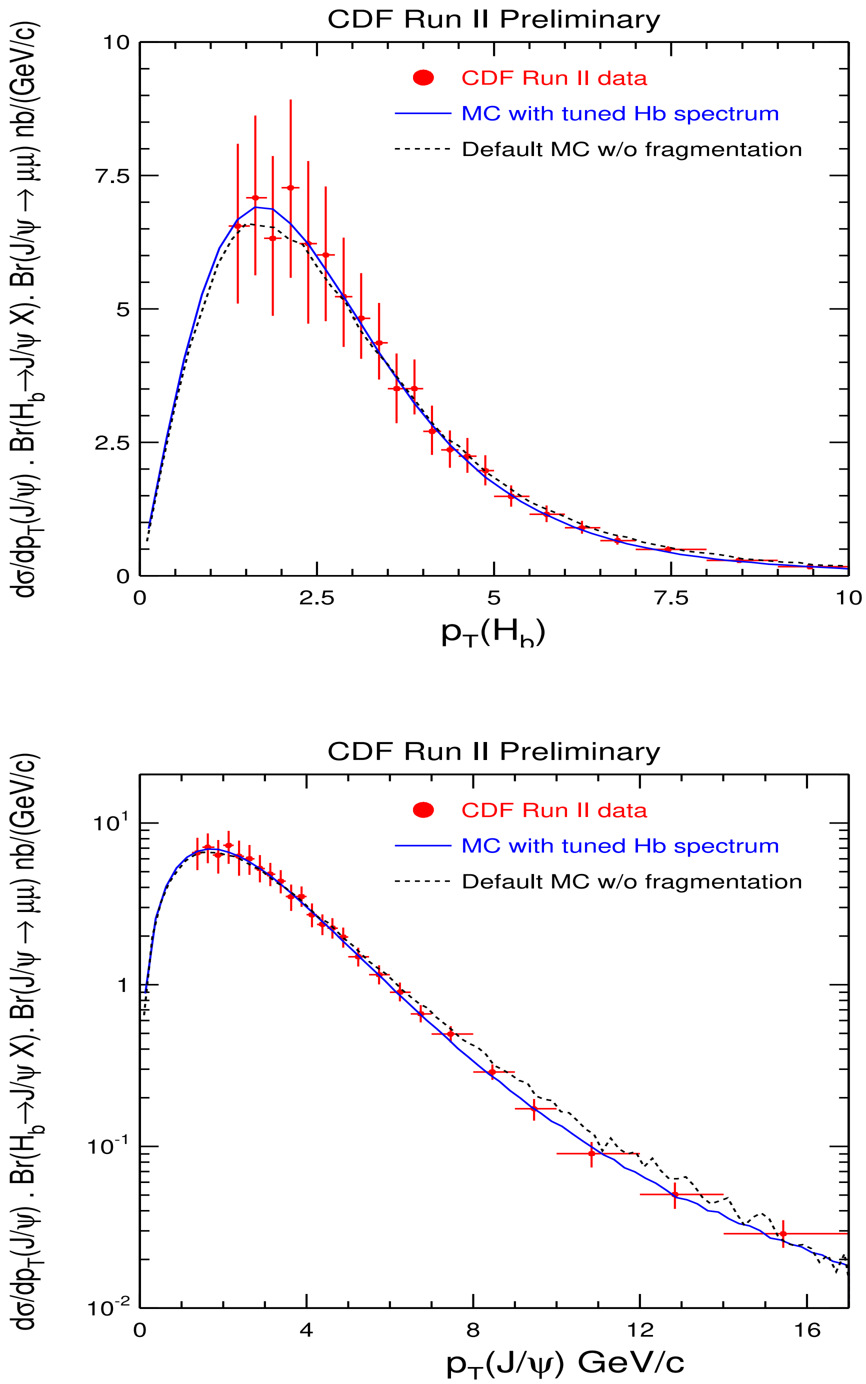

Figure 52: A comparison between the measured $H_b \to J/\psi X$ production spectrum using the default MC input b-hadron momentum spectrum (dashed-line) and the b-hadron momentum spectrum extracted from data (solid-line)

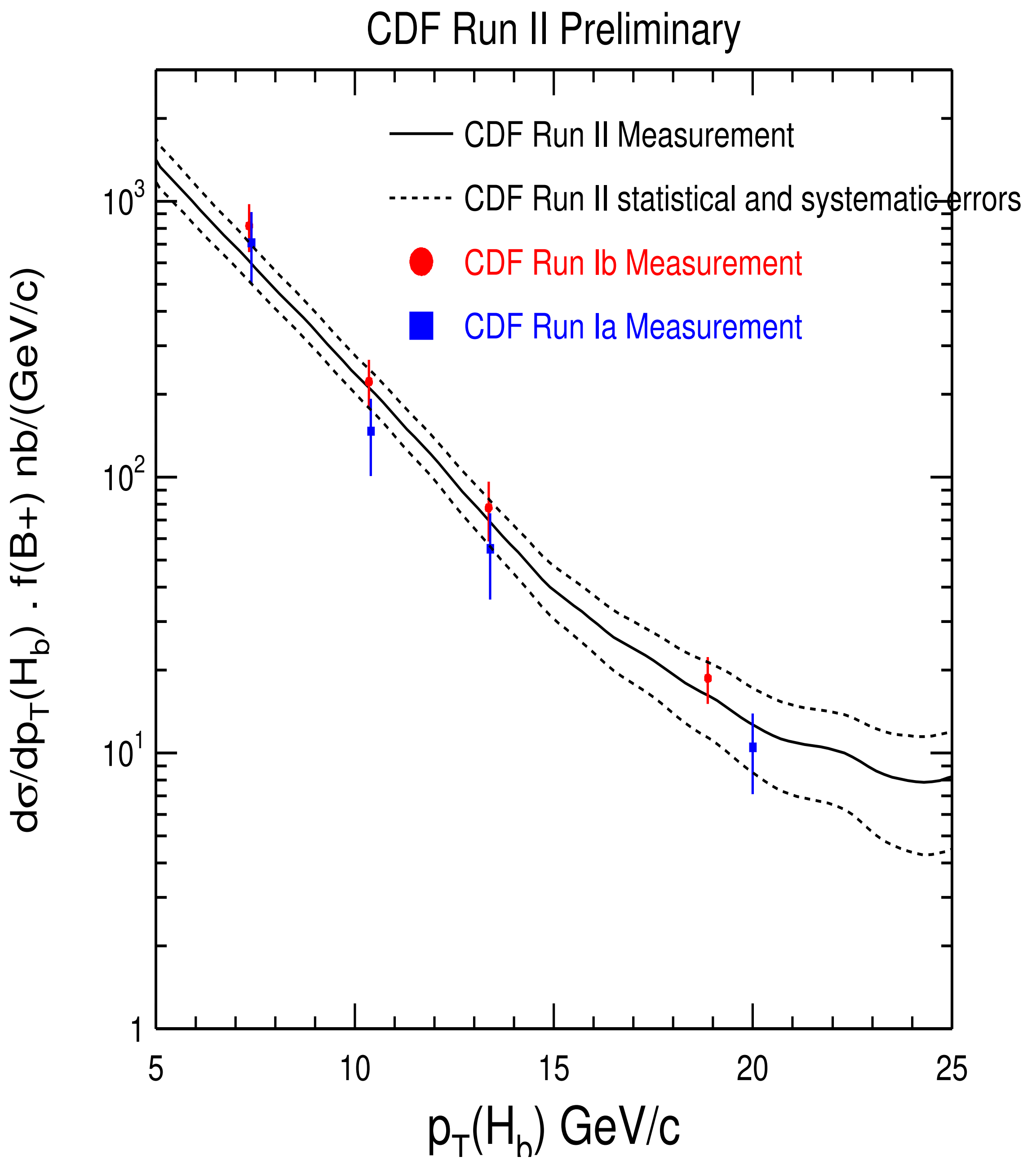

Figure 53: B^+ cross-sections from Run I compared to the Run II results obtained from the inclusive b-hadrons measurement.

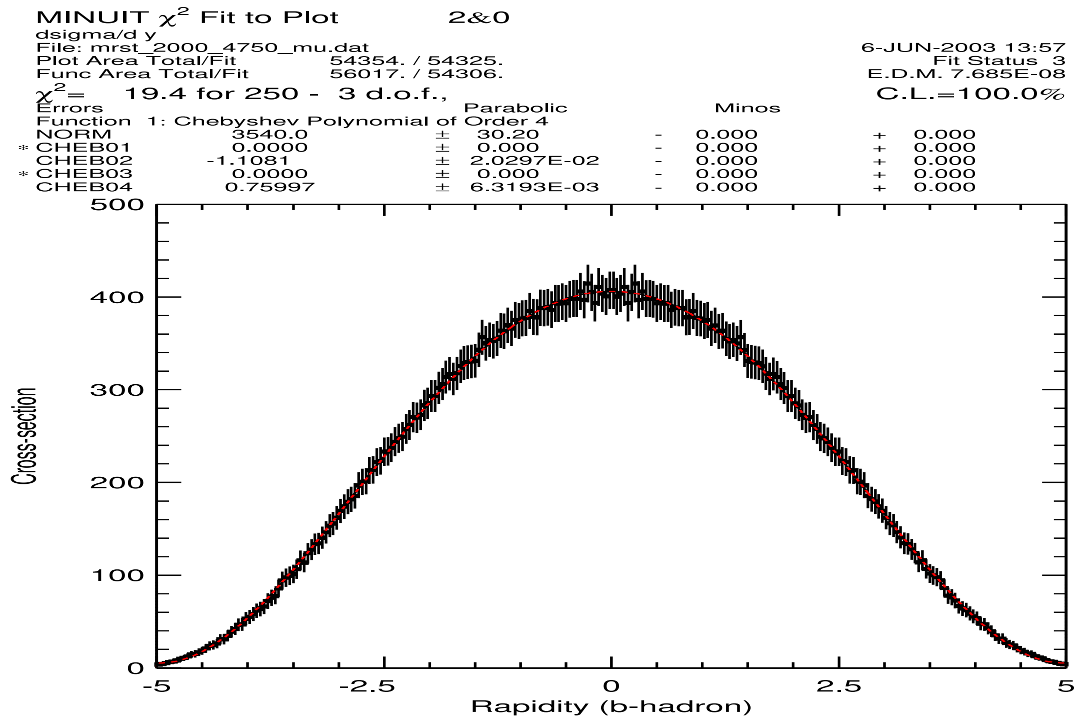

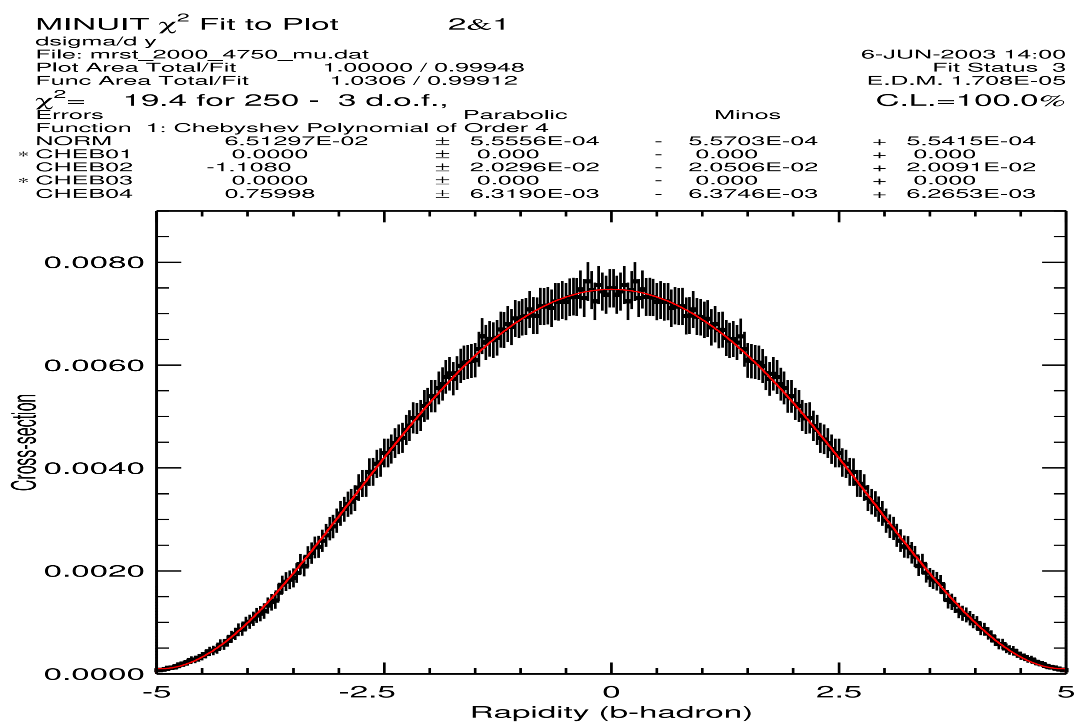

Figure 54: Differential cross-section for $p\bar{p} \rightarrow bX$ as a function of b-quark y. NLO QCD convoluted with the MRST 2000 cross-section, $\mu = \mu_0 = sqrt(m_b^2 + p_T^2)$, $m_b =$ 4.75 GeV/c. Parameteric fit overlaid.

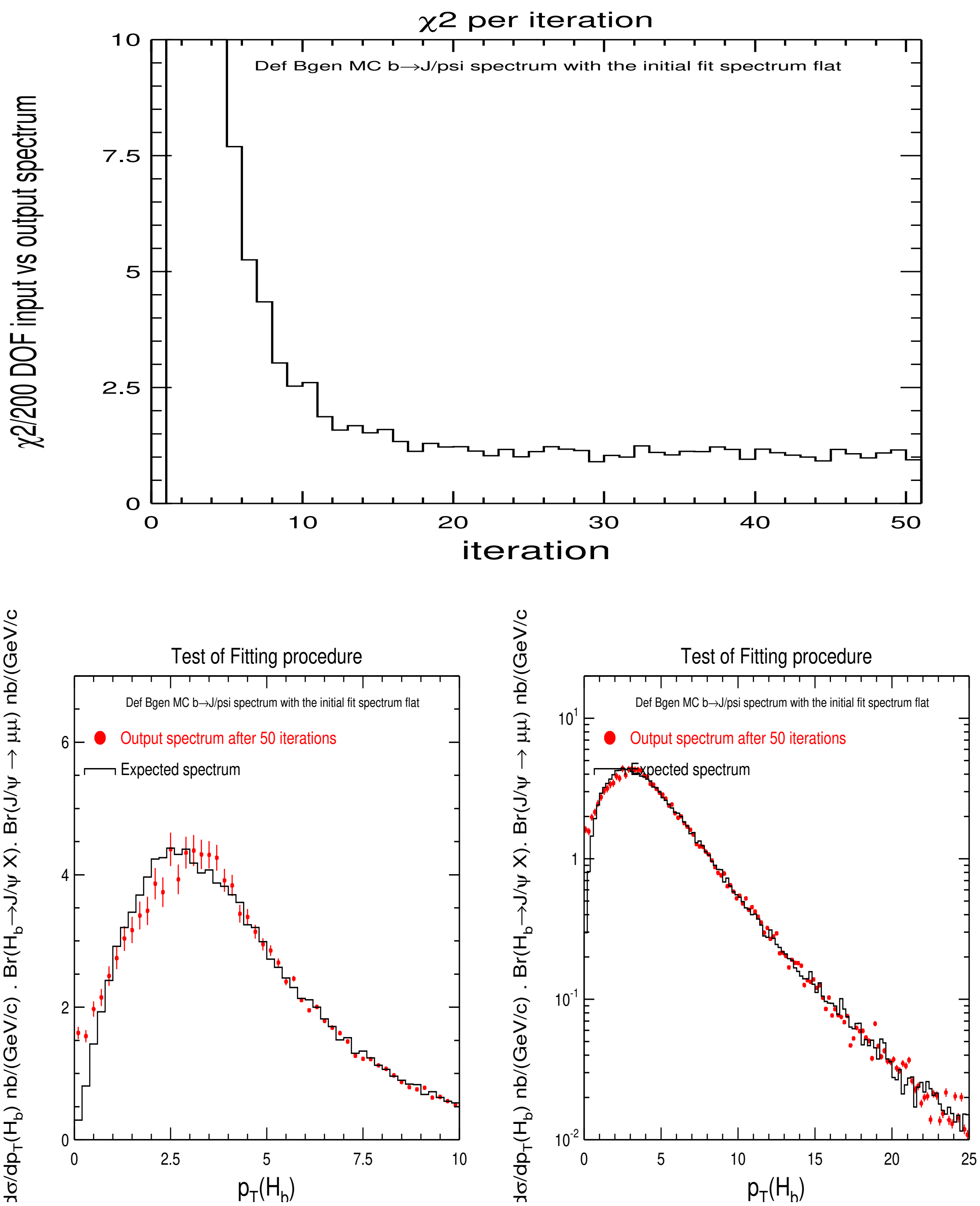

Figure 55: Cross-check of unfolding method. Top plot is the χ^2 comparison of the input and output spectrum vs number of iterations when starting from a flat spectrum. In the bottom plots data points are the measured $p_T(H_b)$ spectrum and the histogram is the expected spectrum on a linear scale and log scale.

A Tables of log-Likelihood Fit Results

The following tables are automatically generated from the MINUIT output of the unbinned loglikelihood fit to the proper decay length of the J/ψ. The program currently used to extract these numbers from the computer logfiles is not sophisticated enough to correct for the large numbers of significant digits.

$p_T(J/\psi)$	$c\tau_b$	f_B	s	$1 - f_{sig}$
1.25-1.5	$456. \pm 0.$	0.0945599973 ± 0.0099	1.00384498 ± 0.0209	0.462994993 ± 0.0133
1.5-1.75	$456. \pm 0.$	0.0919319987 ± 0.0061	0.978923023 ± 0.0138	0.483862013 ± 0.007
1.75-2	$456. \pm 0.$	0.0858160034 ± 0.0054	0.97804302 ± 0.0127	0.501438975 ± 0.0064
2-2.25	$456. \pm 0.$	0.0996339992 ± 0.0052	1.01008403 ± 0.0125	0.531306982 ± 0.0053
2.25-2.5	$456. \pm 0.$	0.0910670012 ± 0.0047	1.00416601 ± 0.0116	0.515726984 ± 0.0055
2.5-2.75	$456. \pm 0.$	0.101911999 ± 0.0047	0.981465995 ± 0.0119	0.511002004 ± 0.0058
2.75-3	$456. \pm 0.$	0.0985290036 ± 0.0046	0.996173978 ± 0.0117	0.500082016 ± 0.0057
3-3.25	$456. \pm 0.$	0.108140998 ± 0.0047	1.00305498 ± 0.0122	0.479523003 ± 0.0063
3.25-3.5	$456. \pm 0.$	0.111437999 ± 0.0049	1.01241505 ± 0.0124	0.473809004 ± 0.0059
3.5-3.75	$456. \pm 0.$	0.111790001 ± 0.005	1.02499795 ± 0.0129	0.468421996 ± 0.0058
3.75-4	$456. \pm 0.$	0.131975994 ± 0.0054	1.00031602 ± 0.0133	0.453213006 ± 0.0066
4-4.25	$456. \pm 0.$	0.114964001 ± 0.0054	1.06024206 ± 0.0145	0.432498008 ± 0.0063
4.25-4.5	$456. \pm 0.$	0.125386998 ± 0.0058	1.02133095 ± 0.0148	0.410423011 ± 0.0074
4.5-4.75	$456. \pm 0.$	0.130845994 ± 0.006	1.03754699 ± 0.015	0.386496007 ± 0.0077
4.75-5	$456. \pm 0.$	0.143967003 ± 0.0066	1.03695297 ± 0.0165	0.386997014 ± 0.0101
5-5.5	$456. \pm 0.$	0.141343996 ± 0.0049	1.04587495 ± 0.0124	0.360955 ± 0.0084
5.5-6	$456. \pm 0.$	0.155883998 ± 0.0056	1.05519199 ± 0.0139	0.346100986 ± 0.0062
6-6.5	$456. \pm 0.$	0.169064 ± 0.0065	1.05752504 ± 0.016	0.318637997 ± 0.0078
6.5-7	$456. \pm 0.$	0.182165995 ± 0.0074	1.08259594 ± 0.0181	0.291720003 ± 0.0104
7-8	$456. \pm 0.$	0.207671002 ± 0.0063	1.06708395 ± 0.0152	0.276513994 ± 0.0069
8-9	$456. \pm 0.$	0.227537006 ± 0.0085	1.083215 ± 0.0199	0.271712005 ± 0.0087
9-10	$456. \pm 0.$	0.248799995 ± 0.011	1.083148 ± 0.0258	0.266292989 ± 0.0132
10-12	$456. \pm 0.$	0.277117997 ± 0.0116	1.07612205 ± 0.0264	0.301899999 ± 0.0132
12-14	$456. \pm 0.$	0.335281014 ± 0.0189	1.11213505 ± 0.0455	0.354759991 ± 0.016
14.0-17.0	$456. \pm 0.$	0.395363986 ± 0.025	1.16718698 ± 0.0635	0.435734004 ± 0.0198
17.0-20.0	$456. \pm 0.$	0.470461994 ± 0.0446	1.17600596 ± 0.1067	0.458591014 ± 0.0336

Table 23: J/ψ pseudo-lifetime signal fit results using L_{xy}/p_T templates.

$p_T(J/\psi)$	M	σ_m	f_2	D	r_2	M_{slope}
GeV/c	GeV/c^2	GeV/c^2		GeV/c^2		GeV/c^{-1}
1.25-1.5	3.09307098 ± 0.0003	0.0127940001 ± 0.0003	0.164683998 ± 0.0245	-0.0328599997 ± 0.0093	4.68528986 ± 0.5968	4.14424419 ± 0.3229
1.5-1.75	3.09325695 ± 0.0002	0.0123899998 ± 0.0002	0.160883993 ± 0.0219	-0.0131759997 ± 0.0037	3.00240493 ± 0.3105	2.95620394 ± 0.1856
1.75-2	3.09359193 ± 0.0002	0.0122039998 ± 0.0002	0.160235003 ± 0.0213	-0.0202769991 ± 0.0043	2.81240392 ± 0.2638	2.03575993 ± 0.1681
2-2.25	3.09431291 ± 0.0003	0.0113829998 ± 0.0003	0.247565001 ± 0.0452	-0.0114679998 ± 0.0025	2.02318001 ± 0.136	0.748299003 ± 0.1527
2.25-2.5	3.09385109 ± 0.0002	0.0124049997 ± 0.0002	0.122247003 ± 0.0262	-0.0214479994 ± 0.0059	2.331954 ± 0.266	0.267886013 ± 0.1543
2.5-2.75	3.09393597 ± 0.0002	0.0125080002 ± 0.0003	0.148276001 ± 0.0382	-0.014347 ± 0.005	2.26142001 ± 0.2914	-0.508508027 ± 0.1552
2.75-3	3.09406304 ± 0.0002	0.0123720001 ± 0.0002	0.140887007 ± 0.0264	-0.0196749996 ± 0.0051	2.418859 ± 0.2375	-1.05372798 ± 0.1583
3-3.25	3.09351301 ± 0.0002	0.0125439996 ± 0.0002	0.162889004 ± 0.0253	-0.0145589998 ± 0.004	2.68924594 ± 0.2922	-1.06436205 ± 0.1684
3.25-3.5	3.094028 ± 0.0002	0.0122819999 ± 0.0003	0.157159001 ± 0.0328	-0.0123910001 ± 0.0037	2.32932496 ± 0.2443	-1.70079505 ± 0.1706
3.5-3.75	3.0944221 ± 0.0004	0.0113089997 ± 0.0006	0.357228011 ± 0.0893	$-0.00555100013 \pm 0.0014$	1.88817501 ± 0.1162	-1.680094 ± 0.1771
3.75-4	3.09384394 ± 0.0002	0.0131160002 ± 0.0003	0.111107998 ± 0.0296	-0.0174460001 ± 0.0067	2.38063693 ± 0.3358	-1.48662496 ± 0.1942
4-4.25	3.09461308 ± 0.0004	0.0114240004 ± 0.0006	0.308016002 ± 0.0909	$-0.00644699996 \pm 0.0019$	1.87490201 ± 0.1365	-2.08580899 ± 0.2058
4.25-4.5	3.09436989 ± 0.0002	0.0131069999 ± 0.0003	0.120118 ± 0.0264	-0.0267999992 ± 0.007	2.34579206 ± 0.3041	-2.25647402 ± 0.227
4.5-4.75	3.09399104 ± 0.0002	0.0141009996 ± 0.0003	0.0936719999 ± 0.0228	-0.0303230006 ± 0.0094	2.60159898 ± 0.3372	-2.15531707 ± 0.2474
4.75-5	3.0939889 ± 0.0002	0.0138419997 ± 0.0003	0.0913790017 ± 0.0205	-0.032331001 ± 0.0133	2.97741199 ± 0.6039	-2.19970989 ± 0.2822
5-5.5	3.09429789 ± 0.0002	0.0143290004 ± 0.0003	0.087402001 ± 0.0187	-0.0273119994 ± 0.0123	2.93309593 ± 0.6087	-2.38460207 ± 0.2357
5.5-6	3.09500098 ± 0.0003	0.0133400001 ± 0.0005	0.219219998 ± 0.0764	-0.0090239998 ± 0.0035	1.88796306 ± 0.1584	-2.30583501 ± 0.2317
6-6.5	3.09489298 ± 0.0002	0.0146559998 ± 0.0003	0.0703530014 ± 0.023	-0.0301249996 ± 0.0121	2.41816401 ± 0.4171	-2.21908402 ± 0.2908
6.5-7	3.09451509 ± 0.0003	0.0140930004 ± 0.0004	0.130273998 ± 0.028	-0.0194639992 ± 0.0086	2.90428805 ± 0.5123	-2.38876891 ± 0.3631
7-8	3.09538603 ± 0.0004	0.0151589997 ± 0.0005	0.124943003 ± 0.0575	-0.0163230002 ± 0.0077	1.950652 ± 0.2951	-2.27139091 ± 0.2937
8-9	3.09518695 ± 0.0005	0.0151789999 ± 0.0006	0.198658004 ± 0.0709	-0.010032 ± 0.0039	1.96184099 ± 0.2548	-2.52884507 ± 0.3837
9-10	3.09437704 ± 0.0004	0.0172579996 ± 0.0004	0.0565520003 ± 0.0226	-0.0553309992 ± 0.0241	2.87446189 ± 0.7312	-2.23580289 ± 0.5485
10-12	3.09605289 ± 0.0012	0.0161569994 ± 0.0012	0.244380996 ± 0.1388	-0.0110940002 ± 0.0047	1.90282404 ± 0.4051	-2.13683009 ± 0.4603
12-14	3.09434009 ± 0.0008	0.0216140002 ± 0.0007	$9.99999997E-07 \pm 0.$	$0.00999999978 \pm 0.$	$1. \pm 0.$	-3.78861403 ± 0.603
14.0-17.0	3.09428906 ± 0.0011	0.0231139995 ± 0.001	$9.99999997E-07 \pm 0.$	$0.00999999978 \pm 0.$	$1. \pm 0.$	-3.67772388 ± 0.6122
17.0-20.0	3.09453797 ± 0.0023	0.0284400005 ± 0.0019	$9.99999997E-07 \pm 0.$	$0.00999999978 \pm 0.$	$1. \pm 0.$	-2.54748201 ± 1.0301

Table 24: J/ψ pseudo-lifetime mass fit results using L_{xy}/p_T templates.

$p_T(J/\psi)$	f_-	λ_-	f_+	λ_+	f_{sym}	λ_{sym}	s_{bg}
1.25-1.5	$0. \pm 0.$	$1500. \pm 0.$	$0. \pm 0.$	$500. \pm 0.$	0.0698269978 ± 0.0088	848.165222 ± 86.8918	1.23690796 ± 0.03
1.5-1.75	$0. \pm 0.$	$1500. \pm 0.$	$0. \pm 0.$	$500. \pm 0.$	0.0800039992 ± 0.0061	659.850037 ± 41.121	1.17742896 ± 0.0189
1.75-2	0.00263400003 ± 0.0019	1587.19043 ± 683.3046	0.0160179995 ± 0.0054	845.478394 ± 147.9334	0.0729880035 ± 0.0086	435.950653 ± 37.1888	1.16313303 ± 0.0178
2-2.25	0.00459499983 ± 0.0027	1286.29346 ± 406.3776	0.0184039995 ± 0.005	850.718872 ± 116.5349	0.0714640021 ± 0.0083	420.122223 ± 37.5273	1.129089 ± 0.0149
2.25-2.5	0.00314699998 ± 0.0013	1600.61011 ± 490.326	0.0257799998 ± 0.0045	699.069153 ± 75.9107	0.0813490003 ± 0.0076	339.259979 ± 24.8995	1.13967395 ± 0.0167
2.5-2.75	0.00424899999 ± 0.002	1353.9624 ± 389.3285	0.0192930009 ± 0.0044	825.402161 ± 103.6514	0.0692780018 ± 0.0071	359.645203 ± 31.2714	1.15682805 ± 0.0154
2.75-3	0.00283799996 ± 0.0017	1413.78198 ± 521.4955	0.0231999997 ± 0.0048	549.312805 ± 68.9985	0.0678279996 ± 0.007	346.972748 ± 30.5868	1.15022802 ± 0.0154
3-3.25	0.00283299992 ± 0.0012	1863.93335 ± 598.7278	0.0274550002 ± 0.0049	642.91272 ± 70.7538	0.0706410035 ± 0.0071	325.31369 ± 25.4367	1.16199195 ± 0.0167
3.25-3.5	0.00451700017 ± 0.0028	1022.38458 ± 353.6304	0.0333800018 ± 0.0058	569.955322 ± 58.9023	0.0666109994 ± 0.0087	300.5672 ± 33.1333	1.131235 ± 0.0172
3.5-3.75	0.00275500002 ± 0.0016	1258.03809 ± 498.3446	0.0201370008 ± 0.005	762.436462 ± 109.7385	0.0783009976 ± 0.0077	302.938293 ± 27.8114	1.17060804 ± 0.0182
3.75-4	0.00118599995 ± 0.0008	1863.09766 ± 1016.3584	0.0323139988 ± 0.0051	633.094116 ± 72.8473	0.069724001 ± 0.0078	245.234756 ± 23.4836	1.14983797 ± 0.0194
4-4.25	0.00376400002 ± 0.002	1456.60742 ± 548.7204	0.0424350016 ± 0.0066	537.527588 ± 56.2714	0.0904269964 ± 0.0098	248.950058 ± 28.0606	1.10585296 ± 0.0222
4.25-4.5	0.00318300002 ± 0.0021	1139.51331 ± 536.081	0.0490400009 ± 0.0067	612.255981 ± 61.074	0.0677340031 ± 0.01	238.140488 ± 31.9789	1.17383003 ± 0.0255
4.5-4.75	0.00475199986 ± 0.002	1153.94861 ± 407.8953	0.0615839995 ± 0.008	495.178864 ± 49.0463	0.072044 ± 0.0112	199.917664 ± 23.8401	1.13421905 ± 0.026
4.75-5	$0. \pm 0.$	$1500. \pm 0.$	0.0686929971 ± 0.0088	463.057526 ± 44.7618	0.0758600011 ± 0.0115	217.73645 ± 24.3409	1.15627897 ± 0.029
5-5.5	$0. \pm 0.$	$1500. \pm 0.$	0.0650200024 ± 0.0072	560.293274 ± 45.6782	0.0822279975 ± 0.0091	284.148895 ± 23.7109	1.21592903 ± 0.0246
5.5-6	$0. \pm 0.$	$1500. \pm 0.$	0.0870539993 ± 0.0085	454.128326 ± 36.8579	0.0691919997 ± 0.0099	323.298737 ± 36.3852	1.21651101 ± 0.0281
6-6.5	$0. \pm 0.$	$1500. \pm 0.$	0.107798003 ± 0.0102	464.299744 ± 38.9181	0.0408460014 ± 0.009	342.755493 ± 62.1143	1.27322805 ± 0.0339
6.5-7	$0. \pm 0.$	$1500. \pm 0.$	0.0971880034 ± 0.0127	528.124878 ± 54.0139	0.0823599994 ± 0.0141	255.81102 ± 34.1875	1.26768804 ± 0.0413
7-8	$0. \pm 0.$	$1500. \pm 0.$	0.131977007 ± 0.0117	452.579651 ± 35.4554	0.0751610026 ± 0.0118	301.835327 ± 39.9526	1.26883602 ± 0.0362
8-9	$0. \pm 0.$	$1500. \pm 0.$	0.165932998 ± 0.0154	500.851379 ± 43.7562	0.0548599996 ± 0.0124	364.479675 ± 71.4014	1.31152701 ± 0.0487
9-10	$0. \pm 0.$	$1500. \pm 0.$	0.207512006 ± 0.0199	384.897888 ± 44.8431	0.0303470008 ± 0.0099	902.457947 ± 246.7007	1.36174095 ± 0.0599
10-12	$0. \pm 0.$	$1500. \pm 0.$	0.238517001 ± 0.0202	412.871979 ± 35.1252	0.0609019995 ± 0.0185	133.773636 ± 28.276	1.14051104 ± 0.0573
12-14	$0. \pm 0.$	$1500. \pm 0.$	0.252855986 ± 0.0267	290.072052 ± 38.8052	0.0304659996 ± 0.0125	1167.17712 ± 383.1209	1.04722798 ± 0.0657
14.0-17.0	$0. \pm 0.$	$1500. \pm 0.$	0.189838007 ± 0.0263	453.1008 ± 60.6028	0.0490220003 ± 0.0183	231.004532 ± 80.1661	1.100402 ± 0.0654
17.0-20.0	$0. \pm 0.$	$1500. \pm 0.$	0.204954997 ± 0.0458	432.249603 ± 89.4158	0.0730499998 ± 0.0375	169.676437 ± 81.8434	1.03336704 ± 0.1131

Table 25: J/ψ pseudo-lifetime background fit results using L_{xy}/p_T templates.

$p_T(J/\psi)$	$c\tau_b$	f_B	s_{sig}	$1 - f_{sig}$
2-2.25	449.117065 ± 29.4055	0.105579004 ± 0.0065	1.00652802 ± 0.013	0.529950023 ± 0.0054
2.25-2.5	490.41571 ± 31.8466	0.0909859985 ± 0.0056	1.00375605 ± 0.0121	0.518042028 ± 0.0056
2.5-2.75	437.546082 ± 25.0873	0.107046999 ± 0.0058	0.97537303 ± 0.0124	0.508836985 ± 0.006
2.75-3	421.780945 ± 23.4361	0.104588002 ± 0.0056	0.989548981 ± 0.0122	0.500838995 ± 0.0057
3-3.25	467.114716 ± 24.1818	0.110344 ± 0.0054	1.00058103 ± 0.0125	0.479874998 ± 0.006
3.25-3.5	431.1409 ± 22.2218	0.119093001 ± 0.0057	1.00267899 ± 0.0128	0.472283989 ± 0.006
3.5-3.75	431.087463 ± 23.0989	0.116145 ± 0.0057	1.01629305 ± 0.0132	0.468008995 ± 0.006
3.75-4	507.995514 ± 25.3262	0.127796993 ± 0.0058	1.000512 ± 0.0137	0.45382601 ± 0.0065
4-4.25	446.274261 ± 24.2161	0.118954003 ± 0.0061	1.05400801 ± 0.0149	0.432424992 ± 0.0064
4.25-4.5	463.502045 ± 25.0418	0.127155006 ± 0.0063	1.02168405 ± 0.0151	0.408852011 ± 0.0074
4.5-4.75	494.359222 ± 26.4073	0.129719004 ± 0.0064	1.04103196 ± 0.0156	0.386970013 ± 0.0078
4.75-5	429.207001 ± 22.3327	0.151203007 ± 0.0075	1.02958798 ± 0.0169	0.381431997 ± 0.0144
5-5.5	437.489807 ± 17.6792	0.144245997 ± 0.0054	1.04289305 ± 0.0127	0.364351004 ± 0.0071
5.5-6	445.075256 ± 18.5446	0.158687994 ± 0.0061	1.05310404 ± 0.0143	0.348935008 ± 0.0062
6-6.5	469.317841 ± 20.7973	0.171171993 ± 0.0069	1.05725503 ± 0.0164	0.318765014 ± 0.0079
6.5-7	460.011841 ± 22.1336	0.182078004 ± 0.0079	1.08627796 ± 0.0186	0.293381989 ± 0.01
7-8	434.87735 ± 15.7051	0.212218001 ± 0.0068	1.06117797 ± 0.0156	0.27273801 ± 0.0067
8-9	468.338623 ± 20.7357	0.230744004 ± 0.0089	1.07803702 ± 0.0205	0.272412002 ± 0.0089
9-10	476.503967 ± 25.5454	0.252256006 ± 0.0116	1.05805695 ± 0.0261	0.263574988 ± 0.0141
10-12	495.192169 ± 24.9213	0.278293997 ± 0.0121	1.07516205 ± 0.0273	0.297592998 ± 0.0149
12-14	491.656311 ± 34.9163	0.339069009 ± 0.0198	1.122509 ± 0.0473	0.353935003 ± 0.0164
14.0-17.0	491.45636 ± 39.3628	0.398503006 ± 0.0261	1.15735698 ± 0.0676	0.437489003 ± 0.0204
17.0-20.0	388.231781 ± 48.1671	0.492419988 ± 0.0457	1.10637105 ± 0.1214	0.440903008 ± 0.0348

Table 26: J/ψ pseudo-lifetime signal fit results using F-factors

$p_T(J/\psi)$	M	σ_m	f_2	D	r_2	M_{slope}
GeV/c	GeV/c^2	GeV/c^2		GeV/c^2		GeV/c^{-1}
2-2.25	3.09427094 ± 0.0003	0.0112530002 ± 0.0003	0.260818005 ± 0.0456	-0.0106889997 ± 0.0023	2.05355906 ± 0.1372	0.762409985 ± 0.1555
2.25-2.5	3.09380507 ± 0.0002	0.0122229997 ± 0.0002	0.128051996 ± 0.0264	-0.0202239994 ± 0.0054	2.32154703 ± 0.2638	0.258982986 ± 0.1562
2.5-2.75	3.09391904 ± 0.0002	0.0126670003 ± 0.0003	0.135728002 ± 0.0322	-0.0173550006 ± 0.0057	2.33156991 ± 0.3086	-0.496237993 ± 0.1592
2.75-3	3.09414911 ± 0.0002	0.012329 ± 0.0002	0.141728997 ± 0.0275	-0.0198730007 ± 0.0051	2.36829996 ± 0.222	-1.10500801 ± 0.1601
3-3.25	3.09358191 ± 0.0002	0.012329 ± 0.0003	0.178478003 ± 0.0305	-0.0124850003 ± 0.0034	2.47744203 ± 0.2426	-1.11665702 ± 0.169
3.25-3.5	3.09401894 ± 0.0002	0.012255 ± 0.0003	0.160171002 ± 0.03	-0.0132759996 ± 0.0036	2.37537909 ± 0.2337	-1.73629904 ± 0.1735
3.5-3.75	3.09437299 ± 0.0004	0.0114949998 ± 0.0006	0.337361008 ± 0.1028	$-0.00567599991 \pm 0.0016$	1.87237895 ± 0.1348	-1.66438901 ± 0.1805
3.75-4	3.09387207 ± 0.0002	0.0130070001 ± 0.0003	0.113383003 ± 0.0323	-0.0176860001 ± 0.0067	2.25329995 ± 0.2939	-1.50662005 ± 0.1962
4-4.25	3.09474492 ± 0.0004	0.0114679998 ± 0.0005	0.305907011 ± 0.0885	-0.00699899998 ± 0.002	1.859905 ± 0.1344	-2.11842203 ± 0.2094
4.25-4.5	3.09441304 ± 0.0002	0.013119 ± 0.0003	0.119658999 ± 0.0265	-0.0272230003 ± 0.0072	2.34687996 ± 0.3026	-2.26353192 ± 0.2301
4.5-4.75	3.09399104 ± 0.0002	0.0140580004 ± 0.0003	0.100585997 ± 0.024	-0.0284289997 ± 0.0088	2.56497693 ± 0.3295	-2.11688399 ± 0.2512
4.75-5	3.09390593 ± 0.0002	0.0140439998 ± 0.0003	0.0848509967 ± 0.017	-0.0428359993 ± 0.0204	3.48687911 ± 0.9981	-2.09587312 ± 0.3623
5-5.5	3.0944519 ± 0.0002	0.01406 ± 0.0003	0.107768998 ± 0.0306	-0.0194060002 ± 0.0089	2.54492688 ± 0.429	-2.48423696 ± 0.2195
5.5-6	3.09510994 ± 0.0003	0.0131219998 ± 0.0006	0.249270007 ± 0.087	-0.00805899967 ± 0.003	1.82749903 ± 0.1364	-2.30647492 ± 0.2346
6-6.5	3.09490108 ± 0.0002	0.0146880001 ± 0.0003	0.0635140017 ± 0.0213	-0.0334439985 ± 0.0133	2.44090796 ± 0.4601	-2.21374893 ± 0.297
6.5-7	3.09467793 ± 0.0003	0.0139119998 ± 0.0004	0.137654006 ± 0.0319	-0.0181920007 ± 0.0078	2.7572391 ± 0.455	-2.32684588 ± 0.3609
7-8	3.09557891 ± 0.0004	0.0148839997 ± 0.0005	0.148990005 ± 0.0588	-0.0145850005 ± 0.0059	1.91600096 ± 0.2187	-2.16289496 ± 0.3
8-9	3.09510708 ± 0.0005	0.0152390003 ± 0.0006	0.199359 ± 0.0733	-0.0100919995 ± 0.0041	1.96772504 ± 0.2537	-2.37808204 ± 0.3922
9-10	3.09446812 ± 0.0004	0.0172169991 ± 0.0004	0.0590649992 ± 0.0217	-0.0584109984 ± 0.0236	2.964396 ± 0.7279	-2.06667495 ± 0.587
10-12	3.09543991 ± 0.0009	0.0166790001 ± 0.001	0.194159001 ± 0.0995	-0.0127800005 ± 0.0067	2.16394901 ± 0.5797	-2.04588699 ± 0.4829
12-14	3.09418893 ± 0.0008	0.021551 ± 0.0007	$0. \pm 0.$	$0. \pm 0.$	$1. \pm 0.$	-3.55693793 ± 0.6258
14.0-17.0	3.09412503 ± 0.0011	0.0228310004 ± 0.001	$0. \pm 0.$	$0. \pm 0.$	$1. \pm 0.$	-3.83989191 ± 0.6206
17.0-20.0	3.09476495 ± 0.0024	0.029236 ± 0.0021	$0. \pm 0.$	$0. \pm 0.$	$1. \pm 0.$	-2.81546593 ± 1.0942

Table 27: J/ψ pseudo-lifetime mass fit results using F-factors

$p_T(J/\psi)$	f_-	λ_-	f_+	λ_+	f_{sym}	λ_{sym}	Scale factor
2-2.25	0.00471000001 ± 0.0025	1308.59204 ± 402.1422	0.0189459994 ± 0.0049	832.619751 ± 113.1246	0.0711499974 ± 0.0082	411.882843 ± 37.1627	1.12795901 ± 0.0152
2.25-2.5	0.00297500007 ± 0.0017	1375.16272 ± 493.4795	0.0253870003 ± 0.0048	670.864868 ± 76.5155	0.0814450011 ± 0.0079	343.936127 ± 27.0289	1.13394105 ± 0.0169
2.5-2.75	0.00452899979 ± 0.0021	1333.35327 ± 387.9816	0.0190379992 ± 0.0046	784.532227 ± 104.6029	0.0712310001 ± 0.0075	361.303101 ± 32.3051	1.15191305 ± 0.0158
2.75-3	0.00181100005 ± 0.0015	1392.67188 ± 683.1656	0.0218679998 ± 0.0047	557.814148 ± 72.9062	0.0705050007 ± 0.007	353.994446 ± 30.4669	1.14703906 ± 0.0155
3-3.25	0.00228799996 ± 0.001	1877.31763 ± 675.171	0.0295020007 ± 0.0049	580.727234 ± 62.911	0.0676970035 ± 0.007	320.031219 ± 25.3941	1.15919304 ± 0.0168
3.25-3.5	0.00452300021 ± 0.0031	1023.45563 ± 372.6768	0.0321060009 ± 0.0059	569.249451 ± 62.8553	0.0643289983 ± 0.0088	313.173462 ± 37.2439	1.13547599 ± 0.0172
3.5-3.75	0.00287099998 ± 0.0018	1236.14917 ± 512.8238	0.0206729993 ± 0.0052	748.417969 ± 111.045	0.0778679997 ± 0.0079	311.084625 ± 29.7352	1.16784596 ± 0.0184
3.75-4	0.001208 ± 0.0008	1884.88733 ± 1016.2193	0.0311489999 ± 0.0051	639.748779 ± 76.5544	0.0696230009 ± 0.0078	242.471756 ± 23.3702	1.14727604 ± 0.0195
4-4.25	0.00375599996 ± 0.0021	1479.90283 ± 575.2255	0.042018 ± 0.0067	550.115051 ± 59.1834	0.0907410011 ± 0.0099	255.973694 ± 29.4102	1.10217798 ± 0.0222
4.25-4.5	0.00325300009 ± 0.0022	1142.96106 ± 542.7926	0.0472589992 ± 0.0068	621.43457 ± 65.0971	0.0721020028 ± 0.0104	239.416992 ± 31.497	1.16763198 ± 0.0258
4.5-4.75	$0. \pm 0.$	$1500. \pm 0.$	0.0558470003 ± 0.0082	417.895325 ± 57.0406	0.0643500015 ± 0.0094	359.763214 ± 46.3839	1.15673101 ± 0.0254
4.75-5	$0. \pm 0.$	$1500. \pm 0.$	0.0680039972 ± 0.0095	454.351227 ± 45.5696	0.0766440034 ± 0.0118	219.19281 ± 25.4991	1.15782595 ± 0.0305
5-5.5	$0. \pm 0.$	$1500. \pm 0.$	0.069062002 ± 0.0072	556.423706 ± 44.2467	0.0789010003 ± 0.0089	280.790741 ± 24.1034	1.20547497 ± 0.024
5.5-6	$0. \pm 0.$	$1500. \pm 0.$	0.0856930017 ± 0.0086	469.406891 ± 38.3902	0.0731170028 ± 0.0102	307.352814 ± 33.4873	1.21265101 ± 0.0285
6-6.5	$0. \pm 0.$	$1500. \pm 0.$	0.101108 ± 0.0102	434.694611 ± 39.5741	0.0414290018 ± 0.009	353.630371 ± 64.6724	1.27021801 ± 0.0339
6.5-7	$0. \pm 0.$	$1500. \pm 0.$	0.100373998 ± 0.0128	523.790649 ± 56.1574	0.0804359987 ± 0.014	258.306244 ± 35.5194	1.25937605 ± 0.0414
7-8	$0. \pm 0.$	$1500. \pm 0.$	0.128010005 ± 0.0118	441.903839 ± 36.0874	0.0817079991 ± 0.0127	252.484253 ± 31.5963	1.25075305 ± 0.0367
8-9	$0. \pm 0.$	$1500. \pm 0.$	0.171213001 ± 0.0158	474.820038 ± 41.8505	0.0538019985 ± 0.0126	337.037323 ± 68.3119	1.29077697 ± 0.0498
9-10	$0. \pm 0.$	$1500. \pm 0.$	0.211170003 ± 0.0207	365.239685 ± 42.958	0.0242400002 ± 0.009	935.980591 ± 283.8552	1.37056506 ± 0.0618
10-12	$0. \pm 0.$	$1500. \pm 0.$	0.231802002 ± 0.0209	389.797333 ± 35.7655	0.0653479993 ± 0.02	131.985687 ± 29.1728	1.14166903 ± 0.0613
12-14	$0. \pm 0.$	$1500. \pm 0.$	0.251504004 ± 0.0281	333.880127 ± 42.2986	0.0398360007 ± 0.021	161.406387 ± 65.3114	1.01897097 ± 0.0697
14.0-17.0	$0. \pm 0.$	$1500. \pm 0.$	0.201444998 ± 0.027	436.567657 ± 57.4622	0.0420630015 ± 0.0176	228.028595 ± 87.2867	1.13285005 ± 0.07
17.0-20.0	$0. \pm 0.$	$1500. \pm 0.$	0.193621993 ± 0.0478	451.82077 ± 106.3229	0.0664369985 ± 0.0422	155.271439 ± 85.3811	1.070485 ± 0.1339

Table 28: J/ψ pseudo-lifetime background fit results using F-factors

B Plots of log-Likelihood Fit Results

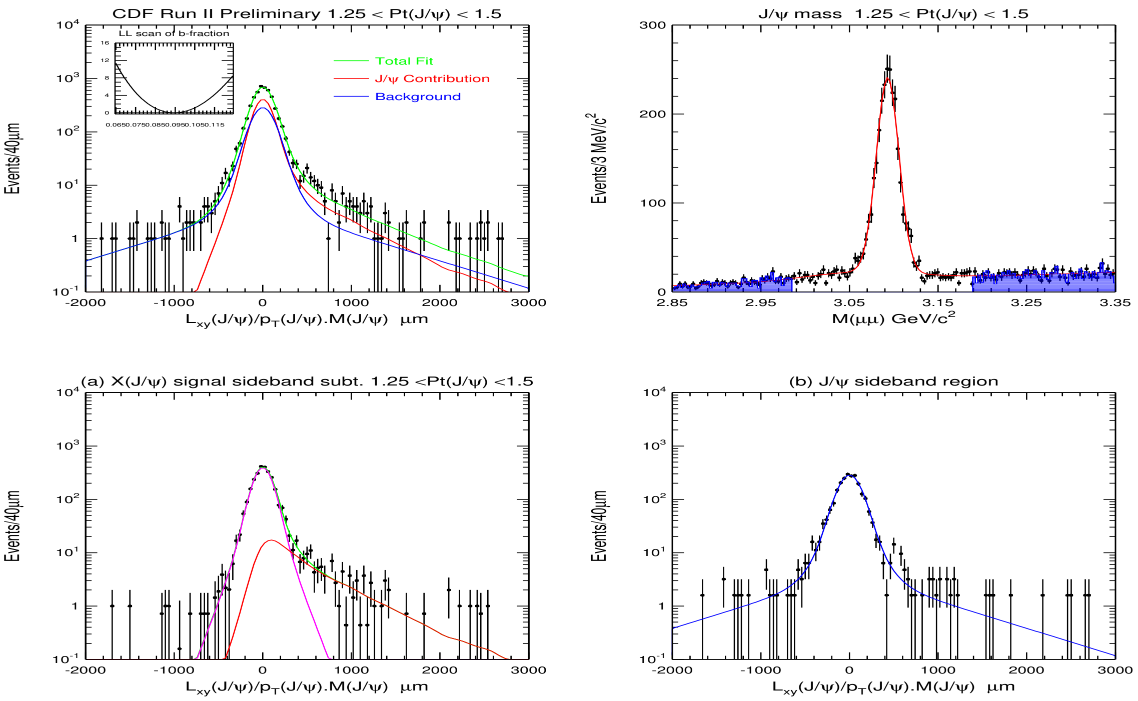

Figure 56: Projection of fit distributions on J/ψ invariant mass and decay length distributions.

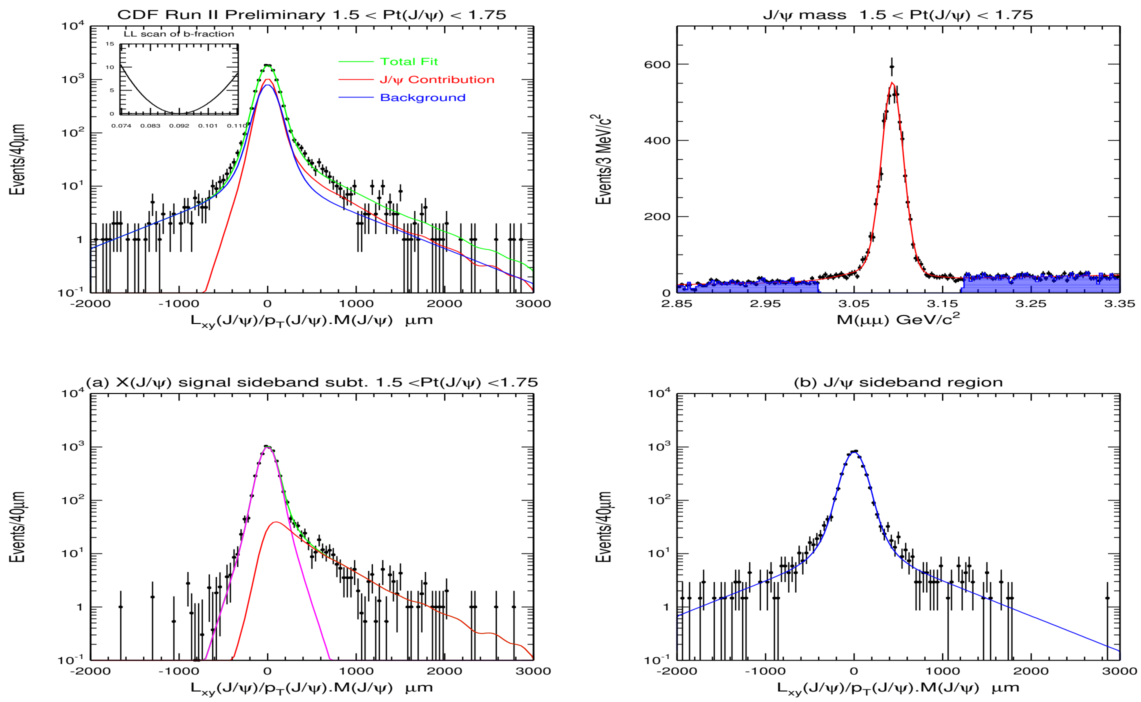

Figure 57: Projection of fit distributions on J/ψ invariant mass and decay length distributions.

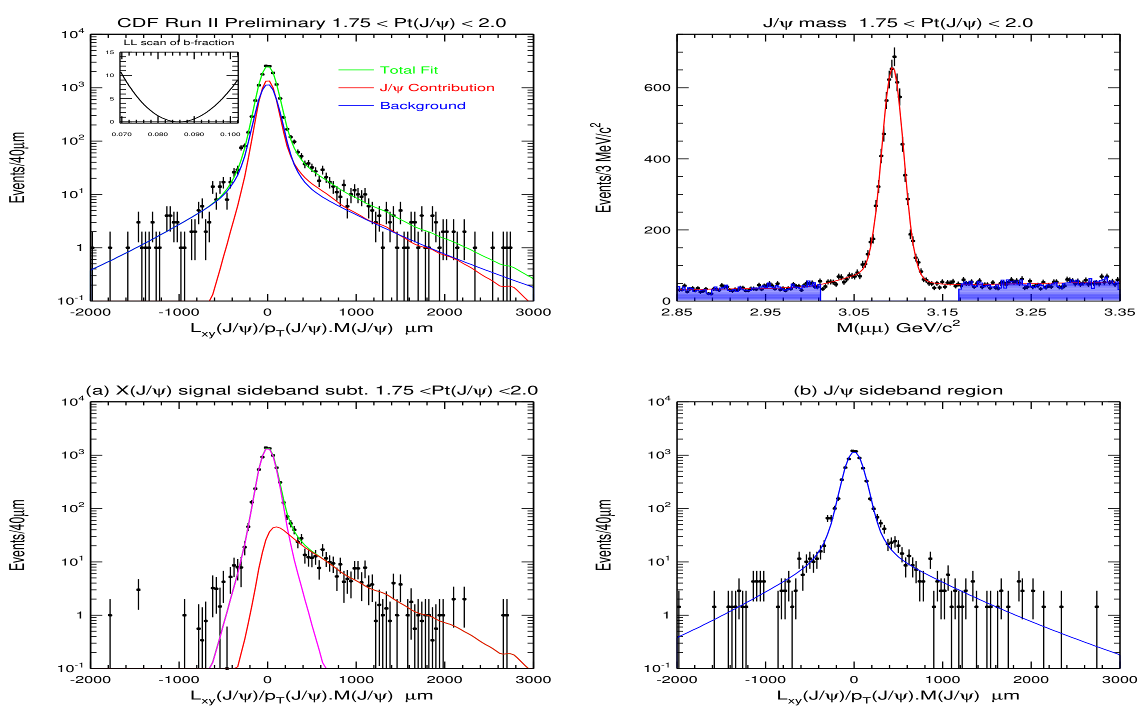

Figure 58: Projection of fit distributions on J/ψ invariant mass and decay length distributions.

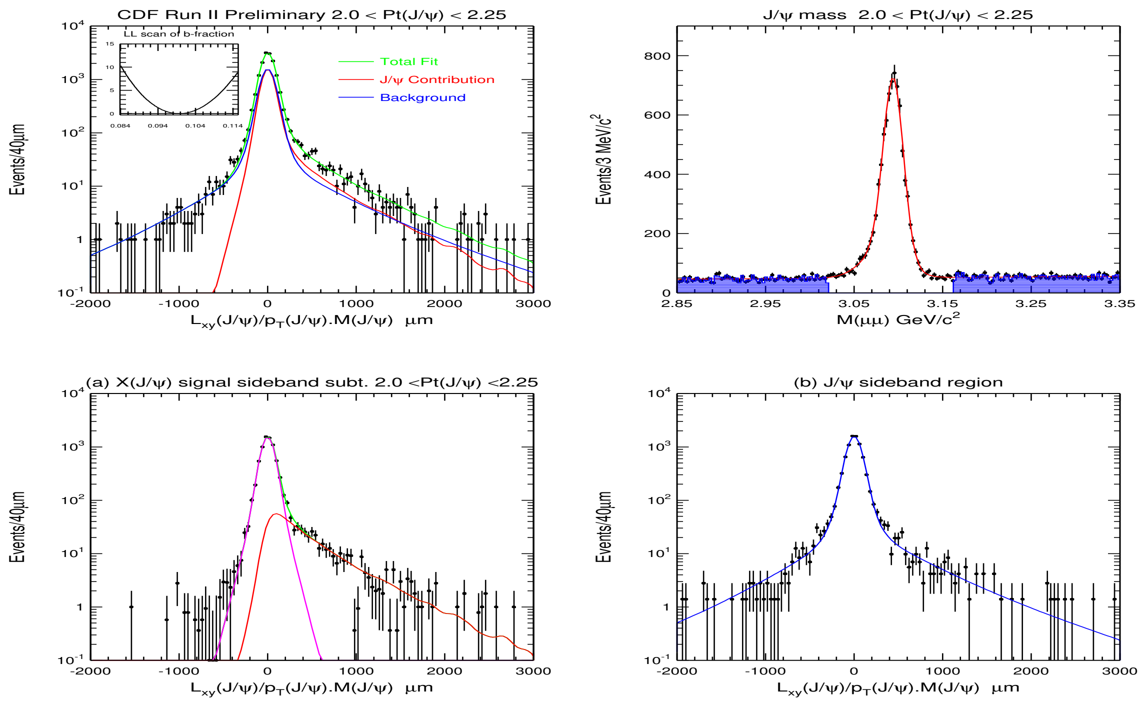

Figure 59: Projection of fit distributions on J/ψ invariant mass and decay length distributions.

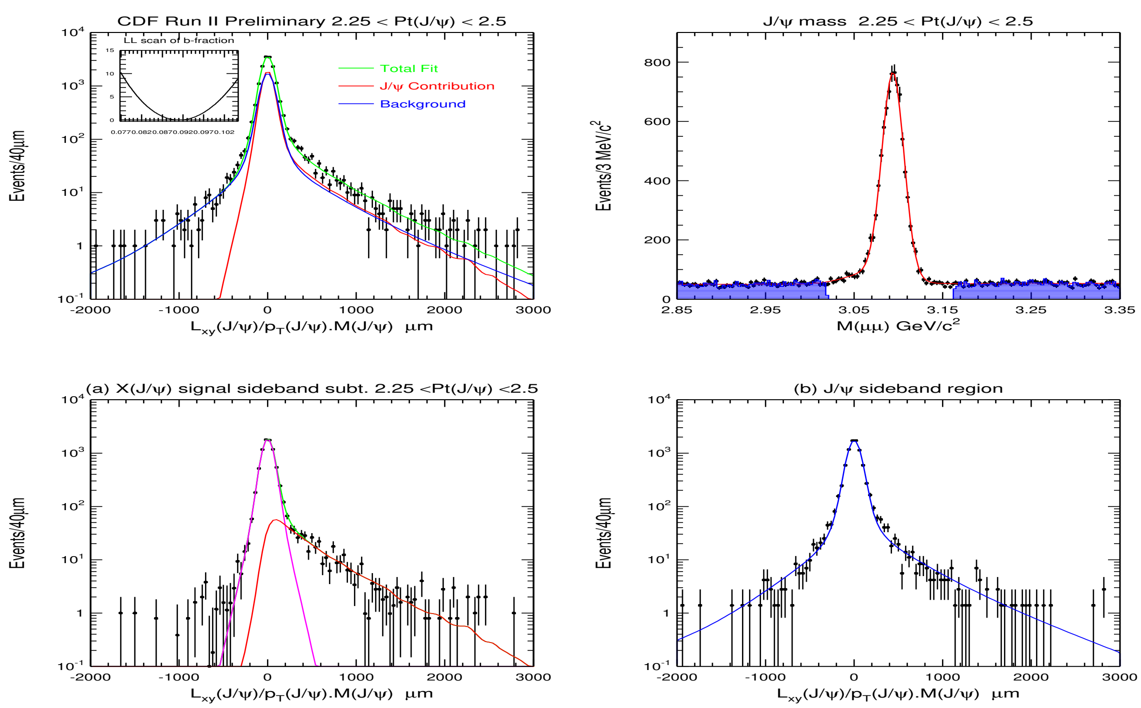

Figure 60: Projection of fit distributions on J/ψ invariant mass and decay length distributions.

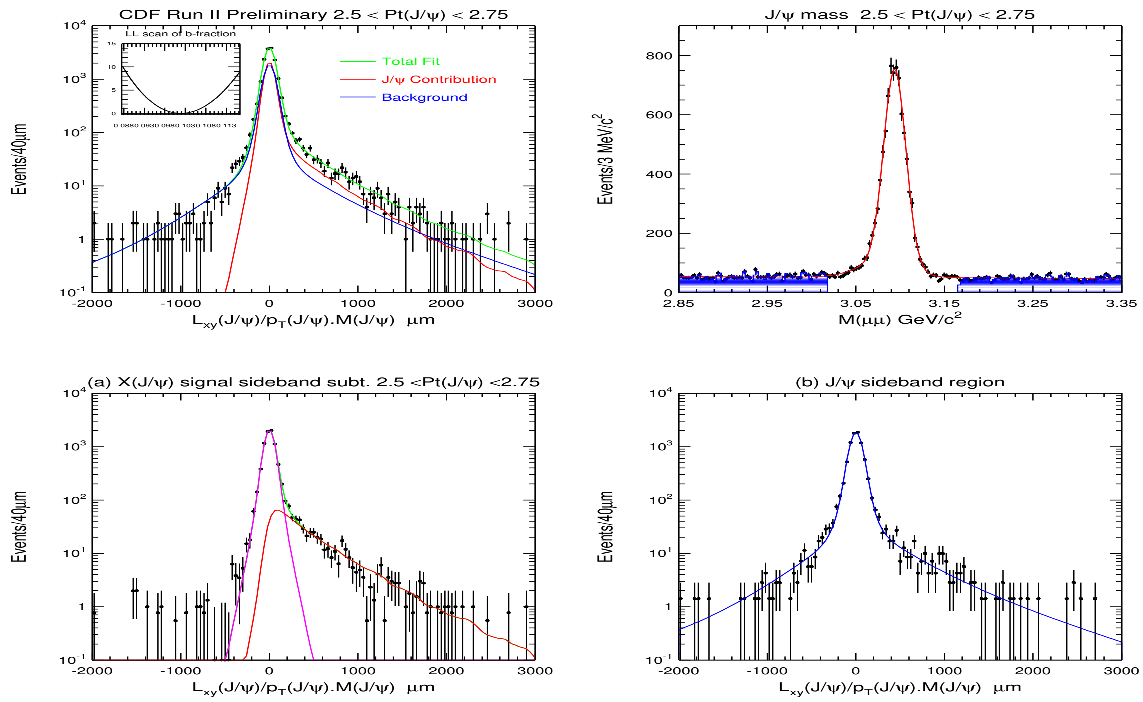

Figure 61: Projection of fit distributions on J/ψ invariant mass and decay length distributions.

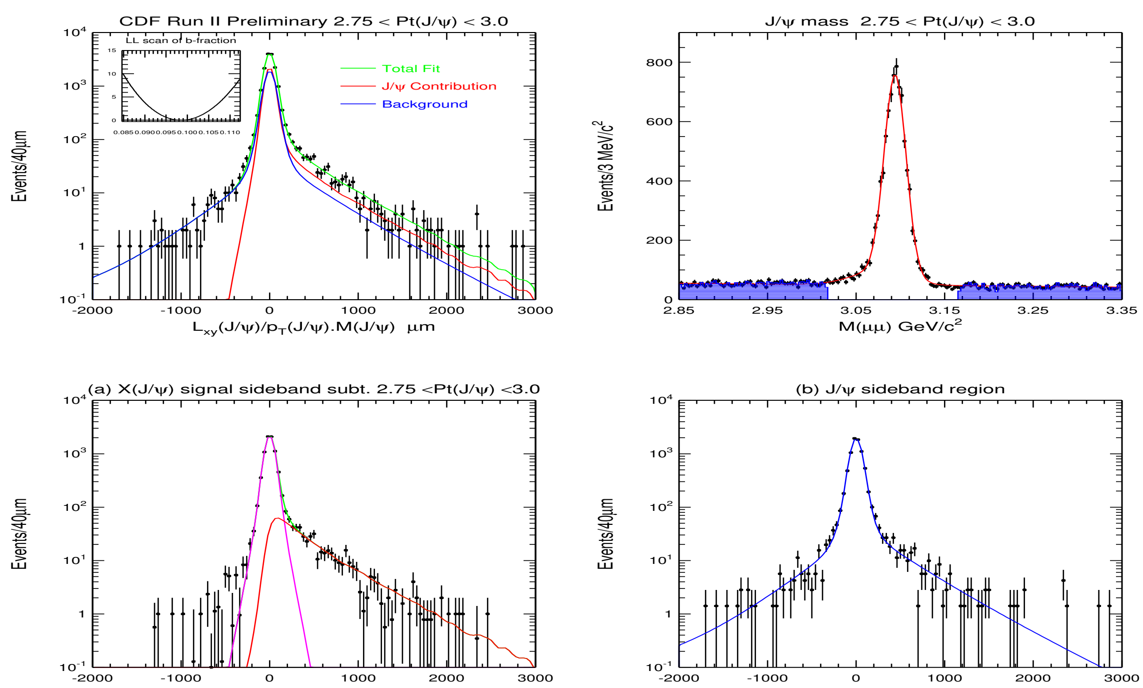

Figure 62: Projection of fit distributions on J/ψ invariant mass and decay length distributions.

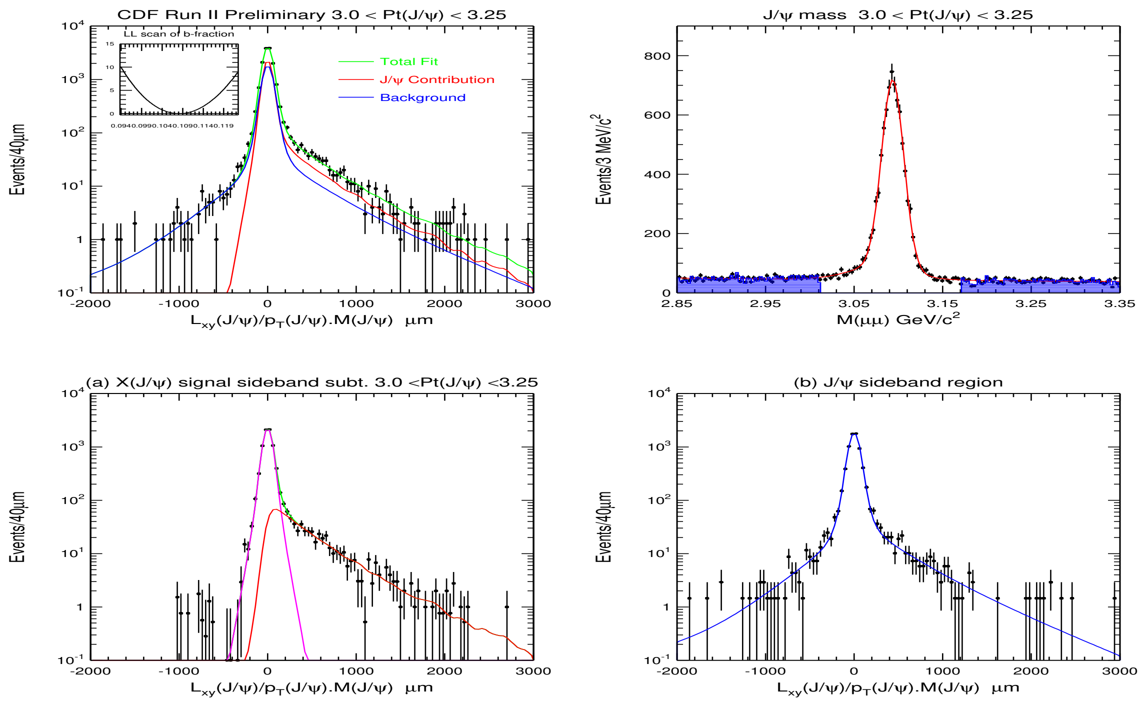

Figure 63: Projection of fit distributions on J/ψ invariant mass and decay length distributions in p_T bin 2.25-2.5 GeV/c using F-factor convolutions.

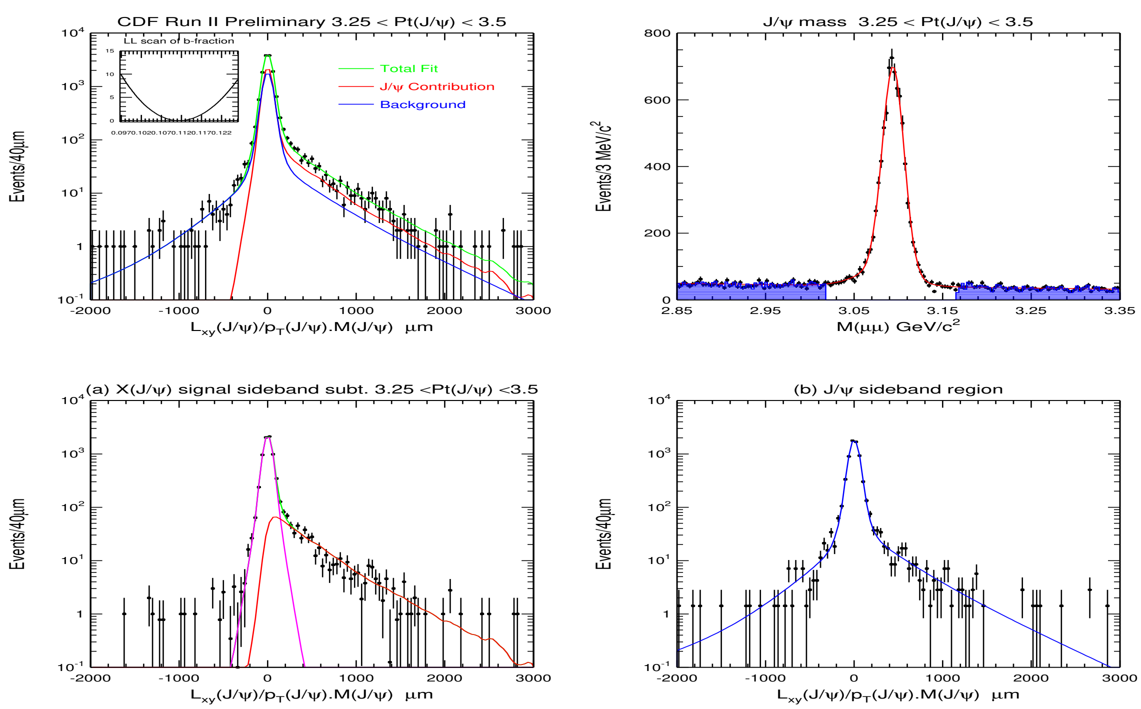

Figure 64: Projection of fit distributions on J/ψ invariant mass and decay length distributions.

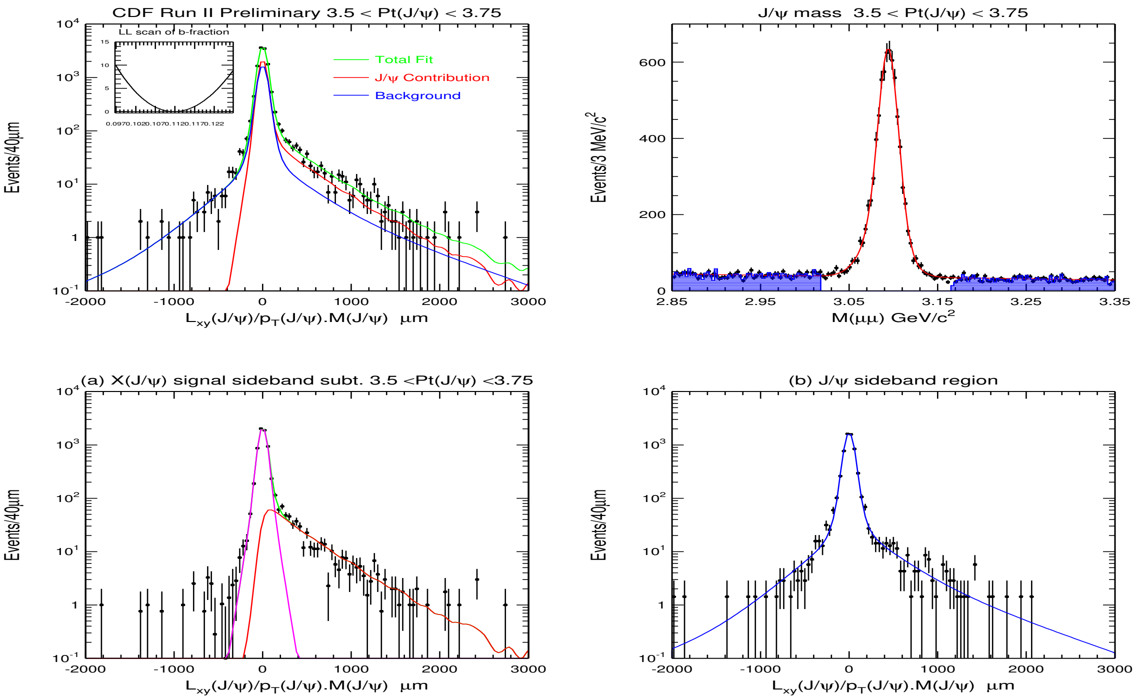

Figure 65: Projection of fit distributions on J/ψ invariant mass and decay length distributions.

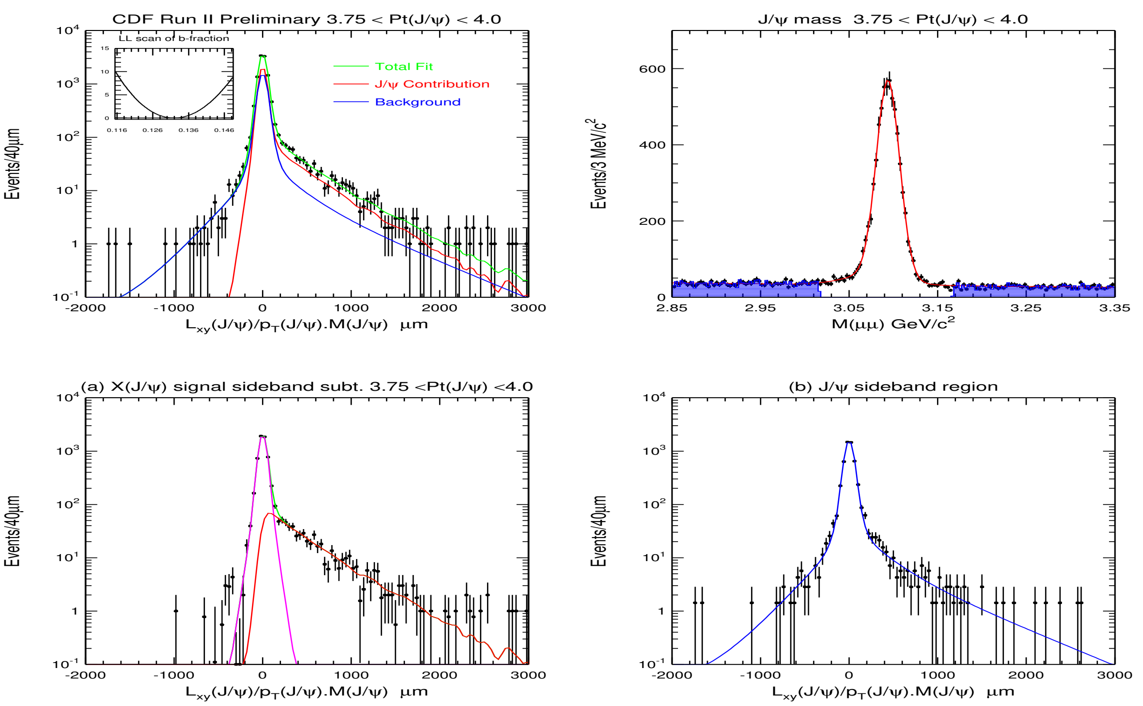

Figure 66: Projection of fit distributions on J/ψ invariant mass and decay length distributions.

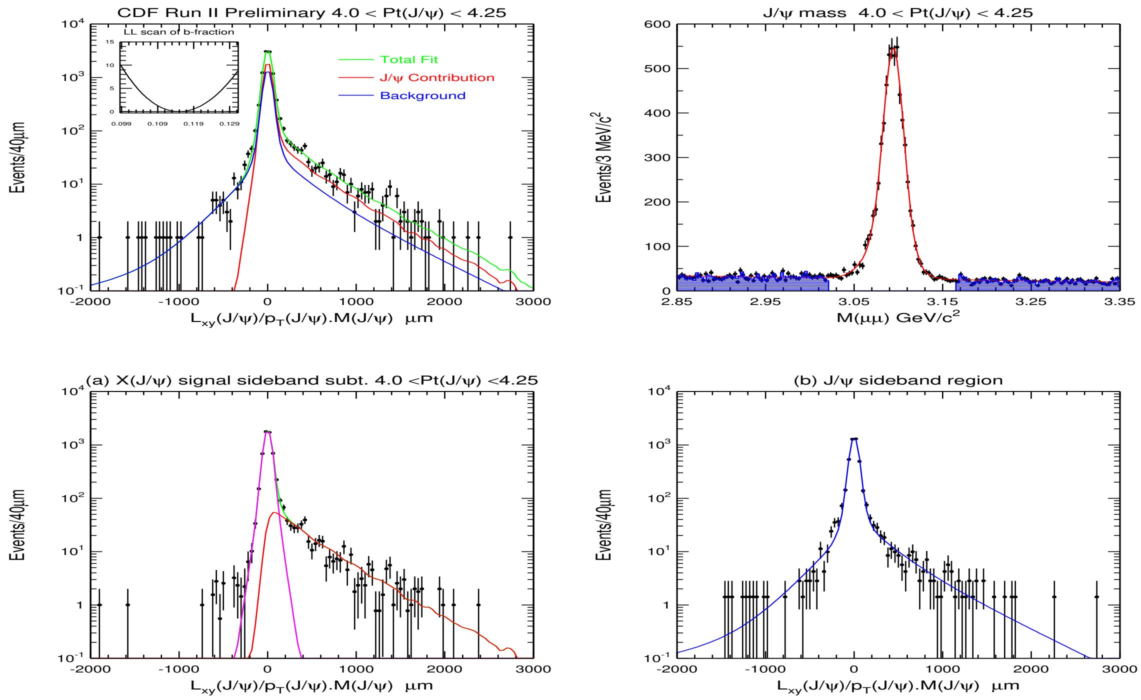

Figure 67: Projection of fit distributions on J/ψ invariant mass and decay length distributions.

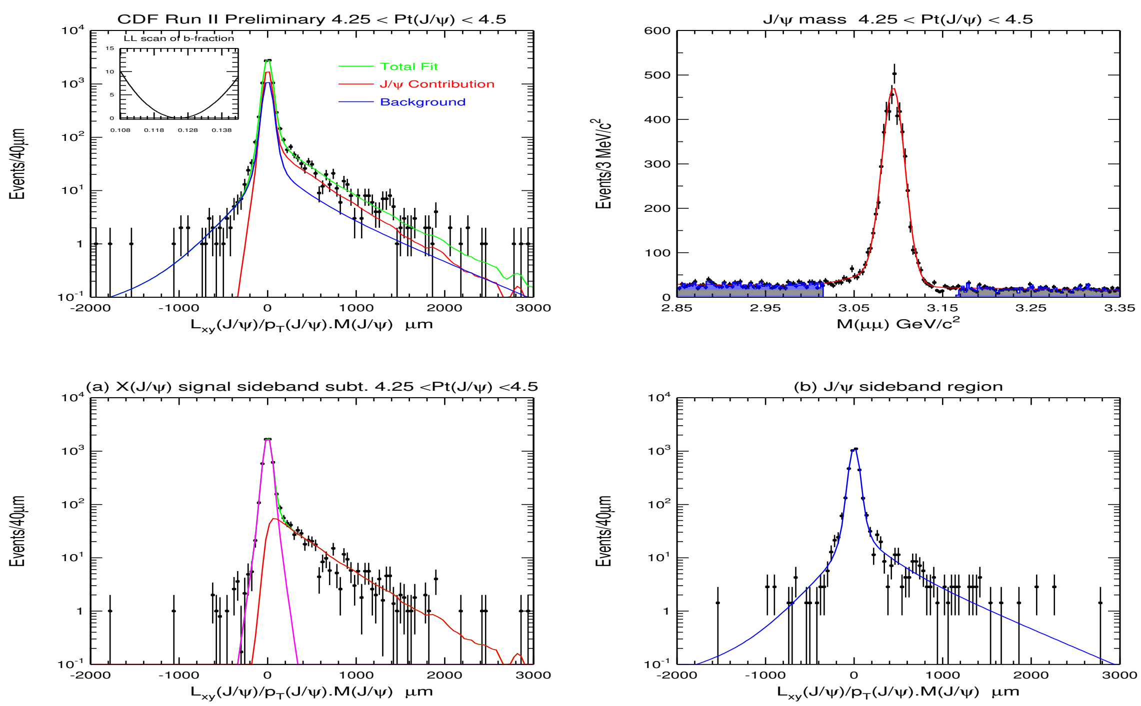

Figure 68: Projection of fit distributions on J/ψ invariant mass and decay length distributions

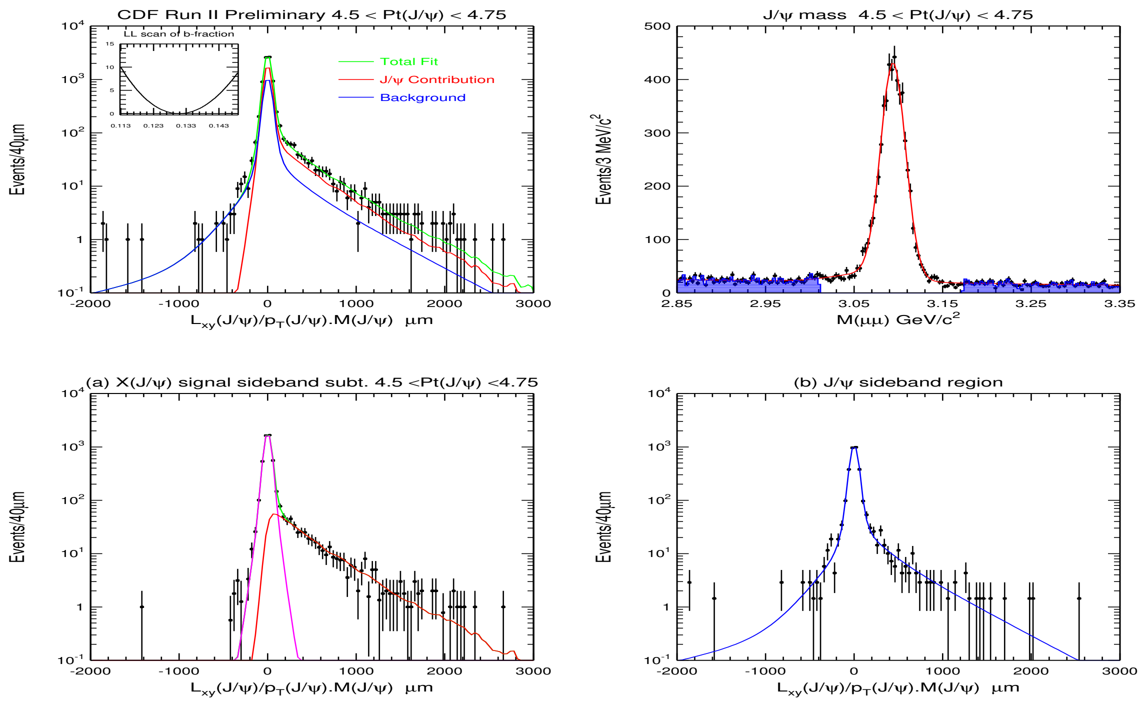

Figure 69: Projection of fit distributions on J/ψ invariant mass and decay length distributions

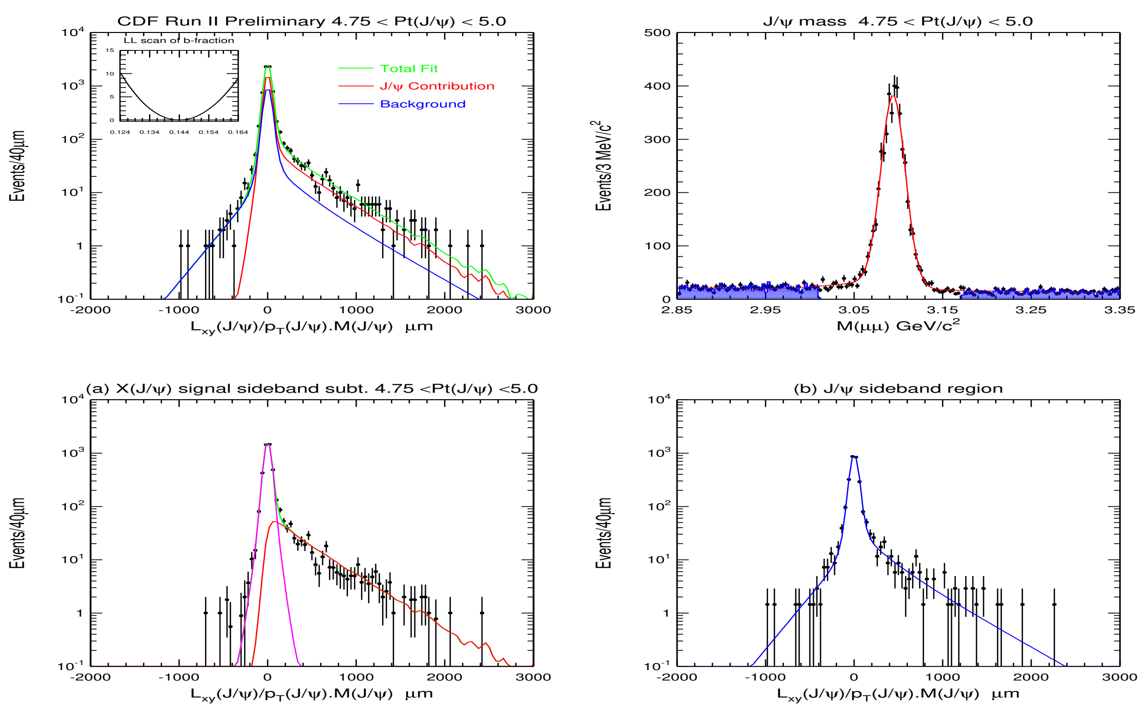

Figure 70: Projection of fit distributions on J/ψ invariant mass and decay length distributions

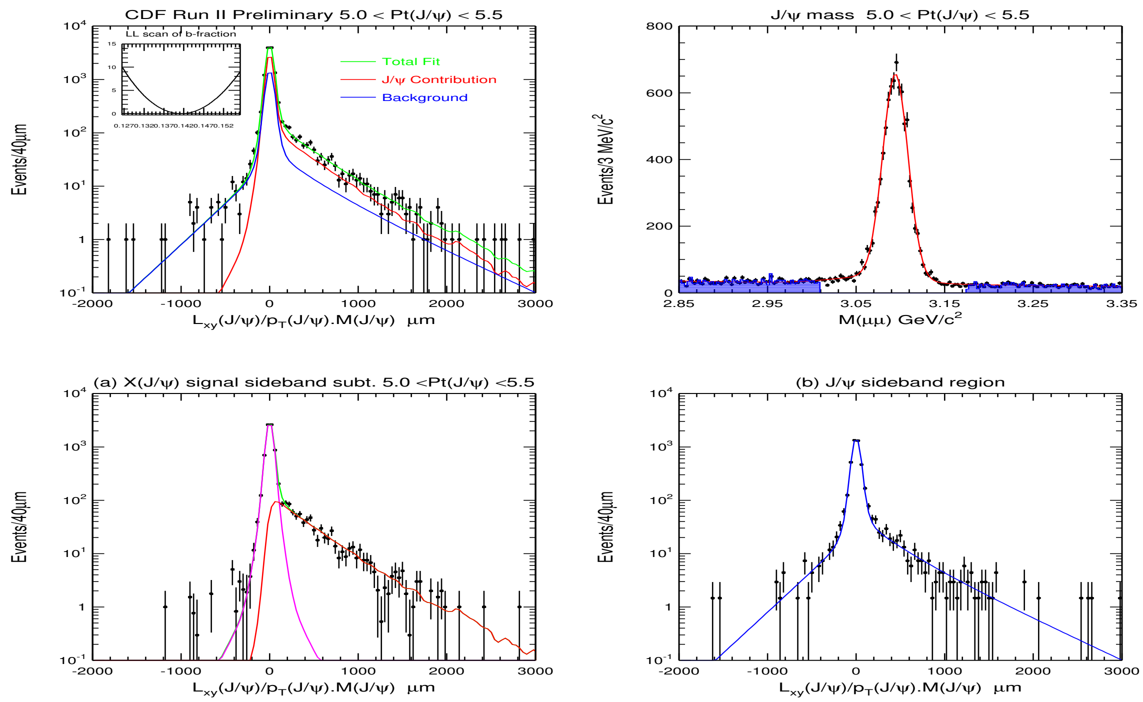

Figure 71: Projection of fit distributions on J/ψ invariant mass and decay length distributions

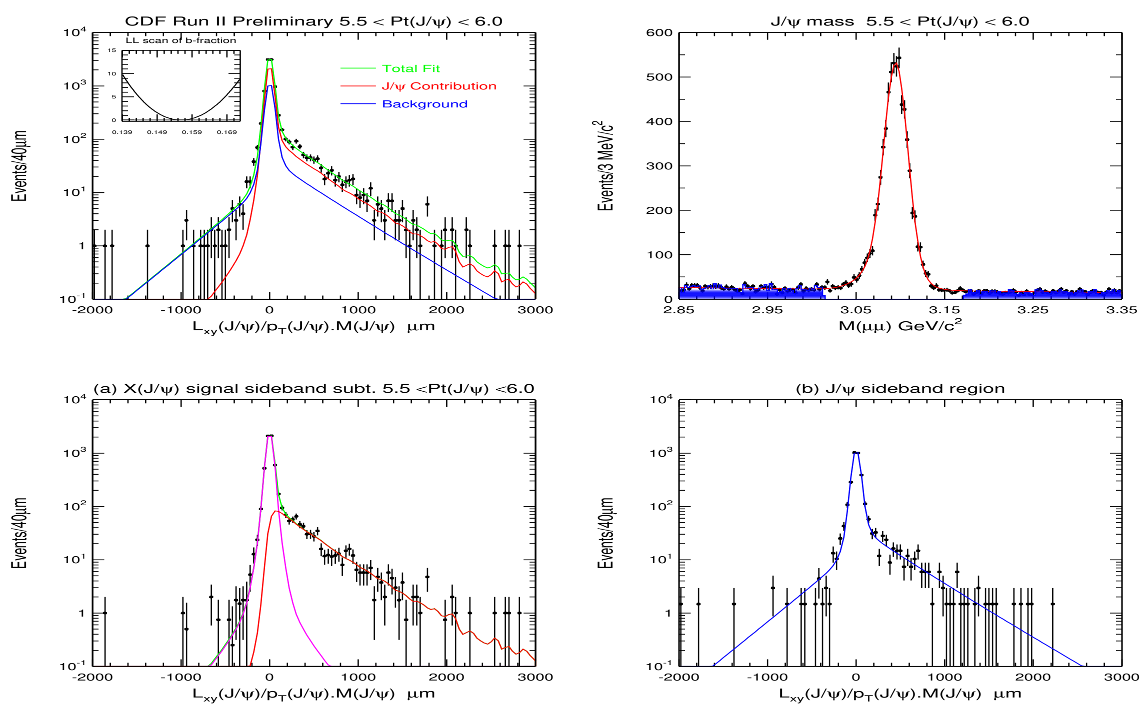

Figure 72: Projection of fit distributions on J/ψ invariant mass and decay length distributions

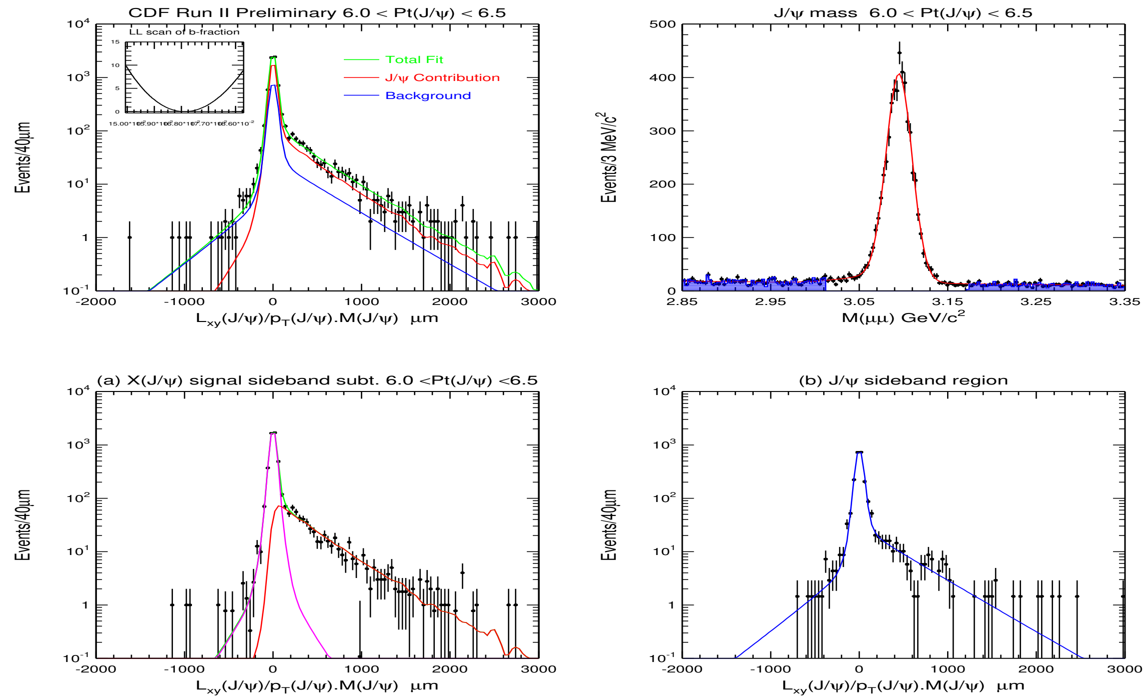

Figure 73: Projection of fit distributions on J/ψ invariant mass and decay length distributions

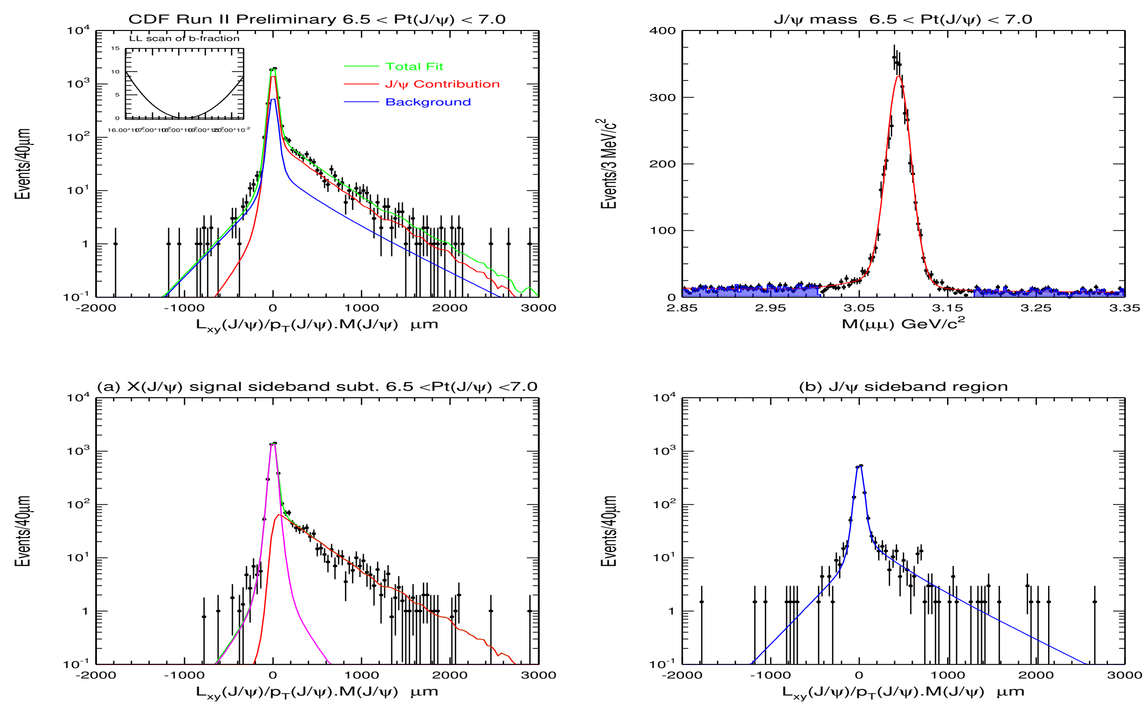

Figure 74: Projection of fit distributions on J/ψ invariant mass and decay length distributions

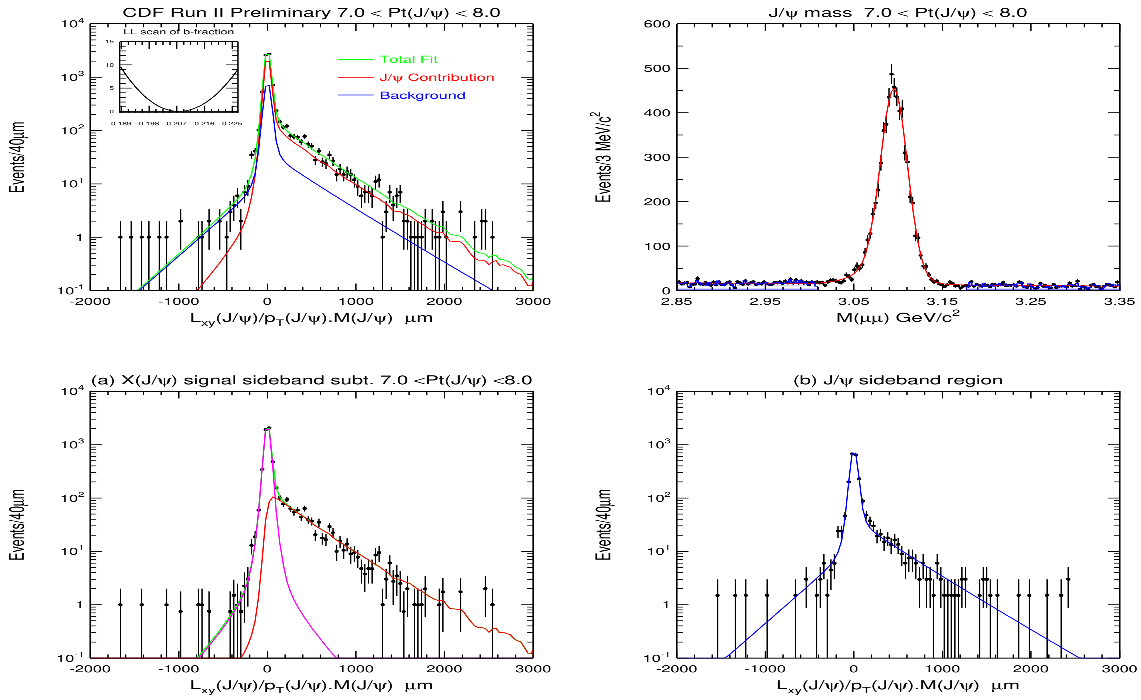

Figure 75: Projection of fit distributions on J/ψ invariant mass and decay length distributions

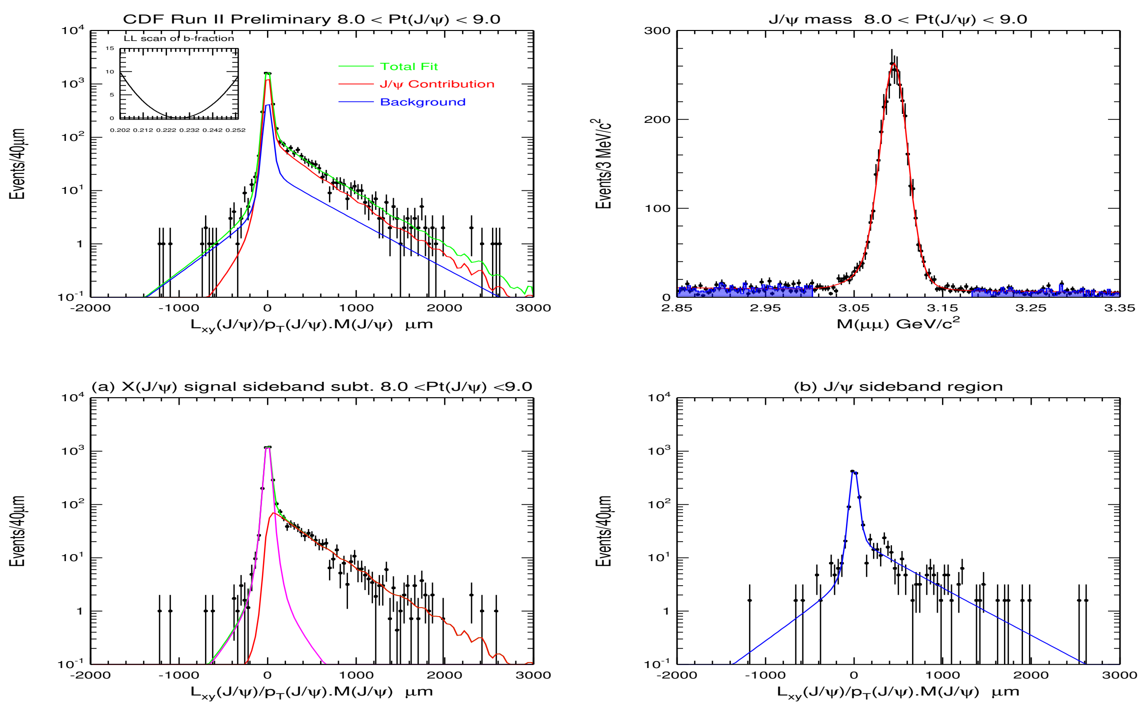

Figure 76: Projection of fit distributions on J/ψ invariant mass and decay length distributions

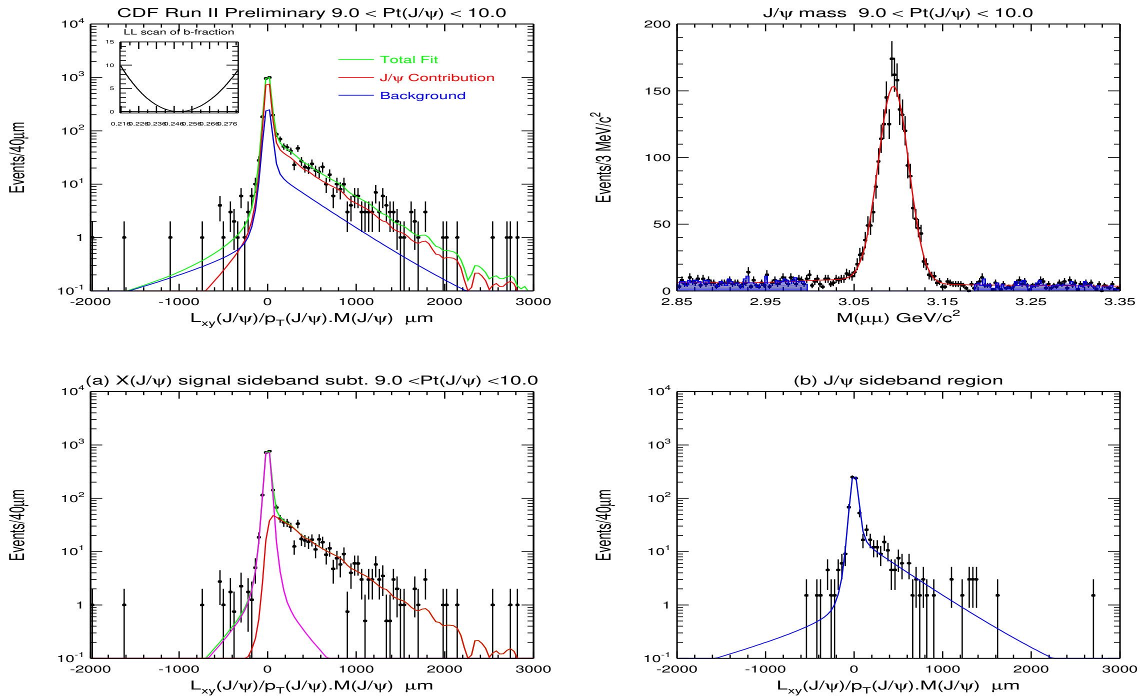

Figure 77: Projection of fit distributions on J/ψ invariant mass and decay length distributions

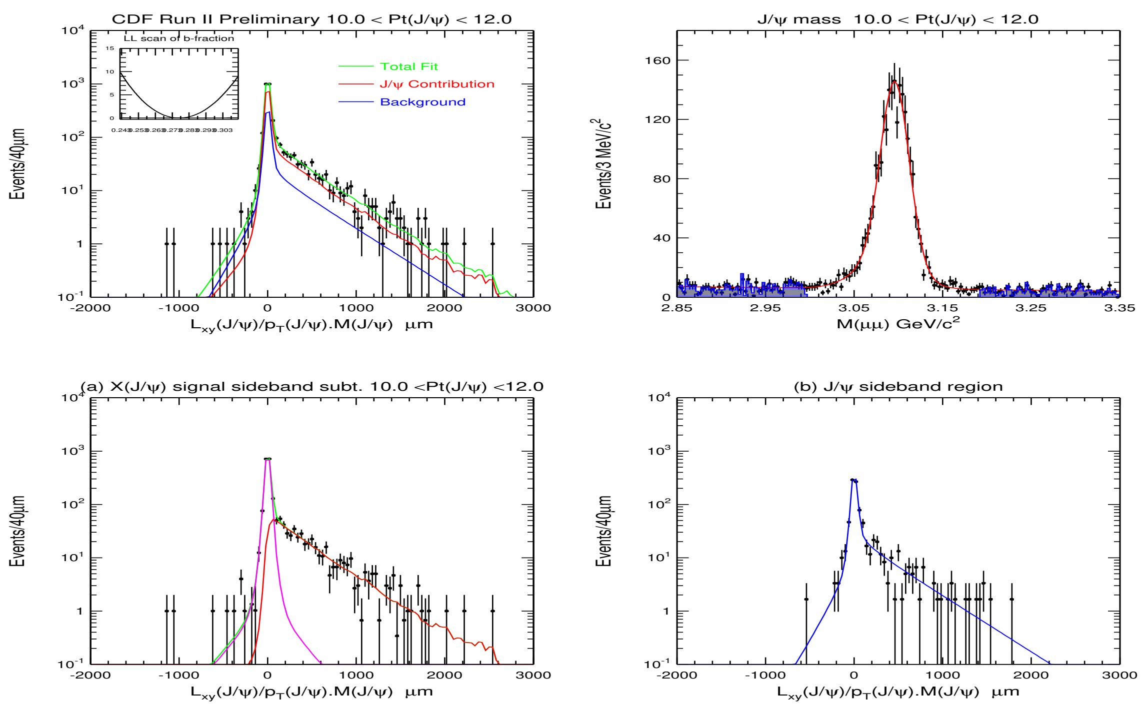

Figure 78: Projection of fit distributions on J/ψ invariant mass and decay length distributions

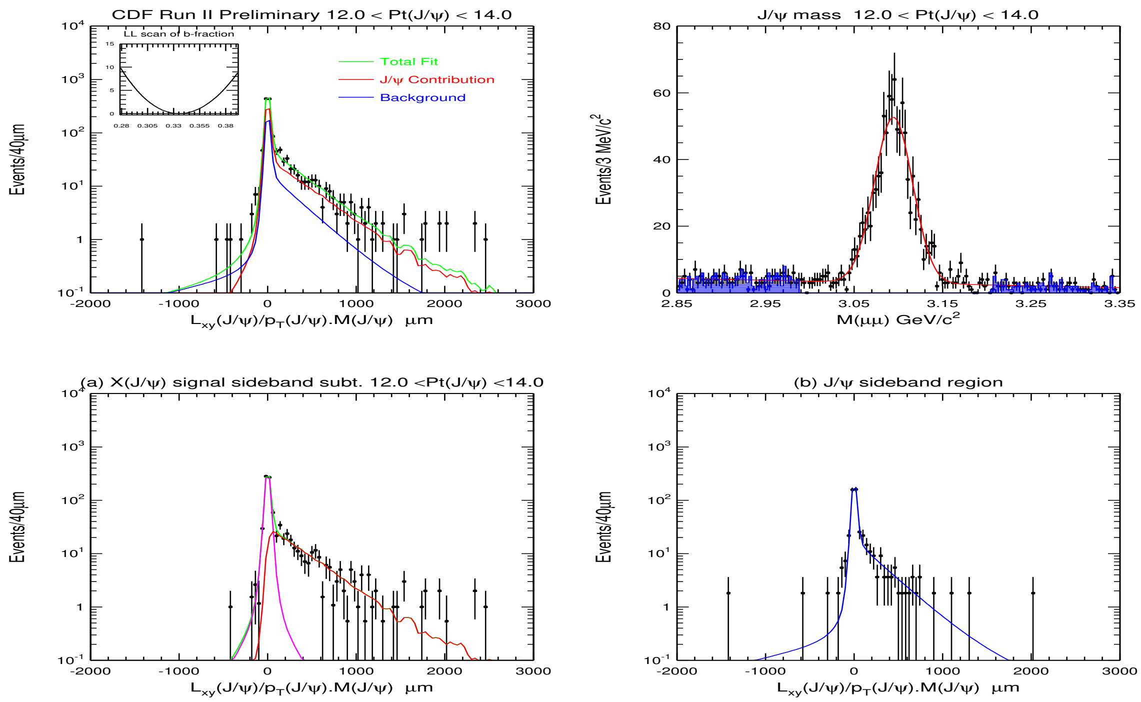

Figure 79: Projection of fit distributions on J/ψ invariant mass and decay length distributions

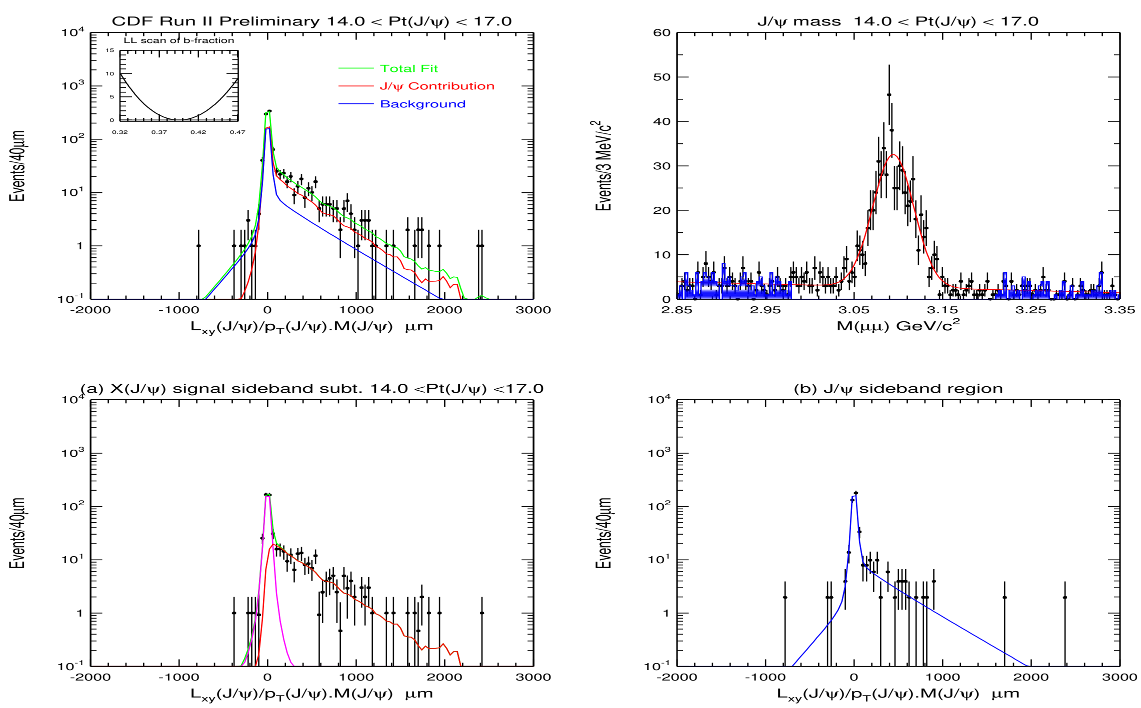

Figure 80: Projection of fit distributions on J/ψ invariant mass and decay length distributions

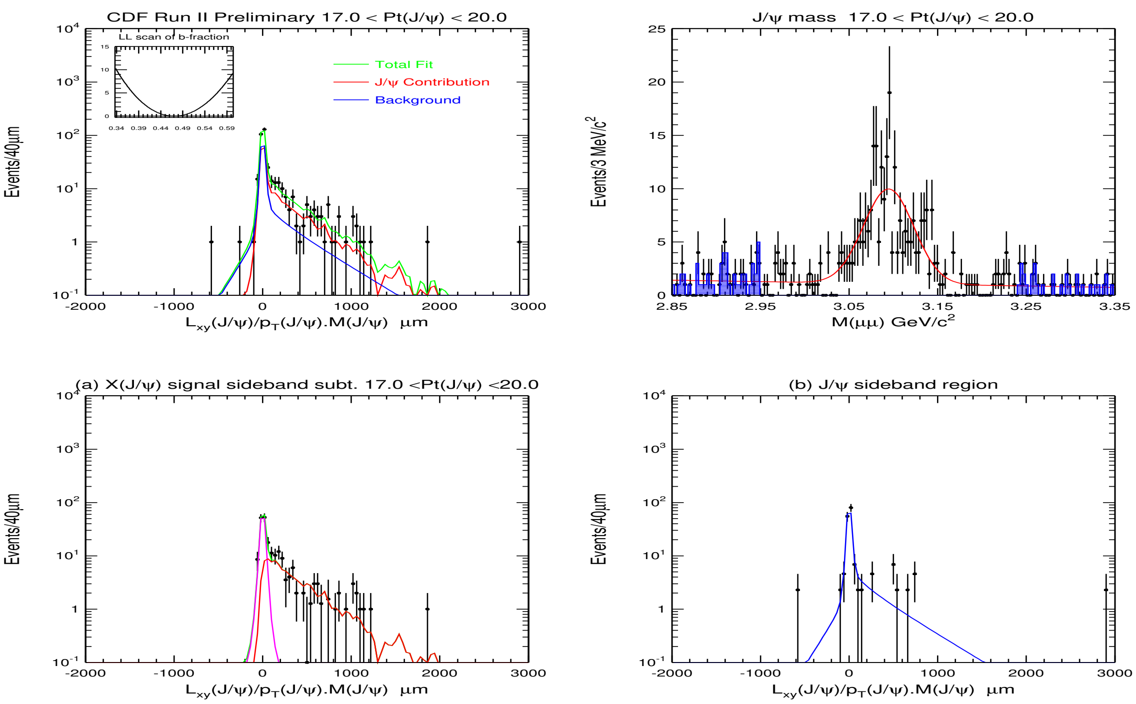

Figure 81: Projection of fit distributions on J/ψ invariant mass and decay length distributions

C MC modeling of the b-hadron production spectrum

The variation in the output b-hadron production spectrum from default Bgenerator as a function of the Peterson parameter and input quark spectra is shown in Figures 82 and 83.

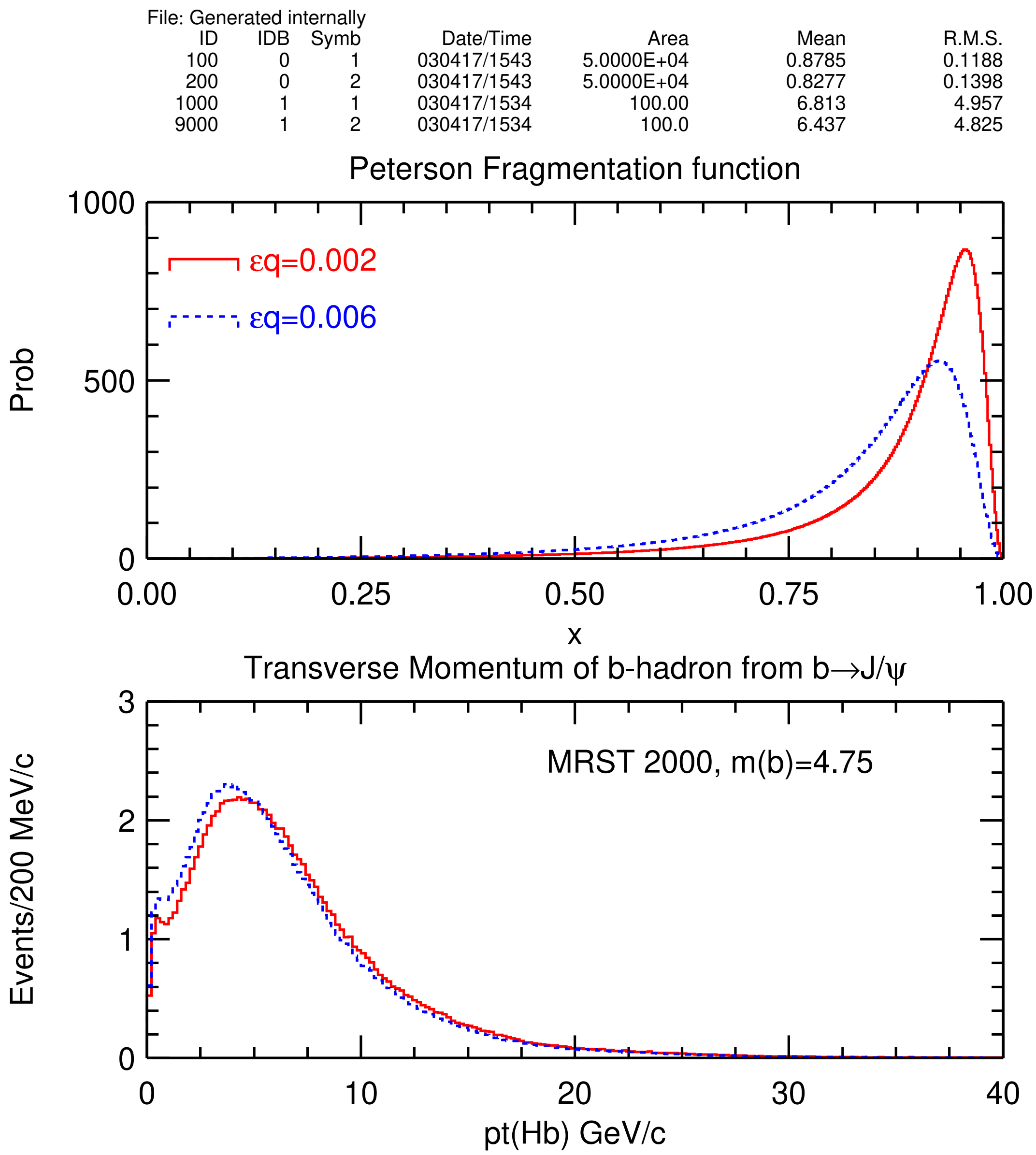

Figure 82: Peterson Fragmentation function (top) b-hadron p_T distrubutions from Bgenerator (bottom). The dashed lines are the distributions using the default Peterson parameter $\epsilon_q = 0.006$ and the solid line is using a Peterson parameter $\epsilon_q = 0.002$

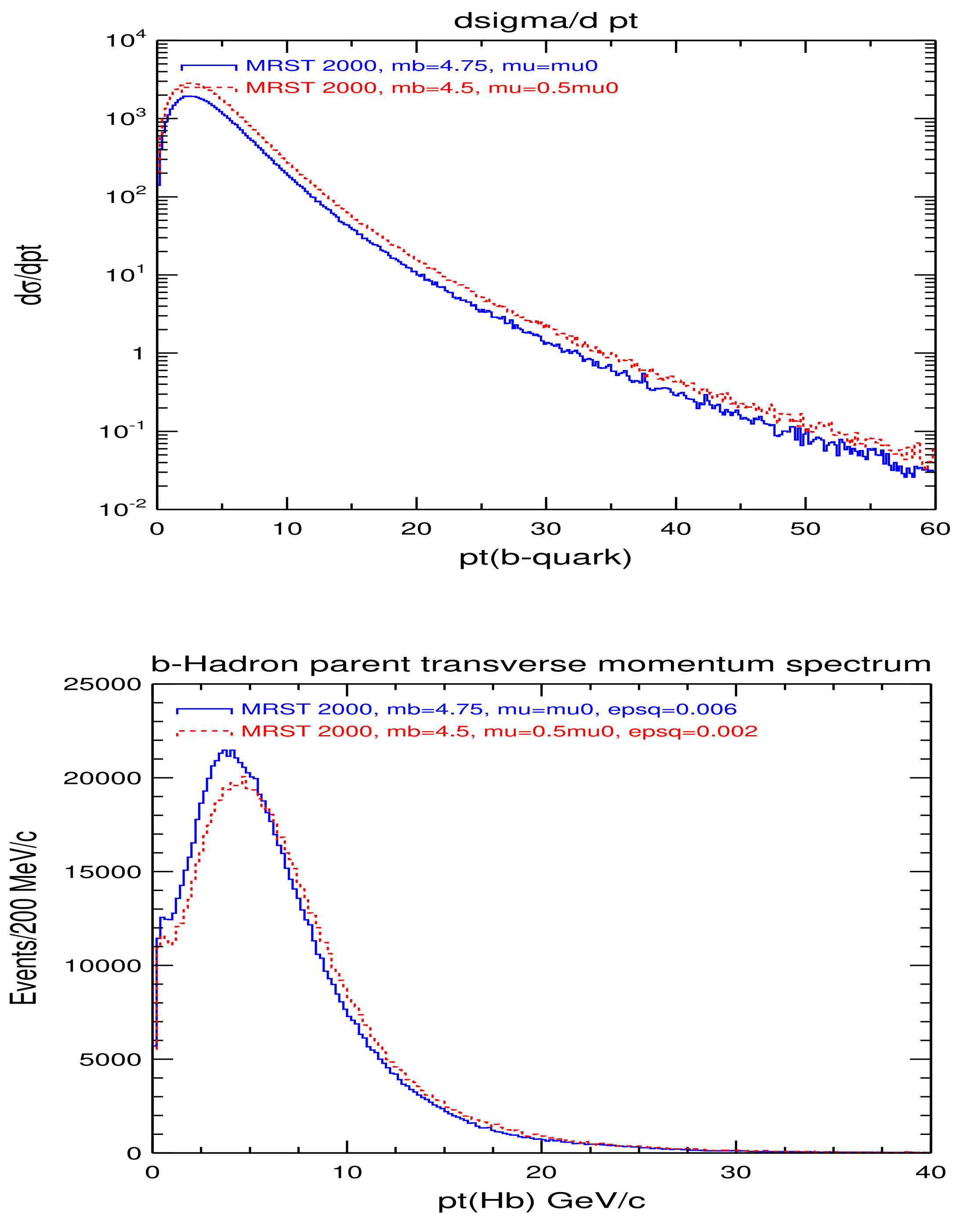

Figure 83: Varying the input to Bgen and the resulting change in b-Hadron transverse momentum distributions for events with J/ψs passing the muon fiducial and trigger selection critirea.

D F-factor distributions

The F-factor distributions in different J/ψ p_T regions are shown in Figure 84 and 85 for a realistic production spectrum and for a flat spectrum respectively. The mean of the F-factor distribution plotted in Figure 86 is approx constant for all values of $p_T(J/\psi) > 1.0$ GeV/c and is found to be ~ 0.83. The RMS of the distribution is determined largely by the $b \to J/\psi X$ decay kinematics and increases with decreasing p_T as is indicated by the errof bars on Figure 86. The F-factor mean as a function of $p_T(J/\psi)$ on a finer scale showing the variation as a function of changes in the production and decay spectra is shown in Figure 87.

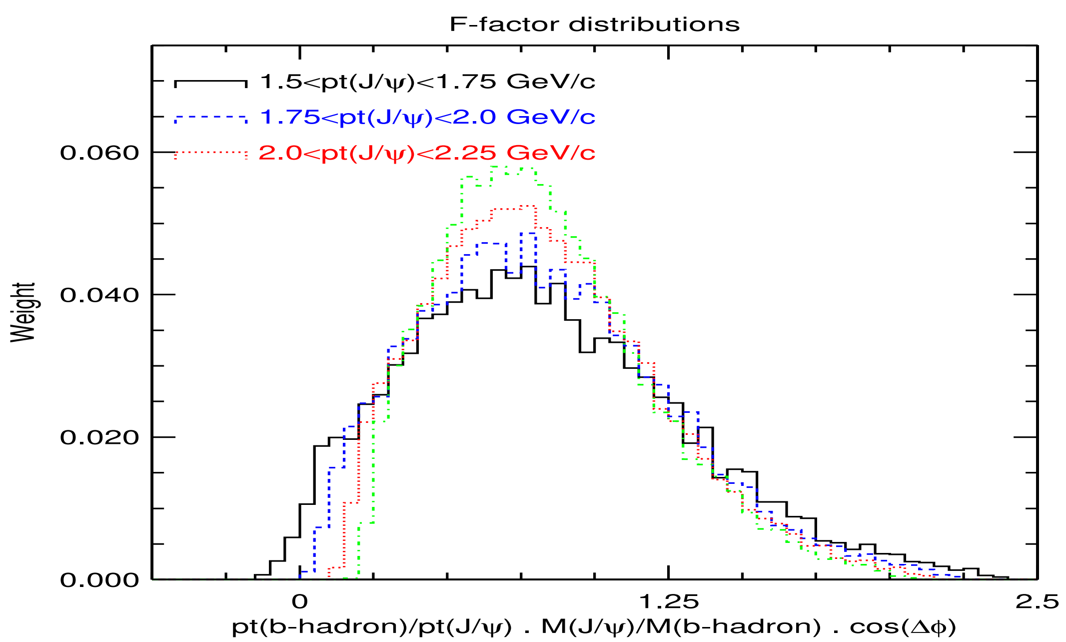

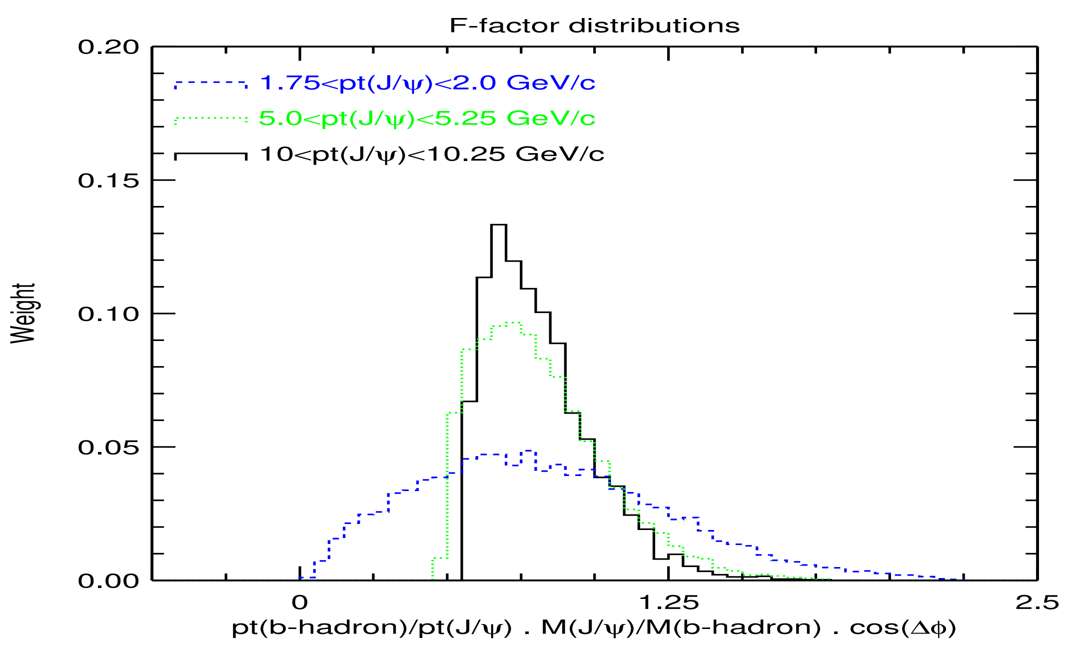

Figure 84: Momentum correction factor, F, distributions from generator level $B \to J/\psi X$ decays in representative J/ψ p_T bins.

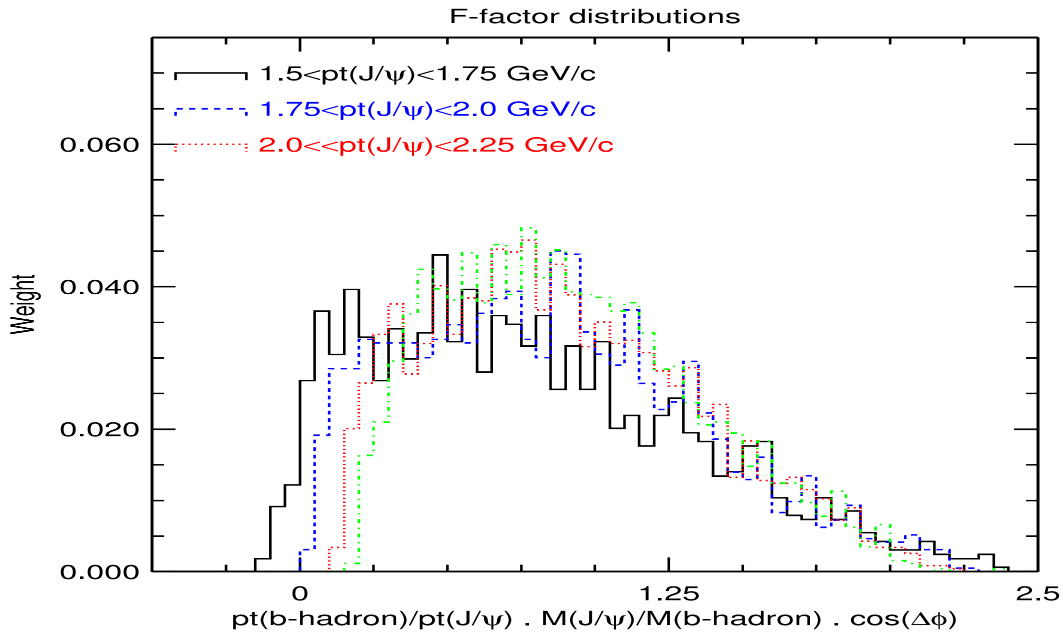

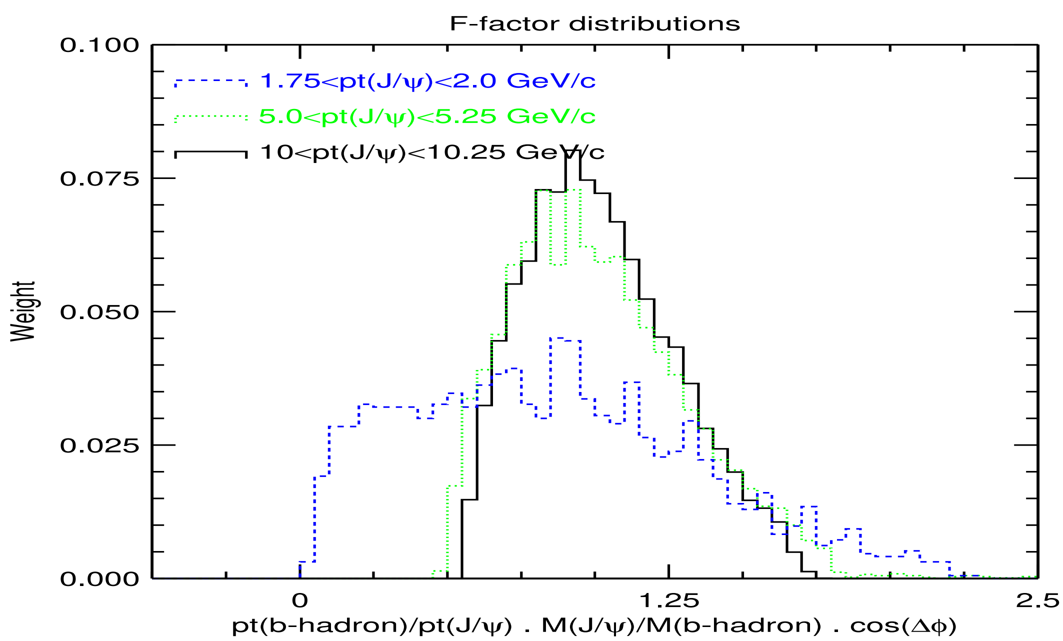

Figure 85: Momentum correction factor, F, distributions from generator level $B \to J/\psi X$ decays in representative J/ψ p_T bins. These distributions are generated using a b-hadron spectrum flat in p_T and y.

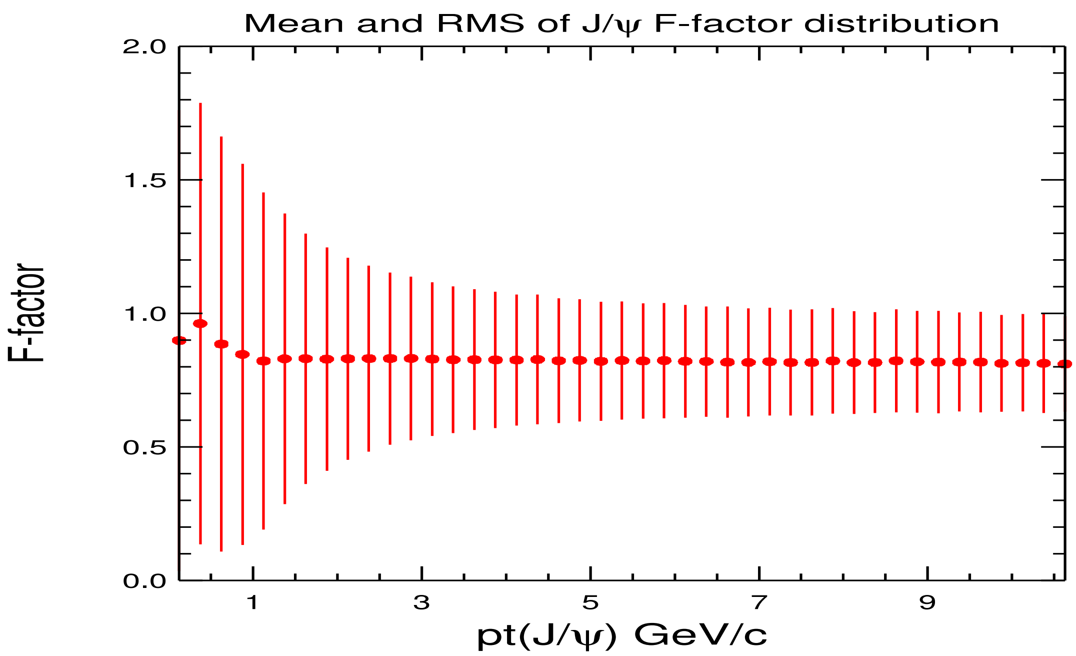

Figure 86: Momentum correction factor, F, mean (points) and RMS (error bars) distributions from generator level $B \to J/\psi X$ decays in all J/ψ p_T bins

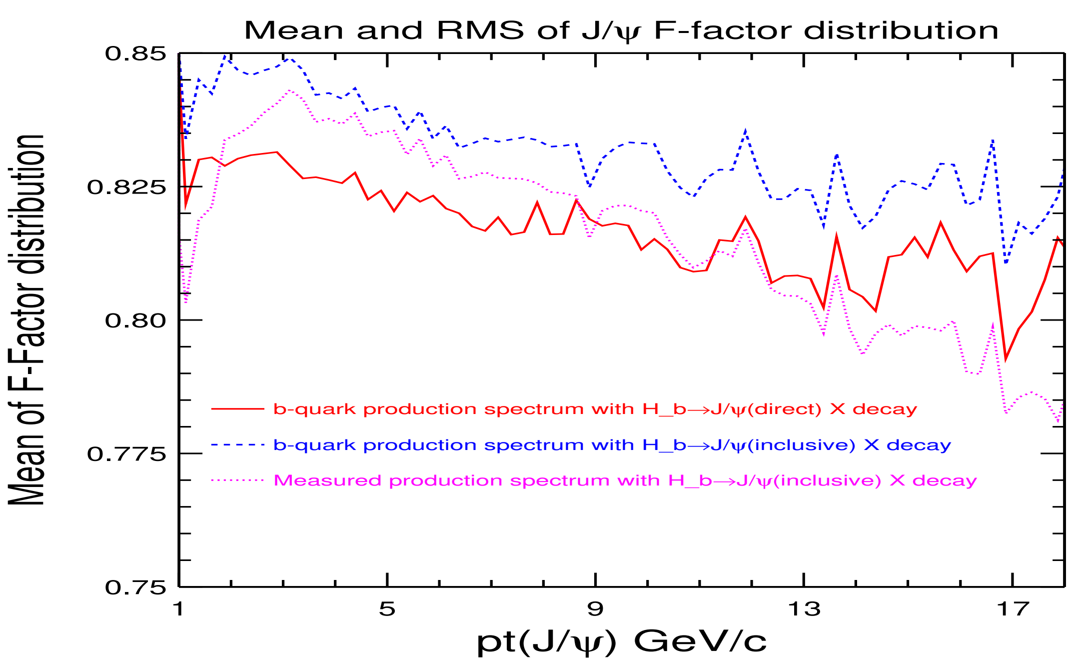

Figure 87: A comparison between the mean of the F-factor distributions as a function of $p_T(J/\psi)$ using different input b-hadron spectra and $b \to J/\psi X$ decay kinematics.

E Fit to J/ψ pseudo $c\tau$ from realistic SVXII $H_b \to J/\psi X$ MC

A full GEANT simulation of the generated $b \to J/\psi X$ events using a patched version of CDF software 4.9.1 including realistic SVXII (without bow misalignments) coverage and beamlines from 20 different runs is performed. Using an unbinned likelihood fit to the reconstructed J/ψ pseudo-lifetime distributions from the MC convoluted with the F-factors distributions and detector resolutions, the b inclusive lifetime is extracted in different $p_T(J/\psi)$ ranges. The MC and fit distributions in 3 representative bins are shown in Figure 88 and are in very good agreement. The value of the b-inclusive lifetime is found to be the same over all the J/ψ transverse momentum range considered, a fit to a straight line yields $c\tau_b(\text{realistic MC}) = (479 \pm 3) + (-0.3 \pm 0.4) * p_T(J/\psi)$. The generated value of $< c\tau_b >$ is 475μm from the lifetimes and mix of b-hadrons generated as listed in Table 1. This cross-check constitutes a proof-of-principle - that the shape of the smeared J/ψ pseudo-lifetime distribution and b-hadron inclusive lifetime can be correctly modeled using a convolution with the F-factor distributions for all J/ψ momenta ≥ 2 GeV/c.

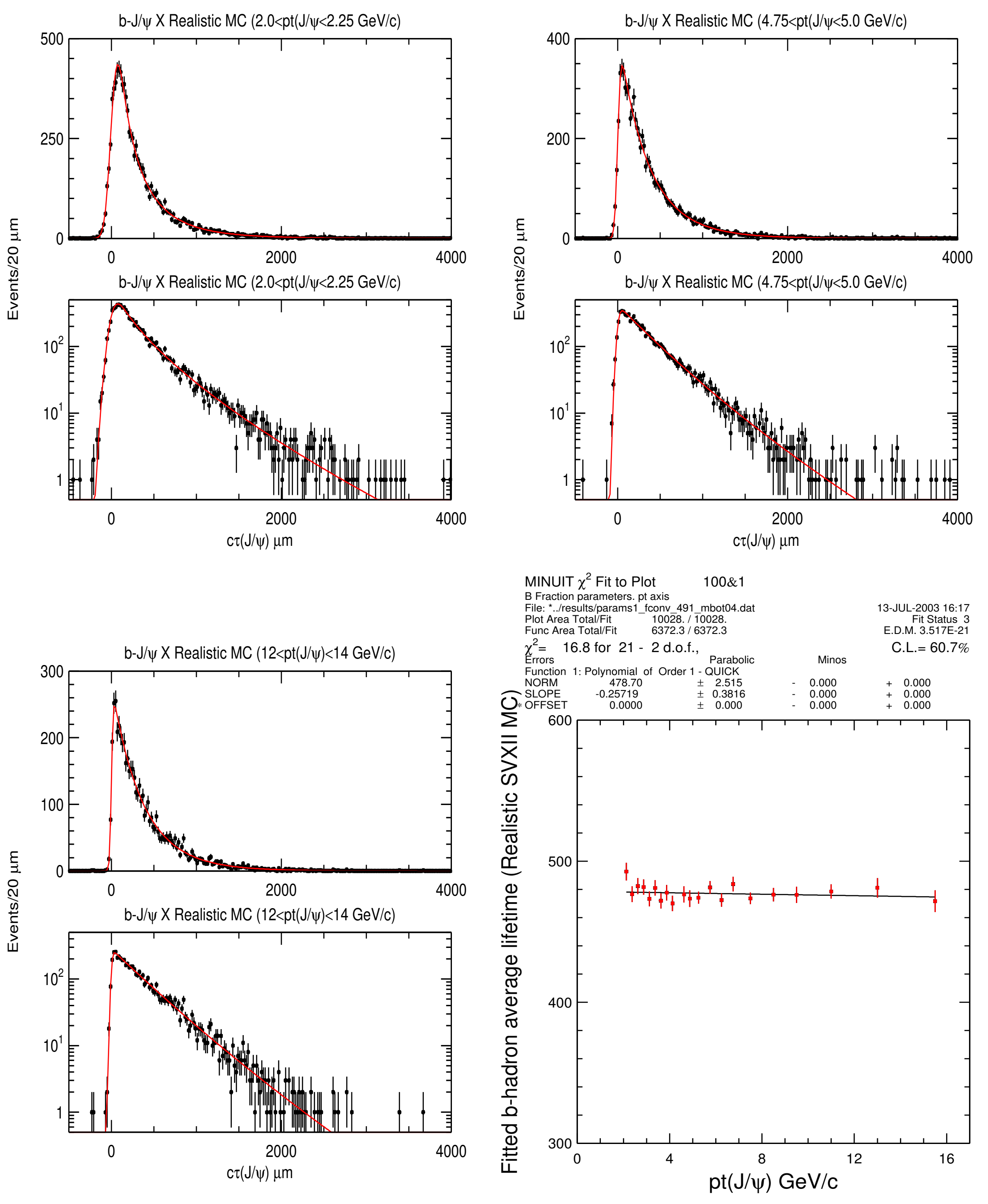

Figure 88: Fit to the realistic MC $b \to J/\psi X$ pseudo-$c\tau$ shape using F-Factors in different $p_T(J/\psi)$ bins. The bottom right plot shows the value of the b hadron inclusive lifetime obtained from the fit in all bins from 2-17 GeV/c. The fit to a straight line is $c\tau_b(\text{realistic MC}) = (479 \pm 3) + (-0.3 \pm 0.4) * p_T(J/\psi)$.

F R_{xy} vs L_{xy}

R_{xy} is defined as the pure flight distance of the J/ψ in the $r-\phi$ plane, and L_{xy} is the signed projection of the J/ψ transverse momenta on the J/ψ flight distance as shown in Figure 10. By construction L_{xy} is shorter than R_{xy}. For prompt J/ψ which are distrubuted randomly in $r-\phi$, $< L_{xy}(prompt) >\sim \pm 0.64 < R_{xy}(prompt) >$, which improves the seperation between the prompt and $H_b \to J/\psi X$ events in the region where the H_b and J/ψ directions are strongly correlated and $L_{xy}(J/\psi) \approx R_{xy}(J/\psi)$. At low momentum J/ψ the angular correction factor could potentially reduce the seperation power between prompt J/ψ and short-lived $H_b \to J/\psi X$ events. The L_{xy} and R_{xy} distributions are compared in Figures 90, 91, 92. Since L_{xy} is a signed quantity distributed symmetrically around 0 for 0 lifetime events, the 2-track flight distance resolution can be measured by examining the L_{xy} distributions of prompt J/ψ in data. We find that the resolution for events with $2.0 < p_T < 3.0$ is $\sigma \sim 50\mu$m including a 30 μm beam spot and increases linearly with p_T after that (Section 5.1). To assess the seperation power between prompt and slow b-hadrons of L_{xy} and R_{xy} below 3.0 GeV/c where the b-fraction is $\sim 9-10\%$, a mixture of prompt J/ψ and $H_b \to J/\psi$ MC events in the ratio 9:1 were generated with beam spot, 2-track vertex postions and COT momenta smeared to match the data. The fraction of b events in the overlap region with the prompt J/ψ for both L_{xy} and R_{xy}, indicated by the shaded region in Figure 93, is counted and the results listed in Table 29 and plotted in Figure 89.

We find that the fraction of H_b events in the overlap region of L_{xy} is less than or equal to the fraction in the R_{xy} distribution for all J/ψ with momenta > 1.25 GeV/c. In addition to slightly improving the separation between H_b and prompt J/ψ in the region > 1.25 GeV/c, the main advantage of using L_{xy} as the kinematic variable to seperate the long-lived J/ψ events is that prompt J/ψ events with negative values of L_{xy} are due to mismeasurements or resolution effects. This allows us to use the negative values of L_{xy} from the dominant prompt J/ψ decays to extract the resolution function from the same data. Below 1.7 GeV/c, real H_b decays will produce -ve values of L_{xy} due to large opening angles between the H_b flight direction and the soft J/ψ. For events with $1 < p_T(J/\psi) < 1.7$ GeV/c the fraction of these b events with -ve tails is $< 10\%$ as listed in Table 30 and is small compared to the resolution effects from prompt J/ψ events (Figure 93); for e.g. early studies indicate the b-fractions in the $1.0 < p_T(J/\psi) < 2.0$ GeV/c bins are $\approx 10\%$ therefore $< 1\%$ of events in the inclusive J/ψ distribution with $L_{xy} < 0$ are from $H_b \to J/\psi X$. Ultimately ,the choice of which flight distance variable to use to separate prompt from b decays is a question of statistical power versus systematic control. Since we extract the b-fractions from

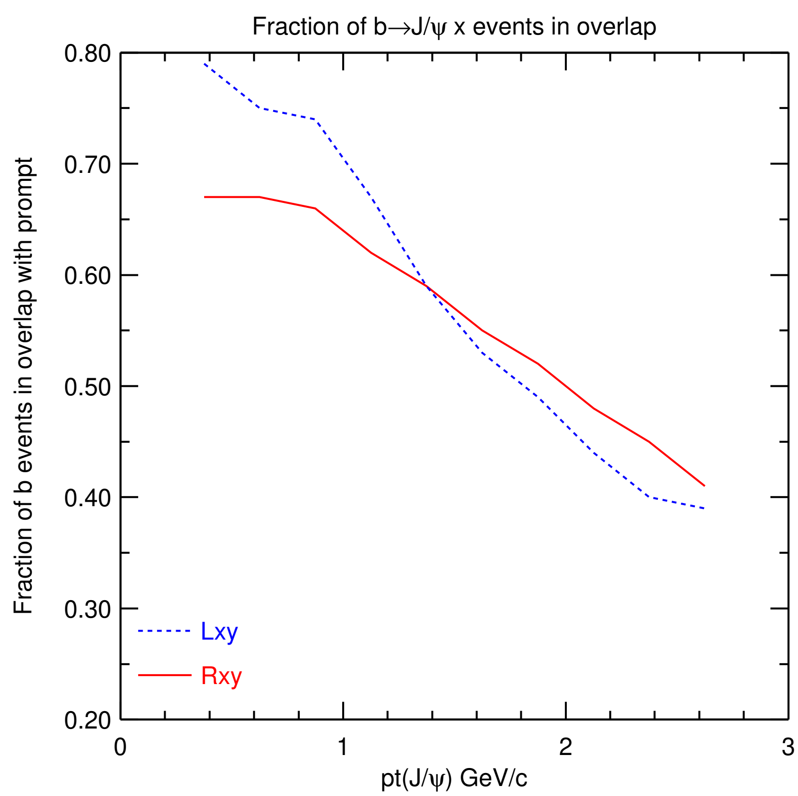

Figure 89: Fraction of $b \to J/\psi$ events in the overlap region of the prompt J/ψ distribution in the lower momentum bins using L_{xy} and R_{xy} values from the MC with Gaussian smearing added. The 2-track vertex resolution is treated as the same for all bins below 3 GeV/c = 40μm and the beam spot is $\sigma_b = 30\mu$m. The MC was produced with a b-fraction of 10% of the total J/ψ. Below 1 GeV/c, the negative L_{xy} tails are longer than the resolution effects in the prompt distribution and the fraction of events listed includes only the events actually below the L_{xy} prompt peak but not the large -ve tails.

$p_T(J/\psi)$ GeV/c	Fraction of b events below R_{xy} peak	Fraction of b events below L_{xy} peak
$0.25 - 0.5$	0.67	0.79
$0.5 - 0.75$	0.67	0.75
$0.75 - 1.0$	0.66	0.74
$1.0 - 1.25$	0.62	0.67
$1.25 - 1.5$	0.59	0.59
$1.5 - 1.75$	0.55	0.53
$1.75 - 2.0$	0.52	0.49
$2.0 - 2.25$	0.48	0.44
$2.25 - 2.5$	0.45	0.40
$2.5 - 2.75$	0.41	0.39

Table 29: Fraction of $b \rightarrow J/\psi$ events in the overlap region of the prompt J/ψ distribution in the lower momentum bins using L_{xy} and R_{xy} values from the MC with Gaussian smearing added. The 2-track vertex resolution is treated as the same for all bins below 3 GeV/c = 40μm and the beam spot is σ_b = 30μm. The MC was produced with a b-fraction of 10% of the total J/ψ. Below 1 GeV/c, the negative L_{xy} tails are longer than the resolution effects in the prompt distribution and the fraction of events listed includes only the events actually below the L_{xy} prompt peak but not the large -ve tails.

J/ψ with momenta > 1 GeV/c - which is sufficient to probe 0 momentum b-hadrons - the signed projection, L_{xy}, is used to extract the b-hadron fraction. In addition, using the quantity $L_{xy}(J/\psi)/p_T(J/\psi)$ in bins of p_T versus using L_{xy} alone reduces our dependence on the J/ψ transverse momentum bin size and placement.

$p_T(J/\psi)$ GeV/c	Fraction of b events with $L_{xy} < 0$
$0.00 - 0.25$	0.42
$0.25 - 0.5$	0.34
$0.5 - 0.75$	0.25
$0.75 - 1.0$	0.16
$1.0 - 1.25$	0.10
$1.25 - 1.5$	0.05
$1.5 - 1.75$	0.01
$1.75 - 2.0$	0.0002
$2.0 - 2.25$	0.0001

Table 30: Fraction of $b \rightarrow J/\psi X$ decays with $L_{xy} < 0$ as a function of J/ψ transverse momenta.

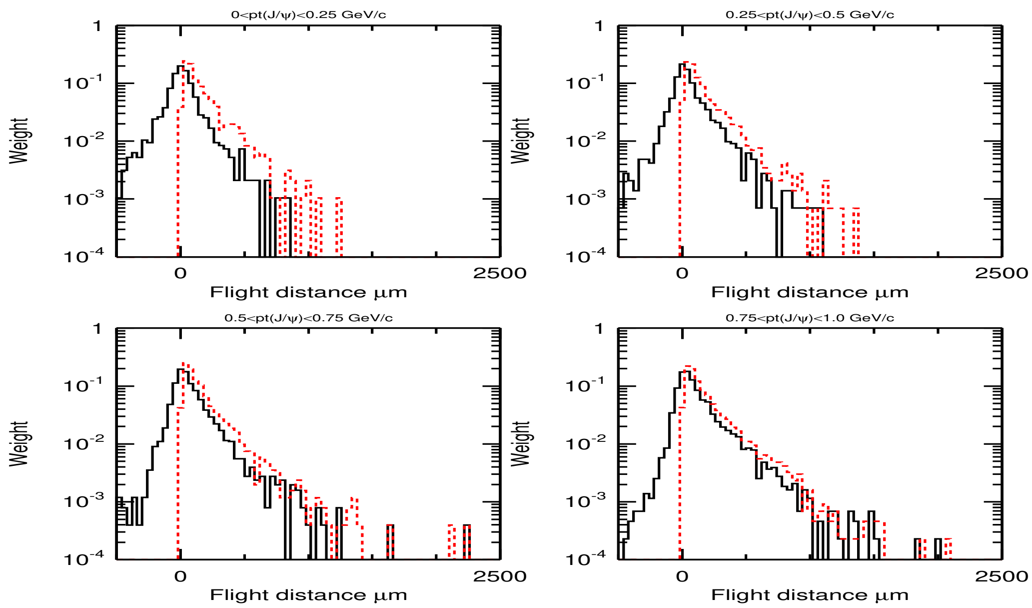

Figure 90: Comparison between the J/ψ from b flight distance in the $r-\phi$, R_{xy} (solid line) and the projection of the J/ψ momentum on R_{xy}, L_{xy} (dashed line). Results are from generator level MC.

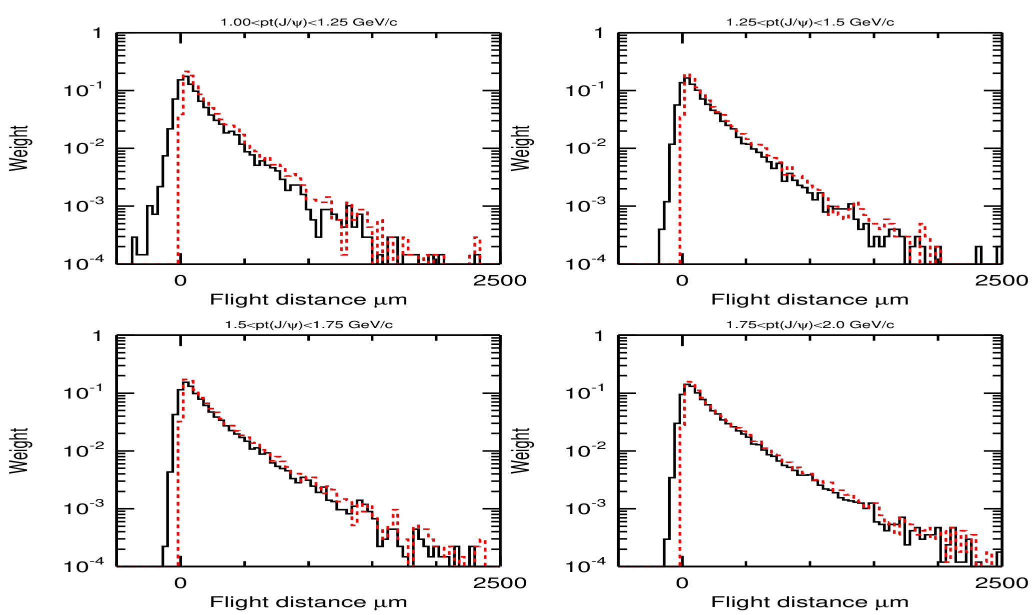

Figure 91: Comparison between the J/ψ from b flight distance in the $r-\phi$, R_{xy} (solid line) and the projection of the J/ψ momentum on R_{xy}, L_{xy} (dashed line). Results are from generator level MC.

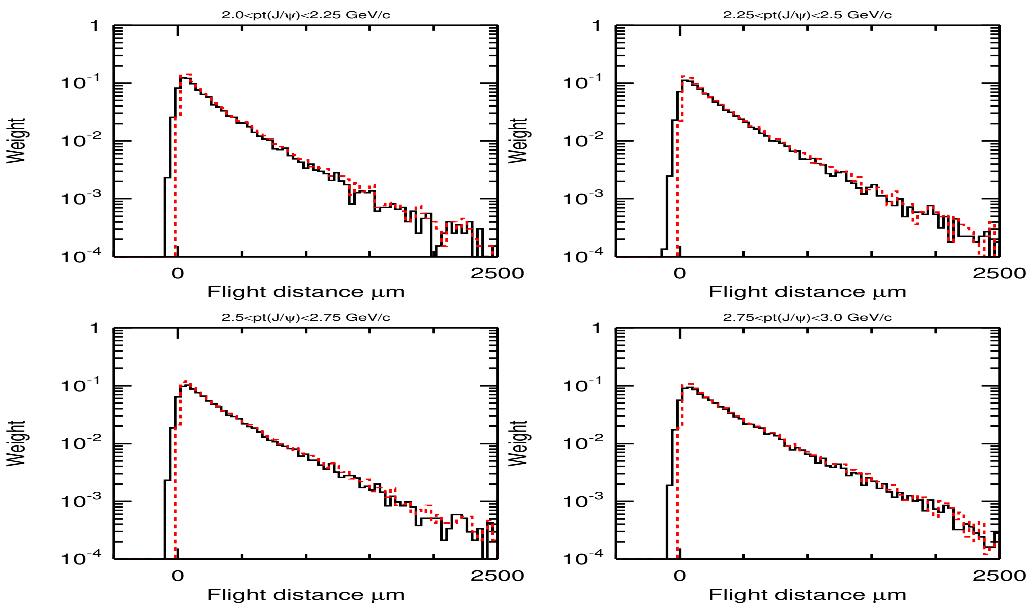

Figure 92: Comparison between the J/ψ from b flight distance in the $r-\phi$, R_{xy} (solid line) and the projection of the J/ψ momentum on R_{xy}, L_{xy} (dashed line). Results are from generator level MC.

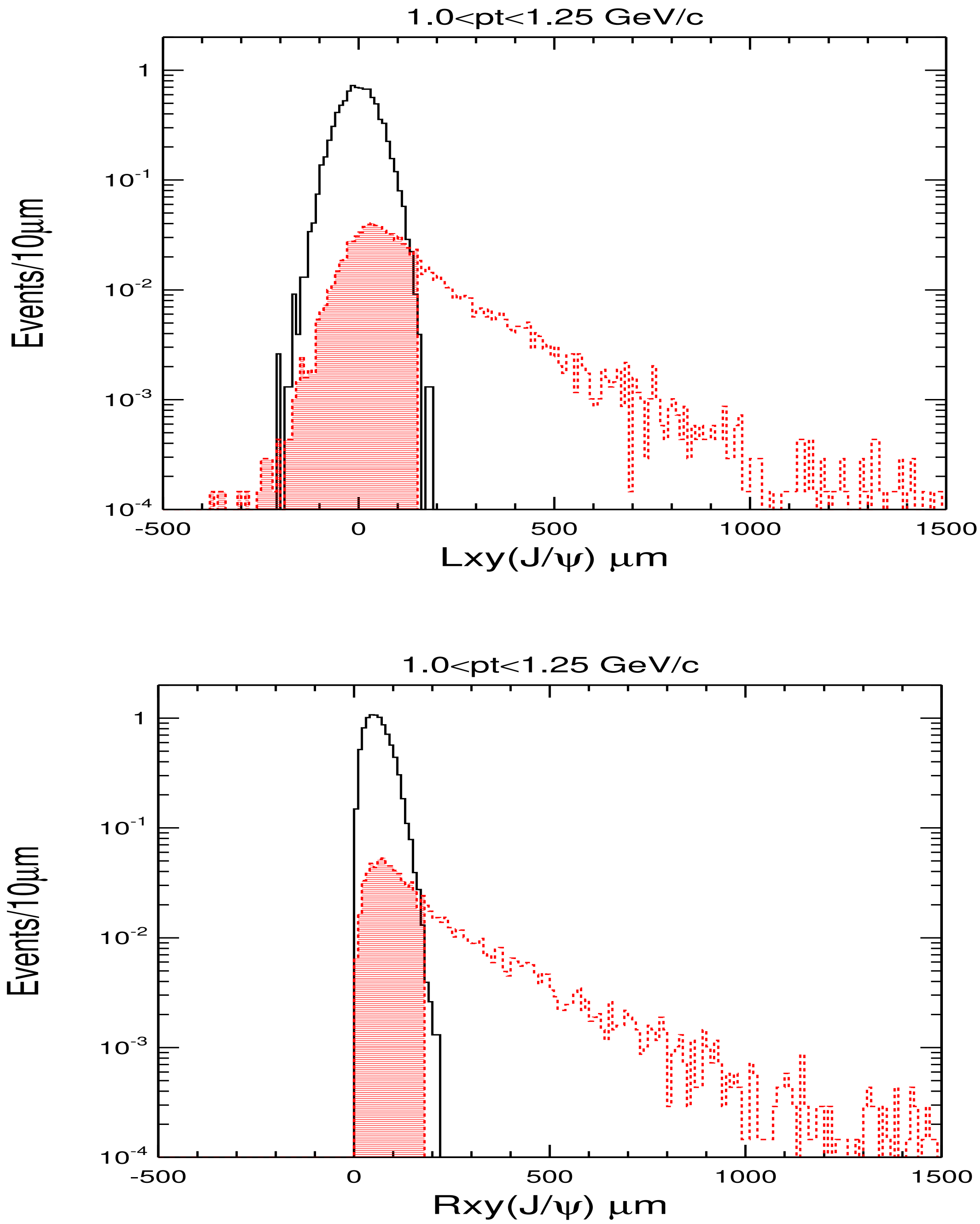

Figure 93: Parameteric MC L_{xy} and R_{xy} distributions of prompt J/psi (black line) and J/ψ from b (dashed line). The shaded area is the fraction of $b \rightarrow J/\psi$ events which are under the prompt peak assuming $b \rightarrow J/\psi X$ is 10% of the inclusive J/ψ.

References

[1] P. Nason, S. Dawson and R. K. Ellis, Nucl. Phys. **B 303**, 607 (1988).
P. Nason *et al.*, Nucl. Phys. **B 327**, 49 (1989), erratum-ibid **B 335** 260 (1989).
W. Beenakker *et al.*, Nucl. Phys. **B 351**, 507 (1991).

[2] J. Binnewies, Bernd A. Kniehl and G. Kramer, Phys. Rev. D58 034016 (1998).

[3] Matteo Cacciari and Paolo Nason, Phys. Rev. Lett. 89 122003 (2002).

[4] J. Binnewies, Bernd A. Kniehl and G. Kramer, Phys.Rev.D60 014006 (1999).

[5] Rick Field, CDF/ANAL/BOTTOM/PUBLIC/5813

[6] Berger-Wagner *et al.* Phys.Rev.Lett. 86,4231 (2001) [hep-ph/0012001]

[7] T. Yamashita *et. al.*, CDF/PHYS/BOTTOM/CDFR/6288

[8] T. LeCompte, /CDF/BOTTOM/PHYS/PUBLIC/6379

[9] Yuri Gotra James Kraus and Ting Miao, CDF/PHYS/TRIGGER/PUBLIC/6162

[10] P. Sphicas, /CDF/DOC/BOTTOM/CDFR/2655 K. Anikeev *et. al.*, CDF/DOC/BOTTOM/CDFR/5092

[11] Particle Data Group, K. Hagiwara *et. al.*., Phys. Rev. D66 010001-1(2002)

[12] S. Anderson *et. al.* hep-ex/0207059 (2002)

[13] B. Aubert *et. al.* BABAR-PUB-02/04, SLAC-PUB-9327

[14] Daniel Young-Joon Kim, “Properties of Inclusive $B \to \psi$ Production”, Ph.D. thesis, Harvard University, Cambridge Mass, January 2002.

[15] M. Bishai, Simon Waschke, /CDF/PHYS/BOTTOM/CDFR/6272

[16] Chakravarti, Laha, and Roy, (1967). “Handbook of Methods of Applied Statistics”, Volume I, John Wiley and Sons, pp. 392-394.

[17] T. Daniels, CDF/THESIS/JET/PUBLIC/4670, page 126.

[18] William Bell *et. al.*, CDF/DOC/BOTTOM/CDFR/5618

[19] http://www-cdf.fnal.gov/upgrades/computing/projects/reconstruction/tracking/talks/030716/shermanTalk.ps

[20] K.Anikeev *et. al.*, CDF/DOC/BOTTOM/CDFR/6023

[21] Thomas J. LeCompte CDF/MEMO/BOTTOM/CDFR/6090

[22] ALBERTO ETCHEGOYEN, THERESA FUESS, VAIA PAPADIMITRIOU CDF/ANAL/TOP/CDFR/1642

List of Tables

List of Figures